



## Spatial networks

Marc Barthélémy \*

*Institut de Physique Théorique, CEA, IPhT CNRS, URA 2306, F-91191 Gif-sur-Yvette, France  
Centre d'Analyse et de Mathématiques Sociales (CAMS, UMR 8557 CNRS-EHESS), Ecole des Hautes Etudes en Sciences Sociales, 54 bd. Raspail,  
F-75270 Paris Cedex 06, France*

---

### ARTICLE INFO

*Article history:*

Accepted 8 November 2010

Available online 23 November 2010

editor: H. Orland

*Keywords:*

Networks

Graphs

Spatial properties

Statistical physics

Geography

Urban systems

---

### ABSTRACT

Complex systems are very often organized under the form of networks where nodes and edges are embedded in space. Transportation and mobility networks, Internet, mobile phone networks, power grids, social and contact networks, and neural networks, are all examples where space is relevant and where topology alone does not contain all the information. Characterizing and understanding the structure and the evolution of spatial networks is thus crucial for many different fields, ranging from urbanism to epidemiology. An important consequence of space on networks is that there is a cost associated with the length of edges which in turn has dramatic effects on the topological structure of these networks. We will thoroughly explain the current state of our understanding of how the spatial constraints affect the structure and properties of these networks. We will review the most recent empirical observations and the most important models of spatial networks. We will also discuss various processes which take place on these spatial networks, such as phase transitions, random walks, synchronization, navigation, resilience, and disease spread.

© 2010 Elsevier B.V. All rights reserved.

---

### Contents

1.	Networks and space .....	3
1.1.	Introduction .....	3
1.2.	Quantitative geography and networks .....	3
1.3.	What this review is (not) about .....	3
2.	Characterizing spatial networks .....	4
2.1.	Generalities on planar networks .....	4
2.1.1.	Spatial and planar networks .....	4
2.1.2.	Classical results for planar networks .....	4
2.1.3.	Voronoi tessellation .....	5
2.2.	Mixing space and topology .....	6
2.2.1.	Basic measures .....	6
2.2.2.	Mixing topology and space .....	9
2.2.3.	Community detection. Motifs .....	12
3.	Empirical observations .....	13
3.1.	Transportation networks .....	13
3.1.1.	Representations .....	13
3.1.2.	Airline networks .....	13
3.1.3.	Bus, subway, railway, and commuters .....	17

\* Corresponding address: Institut de Physique Théorique, CEA, IPhT CNRS, URA 2306, F-91191 Gif-sur-Yvette, France. Tel.: +33 69088120.  
E-mail address: [marc.barthelemy@cea.fr](mailto:marc.barthelemy@cea.fr).

3.1.4.	Cargo ship networks.....	19
3.2.	Infrastructure networks .....	21
3.2.1.	Road and street networks .....	22
3.2.2.	Power grids and water distribution networks.....	26
3.2.3.	The internet.....	27
3.2.4.	Geography in social networks.....	29
3.3.	Origin–destination matrix and mobility networks .....	30
3.3.1.	Importance of human mobility.....	30
3.3.2.	Distribution of the trip duration and length.....	30
3.3.3.	The gravity law .....	33
3.4.	Neural networks .....	39
3.5.	Summary: existence of general features .....	40
4.	Models of spatial networks .....	41
4.1.	Geometric graphs.....	42
4.1.1.	The simplest random geometric graph.....	42
4.1.2.	Random geometric graph in hyperbolic space .....	45
4.1.3.	A scale-free network on a lattice .....	46
4.1.4.	Apollonian networks .....	47
4.2.	Spatial generalization of the Erdos–Renyi graph.....	47
4.2.1.	Erdos–Renyi graph.....	47
4.2.2.	Planar Erdos–Renyi graph .....	48
4.2.3.	The hidden variable model for spatial networks .....	49
4.2.4.	The Waxman model .....	50
4.3.	Spatial small worlds .....	50
4.3.1.	The Watts–Strogatz model.....	50
4.3.2.	Spatial generalizations .....	51
4.4.	Spatial growth models .....	52
4.4.1.	Generalities .....	52
4.4.2.	Preferential attachment and distance selection .....	52
4.4.3.	Growth and local optimization .....	57
4.5.	Optimal networks .....	59
4.5.1.	Hub-and-spoke structure.....	60
4.5.2.	Congestion and centralized organization.....	62
4.5.3.	From the MST to the SPT .....	64
4.5.4.	Adding two antagonistic quantities .....	68
4.5.5.	Beyond trees: noise and loops .....	71
4.6.	Summary: effect of space on networks .....	73
5.	Processes on spatial networks .....	73
5.1.	Ising model.....	73
5.1.1.	Generalities on the Ising model on lattices.....	74
5.1.2.	Ising model on small-world networks .....	74
5.1.3.	Critical fluctuations .....	75
5.2.	Random walks in spatial networks.....	75
5.2.1.	Quantifying the effect of shortcuts .....	75
5.2.2.	Diffusion on power law Watts–Strogatz networks .....	78
5.3.	Synchronization .....	78
5.4.	Navigating and searching .....	79
5.4.1.	Searchable networks .....	79
5.4.2.	Sketch of Kleinberg's proof .....	80
5.4.3.	Searching in spatial scale-free networks .....	82
5.4.4.	Navigability and metric space .....	83
5.4.5.	Effect of cost .....	84
5.4.6.	Routing in social networks .....	84
5.5.	Effect of space on robustness and resilience .....	84
5.5.1.	Percolation and small-worlds .....	84
5.5.2.	Cascade of failures in infrastructures .....	87
5.5.3.	Failure of interdependent networks .....	88
5.6.	Space and the spread of disease.....	89
5.6.1.	SIR on lattices and small-world networks .....	89
5.6.2.	From Euclidean space to networks .....	91
5.6.3.	WiFi and Bluetooth epidemiology .....	94
6.	Summary and outlook .....	95
	Acknowledgements.....	96
	References.....	96

## 1. Networks and space

### 1.1. Introduction

Networks (or graphs) have long been the subject of many studies in mathematics, mathematical sociology, computer science and quantitative geography. In the case of random networks, the first and most important model was proposed by Erdos and Renyi [1,2] at the end of the 1950s and was at the basis of most studies until recently. The interest in networks was however renewed in 1998 by Watts and Strogatz [3], who extracted stylized facts from real-world networks and proposed a simple, new model of random networks. This renewed interest was reinforced after the publication, a year later, of an article by Albert and Barabasi [4] on the existence of strong degree heterogeneities. Strong heterogeneities were in sharp contrast with the random graphs considered so far and the existence of strong fluctuations in real-world networks triggered a wealth of studies. A decade later, we can now find many books [5–10] and reviews on this subject [11–14]. These books and reviews usually discuss spatial aspects of networks very briefly. However, for many critical infrastructures, communication or biological networks, space is relevant: most of people have their friends and relatives in their neighborhood, power grids and transportation networks obviously depend on distance, many communication network devices have short radio range, the length of axons in a brain has a cost, and the spread of contagious diseases is not uniform across territories. In particular, in the important case of the brain, regions that are spatially closer have a greater probability of being connected than remote regions as longer axons are more costly in terms of material and energy [15]. Wiring costs depending on distance are thus certainly an important aspect of brain networks and we can probably expect spatial networks to be very relevant to this rapidly evolving topic. Another particularly important example of such a spatial network is the Internet, which is defined by a set of routers linked by physical cables with different lengths and latency times. More generally, physical distance could be replaced by other parameters, such as a social distance measured by salary, socio-professional category differences, or any quantity which measures the cost associated with the formation of a link.

All these examples show that these networks have nodes and edges which are constrained by some geometry and are usually embedded in a two- or three-dimensional space, and this has important effects on their topological properties and consequently on the processes which take place on them. If there is a cost associated with the edge length, longer links must be compensated by some advantage, such as for example being connected to a well-connected node — that is, a hub. The topological aspects of the network are then correlated to spatial aspects such as the location of the nodes and the length of edges.

### 1.2. Quantitative geography and networks

Spatial networks were actually long ago the subject of many studies in quantitative geography. Objects of study in geography are locations, activities, flows of individuals and goods, and already in the 1970s the scientists working in quantitative geography focused on networks evolving in time and space. One can consult, for example, books such as the remarkably modern ‘Networks analysis in Geography’ by Haggett and Chorley (published in 1969 [16]) or ‘Models in Geography’ [17] to realize that many modern questions in the complex system field are actually at least 40 years old. In these books, the authors discuss the importance of space in the formation and evolution of networks. They develop tools to characterize spatial networks and discuss possible models. Maybe what was lacking at that time were datasets of large networks and larger computer capabilities, but many interesting ideas can be found in these early studies. Most of the important problems, such as the location of nodes of a network, the evolution of transportation networks and their interaction with population and activity density, are addressed in these earlier studies, but many important points still remain unclear and will certainly benefit from the current knowledge on networks and complex systems. Advances in complex networks has already helped researchers to gain new insights on these difficult problems (see for example the recent Handbook on Theoretical and Quantitative Geography [18]) and the present review is an attempt to collect modern results on networks and to help researchers in various fields to reach quantitative answers and realistic modeling. In geography and urban studies, topics of interest would be: understanding the evolution of transportation networks, human mobility, the spatial structure of urban areas, etc. and how these different factors are entangled with each other, in order to propose an integrated approach of scale, mobility, and spatial distribution of activities at various scales.

### 1.3. What this review is (not) about

The importance of spatial networks in current problems, together with the lack of a review specifically on this topic led us to propose the present review article. We will first review the tools to characterize these networks and the empirical properties of some important spatial networks. We then review the most important models of spatial network formation which allow one to understand the main effects of the spatial constraints on the network properties. We will also discuss how space affects various processes taking place on these networks such as walking and searching, resilience, or disease spread.

As mentioned above, spatial networks appear in many different fields, and we will try to cover in some detail the studies in these various areas. However, it is obviously impossible to review all the existing results related to spatial networks. This

implies making some choices, and we basically restricted ourselves to (i) recent topics, (ii) with a sufficient body of literature, (iii) of fundamental research, and (iv) with preferably applications to real-world systems. The goal is to summarize what we understand at this point about the effect of space in networks. In particular, we decided not to discuss here the following subjects (this is not an exhaustive list).

*River networks.* Rivers form spatial networks (which in most cases are essentially trees), and result from the interplay between gravity and the elevation distribution. These networks have been the subject of many studies and we refer the interested reader to the books [8,19] and references therein for a recent account on this subject.

*Sensor, ad hoc, and wireless networks.* There is of course a huge literature on these subjects, which is mostly found in computer and engineering science. In this review, we will discuss some theoretical aspects of these problems, and for more applied problems we refer the interested reader to specialized reviews and books such as [20].

*Spatial games.* Game theory was recently applied to situations where agents are located on the nodes of a network. We refer the interested reader in this particular field to the articles [21,22], for example.

*Mathematical studies of planar maps.* Planar graphs and maps [23] are combinatorial objects which were studied in mathematics and also in physics, where they appear as a natural discretization of random surfaces used in two-dimensional quantum gravity. In particular these mathematical methods allow one to understand the critical behavior of the Ising model on a random planar lattice [24]. We refer the interested reader to the classical book of Ambjorn et al. [25].

The detailed outline of the review is the following. In the Section 2, we introduce the main tools to characterize spatial networks. Many spatial networks are planar, and we recall the main results on planar networks and how to characterize them in Section 2.1. In addition, since spatial networks mix space and topology, we need specific tools and these are described in Section 2.2.

In Section 3, we review the properties of real-world spatial networks such as transportation networks (3.1), infrastructure networks (3.2), mobility networks (3.3), and neural networks (3.4). In these sections, we emphasize the salient stylized facts which allow us to draw some general features of real-world networks in Section 3.5.

In Section 4, we review the most important models of spatial networks. We divide these models into five large categories: we start with random geometric graphs (4.1), followed by spatial generalizations of the Erdos–Renyi graph (4.2) and the Watts–Strogatz model (4.3). We then review models of growing spatial networks in Section 4.4 and we end this chapter with optimal networks in 4.5.

We discuss various processes which take place on spatial networks in Section 5. In particular, we will review the effects of space on transitions in the Ising model (5.1), random walks (5.2), synchronization (5.3), navigation and searching (5.4), robustness (5.5), and disease spread (5.6).

Finally, in Section 6, we give a summary of the review on the effect of space on networks and we end the discussion with a list of open problems that we believe are interesting directions for future research.

## 2. Characterizing spatial networks

### 2.1. Generalities on planar networks

#### 2.1.1. Spatial and planar networks

Loosely speaking, spatial networks are networks for which the nodes are located in a space equipped with a metric. For most practical applications, the space is the two-dimensional space and the metric is the usual Euclidean distance. This definition implies in general that the probability of finding a link between two nodes will decrease with the distance. However, it does not imply that a spatial network is planar. Indeed, the airline passenger networks is a network connecting through direct flights the airports in the world, but is not a planar network.

With this definition of a spatial network links are not necessarily embedded in space: social networks for example connect individuals through friendship relations. In this case, space intervenes in the fact that the connection probability between two individuals usually decreases with the distance between them.

For many infrastructure networks, however, planarity is unavoidable. Roads, rail, and other transportation networks are spatial and to a good accuracy planar networks. For many applications, planar spatial networks are the most important, and most studies have focused on these examples. In this section, we will thus recall some basic results about planar networks and then the standard tools for characterizing networks. In particular, we will focus on the not-so-standard tools which can help in characterizing spatial networks, mixing topological and metric features.

#### 2.1.2. Classical results for planar networks

Basic results on planar networks can be found in any graph theory textbook (see for example [26]) and we will very briefly recall the most important ones.

Basically, a planar graph is a graph that can be drawn in the plane in such a way that its edges do not intersect. Not all drawings of planar graphs are without intersection and a drawing without intersection is sometimes called a plane graph or a planar embedding of the graph. In real-world cases, these considerations actually do not apply, since the nodes and the edges represent in general physical objects.

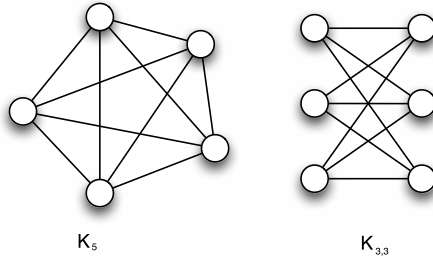


**Fig. 1.** Complete graphs  $K_5$  and  $K_{3,3}$ .

In general it is not a trivial task to check if a graph is planar, and the Kuratowski theorem (see for example the textbook [26]) states that a finite graph is planar if and only if it does not contain a subgraph that is homeomorphic to the graphs  $K_5$  or  $K_{3,3}$  shown in Fig. 1. Many algorithms have been developed to test the planarity of a given network (see for example [27]) and most of these methods operate in  $\mathcal{O}(N)$  time.

There are some very general facts that can be demonstrated for planar graphs, and among them Euler's formula is probably the best known. Euler showed that a finite connected planar graph satisfies the following formula

$$N - E + F = 2 \quad (1)$$

where  $N$  is the number of nodes,  $E$  the number of edges, and  $F$  is the number of faces. This formula can be easily proved by induction by noting that removing an edge decreases  $F$  and  $E$  by one, leaving  $N - E + F$  invariant. We can repeat this operation until we get a tree for which  $F = 1$  and  $N = E + 1$  leading to  $N - E + F = E + 1 - E + 1 = 2$ .

Moreover, for any finite connected planar graph we can obtain a bound. Indeed, any face is bounded by at least three edges and every edge separates two faces at most, which implies that  $E \geq 3F/2$ . From Euler's formula we then obtain

$$E \leq 3N - 6. \quad (2)$$

In other words, planar graphs are always sparse with a bounded average degree  $\langle k \rangle \leq 6$ .

We note here that if we start from a planar point set, we can construct various planar graphs by connecting these points (see the next section on tessellations for example) and by definition the maximal planar graph is the triangulation of a planar point set such that the addition of any edge results in a non-planar graph. Such a network is useful, for example to assess the efficiency of a real-world planar network, and provides an interesting null model. For such a maximal planar graph, the number of edges and faces are maximal and are equal to the bounds  $E = 3N - 6$  and  $F = 2N - 5$ , respectively.

Planar sets thus form faces or cells which have a certain shape. In certain conditions, it can be interesting to characterize statistically these shapes, and various indicators were developed with this goal (see [16] for a list of these indicators). In particular, if  $A$  is the area of a cell, and  $L$  the major axis, the form ratio is defined as  $A/L^2$  or equivalently the elongation ratio given by  $\sqrt{A}/L$ . In the paper [28] on the road network structure, Lämmer et al. use another definition of the form factor of a cell and define it as

$$\phi = \frac{4A}{\pi D^2} \quad (3)$$

where  $\pi D^2$  is the area of the circumscribed circle.

### 2.1.3. Voronoi tessellation

A *tessellation* or tiling of the plane is a collection of plane figures that fills the plane with no overlaps and no gaps. One may also speak of tessellations of parts of the plane or of other surfaces (generalizations to higher dimensions are also possible). A Voronoi diagram is determined by distances to a specified discrete set of points (see for example the Fig. 2). Each site has a Voronoi cell  $V(s)$  consisting of all points closer to  $s$  than to any other site. The segments of the Voronoi diagram are all the points in the plane that are equidistant to the two nearest sites. The Voronoi nodes are the points equidistant to three (or more) sites and, unless there are some degeneracies, all nodes of the Voronoi tessellation have a degree equal to three. The dual graph for a Voronoi diagram corresponds to the Delaunay triangulation for the same set of points.

Voronoi tessellations are interesting for spatial networks in the sense that they provide a natural null model to which one can compare a real-world network.

In particular, an important case is obtained when the points are distributed uniformly and independently in the plane. In this case, one can speak of a Poisson–Voronoi tessellation, for which some statistical properties are known (see [29–31] for a short review on this subject). In particular, the probability that a point has a  $n$ -sided Voronoi cell is given for large  $n$  by [30,31]

$$p_n = \frac{C}{4\pi^2} \frac{(8\pi^2)^n}{(2n)!} \left[ 1 + \mathcal{O}\left(\frac{1}{\sqrt{n}}\right) \right] \quad (4)$$

which at the dominant order behaves as  $p_n \approx n^{-2n}$ .

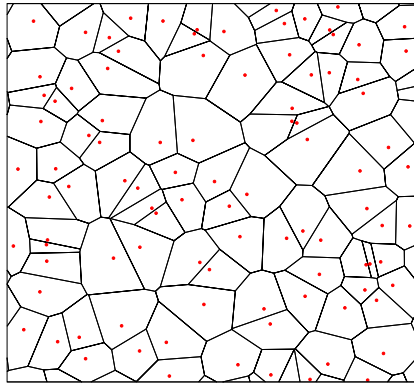


**Fig. 2.** Example of the Voronoi tessellation on a set of points.  
Source: From [29].

## 2.2. Mixing space and topology

### 2.2.1. Basic measures

**2.2.1.1. Adjacency matrix, dual graph.** A graph with  $N$  nodes and  $E$  edges can be described by its  $N \times N$  adjacency matrix  $A$ , which is defined as

$$A_{ij} = \begin{cases} =1 & \text{if } i \text{ and } j \text{ are connected} \\ =0 & \text{otherwise.} \end{cases} \quad (5)$$

If the graph is undirected then the matrix  $A$  is symmetric. The degree of a node is the number of its neighbors and is then given by

$$k_i = \sum_j A_{ij}. \quad (6)$$

The first simple indicator of a graph is the average degree

$$\langle k \rangle = 1/N \sum_i k_i = 2E/N \quad (7)$$

where here and in the following the brackets  $\langle \cdot \rangle$  denote the average over the nodes of the network. In particular the scaling of  $\langle k \rangle$  with  $N$  indicates if the network is sparse (which is the case when  $\langle k \rangle \rightarrow \text{const.}$  for  $N \rightarrow \infty$ ).

The distribution of degree  $P(k)$  is usually a quantity of interest and can display large heterogeneities, such as is observed in scale-free networks (see for example [11]). We indeed observe that for spatial networks, such as airline networks or the Internet, the degrees are very heterogeneous (see 3). However, when physical constraints are strong or when the cost associated with the creation of new links is large, a cut-off appears in the degree distribution [32], and in some case the distribution can be very peaked. This is the case, for example, for the road network and more generally in the case of planar networks, for which the degree distribution  $P(k)$  is of little interest.

In some real-world cases, such as the road network, it is natural to study the usual (or ‘primal’) representation where the nodes are the intersections and the links represent the road segment between the intersection. However, another representation, the dual graph, can be of interest (see [33]). In this road network example, the dual graph is constructed in the following way: the nodes are the roads, and two nodes are connected if there exists an intersection between the two corresponding roads. One can then measure the degree of a node, which represents the number of roads which intersect a given road. Also, the shortest path length in this network represents the number of different roads one has to take to go from one point to another. Finally, we note that even if the road network has a peaked degree distribution its dual representation can display broad distributions [34].

**2.2.1.2. Clustering, assortativity, and average shortest path.** Complex networks are essentially characterized by a small set of parameters, not all of which are relevant for spatial networks. For example, the degree distribution, which has been the main subject of interest in complex network studies, is usually peaked for planar networks, due to the spatial constraints. However, as we will see, the clustering coefficient is important in the characterization of spatial networks. For a node  $i$  of degree  $k_i$  it is defined as

$$C(i) = \frac{E_i}{k_i(k_i - 1)/2} \quad (8)$$

where  $E_i$  is the number of edges among the neighbors of  $i$ . This quantity gives some information about local clustering and is the object of many studies in complex networks. It is also a quantity of interest for spatial networks. Indeed for Erdos–Renyi (ER) random graphs (see Section 4.2) with finite average degree, the average clustering coefficient is simply given by

$$\langle C \rangle \sim \frac{1}{N} \quad (9)$$

where the brackets  $\langle \cdot \rangle$  denote the average over the network. In contrast, for spatial networks, closer nodes have a larger probability to be connected, leading to a large clustering coefficient. The variation of this clustering coefficient in space can thus give valuable information about the spatial structure of the network under consideration.

The clustering coefficient depends on the number of triangles or cycles of length 3 and can also be computed by using the adjacency matrix  $A$ . Powers of the adjacency matrix give the number of paths of variable length. For instance the quantity  $\frac{1}{6}\text{Tr}(A^3)$  is the number  $C_3$  of cycles of length three and is related to the clustering coefficient. Analogously we can define and count cycles of various lengths (see for example [35,36] and references therein) and compare this number to the ones obtained on null models (lattices, triangulations, etc.).

Finally, many studies define the clustering coefficient per degree classes, which is given by

$$C(k) = \frac{1}{N(k)} \sum_{i/k_i=k} C(i). \quad (10)$$

The behavior of  $C(k)$  versus  $k$  thus gives an indication how the clustering is organized when we explore different classes of degrees. However, in order to be useful, this quantity needs to be applied to networks with a large range of degree variations, which is usually not the case in spatial networks.

In general the degrees at the two end nodes of a link are correlated, and to describe these degree correlations one needs the two-point correlation function  $P(k'|k)$ . This quantity represents the probability that any edge starting at a vertex of degree  $k$  ends at a vertex of degree  $k'$ . Higher order correlation functions can be defined, and we refer the interested reader to [7] for example. However, the function  $P(k'|k)$  is not easy to handle and one can define the assortativity [37,38]

$$k_{nn}(k) = \sum_{k'} P(k'|k) k'. \quad (11)$$

A similar quantity can be defined for each node as the average degree of the neighbor

$$k_{nn}(i) = \frac{1}{k_i} \sum_{j \in \Gamma(i)} k_j, \quad (12)$$

where  $\Gamma(i)$  denotes the set of neighbors of  $i$ . There are essentially two classes of behaviors for the assortativity. If  $k_{nn}(k)$  is an increasing function of  $k$ , vertices with large degrees have a greater probability to connect to similar nodes with a large degree. In this case, we speak of an *assortative* network, and in the opposite case of a *disassortative* network. It is expected in general that social networks are mostly assortative, while technological networks are disassortative. However for spatial networks we will see (see Section 3) that spatial constraints usually imply a flat function  $k_{nn}(k)$ .

Usually, there are many paths between two nodes in a connected networks and if we keep the shortest one it defines a distance on the network

$$\ell(i, j) = \min_{\text{paths}(i \rightarrow j)} |\text{path}| \quad (13)$$

where the length  $|\text{path}|$  of the path is defined as its number of edges. The *diameter* of the graph can be defined as the maximum value of all  $\ell(i, j)$  or can also be estimated by the average of this distance over all pairs of nodes in order to characterize the ‘size’ of the network. Indeed for a  $d$ -dimensional regular lattice with  $N$  nodes, this average shortest path  $\langle \ell \rangle$  scales as

$$\langle \ell \rangle \sim N^{1/d}. \quad (14)$$

In a small-world network (see [3] and Section 4.3) constructed over a  $d$ -dimensional lattice,  $\langle \ell \rangle$  has a very different behavior

$$\langle \ell \rangle \sim \log N. \quad (15)$$

The crossover from a large-world behavior  $N^{1/d}$  to a small-world one with  $\log N$  can be achieved for a density  $p$  of long links (or ‘shortcuts’) [39] such that

$$pN \sim 1. \quad (16)$$

The effect of space could thus in principle be detected in the behavior of  $\langle \ell \rangle(N)$ . However, it should be noted that if the number of nodes is too small this can be a tricky task. In the case of brain networks, for example, a behavior typical of a three-dimensional network in  $N^{1/3}$  could easily be confused with a logarithmic behavior if  $N$  is not large enough.

**2.2.1.3. Spectral graph theory.** Spectral graph theory is an important branch of mathematics and allows to obtain insights about the structure of a graph with quantities computed from the eigenvalues of the graph Laplacian [40]. For example, the so-called algebraic connectivity is the smallest non-zero eigenvalue, the distribution of cycle lengths can be computed using a moment expansion of the eigenvalues, and the stationary state of a random walk and synchronization properties are governed by the largest eigenvalue of the adjacency matrix. In a nutshell, spectral graph theory thus studies the adjacency matrices of graphs and connects their eigenvalues to other properties. There are different conventions, but essentially one is interested in the discrete Laplacian on the network defined by

$$L = D - A \quad (17)$$

where  $D_{ij} = k_i \delta_{ij}$  is the identity matrix times the degree  $k_i$  of node  $i$  and  $A$  is the adjacency matrix of the graph. If the graph is undirected the Laplacian is symmetric and if the graph is an infinite square lattice grid of spacing  $a$ , this definition of the Laplacian coincides with the continuous Laplacian  $\nabla^2$  when  $a \rightarrow 0$ . We list here some basic properties of the Laplacian and we refer the interested reader to more advanced material, such as the book [40].

- In the undirected case,  $L$  is symmetric and has real positive eigenvalues  $\lambda_0 = 0 \leq \lambda_1 \leq \dots \leq \lambda_N$ . The multiplicity of  $\lambda_0 = 0$  (whose eigenvector has all components equal) is equal to the number of connected components of the graph.
- The eigenvalue  $\lambda_1$  is called the algebraic connectivity [41] and plays an important role in the characterization of the graph. Roughly speaking, the larger  $\lambda_1$ , the more connected the graph.
- The distribution of eigenvalues is important in many applications. For instance, for random walks, it is related to the return probability and it can also be used (together with the eigenvectors) for visual representations of graphs known as spectral embeddings (see for example [42]). Another example concerns the synchronization of linearly coupled identical oscillators where a master stability function relates the stability of synchronized solutions to the eigenvalues of the Laplacian (more precisely to the ratio  $\lambda_N/\lambda_1$ , see [43,44] for the small-world case).

**2.2.1.4. Betweenness centrality.** The importance of a node is characterized by its so-called centrality. There are however many different centrality indicators, such as the degree, the closeness, etc., but we will focus here on the *betweenness centrality*  $g(i)$ , which is defined as [45–49]

$$g(i) = \sum_{s \neq t} \frac{\sigma_{st}(i)}{\sigma_{st}} \quad (18)$$

where  $\sigma_{st}$  is the number of shortest paths going from  $s$  to  $t$  and  $\sigma_{st}(i)$  is the number of shortest paths going from  $s$  to  $t$  through the node  $i$ . This quantity  $g(i)$  thus characterizes the importance of the node  $i$  in the organization of flows in the network. Note that with this definition, the betweenness centrality of terminal nodes is zero. The betweenness centrality can similarly be defined for edges as

$$g(e) = \sum_{e \in E} \frac{\sigma_{st}(e)}{\sigma_{st}} \quad (19)$$

where  $\sigma_{st}(e)$  is the number of shortest paths going from  $s$  to  $t$  and going through the edge  $e$ .

The betweenness centrality of a vertex is determined by its ability to provide a path between separated regions of the network. Hubs are natural crossroads for paths and it is natural to observe a marked correlation between the average  $g(k) = \sum_{i/k_i=k} g(i)/N(k)$  and  $k$ , as expressed in the following relation [49]

$$g(k) \sim k^\eta \quad (20)$$

where  $\eta$  depends on the characteristics of the network. We expect this relation to be altered when spatial constraints become important, and in order to understand this effect we consider a one-dimensional lattice, which is the simplest case of a spatially ordered network. For this lattice the shortest path between two nodes is simply the Euclidean geodesic, and for two points lying far from each other the probability that the shortest path passes near the barycenter of the network is very large. In other words, the barycenter (and its neighbors) will have a large centrality, as illustrated in Fig. 3a. In contrast, in a purely topological network with no underlying geography, this consideration no longer applies, and if we rewire more and more links (as illustrated in Fig. 3b) we observe a progressive decorrelation of centrality and space, while the correlation with degree increases. In a lattice, the betweenness centrality depends essentially on space and is maximum at the barycenter, while in a network the betweenness centrality of a node depends on its degree. When the network is constituted of long links superimposed on a lattice, we expect the appearance of ‘anomalies’ characterized by large deviations around the behavior  $g \sim k^\eta$ . In order to characterize these anomalies quantitatively [50], one can compute the fluctuations of the betweenness centrality  $\Delta_{MR}(k)$  for a randomized network with the same degree distribution as the original network and constructed with the Molloy–Reed algorithm [51]. We can then consider a node  $i$  to be anomalous if its betweenness centrality  $g(i)$  lies outside the interval  $[\langle g(k) \rangle - \nu \Delta_{MR}(k), \langle g(k) \rangle + \nu \Delta_{MR}(k)]$  where the value of  $\nu$  determines the confidence interval. For  $\nu \approx 1.952$ , the considered interval represents 95% of the nodes in the case of Gaussian distributed centralities around the average.

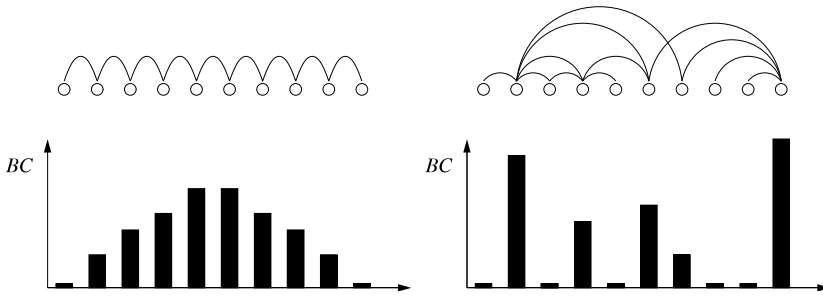


**Fig. 3.** (a) Betweenness centrality for the (one-dimensional) lattice case. The central nodes are close to the barycenter. (b) For a general graph, the central nodes are usually the ones with large degree.

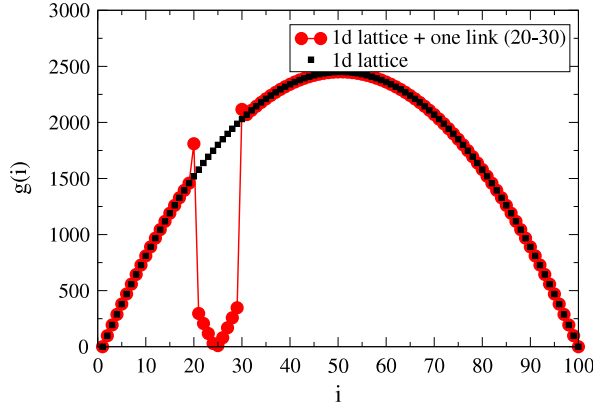


**Fig. 4.** Example of how the addition of a link perturbs the centrality. In black, the betweenness centrality for the 1d lattice (of size  $N = 100$ ) has a maximum at the barycenter  $N/2 = 50$ . The addition of a link between  $a = 20$  and  $b = 30$  decreases the betweenness centrality between  $a$  and  $b$  and increases the betweenness centrality of nodes  $a$  and  $b$ .

The effect of shortcuts and the appearance of anomalies can already be observed in the simple case of a one-dimensional lattice  $i = 1, \dots, N$ . The betweenness centrality in this case is given by  $g_0(i) = (i - 1)(N - i)$  with a maximum at  $i = N/2$  (see Fig. 4). When one link is added between nodes  $a$  and  $b$ , the betweenness centrality of the nodes in the interval  $[a, b]$  decreases. For example, if  $a < N/2 < b$  it is not difficult to see that the variation of the centrality of the node  $N/2$  is bounded by

$$\delta g(N/2) < -a(N - b) \quad (21)$$

which basically means that the shortest paths from a node  $i \in [1, a]$  to a node  $j \in [b, N]$  follow the shortcut and avoid the node  $N/2$ . In contrast, the betweenness centrality of the contact points increases and the betweenness centrality of node  $a$  is now  $g(a) = g_0(a) + \delta g(a)$ , where  $\delta g(a)$  is positive and essentially counts the new pairs of nodes which are connected by a shortest path through the new link  $(a, b)$ .

## 2.2.2. Mixing topology and space

**2.2.2.1. Strengths.** In many cases, the adjacency matrix is not enough to fully characterize a network. This is particularly clear, for example for airline networks, for which the links are also characterized by the average number of passengers  $w_{ij}$  flying on the connection  $(ij)$  (for other networks, such as the Internet it can be the traffic on a cable, etc.). For these weighted networks, the distribution of weights is a first indication of the existence of possible strong heterogeneities [52]. Another important piece of information is the existence of a correlation between the weights and the degrees. Such a correlation can easily be displayed by the study of the *weight strength* of a node  $i$  as defined by [52,53]

$$s_i^w = \sum_{j \in \Gamma(i)} w_{ij} \quad (22)$$

where the sum runs over the set  $\Gamma(i)$  of neighbors of  $i$ . The strength generalizes the degree to weighted networks, and in the case of the air transportation network quantifies the traffic of passengers handled by any given airport. This quantity obviously depends on the degree  $k$ , and increases (linearly) with  $k$  in the case of random uncorrelated weights of average  $\langle w \rangle$  as

$$s^w \sim k\langle w \rangle. \quad (23)$$

A relation between the strength  $s^w(k)$  averaged over the nodes of degree  $k$  of the form

$$s^w = Ak^{\beta_w}, \quad (24)$$

with an exponent  $\beta_w > 1$  (or with  $\beta_w = 1$  but with  $A \neq \langle w \rangle$ ) is then the signature of non-trivial statistical correlations between weights and topology. In particular, a value  $\beta_w > 1$  signals that the typical number of passengers per connection is not constant and increases with  $k$ .

The notion of strength can obviously be extended to many different types of weights. In particular, for spatial networks, one can define [50] the *distance strength* of node  $i$  by

$$s_i^d = \sum_{j \in \Gamma(i)} d_E(i, j) \quad (25)$$

where  $d_E(i, j)$  is the Euclidean distance between nodes  $i$  and  $j$ . This quantity  $s^d$  represents the cumulative distances of all the connections from (or to) the considered airport. Similarly to the usual weight strength, uncorrelated random connections would lead to a linear behavior of the form  $s^d(k) \propto k$ , while otherwise the presence of correlations would be signaled by a behavior of the form

$$s^d(k) \sim k^{\beta_d} \quad (26)$$

with  $\beta_d > 1$ . In such a case, there are correlations between the topology and geography which imply that the typical length of the connection is not constant, as it would be in the case for  $\beta_d = 1$ , but increases with the number of connections.

**2.2.2.2. Indices  $\alpha$ ,  $\gamma$  and variants. Ringness.** Various indices were defined long ago, mainly by scientists working in quantitative geography, following the 1960s and can be found in [16,54,55] (see also the more recent paper by Xie and Levinson [56]). Most of these indices are relatively simple, but give valuable information about the structure of the network, in particular if we are interested in planar networks. These indices were used to characterize the topology of transportation networks. For example Garrison [57] measured some properties of the Interstate highway system and Kansky [58] proposed up to 14 indices to characterize these networks. We will here recall the most important indices, the ‘alpha’ and the ‘gamma’ indices. The simplest index is called the gamma index and is simply defined as

$$\gamma = \frac{E}{E_{max}} \quad (27)$$

where  $E$  is the number of edges and  $E_{max}$  is the maximal number of edges (for a given number of nodes  $N$ ). For non-planar networks,  $E_{max}$  is given by  $N(N - 1)/2$  for non-directed graphs, while for planar graphs we saw in the Section 2.1.2 that  $E_{max} = 3N - 6$  leading to

$$\gamma_p = \frac{E}{3N - 6}. \quad (28)$$

The gamma index is a simple measure of the density of the network, but one can define a similar quantity by counting the number of elementary cycles instead of the edges. The number of elementary cycles for a network is known as the cyclomatic number (see for example [26]) and is equal to

$$\Gamma = E - N + 1. \quad (29)$$

For a planar graph this number is always less or equal to  $2N - 5$ , which leads naturally to the definition of the alpha index (also coined ‘meshedness’ in [59])

$$\alpha = \frac{E - N + 1}{2N - 5}. \quad (30)$$

This index lies in the interval  $[0, 1]$ , being equal to 0 for a tree and to 1 for a maximal planar graph. Using the definition of the average degree  $\langle k \rangle = 2E/N$ , the quantity  $\alpha$  in the large  $N$  limit reads as

$$\alpha \simeq \frac{\langle k \rangle - 2}{4} \quad (31)$$

which shows that in fact for a large network this index  $\alpha$  does not contain much more information than the average degree.

We note that, more recently, other interesting indices have been proposed specifically in order to characterize road networks [56,60]. For example, in [60], Courtat et al. noticed that in some cities the degree distribution is very peaked around 3–4, and they then define the ratio

$$r_N = \frac{N(1) + N(3)}{\sum_{k \neq 2} N(k)} \quad (32)$$

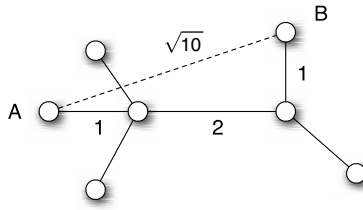


**Fig. 5.** Example of a detour index calculation. The ‘as crow flies’ distance between the nodes  $A$  and  $B$  is  $d_E(A, B) = \sqrt{10}$ , while the route distance over the network is  $d_R(A, B) = 4$ , leading to a detour index equal to  $Q(A, B) = 4/\sqrt{10} \simeq 1.265$ .

where  $N(k)$  is the number of nodes of degree  $k$ . If this ratio is small, the number of dead ends and ‘unfinished’ crossings ( $k = 3$ ) is small compared to the number of regular crossings ( $k = 4$ ). In the opposite case of large  $r_N$ , there is a dominance of  $k = 4$  nodes, which signals a more organized city.

The authors of [60] also define the ‘compactness’ of a city, which measures how much a city is ‘filled’ with roads. If we denote by  $A$  the area of a city and by  $\ell_T$  the total length of roads, the compactness  $\Psi \in [0, 1]$  can be defined in terms of the hull and city areas

$$\Psi = 1 - \frac{4A}{(\ell_T - 2\sqrt{A})^2}. \quad (33)$$

In the extreme case of one square city of linear size  $L = \sqrt{A}$  with only one road encircling it, the total length is  $\ell_T = 4\sqrt{A}$  and the compactness is then  $\Psi = 0$ . At the other extreme, if the city roads constitute a square grid of spacing  $a$ , the total length is  $\ell_T = 2L^2/a$ , and in the limit of  $a/L \rightarrow 0$  one has a very large compactness  $\Psi \approx 1 - a^2/L^2$ .

We end this section by mentioning the ringness. Arterial roads (including freeways, major highways) provide a high level of mobility and serve as the backbone of the road system [56]. Different measures (with many references) are discussed and defined in [56] and, in particular, the *ringness* is defined as

$$\phi_{ring} = \frac{\ell_{ring}}{\ell_{tot}} \quad (34)$$

where  $\ell_{ring}$  is the total length of arterials on rings and the denominator  $\ell_{tot}$  is the total length of all arterials. This quantity, ranging from 0 to 1, is thus an indication of the importance of a ring and to what extent arterials are organized as trees.

**2.2.2.3. Route factor, detour index.** When the network is embedded in a two-dimensional space, we can define at least two distances between the pairs of nodes. There is of course the natural Euclidean distance  $d_E(i, j)$ , which can also be seen as the ‘as crow flies’ distance. There is also the total ‘route’ distance  $d_R(i, j)$  from  $i$  to  $j$  by computing the sum of length of segments which belong to the shortest path between  $i$  and  $j$ . The route factor (also called the detour index or the circuitry or directness [61]) for this pair of nodes  $(i, j)$  is then given by (see Fig. 5 for an example)

$$Q(i, j) = \frac{d_R(i, j)}{d_E(i, j)}. \quad (35)$$

This ratio is always larger than one; and the closer it is to one, the more efficient is the network. From this quantity, we can derive another one for a single node defined by

$$\langle Q(i) \rangle = \frac{1}{N - 1} \sum_j Q(i, j) \quad (36)$$

which measures the ‘accessibility’ for this specific node  $i$ . Indeed, the smaller it is, the easier it is to reach the node  $i$ . Accessibility is a subject in itself (see for example [62]) and there are many other measures for this concept (we refer the interested reader to the articles [63–65]). This quantity  $\langle Q(i) \rangle$  is related to the quantity called ‘straightness centrality’ [66]

$$C^S(i) = \frac{1}{N - 1} \sum_{j \neq i} \frac{d_E(i, j)}{d_R(i, j)} \quad (37)$$

And if one is interested in assessing the global efficiency of the network, one can compute the average over all pairs of nodes (also used in [67])

$$\langle Q \rangle = \frac{1}{N(N - 1)} \sum_{i \neq j} Q(i, j) \quad (38)$$

The average  $\langle Q \rangle$  or the maximum  $Q_{max}$ , and more generally the statistics of  $Q(i, j)$ , is important and contains much information about the spatial network under consideration (see [68] for a discussion on this quantity for various networks). For example, one can define the interesting quantity [68]

$$\phi(d) = \frac{1}{N_d} \sum_{ij/d_E(i,j)=d} Q(i, j) \quad (39)$$

(where  $N_d$  is the number of nodes such that  $d_E(i, j) = d$ ) whose shape can help characterizing combined spatial and topological properties.

**2.2.2.4. Cost and efficiency.** The minimum number of links to connect  $N$  nodes is  $E = N - 1$  and the corresponding network is a tree. We can also look for the tree which minimizes the total length given by the sum of the lengths of all links

$$\ell_T = \sum_{e \in E} d_E(e) \quad (40)$$

where  $d_E(e)$  denotes the length of the link  $e$ . This procedure leads to the minimum spanning tree (MST), which has a total length  $\ell_T^{MST}$  (see also Section 4.5). Obviously the tree is not a very efficient network (from the point of view of transportation for example) and usually more edges are added to the network, leading to an increase of accessibility but also of  $\ell_T$ . A natural measure of the ‘cost’ of the network is then given by

$$C = \frac{\ell_T}{\ell_T^{MST}}. \quad (41)$$

Adding links thus increases the cost but improves accessibility or the *transport performance*  $P$  of the network, which can be measured as the minimum distance between all pairs of nodes, normalized to the same quantity but computed for the minimum spanning tree

$$P = \frac{\langle \ell \rangle}{\langle \ell_{MST} \rangle}. \quad (42)$$

Another measure of efficiency was also proposed in [69,70] and is defined as

$$E = \frac{1}{N(N-1)} \sum_{i \neq j} \frac{1}{\ell(i, j)} \quad (43)$$

where  $\ell(i, j)$  is the shortest path distance from  $i$  to  $j$ . This quantity is zero when all nodes are isolated and is equal to one for the complete graph (for which  $\ell(i, j) = 1$ ). Combinations of these different indicators and comparisons with the MST or the maximal planar network can be constructed in order to characterize various aspects of the networks under consideration (see for example [59]).

Finally, adding links improves the resilience of the network to attacks or dysfunctions. A way to quantify this is by using the *fault tolerance* ( $FT$ ) (see for example [71]) measured as the probability of disconnecting part of the network with the failure of a single link. The benefit/cost ratio could then be estimated by the quantity  $FT/\ell_T^{MST}$ , which is a quantitative characterization of the trade-off between cost and efficiency [71].

### 2.2.3. Community detection. Motifs

**2.2.3.1. Community detection.** Community detection in graphs is an important topic in complex network studies (see the review [72]), but after almost a decade of efforts, there is no definitive method for the identification of communities, but rather many different methods with their respective advantages and drawbacks.

Loosely speaking, a community (or a ‘module’) is a set of nodes which have more connections among themselves than with the rest of nodes. One of the first and simplest methods to detect these modules is the modularity optimization, which consists in maximizing the quantity called modularity, defined as [73]

$$Q = \sum_{s=1}^{n_M} \frac{\ell_s}{E} - \left( \frac{d_s}{2E} \right)^2 \quad (44)$$

where the sum is over the  $n_M$  modules of the partition,  $\ell_s$  is the number of links inside module  $s$ ,  $E$  is the total number of links in the network, and  $d_s$  is the total degree of the nodes in module  $s$ . The first term of the summand in this equation is the fraction of links inside module  $s$  and the second term represents the expected fraction of links in that module if links were located at random in the network (and by keeping the same degree distribution). The number of modules  $n_M$  is also a variable whose value is obtained by the maximization. If for a subgraph  $S$  of the network the first term is much larger than the second, it means that there are many more links inside  $S$  than one would expect by random chance, so  $S$  is indeed a module. The comparison with the null model represented by the randomized network is however misleading and small

modules connected by at least one link might be seen as one single module. This resolution limit was demonstrated in [74], where it was shown that modules of size  $\sqrt{E}$  or smaller might not be detected by this method. Modularity detection was however applied in many different domains, and is still used. In the case of spatial networks, it is the only method which has been used so far, but it is clear that community detection in spatial networks is a very interesting problem which might receive a specific answer. In particular, it would be interesting to see how the classification of nodes proposed in [75] applies to spatial networks.

**2.2.3.2. Motifs.** *Motifs* are particular subgraphs that are over-represented in the network with respect to an uncorrelated random network with the same degree distribution. The concept of motifs is particularly important for biological networks [76] but can be applied to any type of networks, including spatial networks. In many networks found, for example, in biology or ecology, a surprisingly small number of motifs exists and each type of network has its own characteristic set of motifs. The occurrence of a particular motif is characterized by its normalized Z-score, a measure for its abundance in the network. The similarity of the motif distributions between different networks can be a signature of the ubiquity of simple processes occurring in human interactions, good exchanges, etc.

### 3. Empirical observations

In this chapter we will review the most salient properties of real-world spatial networks. We will focus on features connected to the spatial aspects of these networks and we will give references to other aspects.

We will begin with transportation networks, which are emblematic of spatial networks. Generally speaking, transportation networks are structures that convey energy, matter or information from one point to another. They appear in a variety of different fields, including city streets [59,77], plant leaves [78], river networks [19], mammalian circulatory systems [79], networks for commodities delivery [80], technological networks [81], and communication networks [5]. The recent availability of massive data sets has opened up the possibility for a quantitative analysis and modeling of these different patterns. In a second part, we review the recent results obtained for infrastructure networks such as roads, power grids or the Internet. In particular, we will also discuss the geographical aspects of social networks. We then review the recent results on mobility networks which describe the statistics of human movements. We end this chapter with studies on neural networks, including the brain, which is an important example of a complex network with a spatial component. Finally, at the end of this chapter we recap the discussion in the form of a table (see Table 2).

#### 3.1. Transportation networks

The paper of Watts and Strogatz [3] triggered many studies on networks and, in particular, motivated empirical analysis of various networks, for example transportation networks. These networks control many aspects of our society and influence many modern problems, such as disease spread, congestion, urban sprawl, and the structure of cities (see for example the books [82] and [55]). In this section we review the main results concerning their structure.

##### 3.1.1. Representations

In [83], Kurant and Thiran discuss very clearly the different ways to represent a transportation system (Fig. 6). Indeed, the simplest representation is obtained when the nodes represent the stations, and links represent the physical connections. One could, however, construct other networks, such as the space-of-stops or the space-of-changes (see Fig. 6). One also finds in the literature on transportation systems, the notions of  $L$  and  $P$ -spaces [84,87], where the  $L$ -space connects nodes if they are consecutive stops on a given route. The degree in  $L$ -space is then the number of different nodes one can reach within one segment, and the shortest path length represents the number of stops. In the  $P$ -space, two nodes are connected if there is at least one route between them, so the degree of a node is the number of nodes that can be reached directly. In this  $P$ -space, the shortest path represents the number of connections needed to go from one node to another.

##### 3.1.2. Airline networks

The airline transportation infrastructure is an important example of a spatial network. The nodes are identified as the airports, which are located in a two-dimensional space. The location of the nodes are not uniformly distributed and are determined by exogenous factors. The links represent the existence of a direct flight among them, and obviously this network, even if clearly spatial, is not planar.

**3.1.2.1. Weight and spatial heterogeneity.** The usual characteristics of the worldwide air-transportation network using the International Air Transportation Association (IATA) database IATA<sup>1</sup> have been presented in [52]. The network is made of  $N = 3880$  vertices and  $E = 18810$  edges (for the year 2002) and displays both small-world and scale-free properties, as also confirmed in different datasets and analysis [88–90]. In particular, the average shortest path length, measured as the

<sup>1</sup> <http://www.iata.org>.

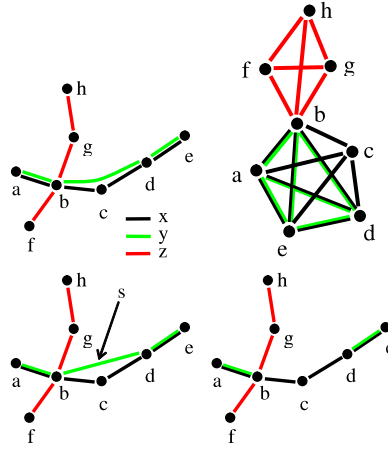


**Fig. 6.** (a) Direct representation of the routes (here for three different routes). (b) Space-of-changes (sometimes called  $P$  space [84–86]). A link connects two nodes if there is at least one vehicle that stops at both nodes. (c) Space-of-stops. Two nodes are connected if they are consecutive stops of at least one vehicle. (d) Space-of-stations. Here two stations are connected only if they are physically connected (without any station in between) and this network reflects the real physical network.

Source: From [83].

average number of edges separating any two nodes in the network, gives the value  $\langle \ell \rangle = 4.37$ , very small compared to the network size  $N$  but largely overestimated due to the presence of long paths between far remote areas (we can expect it to decrease if we weight the paths by their number of passengers).

The degree distribution takes the form

$$P(k) = k^{-\gamma} f(k/k_*) \quad (45)$$

where  $\gamma \simeq 2.0$  and  $f(k/k_*)$  is an exponential cut-off function. The degree distribution is therefore heavy-tailed with a cut-off that finds its origin in the physical constraints on the maximum number of connections that a single airport can handle [32,89,90]. The airport connection graph is therefore a clear example of a spatial (non-planar) small-world network displaying a heavy-tailed degree distribution and heterogeneous topological properties.

The worldwide airline network necessarily mixes different effects. In particular there are clearly two different scales, global (intercontinental) and domestic. The intercontinental scale defines two different groups of travel distances, and for statistical consistency the study [50] focused on a single continental case with the North-American network, constituted of  $N = 935$  vertices with an average degree  $\langle k \rangle \approx 8.4$  and an average shortest path  $\langle \ell \rangle \approx 4$ . The statistical topological properties of the North American network are consistent with the worldwide one: the degree is distributed according to a power law with exponent  $\approx 1.9$  on almost two orders of magnitude, followed by a cut-off indicating the maximum number of connections compatible with the limited airport capacity and the size of the network considered. The spatial attributes of the North American airport network are embodied in the physical spatial distance, measured in kilometers, characterizing each connection. Fig. 7 displays the distribution of the distances of the direct flights. These distances correspond to Euclidean measures of the links, and clearly show a fast decaying behavior reasonably fitted by an exponential. The exponential fit gives a value for a typical scale of the order 1000 km. The origin of the finite scale can be traced back to the existence of physical and economical restrictions on airline planning in a continental setting. However, in a recent paper [91] Bianconi, Pin and Marsili studied the connection probability  $p_{ij}$  for two airports and found that for the US airline network (with  $N = 675$  airports and  $E = 3253$  connections) it behaves as a power law dependence of the form  $p_{ij} \propto d_E(i, j)^{-\alpha}$  with  $\alpha \approx 3$  for  $d > 100$  km. Although the two quantities  $p_{ij}$  and  $P(d)$  are different ( $p_{ij}$  is the probability used to construct the network and  $P(d)$  is the resulting distribution obtained on the specific set of airports distributed across the US territory) it is unclear at this stage if these results are consistent.

In addition, these networks are weighted, with the weight on each link representing the maximum number of passengers on the connection. The traffic at a node can then be studied by the weight strength (see Section 2.2.2.1) and behaves here as a power law of the degree

$$s^w \sim k^{\beta_w}, \quad (46)$$

with an exponent  $\beta_w \simeq 1.7$  (Fig. 8), demonstrating the existence of strong correlations between the degree and the traffic. The distance strength (see the Section 2.2.2.1) also behaves as a power law of the degree

$$s^d(k) \sim k^{\beta_d} \quad (47)$$

with  $\beta_d \simeq 1.4$  (Fig. 8). This result shows the presence of important correlations between topology and geography. Indeed, the fact that the exponents appearing in the relations (Eqs. (46) and (47)) are larger than one has different meanings. While

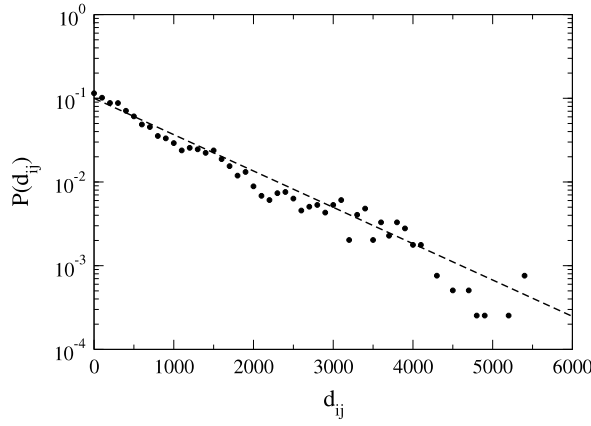


**Fig. 7.** Distribution of distances (in km) between airports linked by a direct connection for the North American network. The straight line indicates an exponential decay with scale of order 1000 km.

Source: From [50].

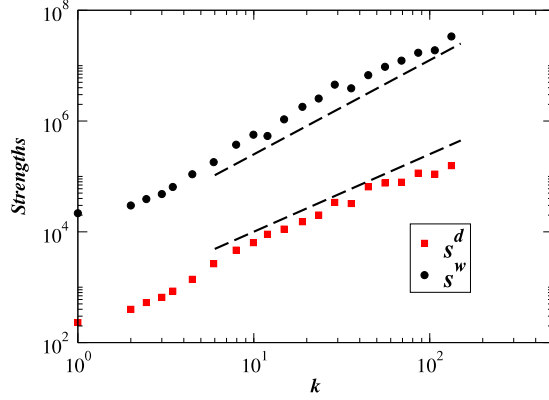


**Fig. 8.** Weight and distance strengths versus degree for the North American network. The dashed lines correspond to the power-laws with exponents  $\beta_d \simeq 1.4$  and  $\beta_w \simeq 1.7$ .

Source: From [50].

Eq. (46) means that larger airports have connections with larger traffic, Eq. (47) implies that they have also farther-reaching connections. In other terms, the traffic and the distance per connection is not constant but increases with  $k$ . As intuitively expected, the airline network is an example of a very heterogeneous network where the hubs have at the same time large connectivities, large weight (traffic) and long-distance connections [52], related by super-linear scaling relations.

**3.1.2.2. Assortativity and clustering.** A complete characterization of the network structure must take into account the level of degree correlations and clustering present in the network. Fig. 9 displays for the North-American airport network the behavior of these various quantities as a function of the degree. An essentially flat  $k_{nn}(k)$  is obtained and a slight disassortative trend is observed at large  $k$ , due to the fact that large airports have in fact many intercontinental connections to other hubs which are located outside of North America and are not considered in this 'regional' network. The clustering is very large and is slightly decreasing at large  $k$ . This behavior is often observed in complex networks and is here a direct consequence of the role of large airports that provide non-stop connections to different regions which are not interconnected among them. Moreover, weighted correlations are systematically larger than the topological ones, signaling that large weights are concentrated on links between large airports which form well inter-connected cliques (see also [52] for more details).

**3.1.2.3. Betweenness centrality.** As discussed in the Section 2.2.1.4, the betweenness centrality is a very interesting quantity which characterizes the importance of a node in the network. The more central the node, the larger the number of shortest paths going through this node. It is thus natural to observe strong correlations between the betweenness centrality and the degree. However, for a lattice, the betweenness centrality is maximal at the barycenter of all nodes and we thus expect for real spatial networks an interesting interplay between the degree of the node and its distance to the barycenter.

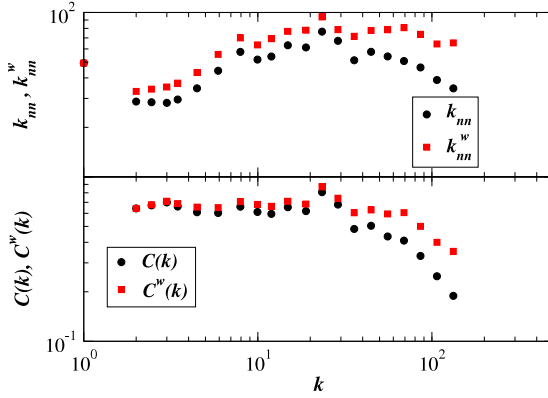


**Fig. 9.** Assortativity and clustering for the North American network. Circles correspond to topological quantities while the squares represent the weighted assortativity and clustering.  
Source: From [50].

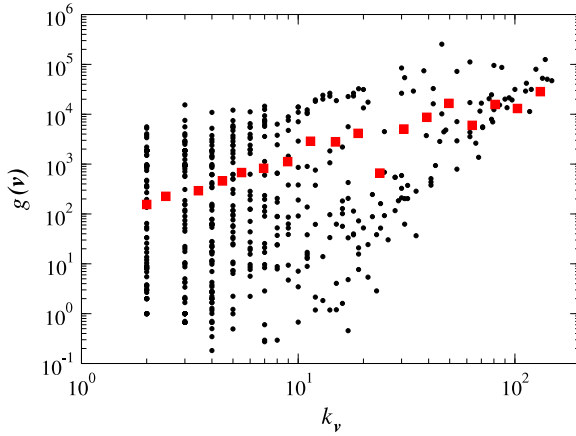


**Fig. 10.** Scatter-plot of the betweenness centrality versus degree for nodes of the North American air-transportation network. The (red) squares correspond to the average betweenness centrality versus degree.  
Source: From [50].

More precisely, it is generally useful to represent the average betweenness centrality for vertices of the same degree

$$g(k) = \frac{1}{N(k)} \sum_{v/k_v=k} g(v), \quad (48)$$

where \$N(k)\$ is the number of nodes of degree \$k\$. For most networks, \$g(k)\$ is strongly correlated with the degree \$k\$. In general, the larger the degree, the larger the centrality. For scale-free networks it has been shown that the centrality scales with \$k\$ as

$$g(k) \sim k^\eta \quad (49)$$

where \$\eta\$ depends on the network [47,49]. For some networks however, the betweenness centrality fluctuations around the behavior given by Eq. (49) can be very large and ‘anomalies’ can occur, in the sense that the variation of the centrality versus degree is not a monotonous function. Guimerà and Amaral [90] have shown that this is indeed the case for the worldwide air-transportation network. This is a very relevant observation in that very central cities may have a relatively low degree and vice versa. Fig. 10 displays the average behavior along with the scattered plot of the betweenness versus degree of all airports of the North American network. In this case we find also very large fluctuations with a behavior similar to that observed in [89].

These different observations call for the need of a network model embedded in real space which can reproduce these betweenness centrality features observed in real networks. More generally these different results point out the importance of space as a relevant ingredient in the structure of networks. In the chapter about models (Section 4) we focus on the interplay between spatial embedding, topology and weights in a simple general model for weighted networks in order to provide a modeling framework considering these three aspects simultaneously.

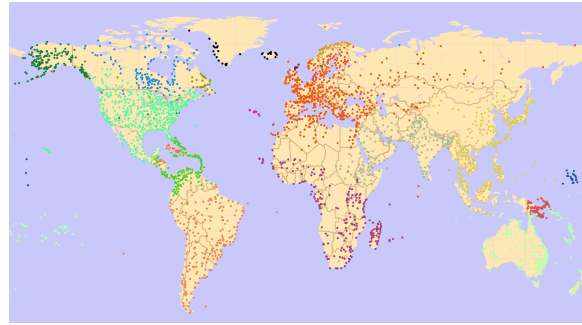


**Fig. 11.** Communities of the worldwide air transportation network obtained with modularity optimization. Each node represents an airport and each color corresponds to a community.

Source: From [90].

**3.1.2.4. Communities.** In [90], Guimera et al. used modularity optimization with simulated annealing (see Section 2.2.3) in order to identify communities defined by the worldwide air network. The obtained result is shown in Fig. 11 where each color corresponds to a community. We can immediately see that most of these communities are actually determined by geographical factors and therefore is not very informative: the most important flows are among nodes in the same geographical regions. More interesting are the spatial anomalies which belong to a community from the modularity point of view but which are in another geographical region. For example, the ‘red’ community of western Europe also contains airports from Asian Russia. More generally, it is clear that in the case of spatial networks, community detection offers a visual representation of large exchange zones. It also allows one to identify the inter-communities links which probably play a very important role in many processes such as disease spread for example.

### 3.1.3. Bus, subway, railway, and commuters

**3.1.3.1. Subways.** One of the first studies (after the Watts–Strogatz paper) on the topology of a transportation network was proposed by Latora and Marchiori [85], who considered the Boston subway network. It is a relatively small network with  $N = 124$  stations. The average shortest path is  $\langle \ell \rangle \sim 16$ , a value which is large compared to  $\ln 124 \approx 5$  and closer to the two-dimensional result  $\sqrt{124} \approx 11$ .

In [86] Sienkiewicz and Holyst study a larger set made of public transportation networks of buses and tramways for 22 Polish cities, and in [92] von Ferber et al. study the public transportation networks for 15 world cities. The number of nodes of these networks varies from  $N = 152$  to 2811 in [86] and in the range [1494, 44629] in [92]. Interestingly enough, the authors of [86] observe a strong correlation between the number of stations and the population, which is not the case for the world cities studied in [92] where the number of stations seems to be independent of the population.<sup>2</sup> For the Polish cities the degree has an average in the range [2.48, 3.08] and in a similar range [2.18, 3.73] for [92]. In both cases, the degree distribution is relatively peaked (the range of variation is usually of the order of one decade) a result consistent with the existence of physical constraints [32].

Due to the relatively small range of variation of  $N$  in these various studies [85,86,92], the behavior of the average shortest path is not clear and could be fitted by a logarithm or a power law as well. We can, however, note that the average shortest path is usually large (of order 10 in [86] and in the range [6.4, 52.0] in [92]) compared to  $\ln N$ , suggesting that the behavior of  $\langle \ell \rangle$  might not be logarithmic with  $N$  but more likely scales as  $N^{1/2}$ , a behavior typical of a two-dimensional lattice.

The average clustering coefficient  $\langle C \rangle$  in [86] varies in the range [0.055, 0.161] and is larger than a value of the order  $C_{ER} \sim 1/N \sim 10^{-3} - 10^{-2}$  corresponding to a random ER graph. The ratio  $\langle C \rangle/C_{ER}$  is explicitly considered in [92] and is usually much larger than one (in the range [41, 625]). The degree-dependent clustering coefficient  $C(k)$  seems to present a power law dependence, but the fit is obtained over one decade only.

In another study [93], the authors study two urban train networks (Boston and Vienna, which are both small,  $N = 124$  and  $N = 76$ , respectively) and their results are consistent with the previous ones.

Due to the limited availability of data, there are less studies on the passenger flows, and the data so far seem to indicate that the flow is broadly distributed [94,95], a feature which seems to be common to many transportation systems (see Table 2).

**3.1.3.2. Rail.** One of the first studies of the structure of the railway network [84] concerns a subset of the most important stations and lines of the Indian railway network and has  $N = 587$  stations. In the  $P$ -space representation (see Section 3.1.1), there is a link between two stations if there is a train connecting them and in this representation, the average shortest path

<sup>2</sup> Incidentally, connecting socio-economical indicators to properties of these networks is certainly a very interesting and difficult question which probably will be addressed in the future.



**Fig. 12.** Physical map of the Swiss railway network.  
Source: From [83].

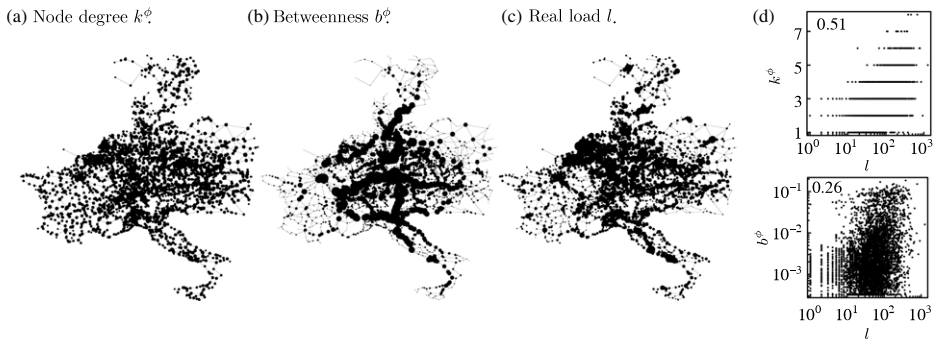


**Fig. 13.** EU rail dataset. (a) Physical layout of the network showing node of size proportional to (a) the degree, (b) the node betweenness centrality, (c) the real load. In (d, top) the degree versus the centrality is shown and in (d, bottom) the betweenness versus the real load. [96].

is of order  $\langle \ell \rangle \approx 5$ , which indicates that one needs 4 connections in the worst case to go from one node to another. In order to obtain variations with the number of nodes, the authors considered different subgraphs with different sizes  $N$ . The clustering coefficient varies slowly with  $N$  and is always larger than  $\approx 0.7$ , which is much larger than a random graph value of order  $1/N$ . Finally, in that study [84], it was shown that the degree distribution behaves as an exponential and that the assortativity  $\langle k_{nn} \rangle(k)$  is flat, showing an absence of correlations between the degree of a node and those of its neighbors.

In [83], Kurant and Thiran study the railway system of Switzerland and major trains and stations in Europe (and also the public transportation system of Warsaw, Poland). The Swiss railway network contains  $N = 1613$  nodes and  $E = 1680$  edges (Fig. 12). All conclusions drawn here are consistent with the various cases presented in this chapter. In particular, the average degree is  $\langle k \rangle \approx 2.1$ , the average shortest path is  $\approx 47$  (consistent with the  $\sqrt{N}$  result for a two-dimensional lattice), the clustering coefficient is much larger than its random counterpart, and the degree distribution is peaked (exponentially decreasing).

Finally, in [96] Kurant and Thiran studied networks by decomposing them into layers (see Fig. 13). In particular, they compare the spatial distribution of the degree, the node betweenness centrality and the real load. As shown in Fig. 13d the correlation between these different indicators is poor (with a Pearson correlation coefficient equal to 0.5 for betweenness centrality- $k$  and 0.26 for the correlation betweenness centrality-real load). As expected from general considerations developed in the Section 2.2.1.4, we see large fluctuations in the relation  $k$  and the betweenness centrality, but surprisingly here, the degree seems to be a better indicator of the real load than the betweenness centrality [96].

**3.1.3.3. Urban commuters network.** As discussed above, it is important to know how the flows of individuals are structured in a dense urban area (Theoretical discussions about this problem can be found in Section 3.3.3 about the so-called gravity law). In [97], Chowell et al. study the simulated movements of 1.6 million individuals during a typical day in the city of Portland (Oregon, USA) and construct a network where the nodes represent the locations (buildings, homes, etc.) and where the edges represent the flow of individuals between these locations (see Fig. 14). The distribution of the outdegree (which is the number of edges leaving a node), and of the corresponding out-traffic, are well-fitted by power laws. The clustering coefficient for different types of locations are all large and, when all activities are aggregated, the corresponding clustering coefficient behaves as  $1/k$  (Fig. 15). It thus seems that at this relatively small scale, space is not constraining enough (or in other words the cost variations are too small) and the important features of spatial networks do not seem to appear here.

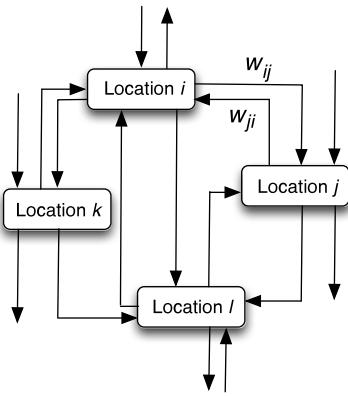


**Fig. 14.** Construction of the network between the locations in Portland as reported in [97]. The weight  $w_{ij}$  on the link  $i - j$  represents the daily traffic from  $i$  to  $j$ . After [97].

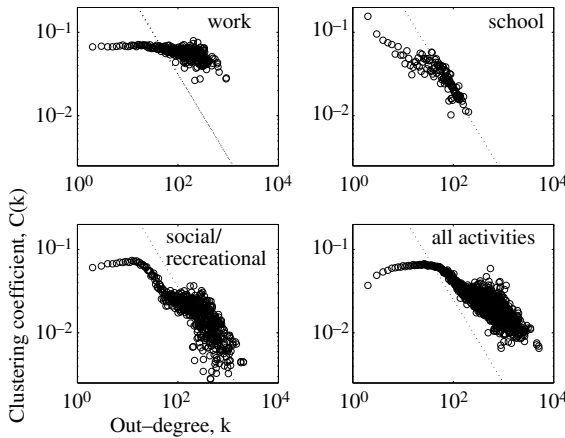


**Fig. 15.** Loglog plots of the clustering coefficient  $C(k)$  as a function of the out-degree for subnetworks constructed from work activities, school activities, social and recreational activities, and all the activities grouped together (the dotted line has slope 1). For social and recreational activities  $C(k) \sim 1/k$ , but for the networks constructed from work activities the clustering coefficient is almost constant.

Source: From [97].

At a larger scale, de Montis et al. [98] studied the network representing the interurban commuting traffic of the island of Sardinia (Italy), which amounts to 375 municipalities and 1.6 million inhabitants. The nodes correspond to towns and the edges to the actual commuting flows among them. This network has a peaked distribution of degrees and, similarly, to the urban case studied in [97], the flows are very heterogeneous and can be fitted by a power law with exponent  $\approx 1.8$ . In contrast with [97], where the relation between the strength and the degree is linear, it is strongly non-linear, with  $\beta \approx 1.9$ , in this inter-urban case.

Still considering commuters, a recent study [99] used modularity optimization to determine communities from this inter-urban commuters-weighted network and showed that there is consistency between the obtained communities and the administrative regions. A similar result was obtained using bank note dispersal in [100]. Community detection was also used on the Belgian mobile phone network to identify communities [101,102]. Community detection thus appears as an interesting tool for scientifically defining administrative boundaries and, more generally, for policy making and planning.

### 3.1.4. Cargo ship networks

The last example of transportation network that we will discuss in this chapter is the cargo ship network [87,103,104]. This network is particularly important, as more than 90% of the world trade is carried by the sea.

Cargo ships are not all the same and can be either bulk dry carriers, oil tankers or can be designed to transport containerized cargo. These different cargo types define different networks which can display different properties [104]. In the case of containerized cargo, many important statistical parameters were measured in [87] and here we summarize their results. The dataset consists of  $N = 878$  ports and 1802 different lines giving 7955 edges. In the  $L$ -space representation (see Section 3.1.1), the nodes are the ports and there is a link between two ports when they are connected by a direct route. The shortest path between two ports in this representation thus represents the number of stops needed to travel between these two nodes. The average degree of the undirected version of this network is  $\langle k \rangle \approx 9$ , the average clustering coefficient

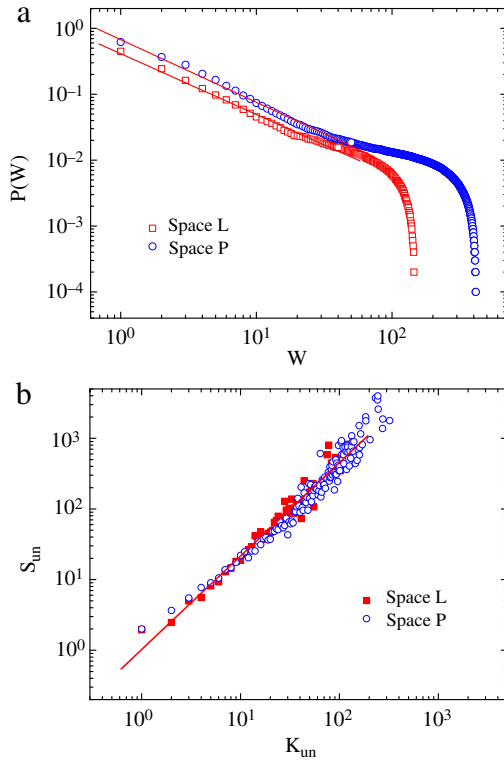


**Fig. 16.** (a) Weight distribution for the worldwide maritime network (the power law fit gives an exponent  $\approx 0.95$ ). (b) Strength versus degree showing a nonlinear behavior (the fit gives an exponent  $\approx 1.3$ ).  
Source: From [87].

is  $\langle C \rangle \approx 0.40$ , which is much larger than  $1/878 \approx 10^{-3}$ . The average shortest path is  $\langle \ell \rangle \approx 3.6$  and the out-, in- and undirected degree distributions seem to be relatively broad, with maximum values as large as  $k \sim 10^2$ . More clearly, the weight (defined as the number of container lines for a given time period) and the strength (see Section 2.2.2) are broadly distributed. The power law fit proposed in [87] gives a behavior for the weight  $P(w) \sim 1/w$  (for  $w < 100$ , see Fig. 16a). The strength (see Section 2.2.2) versus the degree displays a nonlinear behavior (Fig. 16b) typical of these networks. The exponent is of order  $\beta \simeq 1.3$ , not far from the values  $\beta \simeq 1.4\text{--}1.5$  measured for the worldwide network.

For this weighted network, weighted clustering and weighted assortativity were also measured [87], showing that  $C^w(k) > C(k)$  and  $k_{nn}^w(k) > k_{nn}(k)$ , which is the typical sign that most of the traffic takes place on links connecting various hubs. Also this network is weakly assortative with an almost flat  $k_{nn}(k)$ .

The behavior of the betweenness centrality with the degree is interesting and is shown in Fig. 17, where we see that anomalies are very rare: the larger the degree and the larger the betweenness centrality. This particular feature (which makes this network very different from the worldwide air travel network) might come from the fact that geographical constraints are less severe for cargo ships. We saw that the existence of anomalies could be linked to the fact that long links are difficult to create and must be compensated by a large degree. Longer links here are maybe less costly and constraints therefore smaller, leading to less anomalies and to a behavior closer to a power law  $\langle g(k) \rangle \sim k^\eta$  typical of standard non-spatial networks.

Recently, in [104], Kaluza et al. studied a larger dataset (obtained for the year 2007) with 490,517 non-stop journeys between 36,351 distinct pairs of departure and arrival ports. They also found a small average shortest path  $\langle \ell \rangle \approx 2.5$  with more than 50% of possible origin–destination pairs that can be connected by two steps or less. This study confirms the facts that the average clustering is large, and that the degree, weight, and strength distributions are large. The exponent of the weight (defined here as the available space on all ships) distribution is equal to  $\approx 1.7$  and is different from the study [87].

The weight is also very asymmetric (i.e.  $w_{ij} \neq w_{ji}$ ), with 59% of all linked pairs existing in one direction only. This feature can also be observed in other transportation networks (such as mail or freight [105]) and is probably the sign of distribution networks as opposed to travel networks, where basically every individual performs a roundtrip implying symmetrical weights  $w_{ij} \approx w_{ji}$ .

The strength in [104] also scales as a power law of the degree with an exponent  $\simeq 1.46$  not far from the values of the exponents found in other networks. Finally, the betweenness centrality scales well with the degree and displays very few anomalies in agreement with [87]. After these rather standard measurements, the authors of [104] proposed other measurements. They first characterized the community structure (Fig. 18) for three subnetworks of this cargo network

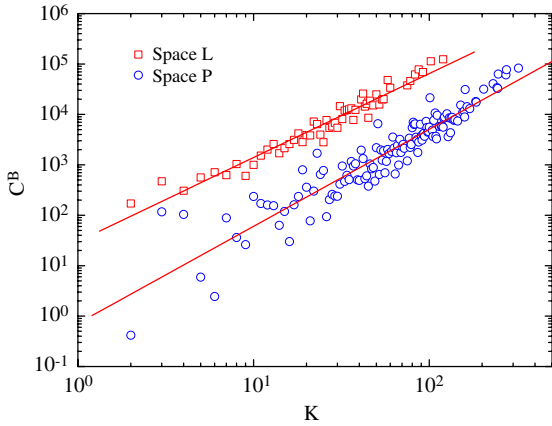


**Fig. 17.** Betweenness centrality versus the degree  $k$ . The power law fit for the  $L$ -space gives 1.66 and 1.93 in the  $P$ -space.  
Source: From [87].

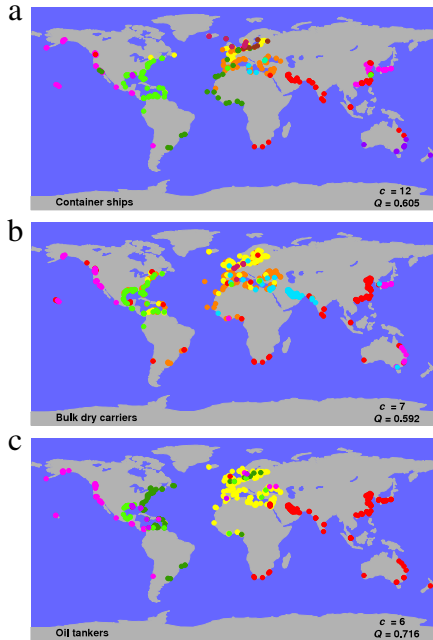


**Fig. 18.** Communities of ports obtained for the cargo networks obtained for different types of ships: (a) container ships, (b) bulk dry carriers, and (c) oil tankers. The optimal values of the number of communities  $c$  and the modularity  $Q$  are shown in the bottom right corner of each panel.  
Source: From [104].

obtained for different ship types (containers, bulk dry carriers, and oil tankers). These communities were obtained by optimizing the modularity  $Q$  (see Section 2.2.3). This procedure might miss some small structures [74] but at large scale can be trusted. Indeed, in this case, groups are observed which are geographically consistent, demonstrating the relevance of this method in this case. One could even think that community detection might be an important tool in geography and in the determination of new administrative or economical boundaries.

Finally, the authors of [104] studied the statistical occurrence of motifs, a method developed in a biological context [76]. In Fig. 19, we reproduce the motif distribution for the three main cargo fleets compared with the results for the Web and social networks, displaying surprising similarities pointing to the existence of ‘superuniversal’ features in complex networks.

### 3.2. Infrastructure networks

Our modern societies depend crucially on infrastructure networks. Movement of people on roads and streets, water and gas distribution, power grids, and communication networks are all networks vital to the good functioning of society. In this chapter, we will review the most important and recent results on their structure in relation to spatial aspects.

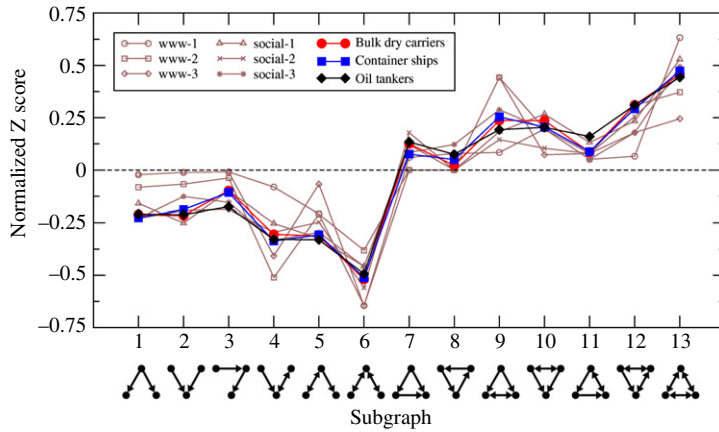


**Fig. 19.** *Z-score for the different motifs shown at the bottom of the figure. Results are shown for the three main cargo fleets and for comparison with the WWW and social networks.*

Source: From [104].

### 3.2.1. Road and street networks

Despite the peculiar geographical, historical, and social–economical mechanisms that have shaped distinct urban areas in different ways (see for example [106] and references therein), recent empirical studies [28,77,107–112] have shown that, at least at a coarse grained level, unexpected quantitative similarities exist between road networks of very different cities. The simplest description of the street network consists of a graph whose links represent roads, and whose vertices represent road intersections and end points. For these graphs, links intersect essentially only at vertices and are thus planar.<sup>3</sup> Measuring spatial properties of cities through the analysis of the street network is not new and was popularized by Hillier and Hanson [113] under the term ‘space syntax’. In this chapter, we will discuss different recent measures of these networks in the light of our current understanding of the structure of networks.

**3.2.1.1. Degrees, lengths, and cell areas.** In [59,77] measurements for different cities in the world are reported. Based on the data from these sources, the authors of [114] plotted (Fig. 20a) the number of roads  $E$  (edges) versus the number of intersections  $N$ . The plot is consistent with a linear fit with slope  $\approx 1.44$  (which is consistent with the value  $\langle k \rangle \approx 2.5$  measured in [59]). The quantity  $e = E/N = \langle k \rangle/2$  displays values in the range  $1.05 < e < 1.69$ , in between the values  $e = 1$  and  $e = 2$  that characterize tree-like structures and  $2d$  regular lattices, respectively. In a study of 20 German cities, Lämmer et al. [28] showed that most nodes have four neighbors (the full degree distribution is shown in Fig. 22) and that for various world cities the degree rarely exceeds 5 [77]. These values are however not very indicative: planarity imposes severe constraints on the degree of a node and on its distribution, which is generally peaked around its average value. Few exact values and bounds are available for the average degree of classical models of planar graphs. In general it is known that  $e \leq 3$ , while it has been recently shown [115] that  $e > 13/7$  for planar Erdős–Renyi graphs ([115] and Section 4.2).

In Fig. 20b, we can see the total length  $\ell_T$  of the network versus  $N$  for the towns considered in [77]. Data are well fitted by a power function of the form

$$\ell_T = \mu N^\beta \quad (50)$$

with  $\mu \approx 1.51$  and  $\beta \approx 0.49$ . In order to understand this result, one has to focus on the street segment length distribution  $P(\ell_1)$ . This quantity has been measured for London in [116] and is shown in Fig. 21. This figure shows that the distribution decreases rapidly and the fit proposed by the authors of [116] suggests that

$$P(\ell_1) \sim \ell_1^{-\gamma} \quad (51)$$

with  $\gamma \simeq 3.36$ , which implies that both the average and the dispersion are well-defined and finite. If we assume that this result extends to other cities, it means that we have a typical distance  $\ell_1$  between nodes which is meaningful. This typical distance between connected nodes then naturally scales as

$$\ell_1 \sim \frac{1}{\sqrt{\rho}} \quad (52)$$

where  $\rho = N/L^2$  is the density of vertices and  $L$  the linear dimension of the ambient space. This implies that the total length scales as

$$\ell_T \sim E\ell_1 \sim \frac{\langle k \rangle}{2} L \sqrt{N}. \quad (53)$$

<sup>3</sup> For roads, highways, etc. planarity can be violated due to bridges but can be considered as a good approximation [28].

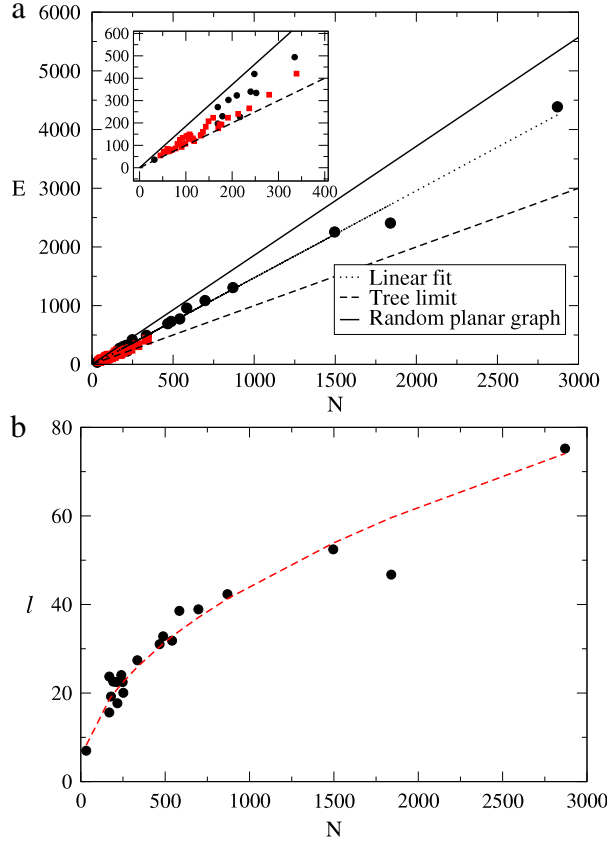


**Fig. 20.** (a) Numbers of roads versus the number of nodes (i.e. intersections and centers) for data from [77] (circles) and from [59] (squares). In the inset, we show a zoom for a small number of nodes. (b) Total length versus the number of nodes. The line is a fit which predicts a growth as  $\sqrt{N}$ .  
Source: Data from [77] and figures from [114].

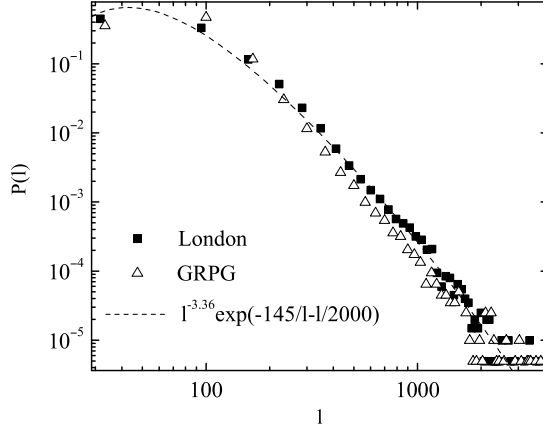


**Fig. 21.** Length distribution  $P(\ell_1)$  for the street network of London (and for the model 'GRPG' proposed in this study [116]).  
Source: From [116]).

This simple argument reproduces well the  $\sqrt{N}$  behavior observed in Fig. 20 and also the value (given the error bars) of the prefactor  $\mu \approx \langle k \rangle L/2$ .

The simplest hypothesis consistent with all the data presented so far, at this stage, is that the road network is an homogeneous and translationally invariant structure. However, this network naturally produces a set of non overlapping cells, encircled by the roads themselves and covering the embedding plane, and surprisingly, the distribution of the area  $A$

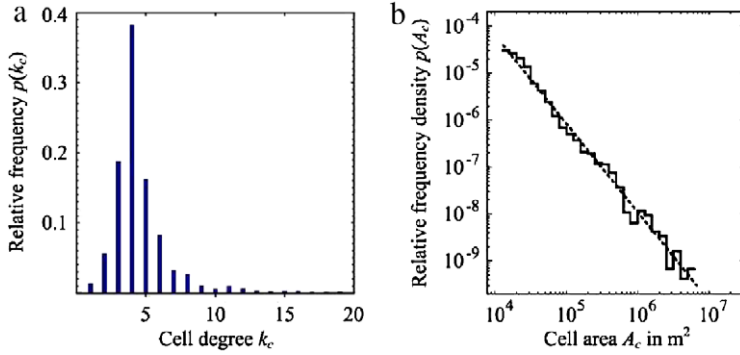


**Fig. 22.** (a) Degree distribution of degrees for the road network of Dresden. (b) The frequency distribution of the cell surface areas  $A_c$  obeys a power law with exponent  $\alpha \approx 1.9$  (for the road network of Dresden).

Source: From [28].

of such cells measured for the city of Dresden in Germany (Fig. 22) has the form

$$P(A) \sim A^{-\alpha} \quad (54)$$

with  $\alpha \simeq 1.9$ . This is in sharp contrast with the simple picture of an almost regular lattice, which would predict a distribution  $P(A)$  peaked around  $\ell_1^2$ . It is interesting to note that if we assume that  $A \sim 1/\ell_1^2 \sim 1/\rho$  and that  $\rho$  is distributed according to a law  $f(\rho)$  (with a finite  $f(0)$ ), a simple calculation gives

$$P(A) \sim \frac{1}{A^2} f(1/A) \quad (55)$$

which behaves as  $P(A) \sim 1/A^2$  for large  $A$ . This simple argument thus suggests that the observed value  $\approx 2.0$  of the exponent is universal and reflects the random variation of the density. However, more measurements are needed at this point in order to test the validity of this hypothesis.

The authors of [28] also measured the distribution of the form factor  $\phi = 4A/(\pi D^2)$ , (the ratio of the area of the cell to the area of the circumscribed circle) and found that most cells have a form factor between 0.3 and 0.6, suggesting a large variety of cell shapes, in contradiction with the assumption of an almost regular lattice. These facts thus call for a model radically different from simple models of regular or perturbed lattices.

Finally, we note that the degree distribution in the dual representation has been studied [34] for the road network in the US, England, and Denmark and displays broad fluctuations with a power law distribution with exponent  $2.0 < \gamma < 2.5$ .

**3.2.1.2. Betweenness centrality.** The importance of a road can be characterized by its traffic, which can be measured by sensors (see for example [117]).<sup>4</sup> If we assume that the traffic between all pairs of nodes is the same, a natural proxy for the traffic is the betweenness centrality. Even if the underlying assumptions are not correct, the spatial distribution of the betweenness centrality gives important information about the coupling between space and the structure of the road network.

Lämmer et al. [28] studied the German road network and obtained very broad distributions of betweenness centrality with a power law exponent in the range [1.279, 1.486] (for Dresden  $\approx 1.36$ ). These broad distributions of the betweenness centrality signals the strong heterogeneity of the network in terms of traffic, with the existence of a few very central roads, which very probably points to some congestion traffic problems. Also the absence of a scale in a power law distribution suggests that the importance of roads is organized in a hierarchical way, a property expected for many transportation networks [118]. However, the broadness of the betweenness centrality distribution does not seem to be universal. Indeed, in [110,119], the betweenness centrality distribution is peaked (depending on the city either exponentially or according to a Gaussian), which signals the existence of a scale and therefore of a finite number of congested points in the city. The betweenness centrality is in itself interesting since it points out the important zones which potentially are congested. The Figs. 23 and 24 display the spatial distribution of the betweenness centrality for various cities. As expected, zones which are central from a geographical point of view also have a large betweenness centrality. However, we see that other roads or zones can have a large betweenness centrality, pointing to a complex pattern of flow distribution in cities.

In addition to having a relationship with the traffic, and possibly the congestion, a recent paper [120] proposes an interesting direction, which is in the general context of connecting topological measures of the networks and socio-economical indices. In particular, Strano et al. [120] show that there is a clear correlation between the betweenness centrality and the presence of commercial activities.

<sup>4</sup> The traffic between two zones given by the origin–destination matrix (see Section 3.3) is however much more difficult to obtain.



**Fig. 23.** Betweenness centrality for the city of Dresden. The width of the links corresponds to the betweenness centrality.  
Source: From [28].

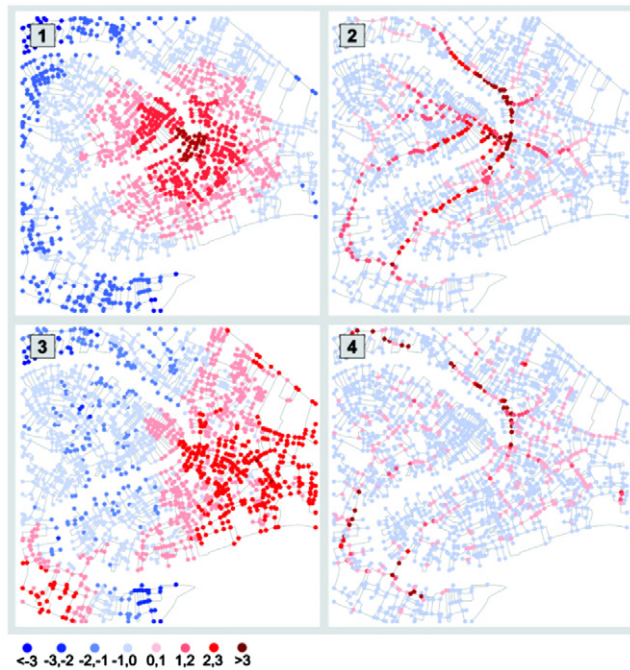


**Fig. 24.** Color-coded maps for different centralities in Venice, Italy (see [110]). (1) Closeness, (2) Betweenness centrality, (3) Straightness, (4) Information (from blue to red the centrality increases).  
Source: From [110].

**3.2.1.3. Other measures.** Buhl et al. [59] measured different indices for 300 maps corresponding mostly to settlements located in Europe, Africa, Central America, and India. They found that many networks depart from the grid structure with an alpha index (or Meshedness) usually low. For various world cities, Cardillo et al. [77] found that the alpha index varies from 0.084 (Walnut Creek) to 0.348 (New York City), which reflects in fact the variation of the average degree. Indeed for both these extreme cases, using Eq. (31) leads to  $\alpha_{NYC} \simeq (3.38-2)/4 \simeq 0.345$  for New York City and  $\alpha_{WC} \simeq (2.33-2)/4 \simeq 0.083$  for Walnut Creek. This same study seems to show that triangles are less abundant than squares (except for cities such as Brasilia or Irvine).

Measures of efficiency are relatively well correlated with the alpha index but displays broader variations demonstrating that small variations of the alpha index can lead to large variations in the shortest path structure. Cardillo et al. plotted the relative efficiency (see Section 2.2.2.4)

$$E_{rel} = \frac{E - E^{MST}}{E^{GT} - E^{MST}} \quad (56)$$

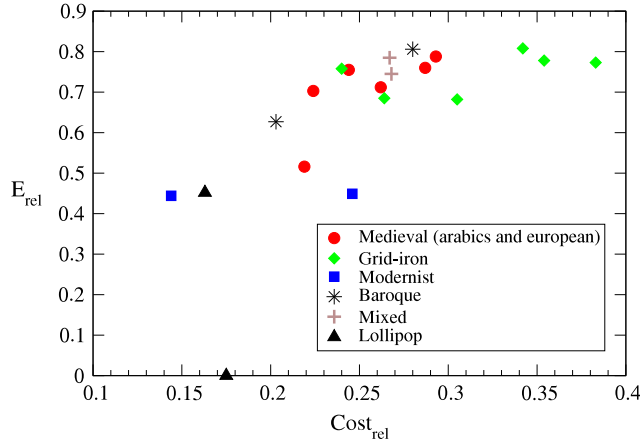


**Fig. 25.** Relative efficiency versus relative cost for 20 different cities in the world. In this plot the point (0, 0) corresponds to the MST and the point (1, 1) to the greedy triangulation.

Source: From [77].

versus the relative cost

$$C_{\text{rel}} = \frac{C - C^{\text{MST}}}{C^{\text{GT}} - C^{\text{MST}}} \quad (57)$$

where GT refers to the greedy triangulation (the maximal planar graph) and MST to the minimal spanning tree. The cost is here estimated as the total length of segments  $C \equiv \ell_T$  (see Section 2.2.2.4). The obtained result is shown in Fig. 25, which demonstrates two things. First, it shows – as expected – that efficiency is increasing with the cost with an efficiency saturating at  $\sim 0.8$ . In addition, this increase is slow: typically, doubling the value of  $C$  shifts the efficiency from  $\sim 0.6$  to  $\sim 0.8$ . Second, it shows that most of the cities are located in the high cost-high efficiency region. New York City, Savannah and San Francisco have the largest value of the efficiency ( $\sim 0.8$ ) with a relative cost value around  $\sim 0.35$ . It seems, however, at this stage difficult to clearly identify different classes of cities, and further studies with a larger number of cities is probably needed in order to confirm the typology proposed in [77].

Finally, we mention the recent study [121] on the street and subway networks of Paris and London. The accessibility in these cities is studied in terms of self-avoiding random walks displaying several differences. In particular, Paris seems to have a larger average accessibility than London, probably due to a large number of bridges.

### 3.2.2. Power grids and water distribution networks

Power grids are one of the most important infrastructure in society. In modern countries, they have evolved for a rather long time (sometimes a century) and are now complex systems with a large variety of elements and factors contributing to their functioning. This complexity leads to the relatively unexpected result that their robustness is actually not very well understood and that large blackouts such as the huge August 2003 blackout in North America call for the need of a better understanding of these networks.

The topological structure of these networks has been studied in different papers, such as [32,122,123]. In particular, in [32] and [122], the authors studied the Southern Californian and the North American power grids. In these networks the nodes represent the power plants, distribution and transmission substations, and the edges correspond to transmission lines. These networks are typically planar (see for example the Italian case, Fig. 26) and we expect a peaked degree distribution, decreasing typically as an exponential of the form  $P(k) \sim \exp(-k/\langle k \rangle)$  with  $\langle k \rangle$  of order 3 in Europe and 2 in the US. The other studies on US power grids confirm that the degree distribution is exponential (see Fig. 27). In [122], Albert, Albert, and Nakarado also studied the load (a quantity similar to the betweenness centrality) and found a broad distribution. The degree being peaked, we can then expect very large fluctuations of load for the same value of the degree, as expected in general for spatial networks (see Section 2.2.1.4). These authors also found a large redundancy in this network with, however, 15% of cut-edges.

Also, as expected for these networks, the clustering coefficient is rather large and even independent of  $k$ , as shown in the case of the Western US power grid (see Fig. 28).

Besides the distribution of electricity, our modern societies also rely on various other distribution networks. The resilience of these networks to perturbations is thus an important point in the design and operating of these systems. In [125], Yazdani and Jeffrey studied the topological properties of the Colorado Springs Utilities and the Richmond (UK) water distribution networks (shown in Fig. 29). Both these networks (of size  $N = 1786$  and  $N = 872$ , respectively) are sparse planar graphs with very peaked distributions (the maximum degree is 12).

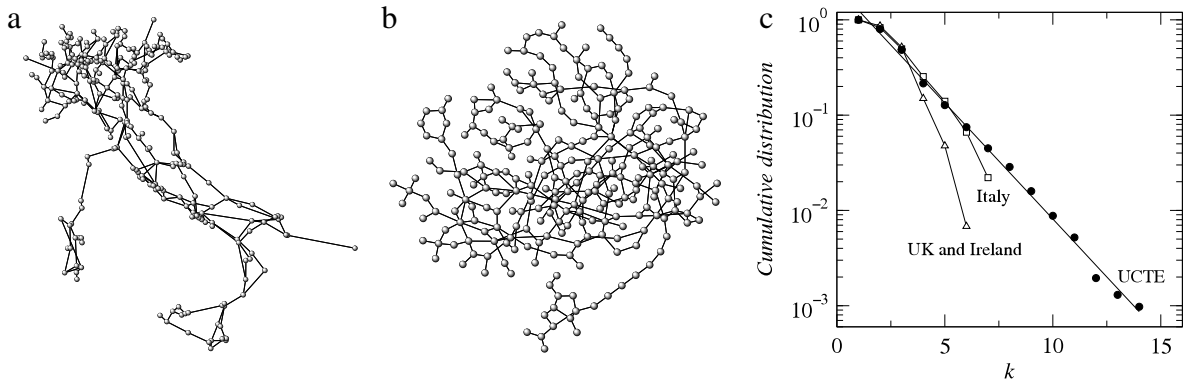


**Fig. 26.** (a) Map of the Italian power grid. (b) Topology of the Italian power grid. (c) Degree distribution for the European network (UCTE), Italy and the UK and Ireland. In all cases the degree distribution is peaked and can be fitted by an exponential.  
Source: From [123].

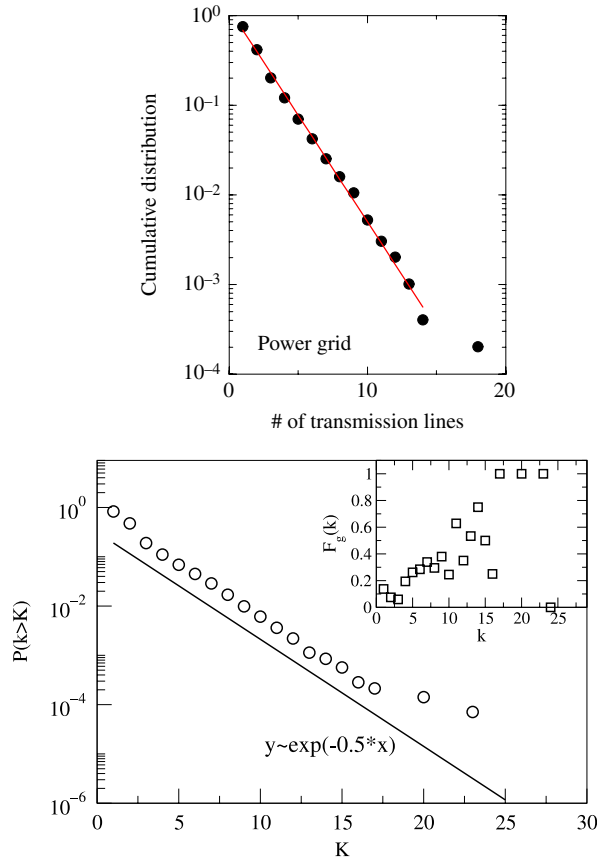


**Fig. 27.** Degree distribution of substations in Southern California (top panel) and for the North American power grid (bottom panel). In both cases, the lines represent an exponential fit.  
Source: From [32,122], respectively.

### 3.2.3. The internet

The Internet is the physical layout for the WWW which organizes the information and makes it accessible. At a small scale, the Internet is a network of routers connected by wires. At a larger scale, the routers are grouped according to an administrative authority, the autonomous system (AS), and at this level the Internet can be seen as a set of interconnected AS.

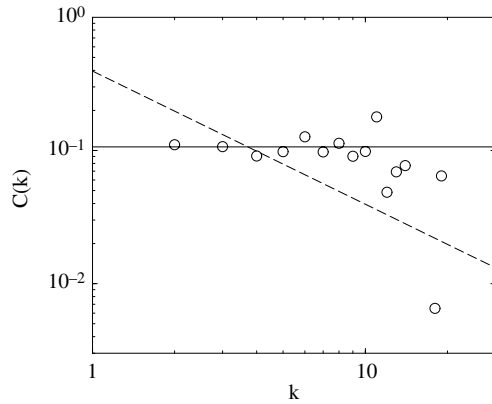


**Fig. 28.** Scaling of the clustering  $C(k)$  for the Power Grid of the Western United States. The dashed line has a slope  $-1$  and the solid line corresponds to the average clustering coefficient.

Source: From [124].

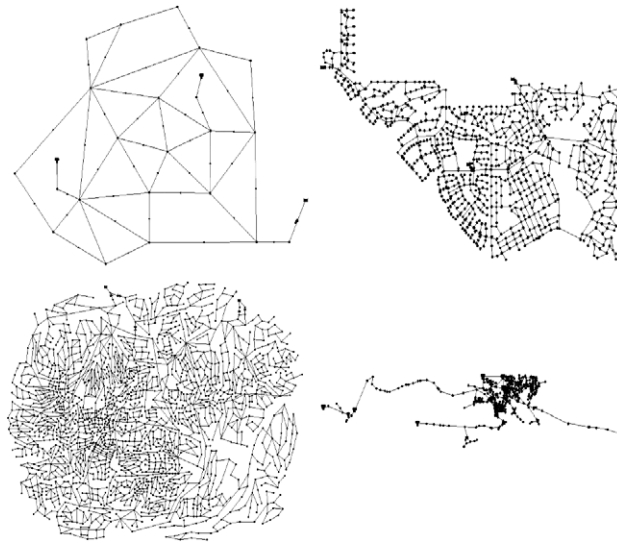


**Fig. 29.** Representation of water distribution networks. Left panels (from top to bottom): Synthetic networks ('Anytown' [126], and 'EXNET' [127]). Top-right panel: Colorado Spring Utilities network. Bottom-right panel: Richmond (UK) water distribution network.

Source: From [125].

There is obviously a very large literature in computer science (but also in statistical physics [5]) about the Internet and its structure. Here we will briefly give some characteristics of this important network that we believe are related to the spatial aspects of the Internet.

The nodes of this network (routers) are distributed among different countries and one expects a non-uniform distribution depending on socio-economical factors. Indeed, this distribution as been shown in [128] to form a fractal set of dimension  $d_f \simeq 1.5$  strongly correlated with the population density.<sup>5</sup> Concerning the links, there is an obvious cost associated with their length and one expects a rapidly decreasing length distribution. In most models (in particular for the Waxman model [131], see also Section 4.2.4), the link distribution is assumed to be an exponential of the form  $e^{-d/d_0}$ , but the authors of [128] seemed to observe results consistent with a slower decay,  $P(d) \sim 1/d$ , over one decade.

The clustering coefficient for the Internet is maybe more interesting. At the AS level, it varies [124] as  $C(k) \sim 1/k$ , a behavior typical of many scale-free networks [12]. However, in sharp contrast with this result, if we do not aggregate the nodes and stay at the router level, we observe [124], a clustering coefficient approximately constant (Fig. 30).

All these different results suggest that the location of nodes is given exogenously and should be the input of a realistic model. Once the location of the nodes is given, the link length distribution and the behavior of the clustering coefficient suggest that there is a competition between preferential attachment and a spatial dependence model that we will discuss in the next Section 4.2.

<sup>5</sup> The fractal dimension here is the usual one—see for example the book [129], and is not the fractal dimension that could be defined for a network [130].

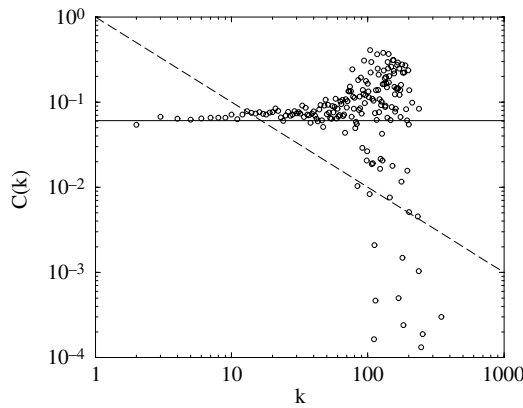


**Fig. 30.** Scaling of the clustering  $C(k)$  for the Internet at the router level. The dashed line has a slope  $-1$  and the solid line corresponds to the average clustering coefficient.

Source: From [124].

### 3.2.4. Geography in social networks

With the development of information technologies, we can now have an idea about some aspects of the structure of social networks. In particular, as expected, space is also important in social networks. It is indeed reasonable to think that in order to minimize their effort and to maintain social ties [132] most individuals will connect with their spatial neighbors. As a measure of social ties, Lambiotte et al. [133] used mobile phone data for 3.3 million customers in Belgium. For each customer, a certain number of attributes is known, in particular the zip code of the address where the bill is sent. After some filtering procedures, the resulting network is made of 2.5 million nodes (customers) and 5.4 million links, giving an average degree  $\langle k \rangle = 4.3$ . The degree distribution is peaked (the power law fit proposed in [133] gives an exponent  $\gamma \approx 5$ ) and the probability  $P(r)$  that two connected individuals are separated by an Euclidean distance  $r$  is found to behave as [133]

$$P(r) \sim r^{-2} \quad (58)$$

over distances in the range 1–100 km. The exponent describing the decay with distance is thus equal to 2.0 in this example and supports the idea of a gravity law (see Section 3.3.3) even in the context of social ties. This result is also consistent with the measure obtained for the inter-city phone intensity exponent (see [134] and Section 3.3.3.4). According to Kleinberg's navigability theorem [135], this result also shows that this social network is navigable (see Section 5.4 for a discussion on navigability).

However, another study [136] on a social network of more than one million bloggers in the USA shows convincingly that the proportion of pairs of nodes at distance  $d$  which are friends decays as

$$P(d) - \varepsilon \sim d^{-\alpha} \quad (59)$$

where  $\alpha \approx 1$  and where  $\varepsilon \approx 5 \times 10^{-6}$ . In addition, this exponent  $\alpha$  of order one is confirmed in another studies [137–139] on Facebook users and on email communications. Interestingly, a recent paper [140] showed that this spatial scaling  $P(d) \sim 1/d$  is consistent with Eq. (58) for a uniform  $2d$  density and could result from the fact that most individuals tend to maximize the diversity of their friendships (which can be seen as the maximization of information entropy). The plateau observed in [136] at  $\varepsilon > 0$  shows that above a certain distance (here of the order  $\approx 1000$  km), the probability  $P(d)$  flattens to a constant value independent of distance and which probably results from complex processes acting in social networks. For this network, on an average of eight neighbors, we then have on average 5.5 friends living in the proximity while only 2.5 result from non-geographic processes (for a discussion about navigability on this network, see Section 5.4.6). This is consistent with the results of [137], where it is shown that about 40% of emails were sent within the same city (for this particular panel of individuals).

Although more measures are needed in order to confirm the value of the exponent  $\alpha$  (and we expect rapid developments on this topic), the existence of an important spatial component in social networks is rather clear, and at this point it seems that on average the majority of our friends are in our spatial neighborhood. This is confirmed in a recent paper [141] which measured a variety of parameters on four different online social networks (BrightKite, FourSquare, LiveJournal, Twitter) and showed in particular that there is a majority of short-distance links between users. This dependence with space seems to go even beyond friendship, and applies to other social processes such as collaborating and writing a paper together [142]. In fact, the strong association between friendship and spatial location led Backstrom, Sun and Marlow [138] to propose an algorithm – which exceeds IP-based geolocation – to predict the location of people in Facebook who didn't provide this information.

Clustering seems also to be large, as shown in [133,138]. In particular, Lambiotte et al. [133] studied the probability  $c(d)$  that a link of length  $d$  belongs to a triangle. This probability decreases with distance and reaches a plateau at around 0.32,

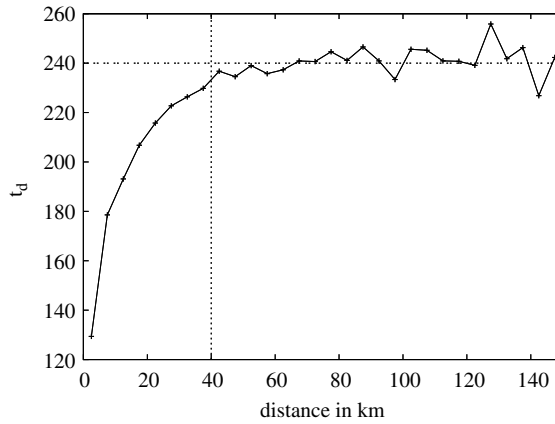


**Fig. 31.** Average duration  $t_d$  of a phone call as a function of the distance  $d$ . A saturation is observed for distances greater than 40 km.  
Source: From [133].

above 40 km. It is interesting to note also that the average duration of a phone call depends also on the distance (see Fig. 31) and saturates to a value of about 4 min for the same value,  $d > 40$  km, obtained for  $c(d)$ . These results led these authors to suggest that two communication regimes exist: a short distance ‘face-to-face’ regime with short communication durations and a large clustering coefficient, and another long-distance regime with smaller clustering and longer communications.

### 3.3. Origin–destination matrix and mobility networks

#### 3.3.1. Importance of human mobility

Knowing the flow of individuals from one point to another in a city or a country is a very important piece of information upon which many models and studies depend. First, it is related to the fundamental problem in geography and spatial economics of the location of activities and their spatial distribution. Second, it is a key ingredient in the epidemiology of infectious diseases (see Section 5.6). These diseases transmit between humans in close proximity and contaminate the population as they travel and interact. Clues on the statistics of human movements and interactions is thus fundamental. At a global level, for example, the spread of infectious diseases such as influenza is – in addition to seasonal effects – largely controlled by air travel patterns (see [143] and Section 5.6). Third, statistics about individual movements are important for more commercial applications, such as geomarketing for example. Finding the best spot to place your advertisement depends on the number of people going through this location and thus implies knowing the flows, or at least the dominant flows, of individuals in the area under consideration.

A simple way to formalize this problem is to divide the area of interest into different zones labeled by  $i = 1, \dots, N$  and to count the number of individuals going from location  $i$  to location  $j$ . This number is called the origin–destination (OD) matrix and is denoted in this review by  $T_{ij}$ . This quantity is at the core of many transportation models, and its properties have been discussed in a large number of papers. It defines a network, directed and weighted, and in the general case is time-dependent. This quantity is, of course, very different from a ‘segment’ measurement, where we can easily count the number of individuals going through an individual segment of the transportation system under consideration (it can be one of the links of the airline network, a segment of road, etc.). In contrast, the OD matrix is usually extremely difficult and costly to obtain and measure.

Despite all the difficulties in measuring the OD matrix, recent technological advances, such as GPS, the democratization of mobile phones, together with geosocial applications, etc. allow for precise measurements on large datasets, and point to the possibility of quantitatively understanding urban movements. In the next sections we will then review some recent results in this field.

#### 3.3.2. Distribution of the trip duration and length

The duration and length of trips in urban areas is obviously of great importance and, in particular, daily trips can characterize the economical efficiency of an urban area. In particular, the duration of daily journey-to-work trips give a good indication of the economical health and efficiency of a given region. For many different reasons, it is then important to understand the factors governing the behavior of the statistics of daily trips. In particular, in the perspective of convergence to sustainable cities, we need to understand such factors in order to reduce energy and environmental problems. We are now at the stage where increasingly more data is available and it will soon become possible to characterize the statistics of human movements at many different scales and in particular at the urban scale.

The important case of the statistics of daily commuter travel is an old problem and has been discussed at length in the transportation research literature. One can find various empirical observations for different urban areas (see for

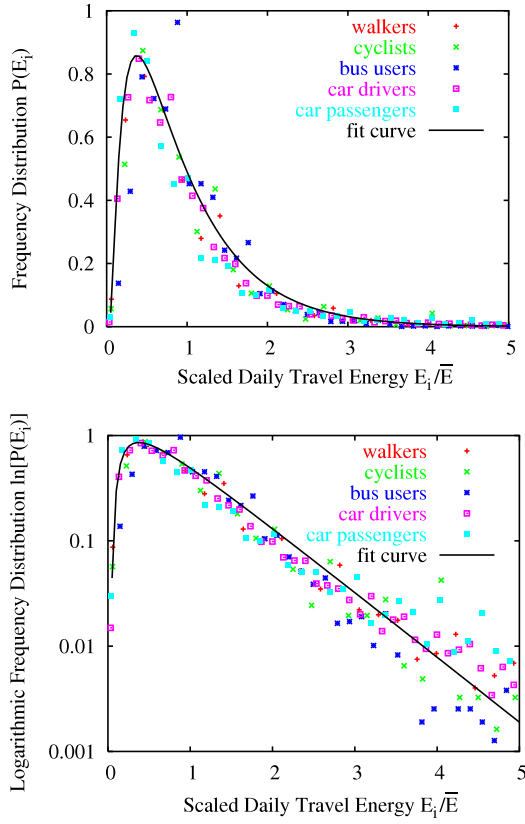


**Fig. 32.** Universal travel energy distribution in (a) linear representation and in (b) semilogarithmic representation. The solid line is the fit obtained for  $\alpha = 0.2$  and  $\beta = 0.7$ .

Source: From [147].

example [144] a short review on this subject) and also some theoretical discussions (see for example [144]). An important theoretical discussion was triggered by Zahavi [145], who suggested that the average daily travel time at the regional scale varies little over space and time. This hypothesis is interesting, in the sense that it is the first step towards some ‘physical laws’ ruling human movement. This hypothesis of a constant time (and money) budget, can be rephrased as the ‘rational locator hypothesis’, states that individuals maintain (if they can choose) steady commute travel times by adjusting their home-to-work distance (see for example [146]).

Koelbl and Helbing [147] proposed that the travel time can be understood in terms of a travel energy budget. More precisely, they found empirically that the average travel time for each daily transportation mode considered (walk, bicycle, car, bus, train) has been approximately constant for over 27 years (the data considered was obtained for the UK in the period 1972–1998, see the end of this chapter for a discussion on this point). This result suggests that there is a travel time budget associated with each transportation mode and the main idea put forward in [147] is that the energy consumed by individuals for travel is constant and mode-independent

$$E \approx \bar{t}_i p_i \quad (60)$$

where  $E \approx 615$  kJ is the estimated average daily energy budget,  $\bar{t}_i$  the average travel time for mode  $i$ , and  $p_i$  the energy consumption rate for mode  $i$  (which varies from  $\approx 4$  kJ/min for a train passenger to  $\approx 15$  kJ/min for walking).

A further observation is that the individual travel time (for a mode  $i$ ) rescaled by the average time of the corresponding mode  $\tau_i = t/\bar{t}_i$  follows a universal probability distribution, which in terms of energy  $E_i = p_i t = \bar{E} \tau_i$  reads

$$P(E_i) \sim e^{-\alpha \bar{E}/E_i - \beta E_i/\bar{E}} \quad (61)$$

where  $\alpha$  and  $\beta$  are fitting parameters. This distribution reflects the variation between individuals but displays a universal behavior among modes. The collapse is shown in Fig. 32. The exponential term  $e^{-\beta E_i/\bar{E}}$  corresponds to the canonical energy distribution when the average energy is fixed (and can be recovered by maximizing the entropy with the normalization and the fixed average energy constraints). The term  $\exp(-\alpha \bar{E}/E_i)$  suppresses the short trips, reflecting what is called the *Simonson effect* (see [147] and references therein), and leads to the selection of a less costly transportation mode. Indeed if the trip is too short for a given transportation mode, the energy spent for preparation can be larger than the energy needed for the trip itself and a less costly transportation mode is then more efficient.

These results of Koelbl and Helbing have, however, been challenged in other empirical studies. In [146], Levinson and Wu showed that the average daily travel seems to be constant over time for a given city, but varies from one city to another. The average travel time for a given city then depends on structural parameters characterizing the city (such as population, density, transportation networks, congestion, etc.). In another study [148] on three travel surveys (for France, UK, and Belgium), Hubert and Toint criticize the validity of the hypothesis of constant average daily human energy expenditure Eq. (60). However, they show that the distribution of the normalized travel time seems to be the same for the three different countries of this study, pointing to the possible existence of universal features of human movement.

It is clear at this point that a ‘unified theory’ of human travel behavior is still needed as well as other empirical studies, but the analysis presented in [147] at least shows that tools from statistical physics can play a role in transportation research and more generally in uncovering universal patterns in human behavior.

**3.3.2.1. Mobile phone and GPS studies.** As discussed above, obtaining OD matrices is a very difficult and crucial task. While traditional surveys are costly and incomplete, mobile phone data give more complete information. In particular, in large urban areas, the density of antennas is large enough so that triangulation gives a relatively accurate indication of the users’ location (mobile devices such as phones are regularly in contact with emitters and triangulation allows one to determine the location of the device at a resolution scale given by the local density of emitters). For all these reasons, mobile phone data were recently used to detail individual trajectories [149], to identify ‘anchor points’ where individuals spend most of their time [150,151], or statistics of trip patterns [152,153]. Results and studies are so numerous now that we will focus on a small subset only and refer the interested reader to [153] and references therein.

Gonzalez et al. [152] used a set of mobile phone data at a national level and found that the distribution of displacement of all users can be fitted by a Levy law of the form

$$P(\Delta r) \sim \frac{1}{(\Delta r_0 + \Delta r)^\beta} e^{-\Delta r/\kappa} \quad (62)$$

where  $\beta \simeq 1.75$ ,  $\Delta r_0 \simeq 1.5$  km. The cutoff value  $\kappa$  depends on the protocol used and varies from  $\kappa \simeq 400$  km (for protocol  $D_1$ ) and  $\kappa \simeq 80$  km (for the protocol  $D_2$ ). The protocol  $D_1$  consists in recording trajectories (of 100,000 users) when the user initiates or receives a call or SMS. The protocol  $D_2$  captures the location of 206 mobile phones every two hours for an entire week. The origin of the data is not indicated in this paper, and could mix both rural and urban areas, thus being a cause of the observed behavior. However, this type of approach is very promising and will certainly lead in the future to interesting insights about human movement behavior in various areas.

We note that the measured value for the exponent  $\beta$  is not far from the value 1.6 observed in [154]. In this study, Brockmann et al. used data for the movements of banknotes across the USA using the ‘Where is George’ database, a system based on voluntary reporting. They found that the distance distribution is also Levy distributed. However, the presence of a given banknote at a given location and at a certain time depends on many processes, such as the diffusion of the bills and also on the probability to actually use a banknote, and of course to report its location to the Whereisgeorges.com website. Such crucial factors were not taken into account in [154], and it is therefore difficult to assess the validity of the obtained Levy law.

We note here that in a recent paper [155], Song et al. proposed a model of human mobility in order to understand the power laws observed in [152,154]. In particular, this model includes the two following ingredients in the description of human displacements: first, the tendency to explore additional locations decreases with time, and second, there is large probability to return to a location visited before. This model gives relations between different scaling exponents and values which are consistent with empirical fits [155]. However, it is still unclear at this stage at which scale this study applies and how it can be reconciled with the previous studies showing a peaked distribution of travel times.

GPS is another interesting tool in order to characterize individual trajectories. Recent studies [156,157] used GPS data of private vehicles for the city of Florence (Italy) and have shown that the *total* daily length trip is exponentially distributed (see Fig. 33).

$$P(\ell_T) \sim e^{-\ell_T/l_0} \quad (63)$$

and seems to be independent of the structure of road network, pointing to a general mechanism which needs to be uncovered. In particular, the authors suggest a relation between this distribution and Maxwell distributions. This seems to be actually reminiscent of the general argument proposed by Koelbl and Helbing (see [147] and previous Section 3.3.2) and indeed points to the possible existence of more general principles governing human movements.

**3.3.2.2. RFIDs.** At an intra-urban scale, and even at the scale of social networks, RFIDs might provide interesting insights. RFID stands for Radio Frequency Identification and is a technology similar to the bar code and composed of a tag which can interact with a transceiver that processes all the information contained in the tag. RFIDs are used in many different instances, from tagging goods to the Oyster card system in London. In fact, it can be used anywhere a unique id is needed, and the tag can carry simple or more complex information about the carrier. RFIDs can also be used for dynamical measures of social networks, such as in the sociopatterns project (see <http://www.sociopatterns.com>).

The Oyster card system in London provides information about instantaneous flows of individuals in the subway system. Since 2003, some 10 million RFID cards have been issued to commuters using the London transport network. In [95], these

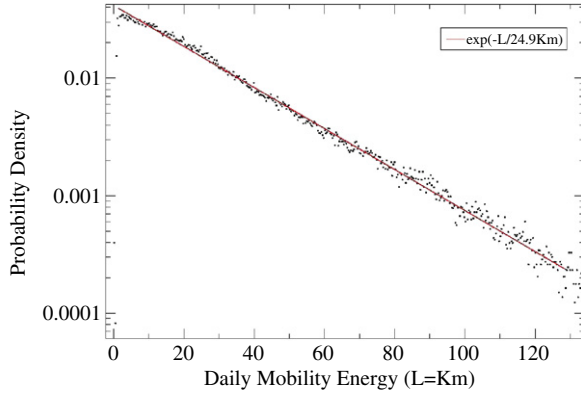


**Fig. 33.** Distribution of total length of daily trips. The exponential fits gives a slope  $L_0 \simeq 25$  km.  
Source: From [157].

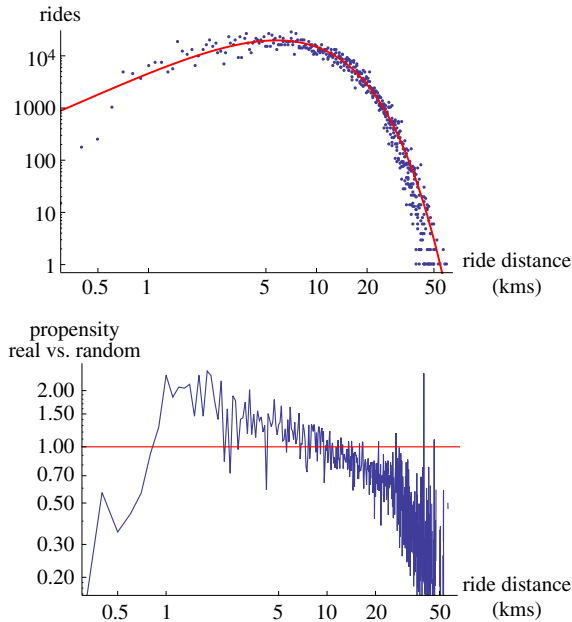


**Fig. 34.** Ride distance distribution. (a) Plot of the histogram of distances for observed rides. This distribution can be fitted by a negative binomial law with parameters  $r = 2.61$  and  $p = 0.0273$ , corresponding to a mean  $\mu = 9.28$  km and standard deviation  $\sigma = 5.83$  km. This distribution is not a broad law (such as a Levy flight for example), in contrast with previous findings using indirect measures of movements [152,154]. (b) Ride distance propensity. Propensity of achieving a ride at a given distance with respect to a null-model of randomized rides.  
Source: From [95].

individual trajectories were analyzed, displaying evidence for a polycentric organization of activity in this urban area. These authors also found that in agreement with many other transportation networks, the traffic is broadly distributed (according to a power law with exponent  $\approx 1.3$ ) but also that the displacement length distribution is peaked (see Fig. 34).

### 3.3.3. The gravity law

The origin–destination matrix contains a large amount of information and allows one to test some ideas about the structure of human movements. In particular, it was suggested (see for example the book [158]) more than 50 years ago that the number of trips from location  $i$  to location  $j$  follows the ‘Gravity’ law

$$T_{ij} = K \frac{P_i P_j}{d_{ij}^\sigma} \quad (64)$$

where  $d_{ij} = d_E(i, j)$  is the Euclidean distance between these two locations,  $P_{i(j)}$  is the population at location  $i$  ( $j$ ) and where  $\sigma$  is an exponent whose value actually depends on the system. This idea was generalized to many other situations, such as

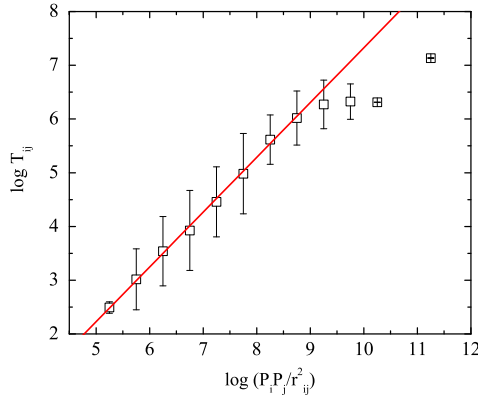


**Fig. 35.** Traffic flow between  $i$  and  $j$  as a function of the variable  $P_i P_j / d_{ij}^2$ . The line has a slope equal to 1.02.  
Source: From [161].

the important case in economics of international trade [159,160]. In this case, the volume of trade between two countries is given in terms of their economical activity and their distance.

More generally the gravity law (see the theoretical discussion in the Section 3.3.3.5) is written in the form

$$T_{ij} \sim P_i P_j f(d(i, j)) \quad (65)$$

where the deterrence function  $f$  describes the effect of space.

In the next sections, we will focus on the most recent measures concerning highways [161], commuters [162], cargo ship movements [104], and phone communications [134]. We then end this chapter with a theoretical discussion on the gravity law.

**3.3.3.1. Worldwide commuters.** Balcan et al. [162] recently studied flows of commuters on the global scale. They studied more than  $10^4$  commuting flows worldwide between subpopulations defined by a Voronoi decomposition and found that the best fit is obtained by a gravity law of the form

$$T_{ij} = C P_i^\alpha P_j^\gamma e^{-d_{ij}/\kappa} \quad (66)$$

where  $C$  is a proportionality constant, and where the exponents are: for  $d \leq 300$  km,  $(\alpha, \gamma) \simeq (0.46, 0.64)$ ,  $\kappa = 82$  km, and for  $d > 300$  km:  $(\alpha, \gamma) \simeq (0.35, 0.37)$ , and  $\kappa$  not available. We note an asymmetry in the exponent at small scales which probably reflects the difference between homes and offices, and which does not hold at large scale where homogenization seems to prevail.

At this granularity level, there is then a dependence of the traffic on populations and distances with specific exponents and with exponentially decreasing deterrence function. At a smaller scale, different results for US commuters were obtained in [163], and as suggested in [162] the observed differences might have originated in the different granularities used in these studies (a problem known as the ‘modifiable areal unit problem’ in geography). Indeed, in [162], the granularity is defined by a Voronoi decomposition, while in [163], counties are used which are administrative boundaries, not necessarily well consistent spatially with gravity centers of mobility processes.

**3.3.3.2. Korean highways.** In [161], Jung et al. studied the traffic on the Korean highway system for the year 2005. The system consists of 24 routes and 238 exits, and the total length of the system is about 3000 km. The highway network is described by a symmetrized weight matrix  $T_{ij}$ , which represents the traffic flow between  $i$  and  $j$ . The in- and out-traffic are well correlated with population, as already seen in the worldwide airline network [143], where the population  $P_i$  of city  $i$  scales with the strength  $s_i$  as

$$P_i \sim s_i^\alpha \quad (67)$$

with  $\alpha \approx 0.5$ , while it is close to one in [98,161]. For 30 cities with population larger than 200,000, Jung et al. study the traffic flow  $T_{ij}$  as a function of the population of the two cities  $P_i$  and  $P_j$ , with the distance  $d_{ij}$  between  $i$  and  $j$ , and used the original formulation of the gravity law

$$w_{ij} \sim \frac{P_i P_j}{d_{ij}^\sigma} \quad (68)$$

with  $\sigma = 2$  (see Fig. 35).

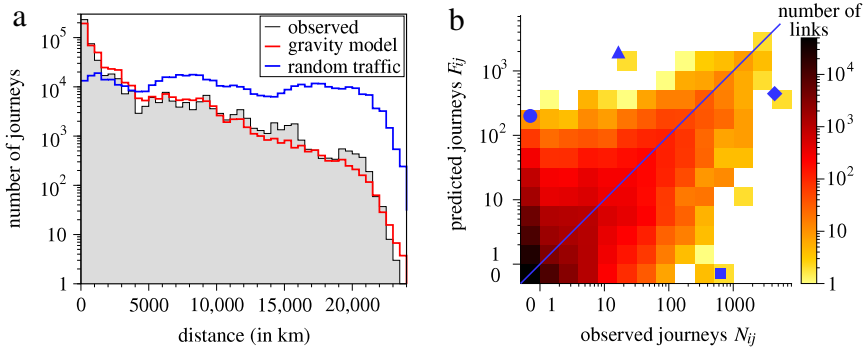


**Fig. 36.** (a) Histogram of port to port distances traveled in the global cargo ship network. The red line represents the gravity model, the blue line a random null model. (b) Count of port pairs with  $N_{ij}$  observed and  $F_{ij}$  predicted journeys.

Source: From [104].

**3.3.3.3. Global cargo ship.** In [104], Kaluza et al. applied the gravity law to the global cargo ship network. They used the general form of the gravity law, where the number of trips  $T_{ij}$  is given as (see the discussion in the Section 3.3.3.5)

$$T_{ij} = A_i B_j O_i I_j f(d_{ij}) \quad (69)$$

where  $O_i$  is the total number of departures from node  $i$  and  $I_j$  the total number of arrivals at node  $j$ . The coefficients  $A_i$  and  $B_j$  are normalization prefactors such that  $\sum_j T_{ij} = O_i$  and  $\sum_i T_{ij} = I_j$ .

The deterrence function used in [104] is a two parameter truncated power law  $f(d) = d^{-\sigma} \exp(-d/\kappa)$ . The best correlation was obtained for  $\kappa = 4900$  km and  $\sigma = 0.59$ . As shown in Fig. 36, this fit compares extremely well with the empirical data. In order to test the dispersion on all origin–destination pairs, Kaluza et al. [104] plot the observed number  $N_{ij}$  of trips between  $i$  and  $j$  with the prediction  $F_{ij}$  obtained with the gravity model. A perfect agreement would give a diagonal  $F_{ij} = N_{ij}$ , but here we observe some dispersion (with a small Kendall's tau of  $\tau = 0.433$ ), showing that even if the gravity law is able to reproduce the histogram, it is not accurate enough to predict the actual flow between a given origin and destination pair.

**3.3.3.4. Inter-city phone communications.** Mobile phone data open a new way to analyze geographical structure at various scales and in particular allows one to exhibit the spatial features of social networks. In a recent paper [134], Krings et al. study the network of mobile phone customers and analyze the geographical pattern of 2.5 million customers. After aggregating by city, these authors found that the inter-city communication intensity follows a gravity law

$$L_{ij} \propto \frac{P_i P_j}{d_E(i, j)^2} \quad (70)$$

where  $L_{ij}$  is the total communication time between cities  $i$  and  $j$  (for a period of six months). This result, showing a power law decay with exponent 2, is in agreement with other studies on the influence of space on social networks (see [133] and Section 3.2.4). More generally, going beyond the topological structure of the social network and including other socio-economical parameters is probably a very interesting research direction which will be developed in the future.

**3.3.3.5. Theoretical discussion.** The problem of estimating the number of trips from one zone to another is an old problem which excited the curiosity of many scientists a long time ago. It is reasonable to think that the number of trips between two locations  $i$  and  $j$  is proportional to the number of possible contacts given by  $P_i P_j$  and also decreases with distance, or equivalently with time and more generally with the cost of traveling from  $i$  to  $j$ . Readers interested in the theoretical developments of this model can find a full account in the book [158]. It is interesting to note that in this book devoted to the gravity model, and which is one of the most cited references in this field, all the chapters are devoted to theoretical and mathematical discussions, with no attempt to compare the results with empirical observations.

There are obviously many factors which control the origin–destination matrix: land use, location of industries and residential areas, accessibility, etc., and it seems difficult to provide a general and simple enough model. The gravity law in its simplest form retains the population and the distance as relevant factors (more elaborated forms with up to dozen of parameters were used in practical applications). However, given the importance of this law for many practical applications and its extensive use in simulations (in epidemiology for example), we believe that an extensive meta-analysis for different modes, geographical regions and granularities is greatly needed. Thanks to the increasing availability of data, we can expect in the future a more systematic investigation of this problem, and we try to provide here a first step in this direction and show in Table 1 a list of various (essentially recent) results obtained empirically. As we can observe in this table, there are multiple choices for the deterrence function and various values of the exponent as well. Particularly puzzling is the existence of different values for the exponent  $\sigma$  (which can vary from  $\approx 0.5$  to  $\approx 3$ ) and the different deterrence function for commuters. As suggested in [162], the observed differences might originate from the different granularities used in these

**Table 1**

List of various empirical studies on the gravity law (we essentially focused on recent and illustrative results).

Network [Ref.]	$N$	Gravity law form	Results
Railway express [164]	13	$P_i P_j / d_{ij}^\sigma$	$\sigma = 1.0$
Korean highways [161]	238	$P_i P_j / d_{ij}^\sigma$	$\sigma = 2.0$
Global cargo ship [104]	951	$O_i l_j d_{ij}^{-\rho} \exp(-d_{ij}/\kappa)$	$\sigma = 0.59$
Commuters (worldwide) [162]	n/a	$P_i^\alpha P_j^\gamma \exp(-d_{ij}/\kappa)$	$(\alpha, \gamma) = (0.46, 0.64)$ for $d < 300$ km $(\alpha, \gamma) = (0.35, 0.37)$ for $d > 300$ km
US commuters by county [163]	3109	$P_i^\alpha P_j^\gamma / d_{ij}^\sigma$	$(\alpha, \gamma, \sigma) = (0.30, 0.64, 3.05)$ for $d < 119$ km $(\alpha, \gamma, \sigma) = (0.24, 0.14, 0.29)$ for $d > 119$ km
Telecommunication flow [134]	571	$P_i P_j d_{ij}^{-\sigma}$	$\sigma = 2.0$

studies. Indeed, in [162], the granularity is defined by a Voronoi decomposition, while in [163], counties are used which are administrative boundaries and not necessarily spatially consistent with mobility processes (a problem known as the *modifiable areal unit problem* in geography). In addition, the different exponents could depend on the transportation mode used, of the scale, or other effects linked to the heterogeneity of users and trips.

In this short discussion, we thought that it could be useful to recall the classical optimization problem and one of the most important derivations of the gravity law which uses entropy maximization, and also to give a simple statistical argument which could shed light on the most important mechanisms in this problem.

#### Optimization

We first recall the classical approach which is at the basis of many studies (see for example [158]). We are interested in this problem in determining the OD matrix  $T_{ij}$  given the constraints

$$\sum_j T_{ij} = T_i \quad (71)$$

$$\sum_i T_{ij} = T_j. \quad (72)$$

These represent  $2N$  constraints for  $N^2$  unknowns and as long as  $N > 2$  many different choices for  $T_{ij}$  are possible. If we assume that the transport from  $i$  to  $j$  has a cost  $C_{ij}$ , we can then choose  $T_{ij}$  such that the total cost

$$C = \sum_{ij} T_{ij} C_{ij} \quad (73)$$

is minimum. This is the classical transportation problem and can be traced back to the 18th century and Monge [158]. Another approach consists in requiring that  $T_{ij} = T_{ij}^0 r_i s_j$ , where  $T^0$  is a given set of interzonal weights and where  $s_j$  and  $r_i$  are given constants. For an extensive discussion on this latter approach, see [158].

#### Entropy maximization

Interestingly enough, the gravity model can be shown to result essentially from the maximization of entropy [165]. Wilson, a physicist who became interested in transportation research, very early proposed that the trips  $T_{ij}$  are such that the quantity

$$\Omega = \frac{T!}{\prod_{ij} T_{ij}!} \quad (74)$$

is maximal, which corresponds to trip arrangements with the largest number of equivalent configurations (or microstates in the statistical physics language). In this expression,  $T = \sum_{ij} T_{ij}$  is the total number of trips and the maximization is subject to the natural constraints on the origin-destination matrix

$$\sum_j T_{ij} = T_i \quad (75)$$

$$\sum_i T_{ij} = T_j \quad (76)$$

and to a cost constraint

$$\sum_{ij} T_{ij} C_{ij} = C \quad (77)$$

where  $C_{ij}$  is the cost to travel from  $i$  to  $j$  and where  $C$  is the total quantity of resources available. This maximization is easy to perform with the help of Lagrange multipliers, and one obtains

$$T_{ij} = A_i B_j T_i T_j e^{-\beta C_{ij}} \quad (78)$$

where  $A_i$ ,  $B_j$  and  $\beta$  are such that the constraints are met. Of course, even if in this expression we do not have explicit expressions of  $A_i$  and  $B_j$ , the most important problem at this point is how to express the cost. In order to recover a power law distribution, one needs a logarithmic dependence on distance:  $C_{ij} = a \ln d_E(i, j)$ , which leads to  $T_{ij} \propto d_E(i, j)^{-\beta a}$ . If the cost is proportional to distance, the number of trips decays exponentially with distance. We thus recover two of the most important forms used in empirical studies and in the model, but the exact form of the cost dependence with distance remains unsolved.

There is a long discussion about the validity of this approach in [158] but we note that it assumes in particular that all individuals act independently from each other. This is obviously not correct when we introduce congestion, which induces correlations between individuals. In such conditions, it is clear that individual choices are correlated and that this entropy maximization can give reasonable results in the limit of small traffic only.

#### *A simple statistical argument*

As proposed in [166], a statistical approach could be helpful in the determination of important features of roads and traffic, and more generally can give insights into the structure of cities. As discussed above, the exact empirical measure of  $T_{ij}$  is extremely difficult, but we have access to more coarse-grained information such as for example the total number  $\ell_d$  of miles driven in 357 US cities.<sup>6</sup> For a given city of total area  $A$  and population  $P$ , it is natural to test for simple scalings such as the one observed in other systems [167,168]. In particular, the natural length scale for a city of area  $A$  is given by  $\sqrt{A}$ , and we thus expect a scaling for  $\ell_d$  of the form

$$\frac{\ell_d}{\sqrt{A}} \sim P^\beta. \quad (79)$$

As suggested in [166], we can explore two extreme cases of mobility in urban areas. If every individual is going to its next nearest neighbor (located at a typical distance  $1/\sqrt{\rho}$ , where  $\rho = P/A$  is the average density of the city), the total distance  $\ell_d$  is given by

$$\ell_d = P \times \frac{1}{\sqrt{\rho}} = \sqrt{AP} \quad (80)$$

implying that  $\ell_d/\sqrt{A}$  scales as  $P^\beta$  with  $\beta = 1/2$ .

On the other hand, if the individuals are going to random points in the city, the typical distance is given by  $\sqrt{A}$  and the total vehicle miles is given by

$$\ell_d \sim P \times \sqrt{A} \quad (81)$$

which implies  $\beta = 1$ .

Following [166], we plot in Fig. 37a the total number  $\ell_d$  of miles driven by the whole population  $P$  of the city and rescaled by  $\sqrt{A}$  for all the 367 US cities in the database. We obtain the result  $\beta \simeq 0.6$  (in [166] this exponent is 0.66 for a slightly larger dataset) with an excellent correlation coefficient. We are thus in an intermediate situation between the two extremes described above, showing that the commuting pattern is probably a mixture of centralized trips (to a central business district for example) and more local trips, or could also result from centralized patterns to many different centers, and could thus be a signature of a polycentric organization.

The total number of miles of built lanes was also studied in [166], and essentially scales as  $\sqrt{PA}$ , which means that the road network is essentially a lattice of spacing  $1/\sqrt{\rho}$ , in agreement with the results shown in Section 3.2.1.1.

Using hand-waving arguments, we can explore the consequences of the empirical result  $\beta \simeq 0.6$  on the general properties of the trip distribution. Since  $T_{ij}$  is the number of trips from a zone  $i$  to a zone  $j$ , the total distance traveled is given by

$$\ell_d = \sum_{i,j} T_{ij} d_{ij} \quad (82)$$

and we can assume that the total number of trips is proportional to the total number of individuals

$$P = \sum_{i,j} T_{ij} \quad (83)$$

(in these Eqs. (82) and (83) some irrelevant constant factors are omitted). The simplest assumption is that the trip distribution depends on the distance  $T_{ij} = f(d_{ij})$  and we can assume that  $f(x) = Cx^{-\tau}$ . This is in fact a very general case, as the exponential case is in a statistical sense reproduced by this form with  $\alpha > 2$ .

---

<sup>6</sup> Source: <http://www.census.gov>.

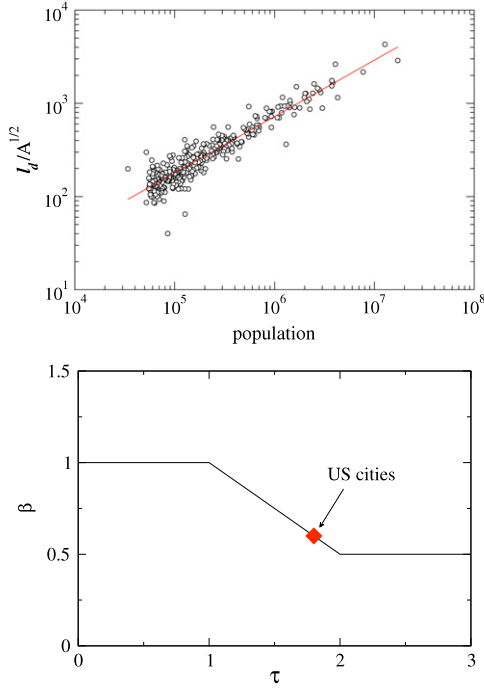


**Fig. 37.** (a) Total rescaled vehicle-miles  $\ell_d/\sqrt{A}$  versus  $N$  for 357 US cities. The line is a power law fit with exponent  $\beta = 0.60$  (the correlation coefficient is  $r^2 = 0.94$ ). (b) Exponent  $\beta$  versus  $\tau$ . The red diamond corresponds to the empirical measure  $\beta \approx 0.6$  predicting  $\tau \approx 1.8$ .

We will assume that the distance is uniformly distributed and we consider the continuous limit, which reads

$$P = \sum_{ij} f(d_{ij}) \simeq C \int_a^L x^{-\tau} dx \quad (84)$$

$$\ell_d = \sum_{ij} f(d_{ij}) d_{ij} \simeq C \int_a^L x^{1-\tau} dx \quad (85)$$

where  $a$  is the smallest distance given by  $a \sim 1/\sqrt{\rho} \sim L/\sqrt{P}$  and where the upper bound is the maximum distance  $L \sim \sqrt{A}$ . We have to separate three cases depending on the value of  $\tau$  (in the following we will keep the dominant terms, knowing that  $a \ll L$ ).

(i) Case  $\tau < 1$ .

In this case, the leading terms are

$$\ell_d \sim CL^{2-\tau} \quad (86)$$

$$P \sim CL^{1-\tau} \quad (87)$$

leading to  $\ell_d \sim P\sqrt{A}$ .

(ii) Case  $1 < \tau < 2$ .

In this case, the dominant terms are

$$\ell_d \sim CL^{2-\tau} \quad (88)$$

$$P \sim Ca^{1-\tau} \quad (89)$$

leading to  $\ell_d \sim P^{\frac{3-\tau}{2}}\sqrt{A}$ .

(iii) Case  $\tau > 2$ .

In this case, the dominant terms are

$$\ell_d \sim Ca^{2-\tau} \quad (90)$$

$$P \sim Ca^{1-\tau} \quad (91)$$

leading to  $\ell_d \sim \sqrt{PA}$ .

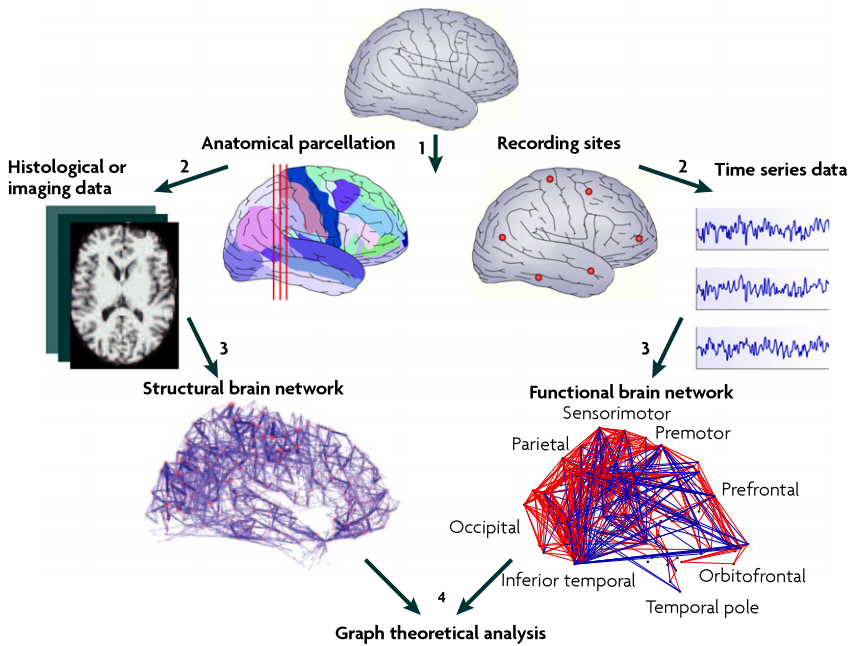


**Fig. 38.** Structural and functional brains can be studied with graph theory by the following different methods shown step-by-step in this figure.  
Source: From [15].

These results can be summarized in Fig. 37b. In particular, we can see on this plot that the empirical result  $\beta = 0.6$  corresponds to the value  $\tau = 1.8$ . If we had an exponential behavior we would have observed a value  $\tau > 2$ , but instead the simple argument presented here suggests the behavior

$$T_{ij} \sim \frac{1}{d_{ij}^\tau} \quad (92)$$

with  $\tau = 1.8$  slightly less than 2. This simple scaling argument leads to a result in agreement with the gravity law and signals a slow decay of the trip volume with distance and the simultaneous existence of trips at many different length scales. Scaling arguments could thus help in understanding the commuting patterns, and reveal interesting features of spatial patterns in the city.

Various factors could be at the origin of the different behaviors observed in gravity law studies (different deterrent functions, different exponents, etc.). In particular, we can list the following factors which could play an important role:

- *Importance of transportation modes.* It is at this point unclear if the gravity law is the same for all modes. Also, the cost of a given transportation mode can vary in time (which was the case for air travel when jets appeared, and is the case for cars with increasing oil prices) and the gravity law could in principle vary in time.
- *Importance of scale and discretization.* As discussed in this chapter, it is important to use a discretization which is consistent with mobility processes. Also, a discussion of scale is probably important, as it can already be seen on the trip length distribution, which seems to display peaked laws at the urban scale and a broad distribution at national scales.
- *Nature of the trip. Heterogeneity of users.* These factors are well known in transportation research, and it could be necessary to distinguish different trips (commuting, travel, etc.) in order to get consistent gravity laws. Users are also very heterogeneous, and it is unclear at this stage if we need to distinguish between different populations with different behaviors.

### 3.4. Neural networks

The human brain, with about  $10^{10}$  neurons and about  $10^{14}$  connections, is one of the most complex networks that we know of. The structure and functions of the brain are the subjects of numerous studies, and recent techniques such as electroencephalography, magnetoencephalography, functional MRI, etc., can be used in order to produce networks for the human brain (see Fig. 38, and for a clear and nice introduction see for example [15,169]).

Brain regions that are spatially close have a larger probability of being connected than remote regions, as longer axons are more costly in terms of material and energy [15]. Wiring costs depending on distance is thus certainly an important aspect of brain networks and we can expect spatial networks to be relevant in this rapidly evolving topic. So far, many measures seem to confirm a large value of the clustering coefficient, and a small-world behavior with a small average shortest-path

length [170,171]. It also seems that neural networks do not optimize the total wiring length, but rather the processing paths, thanks to shortcuts [172]. This small world structure of neural networks could reflect a balance between local processing and global integration with rapid synchronization, information transfer, and resilience to damage [173].

In contrast, the nature of the degree distribution is still under debate, and a recent study on the macaque brain [174] showed that the distribution is better fitted by an exponential rather than a broad distribution. Besides the degree distribution, most of the observed features were confirmed in latest studies, such as [175], where Zalesky et al. propose to construct the network with MRI techniques where the nodes are distinct grey-matter regions and links represent the white-matter fiber bundles. The spatial resolution is of course crucial here, and the largest network obtained here is of size  $N \approx 4000$ . These authors find large clustering coefficients, with a ratio to the corresponding random graph value of order  $10^2$  (for  $N \approx 4000$ ). Results for the average shortest path length  $\langle \ell \rangle$  are however not so clear due to relatively low values of  $N$ . Indeed, for  $N$  varying from 1000 to 4000,  $\langle \ell \rangle$  varies by a factor of order 1.7–1.8 [175]. A small-world logarithmic behavior would predict a ratio

$$r = \frac{\langle \ell \rangle(N = 4000)}{\langle \ell \rangle(N = 1000)} \sim \frac{\log(4000)}{\log(1000)} \approx 1.20 \quad (93)$$

while a 3-dimensional spatial behavior would give a ratio of order  $r \approx 4^{1/3} \approx 1.6$ , which is closer to the observed value. However, larger sets would be needed to be sure about the behavior of this network concerning the average shortest path and to distinguish a  $\log N$  behavior from the  $N^{1/3}$  behavior expected for a three-dimensional lattice.

However, things are more complex than it seems, and even if functional connectivity correlates well with anatomical connectivity at an aggregate level, a recent study [176] shows that strong functional connections exist between regions with no direct structural connections, demonstrating that the structural and functional properties of neural networks are entangled in a complex way and that future studies are needed in order to understand this extremely complex system.

### 3.5. Summary: existence of general features

Through the different examples presented in this chapter, we see that some general features emerge. Space implies a cost associated to distance and the formation of long links must be justified for ‘good economical’ reasons, such as a large degree for example. This simple observation leads to various effects that we summarize here.

In Table 2, we summarize the main empirical features discussed in this chapter.

- **Network typology.** We can roughly divide spatial networks in two categories. The first one consists in planar networks. These networks possess many features similar to lattices, but in some cases (such as the road network) display very distinctive features which call for new models. The other category consists in spatial, non-planar networks such as the airline network, the cargo ship network, or the Internet, where nodes are located in spaces, and edges have a cost related to their length, but where we can have intersecting links. We note here that in some cases, such as for the Internet, the point distribution is not always uniform and could play an important role.
- **Effect of space on  $P(k)$ .** Spatial constraints restrict the appearance of large degrees and  $P(k)$  is usually peaked. Constraints are stronger for planar networks and for non-planar spatial networks such as airlines the degree distribution can be broad.
- **Effect of space on the link distribution.** Here also the spatial constraints severely limit the length of the links. For planar networks, such as roads and streets, the distribution is peaked, while in other networks, such as the Internet or the airline network, the distribution can be broader.
- **Effect of space embedding on clustering and assortativity.** Spatial constraints imply that the tendency to connect to hubs is limited by the need to use small-range links, which explains the almost flat behavior observed for the assortativity. Connection costs also favor the formation of cliques between spatially close nodes and thus increase the clustering coefficient.
- **Effect of space on the average shortest path.** The average shortest path for 2d planar networks scales as  $N^{1/2}$ , as in a regular lattice. When enough shortcuts (such as in the Watts–Strogatz model) are present, this  $\sqrt{N}$  behavior is modified and becomes logarithmic. However, in some three-dimensional situations, such as in the brain for example, it is difficult in some experiments to distinguish a  $\log N$  from a  $N^{1/3}$  behavior.
- **Effect of spatial embedding on topology-traffic correlations.** Spatial constraints induce strong non-linear correlations between topology, traffic and distance. The reason for this behavior is that spatial constraints favor the formation of regional hubs and locally reinforce the preferential attachment, leading for a given degree to a larger strength than the one observed without spatial constraints. Essentially, long-range links can connect to hubs only, which yields a value  $\beta_d > 1$ . The existence of constraints, such as spatial distance selection, induces some strong correlations between topological (degree) and non-topological quantities such as weights or distances.
- **Effect of space embedding on centrality.** Spatial constraints also induce large betweenness centrality fluctuations. While hubs are usually very central, when space is important central nodes tend to get closer to the gravity center of all points. Correlations between spatial position and centrality compete with the usual correlations between degree and centrality, leading to large fluctuations of centrality at fixed degree.

**Table 2**

List of different networks with their main characteristics: number of nodes  $N$ ; average degree  $\langle k \rangle$ ; average clustering coefficient  $\langle C \rangle$ ; average shortest path  $\langle \ell \rangle$ ; the nature of the degree and weight distributions  $P(k)$ ,  $P(w)$ ; the scaling of the strength with the degree  $s(k) \sim k^\beta$ ; and the relation between the centrality and the degree when it exists,  $g(k) \sim k^\mu$ . ‘PL( $x$ )’ means that a power law fit was measured and  $x$  is the value of the exponent. \* existence of many anomalies and \*\* few anomalies. For road networks  $M$  denotes the meshedness (denoted by  $\gamma$  in Section 2.2.2.2).

Network [Ref.]	$N$	$\langle k \rangle$	$\langle C \rangle$	$\langle \ell \rangle$	$P(k); P(w)$	$\beta$	$\mu$
<b>Transportation networks</b>							
Chinese Airline network [88]	128	18.2	0.733	2.1	Unclear; broad	n/a	n/a
Indian Airline network [177]	79	5.77	0.66	2.3	PL (2.2); broad	1.4	n/a
USA Airline network [178]	935	8.4	n/a	4.0	PL (1.9); broad	1.7	1.2*
Global Airline network [89]	3883	6.7	0.62	4.4	PL (2.0); n/a	n/a	n/a*
Global Airline network [52]	3880	9.7	n/a	4.4	PL (1.8); broad	1.5	n/a*
Boston Subway [85]	124	n/a	n/a	15.5	n/a; n/a	n/a	n/a
Seoul Subway [94]	380	2.23	n/a	20.0	n/a; broad	n/a	n/a
Beijing Subway [179]	132	3.2	0.15	12.6	Peaked; peaked	1.1	n/a
Shanghai Subway [179]	151	4.6	0.21	7.1	Peaked; peaked	1.1	n/a
Nanjing Subway [179]	47	2.9	0.09	12.4	Peaked; peaked	1.1	n/a
Polish transportation [86]	[152, 1530]	[2.48, 3.08]	[0.055, 0.161]	[6.83, 21.52]	Peaked; n/a	n/a	≈2.0
World cities Subway [92]	[2024, 44629]	[2.18, 3.73]	~10 <sup>-2</sup>	[6.4, 52]	Peaked; n/a	n/a	2–3
Polish Rail [83]	1533	2.4	0.0092	28.1	Peaked; broad	n/a	n/a
Swiss Rail [83]	1613	2.1	0.0004	46.6	Peaked; broad	n/a	n/a
European Rail [83]	4853	2.4	0.0129	50.9	Peaked; broad	n/a	n/a
Indian Rail [84]	587	2.4	0.69	2.2	Peaked; n/a	n/a	n/a
China Cargo ship [103]	162	3.1	0.54	5.9	$k < 20$ ; broad	n/a	1.0**
Worldwide Cargo ship [87]	878	9.0	0.40	3.60	PL (0.95); PL (0.9)	1.3	1.66**
Worldwide Cargo ship [104]	951	76.5	0.49	2.5	broad; PL (1.7)	1.46	n/a**
<b>Mobility networks</b>							
Location network [97]	181,206	29.9	0.058	3.1	PL (2.4); broad	≈1.0	n/a
Commuters Sardinia [98]	375	86.6	0.26	2.0	Peaked; PL (1.8)	1.9	n/a
<b>Infrastructure networks</b>							
Road network [59]	[45, 339]	[2.02, 2.87]	$M \in [0.009, 0.211]$	[4.6, 13.6]	Peaked; n/a	n/a	n/a
Road network [77]	[32, 2870]	[2.09, 3.38]	$M \in [0.014, 0.348]$	[27.6, 312.1]	Peaked; n/a	n/a	n/a
Power grid [180]	341	3.03	n/a	n/a	$k < 12$ ; n/a	n/a	n/a*
Power grid [3]	4941	2.67	0.08	18.7	Peaked; n/a	n/a	n/a
Water network [125]	1786	2.23	0.0008	25.94	Peaked; n/a	n/a	n/a
Water network [125]	872	2.19	0.0402	51.44	Peaked; n/a	n/a	n/a
Internet [38]	3700–10,500	3.6–4.1	0.21–0.29	3.7	PL (2.1); n/a	n/a	n/a
<b>Biological networks</b>							
Human brain [170]	31,503	13.4	0.14	11.4	PL (~2.0); n/a	n/a	n/a
Human brain [170]	17174	6.3	0.13	12.9	PL (~2.1); n/a	n/a	n/a
Human brain [170]	4891	4.1	0.15	6.0	PL (~2.2); n/a	n/a	n/a
C. Elegans [3]	282	7.7	0.28	2.65	Peaked; n/a	n/a	n/a
C. Elegans [172]	277	15.2	0.167	4.0	n/a; n/a	n/a	n/a
Macaque VC [181]	32	9.9	0.55	1.8	Peaked; n/a	n/a	n/a
Macaque [172]	95	50.6	0.643	1.9	n/a; n/a	n/a	n/a
Cat Cortex [181]	65	17.5	0.54	1.9	Peaked; n/a	n/a	n/a

- **Structure of mobility networks.** The different discussions and empirical examples considered in this chapter showed that the average trip duration and length distribution actually depend on many factors, such as the scale considered (urban, inter-urban, national, or global), the population, congestion, or on the transportation mode, etc. Also, it seems that at the urban scale the trip duration and length distributions are peaked laws and that at a larger scale the trip length is distributed according to a broad law with exponent of order 1.6. However, the identification of relevant factors and the constitution of a clear typology is still an open problem, and in the future we can expect a wealth of new results in this area.

Although many results and measures are missing due to the lack of data availability, we see that the main expected effects of spatial constraints are present for most of these networks. Also, traffic properties seem to be relatively ubiquitous, with a broad traffic distribution, and a non-linear strength-degree law with exponent  $\beta$  distributed around 1.5. In the next chapter, we will discuss the various models which attempt to reproduce these different effects.

#### 4. Models of spatial networks

In this chapter we will describe the most important models of spatial networks. We basically divide these models into five large classes (which of course could present non empty overlaps):

- The first class describes *geometric graphs*, which are probably the simplest models of spatial networks. They are obtained for a set of vertices located in the plane, and for a set of edges which are constructed according to some geometric

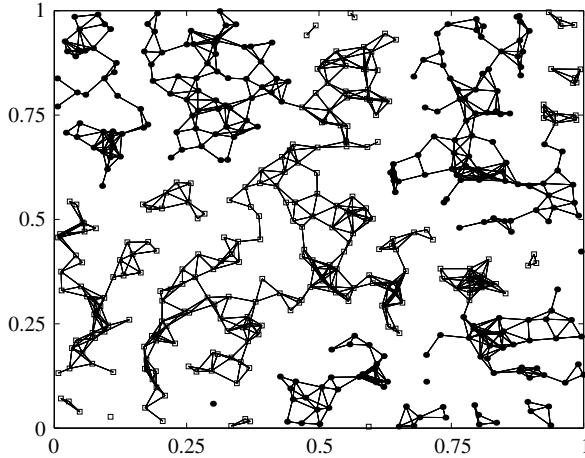


**Fig. 39.** Example of a 2d random geometric graph obtained for  $N = 500$  spheres and  $\langle k \rangle = 5$ .  
Source: From [186].

condition. There is a large body of literature on this rather general subject and we will here focus on a small set of these studies that concern more precisely graphs constructed with an Euclidean proximity condition.

- The second class concerns the Erdos–Renyi model and its spatial generalization, including the spatial hidden variables models. These networks are obtained when the probability to connect two nodes depends on the distance between these nodes. An important example of this class is the Waxman model [131] for the Internet structure.
- The third class comprises spatial variants of the Watts–Strogatz model [3] and could be coined as *spatial small-worlds*. In these cases, the starting point is a  $d$ -dimensional lattice and random links are added according to a given probability distribution for their length.
- The fourth class concerns *spatial growth models*, which can be considered as spatial extensions of the original growth model proposed by Barabasi and Albert [182].
- Finally, the last class concerns *optimal networks* obtained by the minimization of a ‘cost’ function. These networks were already considered long ago in different fields (mathematics, transportation science, computer science) and are now back, following the explosion of studies on complex networks.

#### 4.1. Geometric graphs

A random geometric graph, also called Poisson Boolean model [183], is obtained when the points located in the plane are connected according to a given geometric rule. The simplest rule is a proximity rule which states that nodes only within a certain distance are connected. There is an extensive mathematical literature on geometric graphs and the random case was studied by physicists in the context of continuum percolation (see for example [184,185]).

##### 4.1.1. The simplest random geometric graph

In the framework of complex networks, one of the first studies on random geometric graphs is provided in [186], where the nodes are small spheres of radius  $r$  and two nodes are connected by an edge (see Fig. 39) if they are separated by a distance less than  $2r$  (which is the condition for the intersection of spheres of radius  $r$ ). This network is related to the unit disk graph defined in geometric graph theory as the intersection graph of a family of unit circles in the Euclidean plane: if we draw a vertex at the center of each circle, we connect two vertices if the corresponding circles intersect. This unit disk graph has been used in computer science to model the topology of ad-hoc wireless communication networks where the nodes are wirelessly connected to each other without a base station [188]. The nodes are located in a two-dimensional plane and the area within which a signal can be transmitted to another node is described as a circle (of the same radius if all nodes have the same power to transmit<sup>7</sup>). These random geometric graphs have also been used in continuum percolation models [184,185].

If the volume of the total system is 1, then the probability  $p$  that two randomly chosen vertices are connected is equal to the volume of the sphere of radius  $R = 2r$ , which in  $d$  dimensions reads

$$p = V(R) = \frac{\pi^{d/2} R^d}{\Gamma(1 + d/2)}. \quad (94)$$

<sup>7</sup> The case of random radii has also been considered in the mathematical literature, see for example [187].

In the context of continuum percolation this quantity is the excluded volume  $V_e \equiv p$ . The average degree is then given by  $\langle k \rangle = Np$  and we can then express  $R$  as a function of  $\langle k \rangle$

$$R = \frac{1}{\sqrt{\pi}} \left[ \frac{\langle k \rangle}{N} \Gamma \left( \frac{d+2}{2} \right) \right]^{1/d} \quad (95)$$

which shows that for a given average degree  $\langle k \rangle$  the nodes (spheres) have to become smaller when more nodes are added.

Similarly to the usual ER random graph, there is a critical average degree above which there is a non empty giant component. The authors of [186] computed this critical value  $\langle k \rangle_c$  numerically for different dimensions and proposed the scaling  $\langle k \rangle_c = 1 + bd^{-\gamma}$  with  $b = 11.78(5)$  and  $\gamma = 1.74(2)$ . This relation also states that in infinite dimensions the random geometric graph behaves like a ER graph with  $\langle k \rangle_c = 1$ .

In [189], the authors analytically compute the degree distribution for these random geometric graphs. If we assume that the points are distributed according to a distribution  $p(x)$  and the condition for connecting to nodes  $i$  and  $j$  located at positions  $x_i$  and  $x_j$ , respectively, is  $d_E(i, j) \leq R$ , we can then estimate the degree distribution. If we denote by  $B_R(x)$  the ball of radius  $R$  centered at  $x$ , the probability  $q_R(x)$  that a given node is located in  $B_R(x)$  is

$$q_R(x) = \int_{B_R(x)} dx' p(x'). \quad (96)$$

The degree distribution for a node located at  $x$  is thus given by the binomial distribution

$$P(k; x, R) = \binom{N-1}{k} q_R(x)^k [1 - q_R(x)]^{N-1-k}. \quad (97)$$

In the limit  $N \rightarrow \infty$  and  $R \rightarrow 0$ , the degree distribution for a node located at  $x$  is Poissonian and reads

$$P(k; x, \alpha) = \frac{1}{k!} \alpha^k p(x)^k e^{-\alpha p(x)} \quad (98)$$

where  $\alpha = \langle k \rangle / \int dx p^2(x)$  fixes the scale of the average degree. For example, this expression gives for a uniform density  $p(x) = p_0$  a degree distribution of the form

$$P(k) \sim \frac{(\alpha p_0)^k}{k! k^d} \quad (99)$$

which decays very rapidly with  $k$ . In contrast, if the density decays slowly from a point as  $p(r) \sim r^{-\beta}$ , we then obtain  $P(k) \sim k^{-d/\beta}$ , showing that large density fluctuations can lead to spatial scale-free networks [189].

The average clustering coefficient can also be calculated analytically. The argument [186] is the following. If two vertices  $i$  and  $j$  are connected to a vertex  $k$  it means that they are both in the excluded volume of  $k$ . Now, these vertices  $i$  and  $j$  are connected only if  $j$  is in the excluded volume of  $i$ . Putting all the pieces together, the probability to have two connected neighbors ( $ij$ ) of a node  $k$  is given by the fraction of the excluded volume of  $i$  which lies within the excluded volume of  $k$ . By averaging over all points  $i$  in the excluded volume of  $k$  we then obtain the average clustering coefficient. We thus have to compute the volume overlap  $\rho_d$  of two spheres, which for spherical symmetry reasons depends only on the distance between the two spheres. In terms of this function, the clustering coefficient is given by

$$\langle C_d \rangle = \frac{1}{V_e} \int_{V_e} \rho_d(r) dV. \quad (100)$$

For  $d = 1$ , we have

$$\rho_1(r) = (2R - r)/2R = 1 - r/2R \quad (101)$$

and we obtain

$$\langle C_1 \rangle = 3/4. \quad (102)$$

For  $d = 2$ , we have to determine the area overlapping in Fig. 40, which gives

$$\rho_2(r) = (\theta(r) - \sin(\theta(r)))/\pi \quad (103)$$

with  $\theta(r) = 2 \arccos(r/2R)$  and leads to

$$\langle C_2 \rangle = 1 - 3\sqrt{3}/4\pi \approx 0.58650. \quad (104)$$

Similarly an expression can be derived in  $d$  dimensions [186] which for large  $d$  reduces to

$$\langle C_d \rangle \sim 3\sqrt{\frac{2}{\pi d}} \left( \frac{3}{4} \right)^{\frac{d+1}{2}}. \quad (105)$$

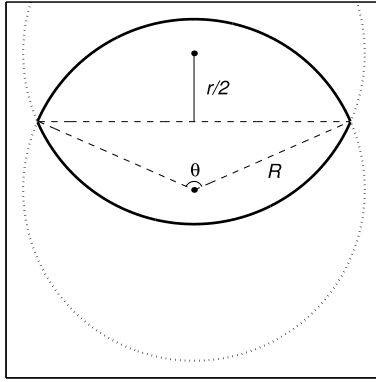


**Fig. 40.** The overlap between the two disks (area comprised within the bold line) gives the quantity  $\rho_2(r)$ .

Source: From [186].

The average clustering coefficient thus decreases from the value  $3/4$  for  $d = 1$  to values of order  $10^{-1}$  for  $d$  of order 10 and is independent of the number of nodes, which is in sharp contrast with ER graphs for which  $\langle C \rangle \sim 1/N$ . Random geometric graphs are thus much more clustered than random ER graphs. The main reason – which is in fact valid for most spatial graphs – is that long links are prohibited or rare. This fact implies that if both  $i$  and  $j$  are connected to  $k$  it means that they are in some spatial neighborhood of  $k$ , which increases the probability that their inter-distance is also small, leading to a large  $\langle C \rangle$ .

**4.1.1.1. Application to ad-hoc networks: calculation of the giant component.** In ad-hoc networks [190], users communicate by means of a short range radio device. This means that a device can communicate with another one if their distance is less than a certain distance that corresponds to the transmission range of the device. The set of connected devices can be used to propagate information at longer distances by going from the source to the destination hop by hop through intermediate nodes. If there is a large density of nodes, alternate routes are even available which allow the information to split into separate flows. Usually the users are mobile and the network evolves in time and it is important to understand the condition for the existence of a giant cluster.

In [190], Nemeth and Vattay explicitly compute the condition for the appearance of a giant component using generating functions such as in [191]. In particular, it is not difficult to show that the fraction  $S$  of nodes which are in the giant component is given by

$$S = 1 - G_0(u) \quad (106)$$

where the generating function  $G_0(x)$  is given by

$$G_0(x) = \sum_k P(k)x^k \quad (107)$$

where  $P(k)$  is the probability that a node has  $k$  neighbors. The quantity  $u$  is the probability of not belonging to the giant component and satisfies

$$u = G_1(u) \quad (108)$$

where  $G_1(x) = G'_0(x)/G'_0(1)$  (see for example [7]).

In the ad-hoc network case, the typical internode distance  $r_0$  depends on the density  $\rho = N/A$  as

$$\rho\pi r_0^2 \sim 1 \Rightarrow r_0 \sim 1/\sqrt{\pi\rho}. \quad (109)$$

The range of the radio devices is denoted by  $r_T$  and the important dimensionless parameter here is  $\sqrt{r_T/r_0}$ . The probability to have  $k$  neighbors is a binomial law of parameter  $\rho\pi r_T^2 = \eta$  and in the limit of large  $N$  (with  $N\eta$  constant) we thus obtain

$$P(k) = e^{-\eta} \frac{\eta^k}{k!}. \quad (110)$$

This particular form of  $P(k)$  allows one to compute  $G_0(x)$  and  $G_1(x)$  and we eventually obtain an implicit equation for  $S$

$$S = 1 - e^{-\eta S}. \quad (111)$$

Or, after inversion

$$\eta = \frac{-\log(1-S)}{S}. \quad (112)$$

This last relation gives the minimum transmission rate in order to get a giant component of size  $NS$ .

Also, in this model one can introduce a probability  $p(r)$  that the devices are connected at distance  $r$ . Different quantities such as the average clustering coefficient can be computed (see [190] for details).

**4.1.1.2. Model of mobile agents for contact networks.** A model for contact networks based on mobile agents was proposed in [192–194]. In this model, individuals are described by disks with the same radius, moving and colliding in a two-dimensional space. The contact network is built by keeping track of the collisions (a link connects two nodes if they have collided). A collision takes place whenever two agents are at a certain distance, and this model can thus be seen as a dynamical version of random geometric graphs. In particular, Gonzalez et al. [194] used this framework to model the sexual interaction network and interestingly enough, found in some cases and for a simple collision rule such that the velocity grows with the number of previous collisions that a scale-free network with exponent  $\gamma = 3$  emerges (such that the velocity grows with the number of previous collisions).

#### 4.1.2. Random geometric graph in hyperbolic space

Motivated by studies on the Internet, a model of random geometric graphs in hyperbolic space was proposed recently (see [195] or the small review article [196]). In their studies, Boguñá, Krioukov and Serrano considered the two-dimensional hyperbolic space  $\mathbb{H}^2$  of constant negative curvature equal to  $K = -\zeta^2 = -1$  and used a polar representation  $(r, \theta)$  for the nodes. They placed  $N$  points distributed uniformly in a disk of radius  $R$  and in the Euclidean disk projection this implies that the nodes have a uniform angle distribution  $U(\theta) = 1/2\pi$  for  $\theta \in [0, 2\pi]$  and that the radial coordinate is distributed according to

$$\rho(r) = \frac{\sinh r}{\cosh R - 1} \approx e^r. \quad (113)$$

They then used the usual geometric graph rule and connect two nodes if their hyperbolic distance is less than  $R$ , which can be written in terms of the connection probability as

$$p_C(x) = \Theta(R - x) \quad (114)$$

where  $\Theta$  is the Heaviside function. The hyperbolic distance  $d$  between two nodes  $(r, \theta)$  and  $(r', \theta')$  is defined by

$$\cosh \zeta d = \cosh \zeta r \cosh \zeta r' - \sinh \zeta r \sinh \zeta r' \cos(\theta' - \theta). \quad (115)$$

The expected degree of a node at point  $X$  located at distance  $r$  from the origin  $O$  is proportional to the area of the intersection of the two disks of radius  $R$  centered at  $O$  and  $X$ , respectively. The disk centered at  $O$  contains all the nodes and the intersection can be calculated leading to the average degree at distance  $r$  (for large  $R$ )

$$\langle k \rangle(r) \approx \frac{4}{\pi} N e^{-r/2}. \quad (116)$$

The average degree of the network is then

$$\langle k \rangle = \int_0^R \rho(r) \langle k \rangle(r) dr \approx \frac{8}{\pi} N e^{-R/2}. \quad (117)$$

The degree distribution is [196]

$$P(k) = 2 \left( \frac{\langle k \rangle}{2} \right)^2 \frac{\Gamma(k-2, \langle k \rangle/2)}{k!} \approx k^{-3} \quad (118)$$

and behaves as a power law with an exponent equal to three, as in the BA model. This network heterogeneity, however, follows directly from the properties of the hyperbolic geometry and not from a preferential attachment mechanism.

Krioukov et al. also considered the case where the node density is not uniform

$$\rho(r) = \alpha \frac{\sinh \alpha r}{\cosh \alpha R - 1} \approx e^{\alpha r}. \quad (119)$$

In this case, it can be shown that the degree distribution is also a power law of the form

$$P(k) \sim k^{-\gamma} \quad (120)$$

where

$$\gamma = \begin{cases} 1 + 2\alpha/\zeta & \text{for } \frac{\alpha}{\zeta} \geq 1/2 \\ 2 & \text{for } \frac{\alpha}{\zeta} \leq 1/2. \end{cases} \quad (121)$$

The power law exponent depends then both on the hyperbolicity  $\zeta$  and  $\alpha$ , through the ratio  $\alpha/\zeta$ , a result expected from an analogy with trees (see [196]). We thus obtain naturally scale-free networks as random geometric graphs on hyperbolic spaces and conversely, it can also be shown that scale-free networks can result from a hidden hyperbolic metric [196].

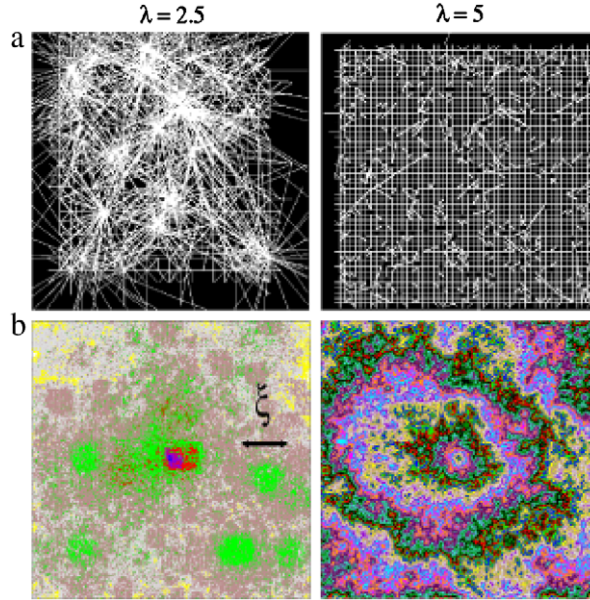


**Fig. 41.** Spatial structure of the network obtained by the method proposed in [197] for different values of the exponent  $\lambda$  of degree distribution. In (a) the networks are shown and in (b) the corresponding chemical shells of equidistant sites form the central node.  
Source: From [197].

In line with random geometric graphs in Euclidean space, there is also a strong clustering for these graphs constructed on hyperbolic space (unfortunately the clustering coefficient cannot be computed analytically).

Finally, the authors of [196] extended their model and introduce an inverse ‘temperature’  $\beta$  akin to usual statistical mechanics in the connection probability

$$p_C(x) = \left(1 + e^{\beta(\zeta/2)(x-R)}\right)^{-1} \quad (122)$$

and showed that this  $\mathbb{H}^2$  model reproduces well the Internet measurements for  $P(k)$ , the assortativity  $k_{nn}(k)$ , and the clustering coefficient  $C(k)$  for  $\alpha = 0.55$ ,  $\zeta = 1$  and  $\beta = 2$ .

#### 4.1.3. A scale-free network on a lattice

As we saw in Section 4.1.1, geometric graphs constructed on uniformly distributed points naturally lead to networks with degrees distributed according to a Poisson distribution. It is, however, interesting to generate spatial graphs with a broad distribution (scale-free network) in order to understand the effect of strong heterogeneity on spatial networks. In [197], Rozenfeld et al. proposed a simple method to construct a scale-free network on a lattice (and in [198] another variant is suggested). This model is defined on a  $d$ -dimensional lattice of linear size  $R$  and with periodic boundary conditions. A random degree  $k$  is assigned to each node on this lattice according to the probability distribution

$$P(k) = Ck^{-\lambda}. \quad (123)$$

The idea is then simple: we connect a randomly chosen node  $i$  to all its neighbors until its degree reaches its assigned value  $k_i$ . The larger  $k$ , the larger the region containing connected neighbors. The size of this region is then given by

$$r(k) = Ak^{1/d} \quad (124)$$

where the prefactor  $A$  essentially depends on the density of nodes. We show in Fig. 41 the obtained networks for two different values of  $\lambda$ . The larger  $\lambda$  and the shorter the links (large  $k$  and therefore long links are very rare), the closer we are to a regular lattice. We can define a chemical shell  $\ell$  as consisting of all sites at minimal distance  $\ell$  from a given site. For large  $\lambda$  these chemical shells are concentric (as in the case of a regular lattice), while for smaller  $\lambda$  the presence of long links destroys this order. Scaling arguments proposed in [197] suggest that the minimal length exponent is given by

$$d_{min} = \frac{\lambda - 2}{\lambda - 1 - 1/d}. \quad (125)$$

This network has then the curious property to have a fractal dimension which stays identical to the Euclidean dimension, but with a minimal length exponent  $d_{min} < 1$  for all  $\lambda$  and  $d > 1$ .

The authors of [198] studied the percolation properties of such a model and found that for these spatial scale-free networks with a degree distribution  $P(k) \sim k^{-\lambda}$ , the percolation threshold in the limit of infinite networks does not go

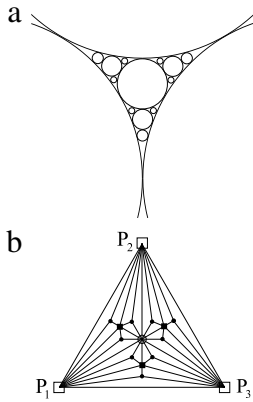


**Fig. 42.** Top: Classical Apollonian packing. Bottom: Apollonian network (showing the first, second and third generation with circles, squares, and dots respectively).

Source: From [199].

towards zero (for  $\lambda > 2$ ), in sharp contrast with non-spatial scale-free networks, which have  $p_c = 0$  for  $\lambda < 3$  (and  $N = \infty$ ).

In a non-spatial scale-free network, there are many short paths between the different hubs of the system easing the percolation. In contrast, for spatial (scale-free) networks there is a high local clustering due to the limited range of links, which naturally lengthen the distance between hubs. This negative assortativity makes it thus more difficult to achieve percolation in such a system, hence the existence of a non-zero threshold. As noted in [198], the spread of a disease too would be easier to control than on a scale-free network (see Section 5.6), which is expected as spatial containment is usually easier to set up.

#### 4.1.4. Apollonian networks

Other models were proposed in order to obtain a spatial scale-free network. In particular, Apollonian networks were introduced by Andrade et al. [199], where they constructed a scale-free network (Fig. 42) from a space-filling packing of spheres and connecting the centers of touching spheres by lines. These networks are simultaneously planar, scale-free (with exponent  $\gamma = 1 + \ln 3 / \ln 2$ ), small-world – in fact ‘ultra-small’ – with an average shortest path varying as

$$\langle \ell \rangle \sim (\log N)^{3/4} \quad (126)$$

and a clustering coefficient larger than 0.8 for large  $N$ . Various quantities for the Apollonian network and one of its variant are also computed and discussed in [200,201]. Due to all these simultaneous properties, Apollonian networks provide an interesting playground to test theoretical ideas.

### 4.2. Spatial generalization of the Erdos–Renyi graph

#### 4.2.1. Erdos–Renyi graph

The Erdos–Renyi (ER) graph [1,2,202] is the paradigm for random graphs, and is in many cases used as a null model. One simple way to generate it is to run through all pairs of nodes and to connect them with a probability  $p$ . The average number of links is then

$$\langle E \rangle = p \frac{N(N - 1)}{2} \quad (127)$$

giving an average degree equal to  $\langle k \rangle = 2\langle E \rangle / N = p(N - 1)$ . This last expression implies that in order to obtain a sparse network, we have to choose a small  $p$  scaling as  $p = \langle k \rangle / N$  for large  $N$ .

The establishment of edges are random, independent events and we thus obtain a binomial distribution for the degree  $k$  of a node

$$P(k) = \binom{N - 1}{k} p^k (1 - p)^{N - k + 1} \quad (128)$$

which can be approximated by a Poisson distribution

$$P(k) \approx e^{-\langle k \rangle} \frac{\langle k \rangle^k}{k!} \quad (129)$$

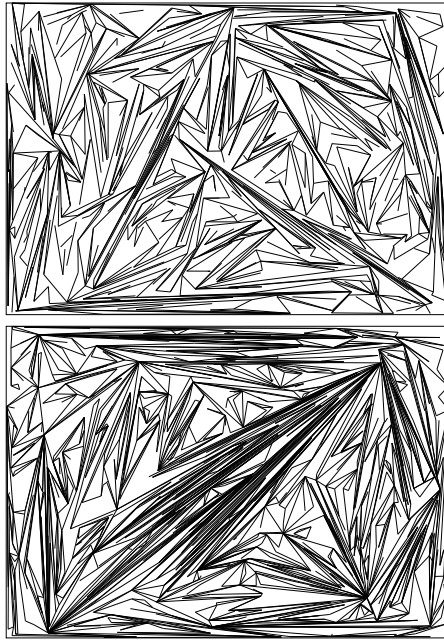


**Fig. 43.** Top: Planar Erdos–Renyi network obtained by rejecting links if they destroy planarity ( $N = 1000$ ). Bottom: Planar Barabasi–Albert network obtained by the same rejection method.

for large  $N$  with  $pN = \langle k \rangle$  constant. Other classical results can easily be derived, such as the clustering coefficient, which can be shown to be  $C = p$ , and the average shortest path  $\langle \ell \rangle \simeq \log N / \log \langle k \rangle$ . In fact for any generalized uncorrelated random graph characterized by a probability distribution  $P(k)$ , it can be shown (see for example [7]) that the average clustering coefficient is

$$\langle C \rangle = \frac{1}{N} \frac{(\langle k^2 \rangle - \langle k \rangle)^2}{\langle k \rangle^3} \quad (130)$$

and that the average shortest path is

$$\langle \ell \rangle \approx 1 + \frac{\log N / \langle k \rangle}{\log \frac{\langle k^2 \rangle - \langle k \rangle}{\langle k \rangle}}. \quad (131)$$

These last two well-known expressions are useful in the sense that they provide a reference to which we can compare results obtained on a specific network in order to understand its features. In particular, we can expect very different behavior for spatial networks signaled by different scaling of these quantities with  $N$ .

#### 4.2.2. Planar Erdos–Renyi graph

The first simple idea to generate a random planar graph would be to first generate a set of points in the two-dimensional space and then to construct an Erdos–Renyi graph by connecting randomly the pairs of nodes. It is clear that in this way we will generate mostly non-planar graphs, but we could decide to keep links which preserve planarity. We would then obtain something like represented in Fig. 43 (top). It is easy to imagine even more extensions of this process, and we could construct a planar BA network by adding in the two-dimensional space nodes (with a random, uniformly distributed location), which will connect according to the preferential attachment. We would then keep the node if it preserves the planarity of the system. We note here that there are some visual similarities with networks obtained by random sequential adsorption of line segments [203] and it would be interesting to understand if there are deeper connections between these problems.

Instead, mathematicians studied closely related networks. If we denote by  $P_N$  the class of all simple labeled planar graphs on  $N$  vertices.<sup>8</sup> We can draw a random planar graph  $R_N$  from this class with a uniform probability [204] and ask some questions [115,205], such as the number of vertices of a given degree, the number of faces of a given size, etc. For instance, the following results have been demonstrated ([115,204,205] and references therein).

- The random planar graph  $R_N$  is connected with probability at least  $1/e$ .

<sup>8</sup> A labeled graph refers to a graph where distinct labels are assigned to all vertices. The labeling thus adds configurations in the counting process of these graphs.

- The number  $\mathcal{N}_u$  of unlabeled planar graphs scales as

$$\mathcal{N}_u \sim \gamma_u^N \quad (132)$$

with  $9.48 < \gamma_u < 32.2$  and the number  $\mathcal{N}_l$  of labeled planar graphs as

$$\mathcal{N}_l \sim \gamma_\ell (N!)^{1/N} \quad (133)$$

where  $27.22685 < \gamma_\ell < 27.22688$ .

- The average number of edges of  $R_N$  is  $\langle E \rangle \geq \frac{13}{7}N$ .
- The degree distribution decreases at least as  $N/\gamma_\ell^k(k+2)!$ .

Other properties can be derived for this class of networks and we refer the interested reader to [115,204,205] and references therein for more results.

#### 4.2.3. The hidden variable model for spatial networks

In the Erdos–Renyi model, the probability  $p$  to connect two nodes is a constant. In certain situations, we could imagine that a node is described by a number of attributes (called *hidden variables* or *fitnesses*) and the connection between two nodes could depend on the respective attributes of these nodes [206,207]. In order to give a concrete example, we assume that there is only one attribute  $\eta$ , which is a real number distributed according to a function  $\rho(\eta)$ . The probability of connection for a pair of nodes  $(i, j)$  is then given by  $p_{ij} = f(\eta_i, \eta_j)$ , where  $f$  is a given function. In the case  $f = \text{const.}$  we recover the ER random graph. The average degree of a node with fitness  $\eta$  is given by

$$k(\eta) = N \int_0^\infty f(\eta, \eta') \rho(\eta') d\eta' \equiv NF(\eta) \quad (134)$$

and the degree distribution is then

$$\begin{aligned} P(k) &= \int \rho(\eta) \delta(k - k(\eta)) \\ &= \rho \left[ F^{-1} \left( \frac{k}{N} \right) \right] \frac{d}{dk} F^{-1} \left( \frac{k}{N} \right). \end{aligned} \quad (135)$$

A surprising result appears if we chose for example an exponential fitness distribution ( $\rho(\eta) \sim e^{-\eta}$ ) and for the function  $f$  a threshold function of the form

$$f(\eta_i, \eta_j) = \theta[\eta_i + \eta_j - z(N)] \quad (136)$$

where  $\theta$  is the Heaviside function and  $z(N)$  a threshold which depends in general on  $N$ . In this case, Caldarelli et al. [206] found a power law of the form  $P(k) \sim k^{-2}$ , showing that a scale-free network can emerge even for a peaked distribution of fitnesses. A spatial variant of this model was proposed in [208] (and discussed together with other models in [209]) where the nodes  $i$  and  $j$  are connected if the following condition is met

$$(\eta_i + \eta_j)h[d_E(i, j)] \geq \phi \quad (137)$$

where  $h[r]$  is a decreasing function and  $\phi$  a constant threshold. For this model, large fitnesses can therefore compensate for larger distances and we will observe large-fitness nodes connected by long links. If the distribution of fitnesses  $f(\eta)$  has a finite support or is strongly peaked around some value, we will have a typical scale  $r_0 = h^{-1}(\phi/2\bar{\eta})$  above which no (or a very few) connections are possible. As a result, the average shortest path will behave as for a lattice with  $\langle \ell \rangle \sim N^{1/d}$  in a  $d$ -dimensional space. For an exponential fitness distribution  $f(\eta) = e^{-\lambda\eta}$  and  $h(r) = r^{-\beta}$ , the authors of [208] find various degree distributions according to the value of  $\beta$ , going to a power-law  $p(k) \sim k^{-2}$  for  $\beta \rightarrow 0$  and to an exponential distribution for  $\beta = d$ . Various other cases were also studied in [206,208] and helped in understanding within this model when scale-free distributions could appear.

Finally, we mention here a generalization to other metrics than the spatial distance [210,211]. In particular, in [210], the probability that two individuals are connected decreases with a particular distance between these individuals. This distance is computed in a ‘social’ space and measures the similarity for different social attributes. This model is able to reproduce some of the important features measured in social networks such as large clustering, positive degree correlations and the existence of dense communities. More recently, Serrano et al. [195] developed the idea of a hidden metric space by using the one-dimensional circle as an underlying metric space in which nodes are uniformly distributed. A degree  $k$  drawn from a law  $P(k) \sim k^{-\gamma}$  for each node and each pair of nodes is connected with a probability  $r(d; k, k')$  that depends on the distance  $d$  between the nodes and also on their respective degrees  $k$  and  $k'$ . In particular, they studied the following form

$$r(d; k, k') = \left( 1 + \frac{d}{d_c(k, k')} \right)^{-\alpha} \quad (138)$$

where  $\alpha > 1$  and where  $d_c \sim kk'$  for example. The probability that a pair of nodes is connected then decreases with distance (as  $d^{-\alpha}$ ) and increases with the product of their degrees  $kk'$ . In this case a long distance can be compensated by large degrees, as is observed in various real-world networks. In this model, in agreement with other models of spatial networks, we observe a large clustering (for  $\alpha$  large enough).

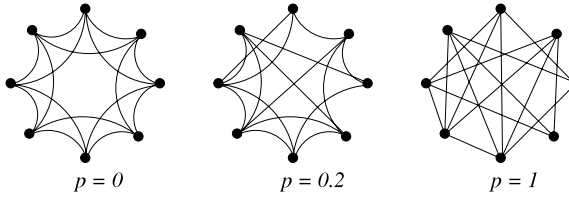


**Fig. 44.** Construction of the Watts-Strogatz model for  $N = 8$  nodes. At  $p = 0$  each node is connected to its four nearest neighbors and by increasing number of edges is rewired.

Source: Adapted from Watts and Strogatz [3].

#### 4.2.4. The Waxman model

The Waxman model [131] is a random network topology generator introduced by Waxman and appears as a spatial variant of the ER model. In this model, the nodes are uniformly distributed in the plane and edges are added with probabilities that depend on the distance between the nodes

$$P(i, j) = \beta e^{-d_E(i, j)/d_0}. \quad (139)$$

The quantity  $d_0$  determines the typical length of the links and  $\beta$  controls the total density of links. In terms of hidden variables the attribute here is the spatial location of the node and the pair connection probability depends on the distance between the nodes. For  $d_0 \rightarrow \infty$ , length is irrelevant and we recover the ER model, while for  $d_0 \sim 1/\sqrt{\rho}$  (where  $\rho$  is the average density of nodes in the plane) long links are prohibited and we are in the limit of a lattice-like graph.

Even though this model is very simple, it served as a first step towards the elaboration of more sophisticated models of the Internet [212]. Also, despite its simplicity, this Waxman model can be used in order to understand the importance of space in different processes taking place on this network. We can cite for example navigation or congestion problems in communication systems (see Section 5.4).

A growth model close to the Waxman model was proposed in [213], where at each time step a new node  $u$  is added in the plane and is connected to existing nodes  $v$  with a probability (if it fails to connect the node is discarded)

$$P(u, v) = \beta e^{-\alpha d_E(u, v)} \quad (140)$$

or even decreasing as power law  $P(u, v) \sim d_E(u, v)^{-\tau}$ . Networks generated with this algorithm have a large clustering coefficient (as expected) and probably a large diameter (although there is no quantitative prediction in [213]).

### 4.3. Spatial small worlds

#### 4.3.1. The Watts-Strogatz model

As early as 1977 spatial aspects of the small-world problem were considered by geographers in the paper [214], but it was only in 1998 that Watts and Strogatz (WS) proposed a simple and powerful network model [3] which incorporated both a spatial component and long-range links. This model is obtained by starting from a regular lattice and by rewiring at random the links with a probability  $p$  (Fig. 44).

The degree distribution of this network has essentially the same features as the ER random graph, but the clustering coefficient and the average shortest path depend crucially on the amount of randomness  $p$ . The average clustering coefficient has been shown to behave as [215]

$$\langle C(p) \rangle \simeq \frac{3(m-1)}{2(2m-1)}(1-p)^3 \quad (141)$$

where the average degree is  $\langle k \rangle = 2m$ . The average shortest path has been shown to scale as [39,216]

$$\langle \ell \rangle \sim N^* \mathcal{F} \left( \frac{N}{N^*} \right) \quad (142)$$

where the scaling function behaves as

$$\mathcal{F}(x) \sim \begin{cases} x & \text{for } x \ll 1 \\ \ln x & \text{for } x \gg 1. \end{cases} \quad (143)$$

The crossover size scales as  $N^* \sim 1/p$  [39,215,216], which basically means that the crossover from a large-world to a small-world occurs for an average number of shortcuts equal to one

$$N^* p \sim 1. \quad (144)$$

The network can thus be seen as clusters of typical size  $N^*(p)$  connected by shortcuts.

The interest of these networks is that they can simultaneously present some features typical of random graphs (with a small-world behavior  $\ell \sim \log N$ ) and of clustered lattices with a large average clustering coefficient (while for ER random graph  $\langle C \rangle \sim 1/N$ ).

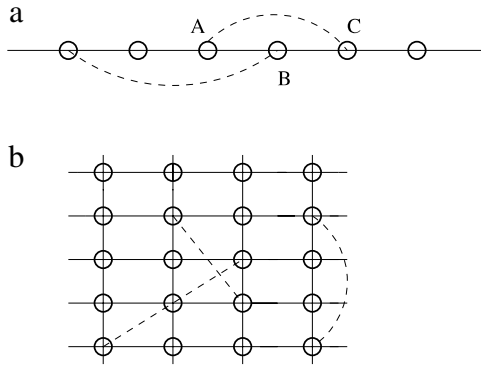


**Fig. 45.** Schematic representation of spatial small-world in (a) one dimension and (b) two dimensions. The dashed lines represent the long-range links occurring with probability  $q(\ell) \sim \ell^{-\alpha}$ .

Source: From [219].

#### 4.3.2. Spatial generalizations

One of the first variants of the Watts–Strogatz model was proposed in [135,217,218] and was subsequently generalized to higher dimensions  $d$  [219]. In this variant (see Fig. 45), the nodes are located on a regular lattice in  $d$ -dimensions with periodic boundaries. The main idea is that if the shortcuts have to be physically realized there is a cost associated with their length. A way to model this is to add links with probability

$$q(\ell) \sim \ell^{-\alpha}. \quad (145)$$

For each node, we add a shortcut with probability  $p$ , which implies that on average there will be  $pN$  additional shortcuts.

Concerning the average shortest path, it is clear that if  $\alpha$  is large enough, the shortcuts will be small and the behavior of  $\langle \ell \rangle$  will be ‘spatial’ with  $\langle \ell \rangle \sim N^{1/d}$ . On the other hand, if  $\alpha$  is small enough we can expect a small-world behavior  $\ell \sim \log N$ . In fact, various studies [217,219,220] discussed the existence of a threshold  $\alpha_c$  separating the two regimes, small- and large-world. We follow here the discussion of [221], who carefully studied the behavior of the average shortest path. The probability that a shortcut is ‘long’ is given by

$$P_c(L) = \int_{(1-c)L/2}^{L/2} q(\ell) d\ell \quad (146)$$

where  $c$  is small but non-zero. The critical fraction of shortcuts  $p^*N = p^*(L)L^d$  then satisfies

$$P_c(L)p^*(L)L^d \sim 1 \quad (147)$$

which means that if we have a fraction  $p > p^*$  of long shortcuts, the system will behave as a small-world. We then obtain

$$p^*(L) \sim \begin{cases} L^{-d} & \text{if } \alpha < 1 \\ L^{\alpha-d-1} & \text{if } \alpha > 1 \end{cases} \quad (148)$$

and a logarithmic behavior  $\log L/L^d$  for  $\alpha = 1$ . For a given value of  $p$  we thus have one length scale

$$L^*(p) \sim \begin{cases} p^{-1/d} & \text{if } \alpha < 1 \\ p^{1/(\alpha-d-1)} & \text{if } \alpha > 1 \end{cases} \quad (149)$$

which in the special case  $\alpha = 0$  was obtained in [222]. We will then have the following scaling form for the average shortest path

$$\langle \ell \rangle = L^* \mathcal{F}_\alpha \left( \frac{L}{L^*} \right) \quad (150)$$

where the scaling function varies as

$$\mathcal{F}_\alpha(x) \sim \begin{cases} x & \text{if } x \ll 1 \\ \ln x & \text{if } x \gg 1 \end{cases} \quad (151)$$

(or even a function of the form  $(\ln x)^{\sigma(\alpha)}$  with  $\sigma(\alpha) > 0$  for  $x \gg 1$ ). The characteristic length for  $\alpha > 1$  thus scales as

$$L^*(p) \sim p^{1/(\alpha-d-1)} \quad (152)$$

and displays a threshold value  $\alpha_c = d + 1$ , a value already obtained with the average clustering coefficient for  $d = 1$  in [219]. For  $\alpha > \alpha_c$ , the length scale  $L^*(p)$  is essentially finite and less than 1, which means that for all values of  $L$  the system has a large-world behavior with  $\langle \ell \rangle \sim L$ . In other words, the links in this case cannot be long enough and the graph can always be coarse-grained to reproduce a regular lattice. In the opposite case  $\alpha < \alpha_c$ , the length  $L^*(p)$  diverges for  $p \rightarrow 0$  and there will always be a regime such that  $L^*(p) \gg L$ , implying a small-world logarithmic behavior.

Finally, we mention a recent numerical study [223] of this model which seems to show that for  $\alpha > d$  there are two regimes. First, for  $d < \alpha < 2d$

$$\langle \ell \rangle \sim (\log N)^{\sigma(\alpha)} \quad (153)$$

with

$$\sigma = \begin{cases} \frac{1/\alpha}{2 - \alpha} & \text{for } d = 1 \\ \frac{4/\alpha}{4 - \alpha} & \text{for } d = 2. \end{cases} \quad (154)$$

The second regime is obtained for  $\alpha > 2d$ , where the ‘spatial’ regime  $\langle \ell \rangle \sim N^{1/d}$  is recovered. We note that, numerically, the scaling prediction of [221] with two regimes only and the result of [223] are however difficult to distinguish. For  $d = 1$  there are no discrepancies ( $\sigma = 1$  for  $\alpha = d = 1$ ), while for  $d = 2$ , the results for  $\alpha = 2$  and  $\alpha = 4$  are consistent with the analysis of [221]. A problem thus exists here for  $d = 2$  and  $\alpha = 3$ , for which  $\sigma = 4/3$ , a value probably difficult to distinguish numerically from corrections obtained at  $\alpha = \alpha_c = d + 1$ .

#### 4.4. Spatial growth models

##### 4.4.1. Generalities

In this part we will review models of growing networks which essentially elaborate on the preferential attachment model proposed by Albert and Barabasi [182,224]. In the preferential attachment, there is a propensity to connect a new node to an already well-connected one [182,224], which is probably an important ingredient in the formation of various real-world networks.

The process to generate such a Barabasi-Albert (BA) network is thus extremely simple. Starting from a small ‘seed’ network, we introduce a new node  $n$  at each time step. This new node is allowed to make  $m$  connections towards nodes  $i$  with a probability

$$\Pi_{n \rightarrow i} \propto k_i \quad (155)$$

where  $k_i$  is the degree of node  $i$ . We refer the interested reader to the various books and reviews which describe in detail this model [5,8,10–13]. In particular, the degree distribution behaves as a power-law with exponent  $P(k) \sim k^{-\gamma}$  with  $\gamma = 3$ , the average shortest path behaves at the dominant order as  $\log N$ , and the average clustering coefficient is given by

$$\langle C \rangle = \frac{m}{8N} (\ln N)^2 \quad (156)$$

while  $C(k) \sim 1/k$ .

However, in many networks, such as transportation or communication networks, distance is a relevant parameter and real-world examples suggest that when long-range links exist, they usually connect to hubs (the well-connected nodes). Many variants of the BA model have been proposed and a few of them are concerned with space. The growth process is the same as for BA, but in addition one has to specify the location of the new node. In most models, the location is taken at random and uniformly distributed in space. The attachment probability is then written as

$$\Pi_{n \rightarrow i} \propto k_i F[d_E(n, i)] \quad (157)$$

where  $F$  is a function of the Euclidean distance  $d_E(n, i)$  from the node  $n$  to the node  $i$ .

When  $F$  is a decreasing function of distance (as in most cases), this form (Eq. (157)) implies that new links preferentially connect to hubs, unless the hub is too far, in which case it could be better to connect to a less connected node but closer in space. In order to have long links, the target node must have a large degree in order to compensate for a small  $F(d)$ , such that  $kF(d) \sim 1$ . This is for instance the case for airlines: Short connections go to small airports while long connections point preferably to large airports, i.e. well-connected nodes.

##### 4.4.2. Preferential attachment and distance selection

Several models including distance have been proposed [128,186,197,198,219,225–228] and we review here the main results obtained in these studies. The  $N$  nodes of the network are supposed to be in a  $d$ -dimensional space of linear size  $L$  and we assume that they are distributed randomly in space with uniform density  $\rho$ . One could use other distributions. For instance in cities the density decreases exponentially from the center [109]. The case of randomly distributed points is interesting since on average it preserves natural symmetries such as translational and rotational invariance, in contrast with lattices.

Essentially two different cases have been considered in the literature.

**4.4.2.1. Finite range case.** In this case, the function  $F(d)$  decreases sharply with distance, typically as an exponential [228]

$$F(d) = e^{-d/r_c} \quad (158)$$

and thus introduces a new scale in the system, the interaction range  $r_c$ . When the interaction range is of the order of the system size (or larger), the distance is irrelevant and the obtained network will be scale-free. In contrast, when the interaction range is small compared to the system size, we expect new properties and a crossover between these two regimes.

The important dimensionless parameters here are the average number  $n$  of points in a sphere of radius  $r_c$

$$n = \rho r_c^d \frac{\pi^{d/2}}{\Gamma(1 + \frac{d}{2})} \quad (159)$$

and the ratio which controls the importance of spatial effects

$$\eta = \frac{r_c}{L} \quad (160)$$

(where  $L$  is the system size). It can then be shown [228] that the degree distribution follows the scaling form valid only for  $\eta \ll 1$

$$P(k) \sim k^{-\gamma} f(k/k_c) \quad (161)$$

with  $\gamma = 3$  and where the cut-off  $k_c$  behaves as

$$k_c \sim n^\beta \quad (162)$$

where  $\beta \simeq 0.13$ . The distance effect thus limits the choice of available connections and thereby limits the degree distribution for large values.

Also, when the distance effect is important we expect a large value of the average clustering coefficient. In the limit of small  $\eta$ , we can expect the result of random geometric graphs (see Section 4.1.1 and [186]) to hold

$$C_0 \equiv \langle C \rangle(\eta = 0) = 1 - 3\sqrt{3}/4\pi \simeq 0.59 \quad (163)$$

(for  $d = 2$ ). We expect to recover this limit for  $\eta \rightarrow 0$  and for an average connectivity  $\langle k \rangle = 6$ , which is a well-known result in random geometry. If  $\eta$  is not too small, the preferential attachment is important and induces some dependence of the clustering coefficient on  $n$ . In addition, we expect that  $\langle C \rangle(\eta)$  will be lower than  $\langle C \rangle(0)$ , since the longer links will not connect to the nearest neighbors. Numerical results show that there is a good collapse (see Fig. 46a) when  $\langle C \rangle(\eta)$  is expressed in terms of  $n$  and is a decreasing function, since when  $n$  increases the number of neighbors of the node will increase, thus decreasing the probability that two of them will be linked.

The average shortest path is described by a scaling ansatz which governs the crossover from a spatial to a scale-free network

$$\langle \ell(N, \eta) \rangle = [N^*(\eta)]^\alpha \mathcal{F}_\alpha \left[ \frac{N}{N^*(\eta)} \right] \quad (164)$$

with

$$\mathcal{F}_\alpha(x) \sim \begin{cases} x^\alpha & \text{for } x \ll 1 \\ \ln x & \text{for } x \gg 1. \end{cases} \quad (165)$$

The typical size  $N^*$  depends on  $\eta$ , and we can find its behavior in two extreme cases. For  $\eta \gg 1$ , space is irrelevant and

$$N^*(\eta \gg 1) \sim N_0 \quad (166)$$

where  $N_0$  is a finite constant. When  $\eta \ll 1$ , the existence of long-range links will determine the behavior of  $\langle \ell \rangle$ . If we denote by  $a = 1/\rho^{1/d}$  the typical inter-node distance, the transition from a large to a small-world will be observed for  $r_c \sim a(N^*)$ , which leads to

$$N^*(\eta \ll 1) \sim \frac{1}{\eta^d}. \quad (167)$$

In Fig. 46b, the ansatz equation (164), together with the results of Eqs. (166), (167) is shown. This data collapse is obtained for  $\alpha \simeq 0.3$  and  $N_0 \simeq 180$  (for  $d = 2$ ). For  $N > N^*$ , the network is a small-world: the diameter grows with the number of points as  $\langle \ell \rangle \sim \log N$ . In the opposite case of the spatial network with a small interaction range, the network is much larger: to go from a point  $A$  to a point  $B$ , we essentially have to pass through most of the points in between and the behavior of this network is much like that of a lattice with  $\langle \ell \rangle \sim N^\alpha$ , although the diameter here is smaller, probably due to the existence of some rare longer links (in the case of a lattice we expect  $\alpha = 1/d$ ). Probably larger networks and better statistics are needed here.

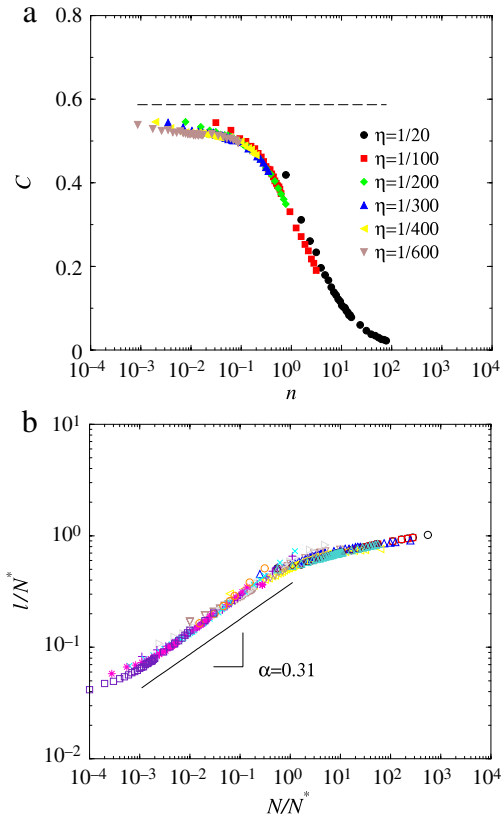


**Fig. 46.** (a) Clustering coefficient versus the mean number  $n = \rho\pi r_c^2$  of points in the disk of radius  $r_c$  (plotted in Log-Lin). The dashed line corresponds to the theoretical value  $C_0$  computed when a vertex connects to its adjacent neighbors without preferential attachment. (b) Data collapse for the average shortest path obtained. The first part can be fitted by a power-law with exponent  $\approx 0.3$ , followed by a logarithmic regime for  $N > N^*$ .  
Source: Both figures from [228].

This model was extended [50] in the case of weighted growing networks in a two-dimensional geometrical space. The model considered consists of growth, and the probability that a new site connects to a node  $i$  is given by

$$\Pi_{n \rightarrow i} = \frac{s_i^w e^{-d_{ni}/r_c}}{\sum_j s_j^w e^{-d_{nj}/r_c}}, \quad (168)$$

where  $r_c$  is a typical scale and  $d_{ni}$  is the Euclidean distance between  $n$  and  $i$ . This rule of *strength driven preferential attachment with spatial selection*, generalizes the preferential attachment mechanism driven by the strength to spatial networks. Here, new vertices connect more likely to vertices which correspond to the best interplay between Euclidean distance and strength.

The weights are also updated according to the following rule already studied in another paper [229]

$$w_{ij} \rightarrow w_{ij} + \delta \frac{w_{ij}}{s_i^w}. \quad (169)$$

for all neighbors  $j \in \Gamma(i)$  of  $i$ .

The model thus contains two relevant parameters: the ratio between the typical scale and the size of the system  $\eta = r_c/L$ , and the ability to redistribute weights,  $\delta$ .

The most important results concerning the traffic are the following. The correlations appearing between traffic and topology of the network are largely affected by space as the value of the exponents  $\beta_w$  and  $\beta_d$  depend on  $\eta$  (for  $\beta_d$  see Fig. 47). Strikingly, the effect of the spatial constraint is to increase both exponents  $\beta_w$  and  $\beta_d$  to values larger than 1 and, although the redistribution of the weights is linear, non-linear relations  $s^w(k)$  and  $s^d(k)$  as a function of  $k$  appear. For the weight strength the effect is not very pronounced, with an exponent of order  $\beta_w \approx 1.1$  for  $\eta = 0.01$ , while for the distance strength the non-linearity has an exponent of order  $\beta_d \approx 1.27$  for  $\eta = 0.02$ .

The nonlinearity induced by the spatial structure can be explained by the following mechanism affecting the network growth. The increase of spatial constraints affects the trend to form global hubs, since long distance connections are less probable, and drives the topology towards the existence of ‘regional’ hubs of smaller degree. The total traffic, however, is

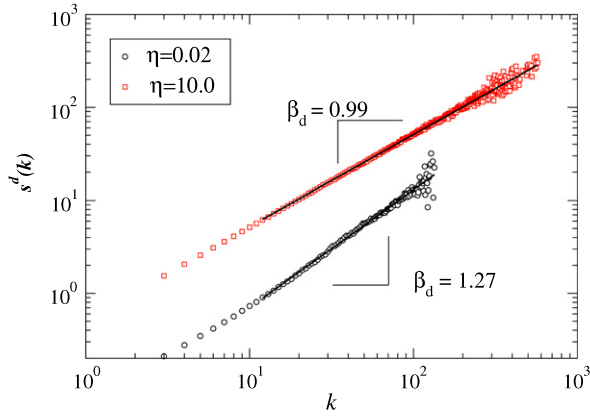


**Fig. 47.** Distance strength versus  $k$  for two different cases ( $\eta = 0.02$  and  $\eta = 10.0$ ). When  $\eta$  is not small, space is irrelevant and there are no correlations between degree and space as signalled by  $\beta_d \approx 1$ . When spatial effects are important ( $\eta = 0.02 \ll 1$ ), non-linear correlations appear and  $\beta_d > 1$ . We observe a crossover for  $k \simeq 10\text{--}20$  to a power-law behavior and the power-law fit over this range of values of  $k$  is shown (full lines).  
Source: From [50].

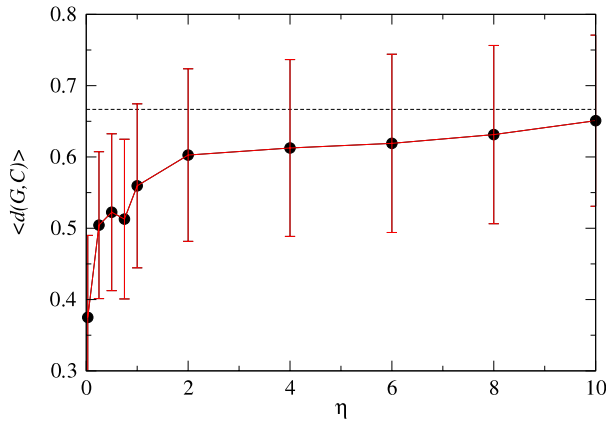


**Fig. 48.** Average Euclidean distance between the barycenter  $G$  of all nodes and the 10 most central nodes ( $C$ ) versus the parameter  $\eta$  (Here  $\delta = 0$ ,  $N = 5,000$  and the results are averaged over 50 configurations.). When space is important (i.e. small  $\eta$ ), the central nodes are closer to the gravity center. For large  $\eta$ , space is irrelevant and the average distance tends to the value corresponding to a uniform distribution  $\langle r \rangle_{unif} = 2/3$  (dotted line).  
Source: From [50].

not changed with respect to the case  $\eta = \infty$ , and is in fact directed towards these regional hubs. These medium-large degree vertices therefore carry a much larger traffic than they would do if global hubs were available, leading to a faster increase of the traffic as a function of the degree, eventually resulting in a super-linear behavior. Moreover, as previously mentioned, the increase in distance costs implies that long range connections can be established only towards the hubs of the system: this effect naturally leads to a super-linear accumulation of  $s^d(k)$  at larger degree values.

The spatial constraints act at both local and global levels of the network structure by introducing a distance cost in the establishment of connections. It is therefore important to look at the effect of space in global topological quantities such as the betweenness centrality. Hubs are natural crossroads for paths and it is natural to observe a correlation between  $g$  and  $k$ , as expressed in the general relation  $g(k) \sim k^\mu$ , where the exponent  $\mu$  depends on the characteristics of the network, and we expect this relation to be altered when spatial constraints become important (see Section 2.2.2). In particular, the betweenness centrality displays relative fluctuations which increase as  $\eta$  decreases, and become quite large. This can be understood by noticing that the probability to establish far-reaching shortcuts decreases exponentially in Eq. (168), and only the large traffic of hubs can compensate this decay. Far-away geographical regions can thus only be linked by edges connected to large degree vertices, which implies a more central role for these hubs. The existence of fluctuations means that nodes with small degree may have a relatively large betweenness centrality (or the opposite), as observed in the air-transportation network (see Fig. 10 and [89]). The present model defines an intermediate situation in that we have a random network with space constraints that introduces a local structure since short distance connections are favored. Shortcuts and long distance hops are present, along with a spatial local structure that clusters spatially neighboring vertices. In Fig. 48, we plot the average distance  $d(G, C)$  between the barycenter  $G$  and the 10 most central nodes. As expected, as spatial constraints become more important, the most central nodes get closer to the spatial barycenter of the network.

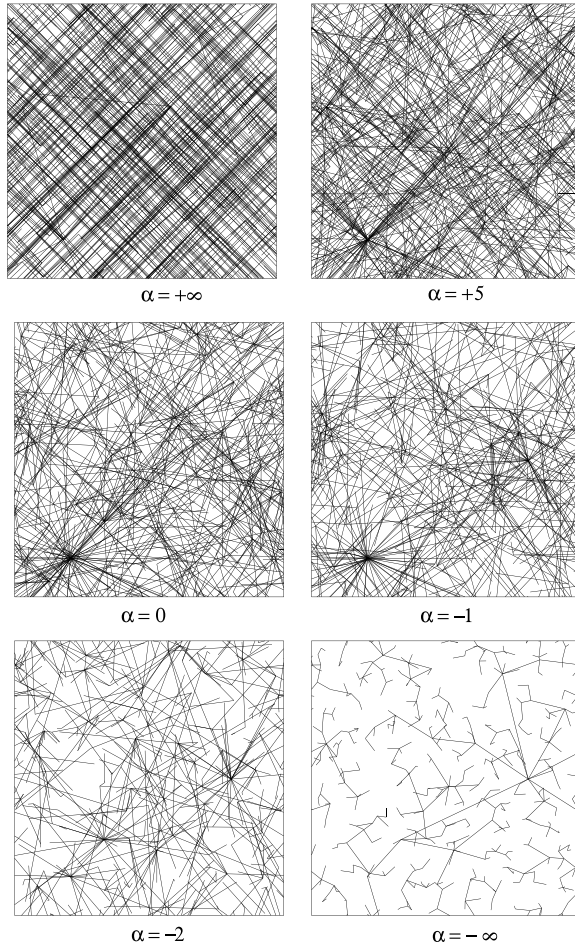


**Fig. 49.** Various networks obtained with the rule  $F(d) = d^\alpha$ .  
Source: From [226].

4.4.2.2. Power law decay of  $F(d)$ . In this case, the function  $F$  in Eq. (157) varies as

$$F(d) = d^\alpha. \quad (170)$$

This problem was considered in [128,226,227]. The numerical study presented in [227] shows that in the two-dimensional case, for all values of  $\alpha$  the average shortest path behaves as  $\log N$ . The degree distribution is however different for  $\alpha > -1$  where it is broad, while for  $\alpha < -1$  it decreases much faster (the numerical results in [227] suggest according to a stretched exponential).

In [226], Manna and Sen study the same model but for various dimensions and for values of  $\alpha$  going from  $-\infty$  to  $+\infty$  where the node connects to the closest and the farthest node, respectively (Fig. 49). These authors indeed find that if  $\alpha > \alpha_c$  the network is scale-free and in agreement with [227] that  $\alpha_c(d = 2) = -1$ , while for large dimensions  $\alpha_c$  decreases with  $d$  (the natural guess  $\alpha_c = 1 - d$  is not fully supported by their simulations). This study was complemented by another one by the same authors [230] in the  $d = 1$  case and where the probability to connect to a node  $i$  is given by (which was already proposed in [128])

$$\Pi_{n \rightarrow i} \sim k_i^\beta d_E(n, i)^\alpha. \quad (171)$$

For  $\alpha > \alpha_c = -0.5$  the network is scale-free at  $\beta = 1$  with an exponent  $\gamma = 3$ . They also find a scale-free network for a line in the  $\alpha-\beta$  plane and also for  $\beta > 1$  and  $\alpha < -0.5$ . The degree-dependent clustering coefficient  $C(k)$  behaves as

$$C(k) \sim k^{-b} \quad (172)$$

where the authors found numerically that  $b$  varies from 0 to 1 (which is the value obtained in the BA case).

#### 4.4.3. Growth and local optimization

**4.4.3.1. A model for the Internet.** In the Internet, the degree distribution is a power law (see for example [5] and references therein) and in order to explain this fact, computer scientists [231] proposed a tree growth model with local optimization. More precisely, at each unit time, a new node  $i$  is connected to an already connected node  $j$  such that the quantity

$$\mathcal{E} = \lambda d_E(i, j) + h_j \quad (173)$$

is minimum. The quantity  $h_j$  is an extensive measure of centrality, which can be either the average shortest path length from  $j$  or the shortest path length to a root node, etc. A new node would then typically like to connect to a very central node, but is limited by the cost measured by the distance. There will thus be an interplay between these two constraints and we can explore the two extremes: for small  $\lambda$ , we obtain a star network. In the opposite case, when  $\lambda$  is large, only distance is important and we obtain some sort of dynamical version of the Euclidean minimum spanning tree. If  $\lambda$  has some intermediate values ( $\lambda$  growing slower than  $\sqrt{N}$  and is larger than a certain constant), we can obtain a network with a power-law degree distribution whose exponent  $\gamma$  depends on  $\lambda$ . For instance if  $\lambda \sim N^{1/3}$  then  $\gamma = 1/6$  (see [231] for other results on this model).

Even if the resulting network is not obtained by minimizing some global function, the addition of new nodes minimizes a cost function, and in this sense we can speak of a *local* minimization.

**4.4.3.2. A model for distribution networks.** Many networks, including transportation and distribution networks evolve in time and increase their service area. Clearly, in these situations the resulting networks are growing and cannot result from a global optimization, but instead local optimization could be a reasonable mechanism to explain the organization of these structures.

In the example of a transportation network such as the train system, the nodes represent the train stations and the edges the rail segments between adjacent stations. In many of these systems, there is also a *root node* which acts as a source of the distribution system, or in the case of the railway can be considered to be the central station. During the evolution of the network at least two factors could be considered. First, the total length of the system, which represents the cost of the infrastructure, should not be too large. Space has another important role here: the transportation system should also allow one to connect two nodes in the network through a shortest path whose length is not too far from the ‘as crow flies’ distance. This efficiency is for example measured by the route factor – or detour index – (see Section 2.2.2.3) which for two nodes  $i$  and  $j$  of the network reads

$$Q(i, j) = \frac{d_R(i, j)}{d_E(i, j)}.$$

For a system with a root node 0, one can then compute the route factor as the average over all nodes except 0

$$q = \frac{1}{N} \sum_{i \neq 0} \frac{d_R(i, 0)}{d_E(i, 0)}. \quad (174)$$

Following these two requirements, Gastner and Newman [232] proposed a model of a growing network where vertices are initially randomly distributed in the two-dimensional plane and where one vertex is designated as the root node 0. A network is then grown from its root by adding an edge between an unconnected node  $i$  to a vertex  $j$  which belongs to the network. The edge is chosen according to a local minimization process such that the quantity

$$\mathcal{E}_{ij} = d_E(i, j) + \alpha \frac{d_R(j, 0)}{d_E(i, 0)} \quad (175)$$

is minimum and where  $\alpha > 0$  is here a parameter controlling the importance of the route factor. For  $\alpha = 0$ , the algorithm always adds a link to the closest vertex and the resulting network is similar to the MST and has a poor route factor [232]. When  $\alpha$  increases, the route factor decreases and the average edge length  $\bar{l}$  (not be confused with the average shortest path  $\langle \ell \rangle$ ) increases (see Fig. 50). In this figure, we see that the route factor  $q$  decreases sharply when  $\alpha$  increases from zero, while the average edge length – which is a measure of the building cost of the network – increases slowly. This suggests that it is possible to grow networks with a small cost but with a good efficiency.

Gastner and Newman [232] also studied a simpler version of this model, where the local minimization acts on the quantity

$$\mathcal{E}'_{ij} = d_E(i, j) + \beta d_R(j, 0) \quad (176)$$

which is similar to the model for the Internet proposed by Fabrikant et al. [231] (see also Section 4.4.3.1) but where the vertices are added one by one. This model produces networks similar to the one obtained with Eq. (175) and self-organizes to networks with small  $q$ , which is not imposed here. This model can be applied to the set of stations of the Boston rail network and produces a network in good correspondence with the real one. Also, the small value of  $q$  is confirmed in different empirical examples, such as sewer systems, gas pipelines, and the Boston subway [232], where the ratio  $\bar{l}/\bar{l}_{MST}$  is in the range [1.12, 1.63] while the route factor is less than 1.6 (and compared to the MST is improved by a factor in the range [1.4, 1.8]).

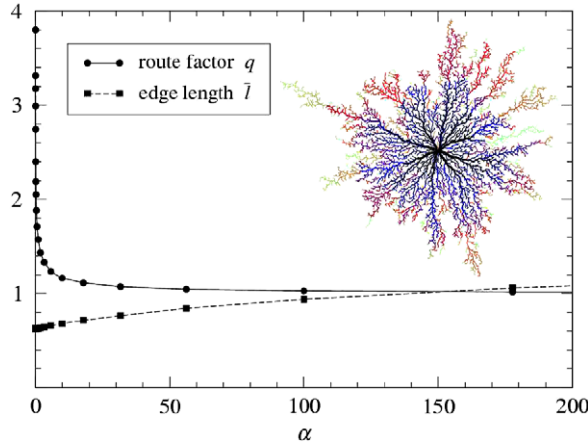


**Fig. 50.** Route factor  $q$  and average edge length  $\bar{l}$  versus  $\alpha$  in Eq. (175). These results are obtained for  $N = 10^4$  vertices and in the inset the network is obtained for  $\alpha = 12$ .  
Source: From [232].

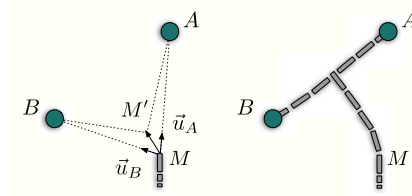


**Fig. 51.**  $M$  is the network's closest point to both centers  $A$  and  $B$ . The road will grow to point  $M'$  in order to maximally reduce the cumulative distance  $\Delta$  of  $A$  and  $B$  from the network.  
Source: From [114].

The networks obtained here are trees, which is a simplification for many of the real-world networks which usually contain loops. In addition, there is also usually an interaction between the density of points and the network, and this co-evolution is not taken into account here. However, this simple model of local optimization seems to capture important ingredients and could probably serve as a good starting point for further improvements.

**4.4.3.3. A model for street and road networks.** In the case of urban street patterns, striking statistical regularities across different cities have been empirically found recently, suggesting that a general and detail-independent mechanism may be in action (see Section 3.2.1). The rationale to invoke a local optimality principle in this context is as in the case of distribution networks based on costs: every new road is built to connect a new location to the existing road network in the most efficient way [233]. The locality of the rule is implemented both in time and space during the evolution and formation of the street network, in order to reflect evolution histories that greatly exceed the time-horizon of planners. The self-organized pattern of streets emerges as a consequence of the interplay of the geometrical disorder and the local rules of optimality.

This local optimization process proposed in [114] can be understood with the simple following example (Fig. 51). We assume that at a given stage of the evolution, two nodes  $A$  and  $B$  still need to be connected to the network. At any time step, each new node can trigger the construction of a single new portion of road of fixed (small) length. In order to maximally reduce their distance to the network, both  $A$  and  $B$  would select the closest points  $M_1$  and  $M_2$  in the network as initial points of the new portions of roads to be built. If  $M_1$  and  $M_2$  are distinct, segments of roads are added along the straight lines  $M_1A$  and  $M_2B$ . If  $M_1 = M_2 = M$ , it is not economically reasonable to build two different segments of roads and in this case only one single portion  $MM'$  of road is allowed. The main assumption here is that the best choice is to build it in order to maximize the reduction of the cumulative distance  $\Delta$  from  $M$  to  $A$  and  $B$ .

$$\Delta = [d(M, A) + d(M, B)] - [d(M', A) + d(M', B)]. \quad (177)$$

The maximization of  $\Delta$  is done under the constraint  $|MM'| = \text{const.} \ll 1$  and a simple calculation leads to

$$\overrightarrow{MM'} \propto \vec{u}_A + \vec{u}_B \quad (178)$$

where  $\vec{u}_A$  and  $\vec{u}_B$  are the unit vectors from  $M$  in the direction of  $A$  and  $B$  respectively. The rule (178) can easily be extended to the situation where more than two centers want to connect to the same point  $M$ . Already in this simple setting non-trivial geometrical features appear. In the example of Fig. 51 the road from  $M$  will develop a bent shape until it reaches the line  $AB$ .

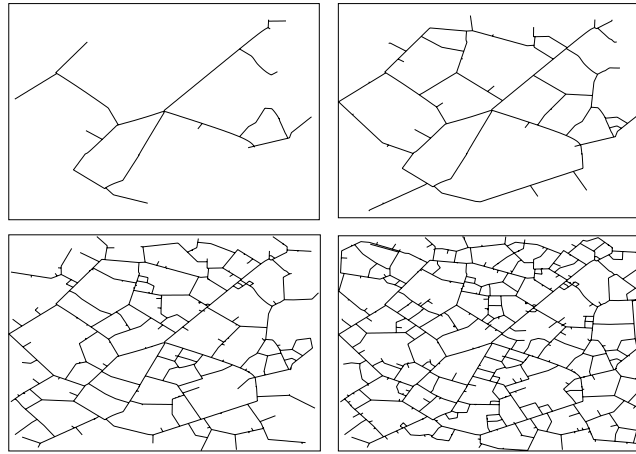


**Fig. 52.** Snapshots of the network at different times of its evolution: for (a)  $t = 100$ , (b)  $t = 500$ , (c)  $t = 2000$ , (d)  $t = 4000$  (the growth rate is here  $\eta = 0.1$ ). At short times, we have almost a tree structure and loops appear for larger density values obtained at larger times (the number of loops then increases linearly with time).

Source: From [114].

and intersects it perpendicularly, as is commonly observed in most urban settings. At the intersection point, a singularity occurs with  $\vec{u}_A + \vec{u}_B \approx 0$ , and one is then forced to grow two independent roads from the intersection to  $A$  and  $B$ .

Interestingly, we note that although the minimum expenditure principle was not used, the rule Eq. (178) was also proposed by Runions et al. [78] in a study of leaf venation patterns.

The growth scheme described so far leads to tree-like structures which are on one side economical, but which are hardly efficient. For example the path length along a minimum spanning tree scales as a power  $5/4$  of the Euclidean distance between the end-points [234,235] and better accessibility is granted if loops are present. The authors of [114,236] followed [78] and assumed that a new node can trigger the construction of more than one portion of road per time step, leading to the existence of loops. This model produces realistic results (some examples are shown in Fig. 52), which are in good agreement with empirical data which demonstrates that even in the absence of a well defined blueprint, non-trivial global properties emerge. This agreement confirms that the simple local optimization is a good candidate for the main process driving the evolution of city street patterns, but it also shows that the spatial distribution of nodes  $\rho(r)$  is crucial. Concerning this last aspect, a more general model describing the co-evolution of the node distribution  $\rho(r)$  and the network was proposed in [236].

Another interesting model was proposed recently by Courtat et al. [60]. In this model, each new ‘settlement’ is added every time step at a certain location and connects to the existing infrastructure network in a way similar to [114]. The city generates a spatial field describing the ‘attractiveness’ of every point. This potential field has a hard repulsion term at short distances and a large distance behavior proportional to the total ‘mass’ of the city (measured by the total length of its roads) and decreasing as a power law with distance. The sum of all influences of all roads then produces local minima, and each new node has its own policy. Among others, the parameter  $\omega$  is related to the ‘wealth’ of the node and controls the number of roads constructed to connect new settlements: if  $\omega = 1$  all possible roads are constructed and in the opposite case,  $\omega = 0$ , only the shortest road is built. Another important parameter in this model is the probability to be at the optimal location controlled by the potential. For small  $P_e$  the city is ‘unorganized’ and nodes are added randomly, while for large  $P_e$  the probability to stick to the optimal location is large. In Fig. 53, we show the different networks obtained by varying the two parameters  $P_e$  and  $\omega$ . The variety of networks obtained by varying two parameters only is remarkable – going from a ‘favella-like’ organization (for large  $P_e$ ) to a highly organized area (for small  $P_e$ ) – and suggests that this approach could provide an interesting first step for the modeling of urban street networks.

Finally, we end this section by noting that there are many other models for roads and urban structures and that we focused here on a physicist-like approach with minimal models. In particular, there are many studies on these problems done by geographers (usually with the help of cellular automata) and we refer the interested reader to articles in the handbook [18] for more references.

#### 4.5. Optimal networks

Although one of the main pillars in complex systems studies is the emergence of a collective behavior without any central planning, it is usually a matter of time scale compared with the typical time horizon of planners. On a short time scale it is reasonable to assume that planning plays a role and that the system under consideration evolves by using an optimization process. On a larger time scale, most systems result from the addition of successive layers and even if each of these layers is the result of an optimization process, it is very likely that the long time result is not an optimum.

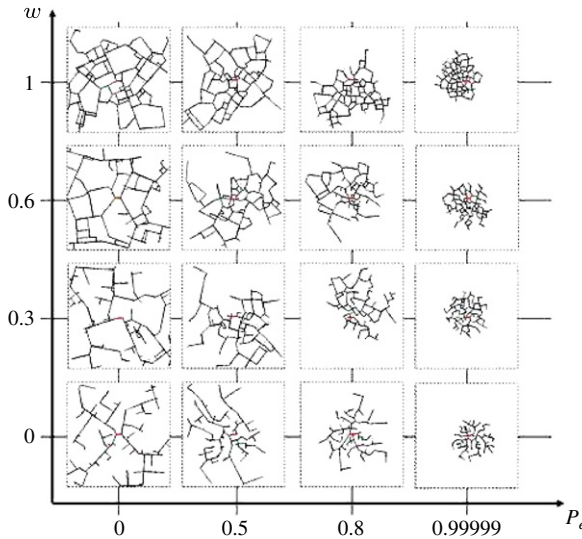


**Fig. 53.** Simulations of the model proposed by Courtat et al. [60]. The different networks are obtained for various values of the parameters  $P_e$  and  $\omega$ . At small values of  $P_e$  the city is organized, while for large  $P_e$  the nodes are added at random. For small  $\omega$ , a minimum number of roads are constructed to connect new nodes, while in the opposite case all possible connections are added.

Source: From [60].

Optimization is however of great importance in many practical engineering problems, and both the problem of optimal networks [27] and of optimal traffic on a network [237,238] have a long tradition in mathematics and physics. It is well known, for example, that the laws that describe the flow of currents in a resistor network [239] can be derived by minimizing the energy dissipated by the network [240]. On the other hand, optimal networks have been shown to be relevant in the study of the mammalian circulatory system [241], food webs [242], general transportation networks [168], metabolic rates [167], river networks [243], and gas pipelines or train tracks [80]. All these studies share the fact that the nodes of the network are embedded in a  $d$ -dimensional Euclidean space, which implies that the degree is almost always limited and the connections restricted to ‘neighbors’ only.

A second broad class of optimal networks where spatial constraints are absent has been also recently investigated. It has been shown, for example, that optimization of both the average shortest path and the total length can lead to small-world networks [244], and more generally, degree correlations [245] or scale-free features [246] can emerge from an optimization process. Cancho and Sole [247] showed that the minimization of the average shortest path and the link density leads to a variety of networks, including exponential-like graphs and scale-free networks. Guimera et al. [248] studied networks with minimal search cost and found two classes of networks: star-like and homogeneous networks. Finally, Colizza et al. [249] studied networks with the shortest route and the smallest congestion, and showed that this interplay could lead to a variety of networks when the number of links per node is changed.

Finally, we note that optimal networks could serve as interesting null models. For example, the (Euclidean) minimum spanning tree (MST) is obtained by connecting all the nodes with a minimum total length, and as an illustration we show in Fig. 54 the MST obtained for the set of stations present in the Paris subway in 2009. In this subway case, the total length is directly connected to the cost of the network and the MST represents the most economical network. The MST, however, has some drawbacks such as a large average shortest path and a large vulnerability to failure, and the real subway network obviously has many redundant links. It is, however, interesting to understand the interplay between costs and efficiency by comparing the actual network with the MST.

As we can see, optimal networks appear in many different branches, such as mathematics, physics and also in engineering. This subject is in fact so broad that it would deserve a whole review to explore its various aspects. In this chapter, we thus made the choice to restrict ourselves to the most recent and relevant statistical studies involving optimal networks and space.

#### 4.5.1. Hub-and-spoke structure

An important example of the result of an optimization process is the hub-and-spoke structure. In this structure, direct connections are replaced with fewer connections to hubs which form a network at a larger scale. The hub-and-spoke structure reduces the network costs, centralizes the handling and sorting, and allows carriers to take advantage of scale economies through consolidation of flows. Such networks have widespread application in transportation, and became in particular important in airline transportation, mainly due to the fact that a carrier has to minimize its costs even if by doing so the average traveling time for a user is not minimized (see the Fig. 55 for an illustration of this difference of designs).

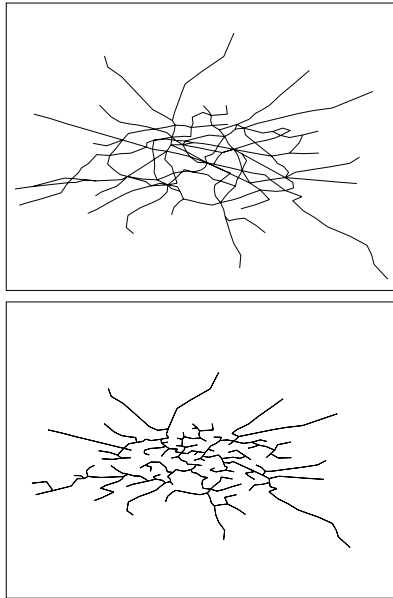


**Fig. 54.** Top: Paris subway network (2009). Bottom: Corresponding Minimum spanning tree.

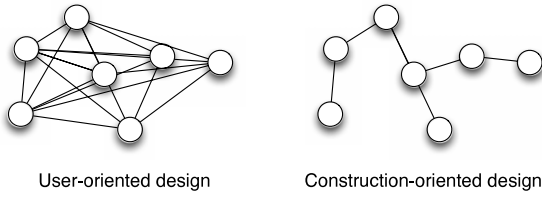


**Fig. 55.** Schematic comparison between a transportation network which optimizes the user travel time and distance (left) and a network which minimizes the construction costs (right).

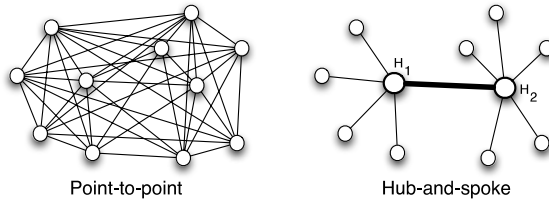


**Fig. 56.** Schematic comparison between a point-to-point transit model which optimizes the user travel time and distance (left) and a hub-and-spoke system (with two hubs  $H_1$  and  $H_2$ ) which minimizes the total operating costs by bundling together the traffic between the two hubs.

One of the first cases where the hub-and-spoke system was observed is in the US, with Delta Air Lines, which had its hub in Atlanta (GA). FedEx also adopted this system in the 1970s, and after the airline deregulation in 1978 most of the airline carriers adopted it as well. This system is based on the construction of regional hubs and the creation of major routes between these hubs (see Fig. 56). One can easily compare the point-to-point (P2P) transit model and the one hub-and-spoke model for  $N$  nodes. In the hub-and-spoke model, there are of the order  $N$  routes to connect all nodes, while in the P2P the number of routes is of the order  $N^2$ . In transportation systems such as airlines, this will lead to fuller planes, larger benefits, and expensive operations such as sorting and accounting packages will be done at the hub only. Obviously, there are also drawbacks. The centrality of the hubs is very large, and overloading at a hub can have unexpected consequences throughout the whole network. In other words, the hub is a bottleneck in the network and in agreement with general results on networks, hubs also constitute the vulnerable points in the network, a failure at a hub being able to trigger large delays which can propagate through the whole network.

An important problem in transportation research is to locate the hub(s) in a system of  $N$  nodes such that a given cost function is minimum. Analytical research on this *hub location problem* began relatively recently with the study [250] and the interested reader can find a short review on this subject in [251]. In the following, we will detail one of the simplest cases, known as the *linearized multiple assignment model* and which can be formulated as follows. We assume that in a system of

$N$  nodes, there is a known origin–destination matrix  $T_{ij}$  (i.e. the flow between  $i$  and  $j$ , see Section 3.3.1). We denote by  $C_{ij}$  the transportation cost per individual to go from  $i$  to  $j$  and the importance of hubs is in the fact that there is a *discount factor*  $0 \leq \alpha \leq 1$  on the links among them. For example in the airline case, bundling flows allows one to use for example larger aircrafts and reduce the passenger-mile costs. This discount factor implies that if  $k$  and  $m$  are two hubs, then the interhub cost on  $k - m$  is given by  $\alpha C_{km}$ . If we denote by  $X_{ij,km}$  the fraction of the flow from  $i$  to  $j$  which is routed via the hubs  $k$  and  $m$ , the function to be minimized is then

$$\mathcal{E} = \sum_{ijkm} T_{ij}[C_{ik} + \alpha C_{km} + C_{mj}]X_{ij,km} \quad (179)$$

under the constraints

$$\sum_k Z_k = p \quad (180)$$

$$\sum_{km} X_{ij,km} = 1 \quad (181)$$

$$\sum_m X_{ij,km} - Z_k \leq 0 \quad (182)$$

$$\sum_k X_{ij,km} - Z_m \leq 0 \quad (183)$$

where  $Z_k = 1$  if  $k$  is a hub and zero otherwise. We look for a solution of this problem with a fixed number  $p$  of hubs. The two last constraints ensure that the flow will not be routed via  $k$  and  $m$  unless both  $k$  and  $m$  are hubs. This type of minimization will lead to the solutions schematically shown in Fig. 56, where the reduction of the number of links is made possible by the establishment of hubs and the bundling of flows between the hubs. For these optimal networks, the total network cost is minimum, but obviously individual travel times are larger (as compared with a point-to-point network).

We just gave the flavor here of this type of approach and there is a huge number of studies on this problem that we cannot cite here because of lack of space. Basically, there is a more practical research direction which amounts to adding more characteristics of real-world networks [251], such as transfer delays for example [252]. There is also a more mathematical point of view (see for example [253]) where optimal properties are discussed. At this point, however, many problems are still unsolved and a statistical approach on the large network properties of this hub-and-spoke minimization problem is probably an interesting direction for future research.

#### 4.5.2. Congestion and centralized organization

In many real-world cases however the pure hub-and-spoke structure is not present and we observe a ring structure around a complicated core or an effective hub (see for example Fig. 57). An interesting discussion on centralization versus decentralization from the perspective of the minimum average shortest path and of the effect of congestion can be found in [254,255]. The idea is then to study the competition between the centralized organization with paths going through a single central hub and decentralized paths going along a ring and avoiding the central hub in the presence of congestion. A simple model of hub-and-spoke structure together with a ring was proposed in [256]. In this model,  $N$  nodes are on a circle and there is hub located at the center of the circle (see Fig. 58). A radial link – a spoke – is present with probability  $p$ . When computing the shortest path, these spokes are assumed to count for 1/2. In other words, the number of hops to go from one site on a ring to another via the central hub (when it is possible) is then equal to 1. In the case of directed links, the shortest path distribution is easy to compute and one finds [256]

$$P(\ell) = \frac{1}{N-1} [1 + (\ell-1)p + \ell(N-1-\ell)p^2] (1-p)^{\ell-1}. \quad (184)$$

In particular, we can check that the two limiting cases are correct: for  $p \rightarrow 0$ , we obtain  $P(\ell) \rightarrow 1/N-1$  giving  $\langle \ell \rangle = N/2$  and for  $p \rightarrow 1$ ,  $P(\ell) \rightarrow \delta_{\ell,1}$  and  $\langle \ell \rangle = 1$ . The general expression for the average shortest path is

$$\langle \ell \rangle = \frac{1}{N-1} \left[ \frac{2-p}{p} N - \frac{3}{p^2} + \frac{2}{p} + \frac{(1-p)^N}{p} \left( N - 2 + \frac{3}{p} \right) \right]. \quad (185)$$

In the undirected case, we have more paths going from one site to the other and the enumeration is a little bit more tedious. The result for the shortest path distribution now reads [256]

$$P(\ell = 1) = \frac{2}{N-1} \left( 1 + \frac{N-3}{2} p^2 \right) \quad (186)$$

$$P(\ell \geq 2) = \frac{1}{N-1} [a_0 + a_1 p + a_2 p^2 + a_3 p^3 + a_4 p^4] (1-p)^{2\ell-4}$$

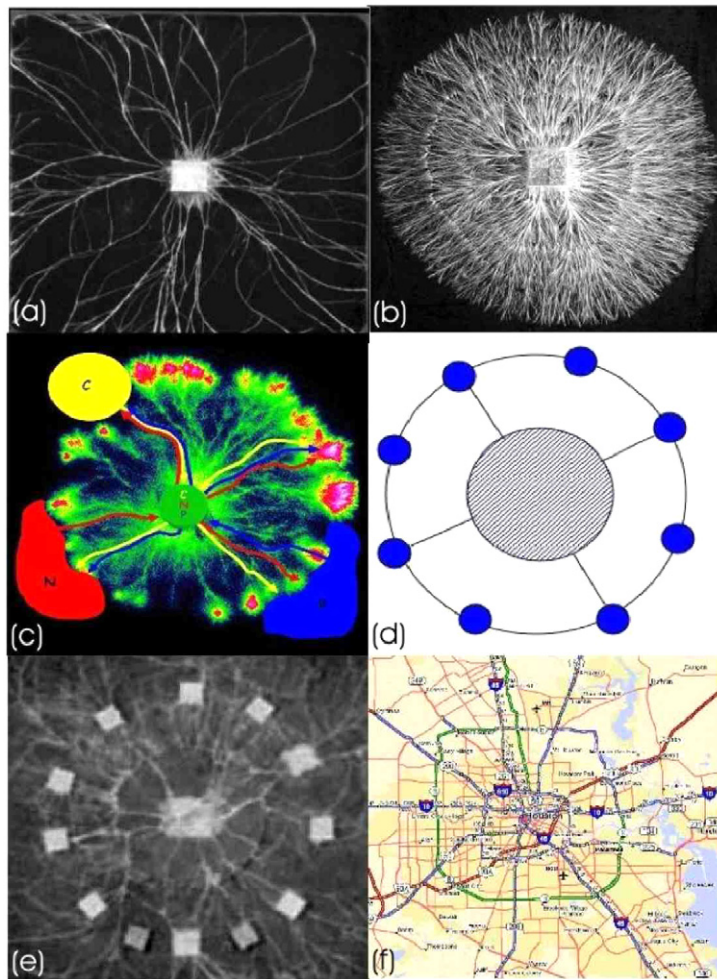


**Fig. 57.** Examples of hub-and-spoke structures with rings. (a)–(c), (e): Typical fungi networks, in (c) a schematic representation of the nutrient flow is shown. (d) The model studied in [254–256] with spokes radiating from a hub. (f) Road network in Houston showing an inner hub with a complicated structure.

Source: From [255].

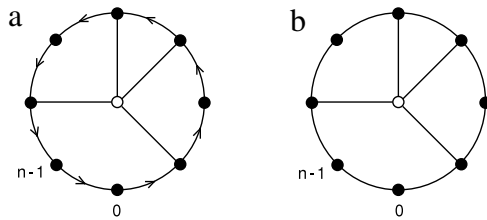


**Fig. 58.** Models proposed in [256] and studied in [254,255] with congestion. A central site is connected to a site on a ring with probability  $p$ . In (a) all the links on the ring are directed and in (b) these links are not directed.

Source: From [256].

where

$$\begin{aligned}
 a_0 &= 2 \\
 a_1 &= 4(\ell - 2) \\
 a_2 &= 2(\ell - 1)(2N - 4\ell - 3) \\
 a_3 &= -2(2\ell - 1)(N - 2\ell - 1) \\
 a_4 &= \ell(N - 2\ell - 1).
 \end{aligned} \tag{187}$$

For both these models a continuous limit can be defined by taking the limit  $N \rightarrow \infty$  and  $p \rightarrow 0$  with  $\rho = pN$  and  $z \equiv \ell/N$  fixed. The shortest path distribution then converges to (in the undirected model)

$$NP(\ell) \rightarrow 2[1 + 2\rho z + 2\rho^2(1 - 2z)]e^{-2\rho z}. \quad (188)$$

The interesting observation made in [254] is that if we now add a cost  $c$  each time a path goes through the central hub, we could expect some sort of transition between a decentralized regime where it is less costly to stay on the peripheral ring to a centralized regime where the cost is not enough to divert the paths from the central hub. The cost could in general depend on how busy the center is and could therefore grow with the number of connections to the hub. In the case of a constant cost  $c$ , the expression for the average shortest path is now [254]

$$P(\ell) = \begin{cases} \frac{1}{N-1} & \text{for } \ell \leq c \\ \frac{1}{N-1}[1 + b_1 p + b_2 p^2](1-p)^{\ell-c-1} & \text{for } \ell > c \end{cases} \quad (189)$$

where  $b_1 = \ell - c - 1$  and  $b_2 = (N - 1 - \ell)(\ell - c)$ . For paths of length  $\ell \leq c$ , there is no point in going through the central hub. In the opposite case, when  $\ell > c$ , we recover a distribution similar to the  $c = 0$  case in [256]. The average shortest path is then

$$\langle \ell \rangle = \frac{(1-p)^{N-c}[3 + (N-2-c)p]}{p^2(N-1)} + \frac{p[2-2c+2N-(c-1)(c-N)p]-3}{p^2(N-1)} + \frac{c(c-1)}{2(N-1)}. \quad (190)$$

In the continuous limit ( $p \rightarrow 0$ ,  $N \rightarrow \infty$  and  $z \equiv \ell/N$  and  $\rho = pN$  fixed), the average shortest path is a function of the various parameters  $\langle \ell \rangle = \langle \ell \rangle(\rho, c, N)$ . In the case of costs increasing linearly with  $\rho$ , the average shortest path displays a minimum when  $\rho$  is varied ( $N$  and  $c$  being fixed). Indeed for  $\rho \rightarrow 0$ , there are no spokes and  $\langle \ell \rangle$  scales as  $N$ . In the opposite case,  $\rho$  large, the cost is also large and it is less costly to go along the ring. In [254], the authors used a simple approximation and found that (with  $c \equiv k\rho$ ), the optimal value of  $\rho$  is

$$\rho^* \approx \sqrt{\frac{N}{k}} \quad (191)$$

a result that is confirmed numerically. This result can actually be rewritten as

$$pc(\rho) \sim 1 \quad (192)$$

which means that the optimal situation is obtained when the average cost of a radial trip through the central hub is of order one: when  $c$  is too large, this trip is too costly and when  $p$  is too small, the existence of this path is too unlikely. The same argument applied to nonlinear cost  $c \sim k\rho^2$  gives the scaling

$$\rho^* \sim (N/k)^{1/3}. \quad (193)$$

For this optimal value, the minimum average shortest path is then of the order the cost

$$\langle \ell \rangle_{min} \sim c(\rho^*). \quad (194)$$

In the linear case  $c = k\rho$ , one obtains

$$\langle \ell \rangle_{min} \sim \sqrt{kN} \quad (195)$$

and in the nonlinear case  $c \sim k\rho^2$ , one obtains

$$\langle \ell \rangle_{min} \sim (kN^2)^{1/3}. \quad (196)$$

These expressions and arguments apply essentially both to the directed and non-directed model.

This study [254] was generalized in [255] to the case of a more complicated cost function such as  $c(\rho) = C\rho + B\rho^2 + A\rho^3$ , where the authors observe different behaviors and a phase transition according to the values of the coefficients  $A$ ,  $B$ , and  $C$ .

These studies show how congestion could have an important impact on the a priori optimal hub-and-spoke structure and favor the transport along a ring. From a more general perspective it would indeed be interesting to observe quantitatively this transition from a purely radial structure and the appearance of a ring for a congestion large enough, as is observed in many urban structures for example.

#### 4.5.3. From the MST to the SPT

There is a obviously a huge literature on optimal networks and we are obliged to restrict ourselves to a small subset of subjects. We will discuss here the prototypes of optimal networks, allowing us to introduce some of the main objects such

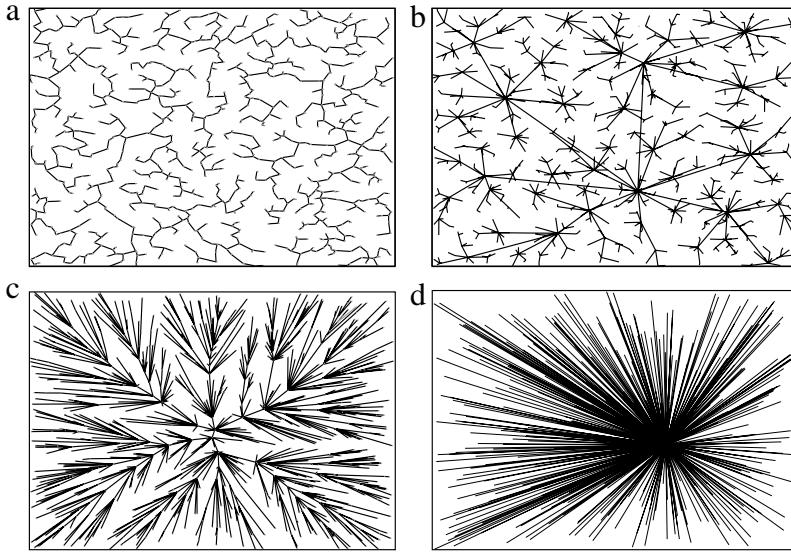


**Fig. 59.** Different spanning trees obtained for different values of  $(\mu, \nu)$  in Eq. (197) obtained for the same set of  $N = 1000$  nodes. (a) Minimum spanning tree obtained for  $(\mu, \nu) = (0, 1)$ . In this case the total distance is minimized. (b) Optimal traffic tree obtained for  $(\mu, \nu) = (1/2, 1/2)$ . In this case we have an interplay between centralization and minimum distance resulting in local hubs. (c) Minimum Euclidean distance tree obtained for  $(\mu, \nu) = (1, 1)$ . In this case centrality dominates over distance and a ‘star’ structure emerges with a few dominant hubs. (d) Optimal betweenness centrality tree obtained for  $(\mu, \nu) = (1, 0)$ . In this case we obtain the shortest path tree which has one star hub (for the sake of clarity, we omitted some links in this last figure). Source: From [258].

as the minimum spanning tree or the shortest path tree. Concerning the topic of connected networks over random points which minimize quantities such as the total route-length, the interested reader can find a recent and modern account about mathematically tractable models in a series of papers by Aldous [68,253,257] and in the references therein.

We will not introduce the different networks one by one but we will adopt a different point of view by introducing a generalized energy inspired by studies on optimal traffic networks [258]. The problem is, given a set of  $N$  nodes located in a 2-dimensional plane, to find the tree connecting them which minimizes the following quantity

$$\mathcal{E}_{\mu\nu} = \sum_{e \in \mathcal{T}} b_e^\mu d_e^\nu \quad (197)$$

where  $d_e$  is the Euclidean length of a link (or it could be another measure of its cost) and  $b_e$  is the betweenness centrality of the link (see Section 2.2.1.4). The exponents  $\mu$  and  $\nu$  control the relative importance of distance against topology as measured by centrality. Fig. 59 shows examples of spanning trees obtained for different values of  $(\mu, \nu)$ .

Case  $(\mu, \nu) = (0, 1)$ .

The energy is then

$$\mathcal{E}_{0,1} = \sum_{e \in \mathcal{T}} d_e \quad (198)$$

and represents the total length of the network. In real-world cases, the cost of the network is connected to this quantity and it makes sense to try to minimize it. Since the nodes are in space, the optimal resulting tree is called Euclidean MST. An example of the two-dimensional MST is shown in the Fig. 59a and many quantities can be calculated in the limit of a large number of nodes. For example, for the 2d case, the average length  $M(N)$  of the longest edge scales as [259]

$$M(N) \sim \sqrt{\frac{\ln N}{N}} \quad (199)$$

which is larger by a non-trivial factor  $\sqrt{\ln N}$  than the typical internode distance which scales as  $1/\sqrt{N}$ . Also, the total length  $\ell_T(N)$  of the  $d$ -dimensional MST is given by the general theorem of Beardwood, Halton, and Hammersley [260] and scales as [261]

$$\ell_T(N) \sim N^{1-1/d} \int_{\mathbb{R}^d} \rho(x)^{\frac{d-1}{d}} dx \quad (200)$$

where  $\rho(x)$  denotes the point distribution in  $\mathbb{R}^d$ . For a uniform distribution in  $d = 2$ , we thus obtain a scaling of the form  $\ell_T(N) \sim \sqrt{N}$ . This scaling can be understood with the following simple argument. In the case of a uniform density  $\rho$ , the

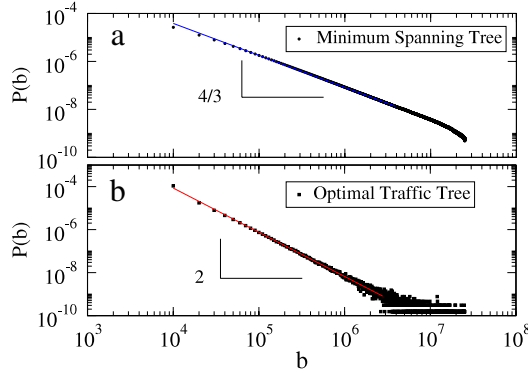


**Fig. 60.** Betweenness centrality distribution for the MST and for the OTT. The lines are power law fits and give for the MST the theoretical result  $\delta = 4/3$  and for the OTT the value  $\delta \simeq 2.0$  ( $N = 10^4$ , 100 configurations).  
Source: From [258].

typical inter-node distance is given by  $1/\rho^{1/d}$ , which scales as  $1/N^{1/d}$ , and we have  $E \propto N$  links, which reproduces the scaling  $\ell_T(N) \sim N \times N^{-1/d}$ .

We note here that an interesting study [262] shows that the minimum spanning tree for weighted networks can be partitioned into two distinct components: the ‘superhighways’ with large betweenness centrality nodes and the ‘roads’ with lower centrality. It would be interesting to study the consequences of these results for the Euclidean minimum spanning tree.

There are many other studies on the MST and it is impossible to quote them all here. We just end this paragraph by noting that the MST has many interesting connections with other problems of statistical physics, such as invasion percolation, directed polymers in random media, random resistor networks and spin glasses (see for example [263–265]).

Case  $(\mu, \nu) = (1/2, 1/2)$ .

We obtain here the optimal traffic tree (OTT) shown in Fig. 59b and which displays an interesting interplay between distance and shortest path minimization [258]. It has been shown that trees can be classified in ‘universality classes’ [266,267] according to the size distribution of the two parts in which a tree can be divided by removing a link (or the sub-basins areas distribution in the language of river network). We define  $A_i$  and  $A_j$  as the sizes of the two parts in which a generic tree is divided by removing the link  $(i, j)$ . The betweenness  $b_{ij}$  of link  $(i, j)$  can be written as  $b_{ij} = \frac{1}{2}[A_i(N - A_i) + A_j(N - A_j)]$ , and the distributions of  $A$ 's and  $b$ 's can be easily derived one from the other. It is therefore not surprising that the same exponent  $\delta$  characterizes both  $P(A) \sim A^{-\delta}$  and  $P(b)$ . While we obtain the value  $\delta = 4/3$  for the MST [266], for the OTT we obtain (Fig. 60) an exponent  $\delta \simeq 2$ , a value also obtained for trees grown with preferential attachment mechanism [11] (see also [268] for a supporting argument). Interestingly, most real-world networks are also described by this value  $\delta \simeq 2$  [269]. The OTT thus tends to have a more uniform centrality with respect to the MST [262], with important consequences on the vulnerability of the network, since there is no clearly designated ‘Achilles’ heel’ for the OTT.

The traffic properties of the OTT are also interesting as the traffic scales as  $T_{ij} \sim d_{ij}^\tau$  with  $\tau \approx 1.5$ , showing that large traffic is carried over large distance and is then dispatched on smaller hubs that distribute it over still smaller regions. Despite the limited range of degrees, we also observe for the strength [52]  $s_i = \sum_j T_{ij}$  a superlinear behavior with the degree. This result demonstrates that the existence of degree–traffic correlations, as observed for the airport network [52], could emerge from a global optimization process. The spatial properties of the OTT are also remarkable and display (Fig. 61) a hierarchical spatial organization where long links connect regional hubs, that, in turn are connected to sub-regional hubs, etc.

Case  $(\mu, \nu) = (1, 1)$ .

The energy is then given by  $\sum_e b_e d_e$  which is proportional to the average shortest path with weights given by the Euclidean distance. If we think of the betweenness centrality as a proxy for the traffic, the energy also represents the total length traveled on the system. An example of such a tree is shown in Fig. 59c.

Case  $(\mu, \nu) = (1, 0)$ .

In this case, the energy equation (197) is proportional to the average betweenness centrality, which is also the average shortest path  $\sum_e b_e \propto \ell$ . The tree  $(1, 0)$  shown in Fig. 59d is thus the shortest path tree (SPT) with an arbitrary ‘star-like’ hub (a small non zero value of  $\nu$  would select as the star the closest node to the gravity center). The total length here scales as

$$\ell_T(N) \sim N \quad (201)$$

with a prefactor proportional to the linear size of the system. Also, we note that if we were not restricted to trees, the solution would of course be the complete graph which gives an average shortest minimal and equal to one.

The minimization of Eq. (197) thus provides a natural interpolation between the MST and the SPT, a problem which was addressed in previous studies [270]. The degree distribution for all cases considered above (with the possible exception of

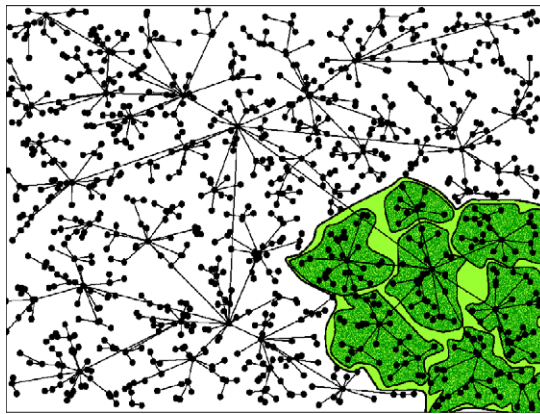


**Fig. 61.** Hierarchical organization emerging for the optimal traffic tree  $(\mu, \nu) = (1/2, 1/2)$  ( $N = 10^3$  nodes). Longer links lead to regional hubs which in turn connect to smaller hubs distributing traffic over smaller regions.  
Source: From [258].

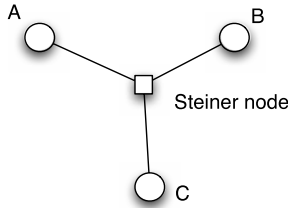


**Fig. 62.** Example of the Steiner tree for three points  $A$ ,  $B$ , and  $C$ . The Steiner point  $S$  is located at the Fermat point of the triangle  $ABC$  and minimizes the total distance  $d(S, A) + d(S, B) + d(S, C)$ . The angles are equal  $(SB, SA) = (SA, SC) = (SC, SB) = 2\pi/3$ .

$(\mu, \nu) = (1, 1)$  – a complete inspection of the plane  $(\mu, \nu)$  is still lacking) is not broad, possibly as a consequence of spatial constraints.

**4.5.3.1. The Steiner problem.** More generally, finding a subgraph that optimizes a global cost function is a very important problem. The Steiner tree is one of the classical (NP-complete) problems which is still studied now [271] because of its importance in many fields such as network reconstruction in biology, Internet multicasting, circuit and distribution network design. It is defined as the following: given a graph with positive weights, it consists in finding a connected subgraph of minimum weight that contains a selected set of ‘terminal’ vertices. Such a subgraph may require the addition of some ‘non-terminal’ nodes, which are called Steiner nodes (see Fig. 62 for an illustration of the three nodes problem). The difference between the Steiner tree problem and the minimum spanning tree problem is that in the Steiner tree problem extra intermediate vertices and edges may be added to the graph in order to reduce the length of the spanning tree.

In [271], the authors show that this problem can be analyzed with tools – such as the cavity equation – coming from statistical physics of disordered, frustrated systems (such as spin glasses, see for example [272]) and can lead to new optimization algorithms.

The Steiner problem is obviously important in transportation science too, where the nodes are considered as cities and the Steiner points as junctions. Recent results on this topic can be found in [257], where the author proposes a rigorous study of the network which minimizes the quantity

$$\mathcal{E} = \sum_e d_e f(e)^\beta \quad (202)$$

where  $\beta$  is a positive exponent,  $d_e$  is the length of the link  $e$ , and where  $f(e)$  is a function describing the flow on edge  $e$ . In this case, the minimum cost can be shown to scale as

$$\ell_T(N) \sim N^{\alpha(\beta)} \quad (203)$$

with

$$\alpha(\beta) = \begin{cases} 1 - \beta/2 & \text{for } \beta \in ]0, 1/2] \\ (1 + \beta)/2 & \text{for } \beta \in [1/2, 1]. \end{cases} \quad (204)$$

There is a transition at  $\beta = 1/2$  which corresponds to a change of regime where short links dominate to another one where long links dominate [257].

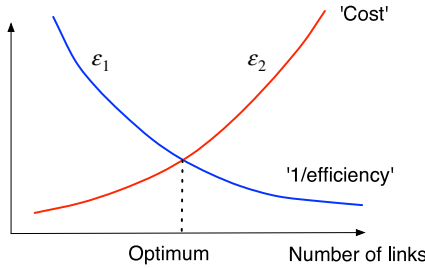


**Fig. 63.** Schematic representation of many optimal network models. The functional to minimize is the sum of two terms which behave in opposite ways when adding links. This leads in general to a non-trivial optimum.

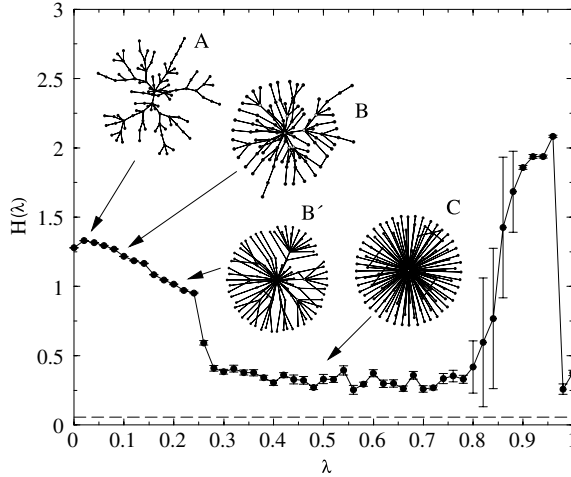


**Fig. 64.** Optimal networks obtained with the minimization of Eq. (207) for different values of  $\lambda$ . The  $y$ -axis represents the degree entropy  $H = -\sum_k p_k \log p_k$  and is small for a heterogeneous network (and large for a lattice).  
Source: From [247].

#### 4.5.4. Adding two antagonistic quantities

After having briefly reviewed the important optimal networks, such as the MST and the SPT, we now discuss some examples which were recently proposed in the literature. In particular, many models of optimal networks minimize a functional  $\mathcal{E}$  which is the sum of two terms which have antagonistic behavior

$$\mathcal{E} = \lambda \mathcal{E}_1 + (1 - \lambda) \mathcal{E}_2 \quad (205)$$

where  $\lambda \in [0, 1]$  and where  $\mathcal{E}_1$  is for example a decreasing function of the number of links and could represent the efficiency (such as the average shortest path for example) and where  $\mathcal{E}_2$  is an increasing function of the number of links for example and could represent the cost as measure by the total length for example (see Fig. 63). This interplay will lead in many cases to interesting solutions.

We will now discuss some simple examples that were considered in the literature. Already in the 1970s optimal network design was a very active field (see for example [273]) and we will focus here on the more recent results.

**4.5.4.1. Link density and average shortest path.** Ferrer i Cancho and Solé [247] minimized the simplest form, which is the combination of the average (normalized by the maximum) shortest path

$$d = \langle \ell \rangle / \langle \ell \rangle_{\max} \quad (206)$$

and the average link density  $\rho = 2E/N(N - 1)$  and reads

$$\mathcal{E} = \lambda d + (1 - \lambda) \rho \quad (207)$$

where  $\lambda \in [0, 1]$ . For  $\lambda = 0$ , the energy is the density and the optimal network is a tree. In the opposite case  $\lambda = 1$ , the optimal network minimizes the average shortest path. For intermediate values of  $\lambda$ , Cancho and Solé obtained different networks (see Fig. 64) and in particular argue that one of the regimes is a scale-free network with a broad distribution of degrees. For the network denoted by 'B' in Fig. 64 they obtained a power law with exponent  $-2$ , for a network of size  $N = 100$  (obviously better statistics on larger networks would be necessary to confirm this result, but this is not an obvious task). This shows that optimization might be a candidate for explaining the emergence of scale-free features.

**4.5.4.2. Total length and average shortest path.** Aldous [253] studied the network which minimizes the total length subject to the average number of hops. More precisely the cost associated to a route  $\pi(i, j) = e_1 e_2 \dots e_m$  going from node  $i$  to node  $j$  is

$$C(\pi) = m\Delta + a \sum_{e \in \pi} d_e \quad (208)$$

where  $\Delta$  and  $a$  are two constants (in [253], the quantity  $a$  is chosen to scale as  $1/\sqrt{N}$  in order to obtain terms of the same order of magnitude). The quantity  $\Delta$  measures the cost of connections and we expect that the larger it is the smaller the number of hubs (and the longer the spokes). The journey time associated with a graph  $G$  is then proportional to

$$T(G) = \sum_{i \neq j} \min_{\pi(i,j)} C[\pi(i, j)] \quad (209)$$

(where  $\pi(i, j)$  is the set of paths from  $i$  to  $j$ ). The total length of the graph is  $\ell_T(G) = \sum_{ij} A_{ij} d_E(i, j)$  and represents the cost (if we assume that the cost is proportional to the length of connection between two adjacent nodes). We thus can have an interplay between the cost represented by the total length and the total journey time leading to a variety of behaviors. If we constrain the routes to have  $m$  average hops, then the minimal total length scales as [253]

$$\ell_T(N) \sim N^{\beta(m)} \quad (210)$$

where the following bounds are obtained:  $\beta(2) = 3/2$ ,  $\beta(3) = 13/10$ ,  $\beta(4) = 7/6$ . The exponent thus decreases when  $m$  increases, which is expected since a smaller average number of hops implies a stronger constraint and thus a longer network. Conversely, if we require the network length  $\ell_T$  to scale as  $N$ , then the average shortest path scales as  $\ln \ln N$  [253].

In [80] an effective length is assigned to each edge

$$\tilde{\ell}_{ij} = \delta + (1 - \delta)d_E(i, j) \quad (211)$$

and the effective distance on a route  $\pi = e_1 e_2 \dots e_m$  between two nodes is given by

$$m\delta + (1 - \delta) \sum_{e \in \pi} d_e \quad (212)$$

which is Aldous' expression Eq. (208) with the correspondence  $\Delta \leftrightarrow \delta$  and  $a \leftrightarrow (1 - \delta)$ . Gastner and Newman [80] then weight the distance with a passenger number  $w_{ij}$  and minimize a combination of the form  $\ell_T(G) + \gamma T(G)$ . We note here that this model was also used together with a gravity model for computing  $w_{ij}$  in [274], where the authors compared the resulting optimal network and the real-world Indian airline network and found a good agreement. Gastner and Newman found for example optimal networks shown in Fig. 65. In particular, this figure illustrates the expected behavior when the connection cost increases (similar results were obtained with the same model in [275]): for  $\delta = 0$ , the connection cost is zero, only distance counts, and the resulting network is essentially a minimal length network, such as a planar network of roads for example. When  $\delta$  increases, and thus the cost associated to connections, we see fewer hubs and longer spokes (the limit being one hub and the corresponding network is the SPT). As noted by Aldous [253], it would be interesting to obtain more quantitative results in order to be able to compare with some real-world data for example.

In [276], Brede also recently revisited this problem in terms of a communication infrastructure with

$$\mathcal{E} = \lambda \ell_T(G) + (1 - \lambda) \langle \ell \rangle. \quad (213)$$

In a communication context, the total length represents the cost associated with the wires and the average shortest path is a measure of the communication efficiency. The number of links is not limited and the nodes are located on a regular lattice of dimension  $d$  with periodic boundary conditions. For  $\lambda = 0$ , we obtain the complete graph which minimizes  $\langle \ell \rangle$  and for  $\lambda = 1$  we obtain a minimum spanning tree (and depending on the dimension we can obtain a chain or a star network). For intermediate values of  $\lambda$ , we obtain different networks interpolating between these two extremes (see Fig. 66).

**4.5.4.3. Total length and synchronization.** A wide range of systems can be described by a system of oscillators coupled through a network of contacts, and synchronization problems have attracted much attention (for a review on synchronization in complex networks see [277]). If each of the oscillators is described by its individual dynamics by  $\dot{\phi}_i = f(\phi_i)$ , the dynamics of the coupled oscillators is governed by the following equation

$$\dot{\phi}_i = f(\phi_i) + \sigma \sum_j A_{ij} [h(\phi_j) - h(\phi_i)] \quad (214)$$

where  $h$  is a given output function. The stability of synchronized solutions is related to the eigenvalues  $\lambda_0 = 0 \leq \lambda_1 \leq \dots \leq \lambda_N$  of the graph Laplacian. More precisely, Pecora and Carroll [43] showed that the stability is related to the ratio, sometimes called ‘synchronizability’, defined as

$$e = \frac{\lambda_N}{\lambda_1} \quad (215)$$

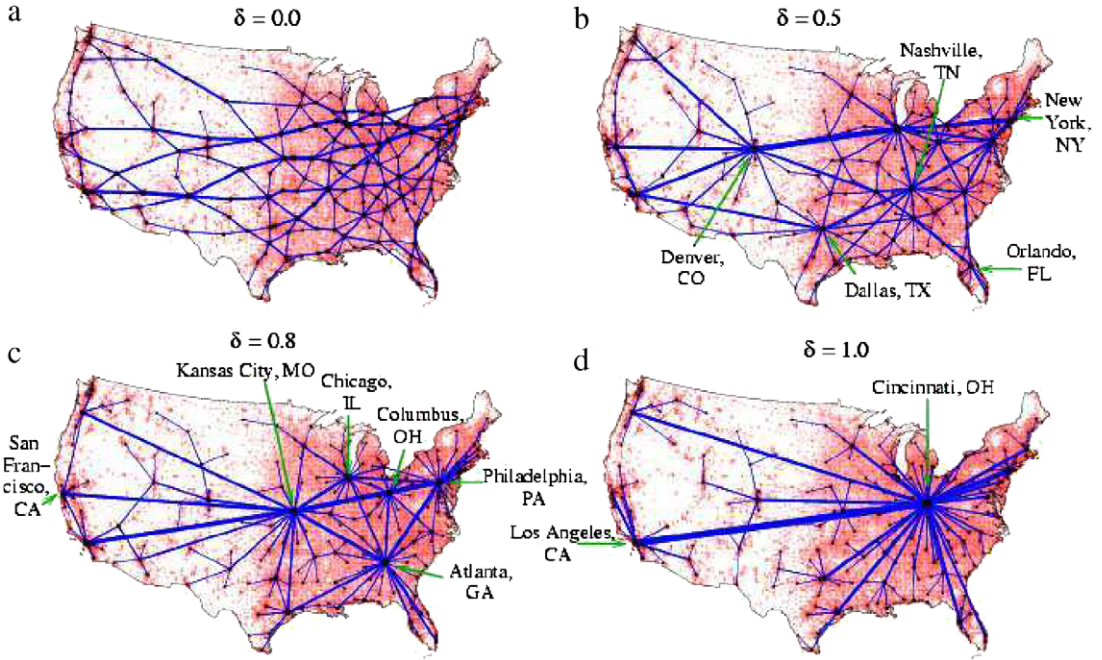


**Fig. 65.** Optimal networks obtained with the minimization of Eq. (212) for different values of  $\delta$ .  
Source: From [80].

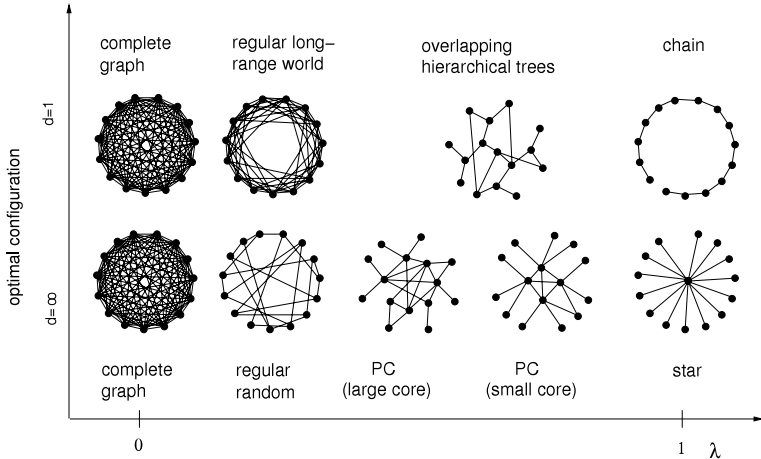


**Fig. 66.** Optimal networks obtained with the minimization of Eq. (213) for different values of  $\lambda$ .  
Source: From [276].

and that the smaller  $e$ , the more stable the synchronized solutions. Donetti et al. [278] proposed to construct networks with a fixed number of nodes and average degree and which optimize synchronizability (i.e. minimizing  $e$ ). The optimal networks are not small-world networks and display peaked distributions of degree, betweenness, average shortest paths, and of loops. An important feature of these networks is that they have a very entangled structure with short  $\langle \ell \rangle$ , large loops and no well-defined structure. In a recent article [279], Brede extended this problem and proposed to minimize both the total amount of wire  $\ell_T(G)$  to connect the network and the synchronizability characterized by  $e$

$$\mathcal{E} = \lambda \ell_T(G) + (1 - \lambda)e. \quad (216)$$

Starting with a one-dimensional chain for  $\lambda = 0$ , one obtains the complete graph which minimizes the synchronizability. For  $\lambda = 1$ , the  $1d$  line is optimal and for intermediate values of  $\lambda$  one obtains the networks shown in Fig. 67. Most links are small and the link length  $l$  distribution goes from a peak distribution to a broader law. A power law fit of the form  $P(l) \sim l^{-\alpha}$  gives a value of the exponent in the range [1, 1.5] (for a random graph with the same degree distribution and no total length constraint, the length distribution is uniform and when there is a total length constraint, the distribution is exponential). This

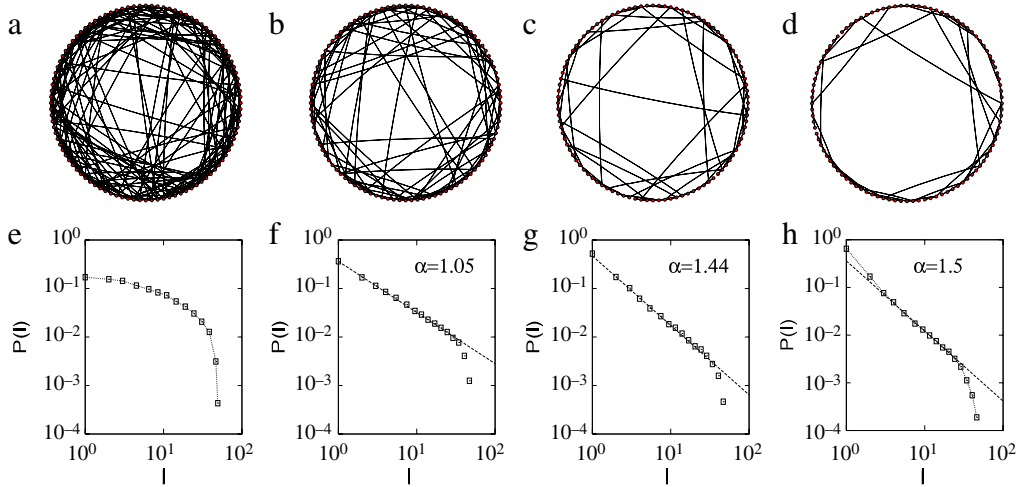


**Fig. 67.** (a)–(d) Examples of networks constructed for different values of  $\lambda = 0.05, 0.3, 0.8$ , and  $0.95$ . (e)–(h) Corresponding link length distribution for these different values of  $\lambda$ . Straight lines in (f)–(h) represent power laws with exponent  $1.05, 1.44$ , and  $1.5$ , respectively.  
Source: From [279].

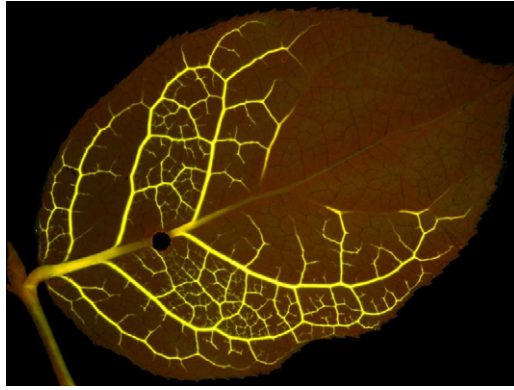


**Fig. 68.** Re-routing of the flow around an injury in a lemon leaf.  
Source: From [282].

result means that small-world networks can display optimal synchronization but with shortcuts covering many different length scales.

In another paper [280], the same author studied the trade-off between enhanced synchronization and total length of wire, but allowing the nodes to rearrange themselves in space with the constraint that the average Euclidean distance among nodes is constant. In this model, depending on the cost of wire, one observes different organization in modules: when the cost of wire  $\lambda$  increases one observes an organization in a large number of modules connected on a ring.

#### 4.5.5. Beyond trees: noise and loops

In most examples studied in literature (including the ones presented above), the optimal networks are trees. However, in many natural networks such as veins in leaves or insect wings, one observes many loops. Very recently, two studies which appeared simultaneously [281,282] proposed possible reasons for the existence of a high density of loops in many real optimal networks. In particular, it seems that the existence of fluctuations is crucial in the formation of loops. Maybe more related to the botanic evolution of leaves, the resilience to damage also naturally induces a high density of loops (see Fig. 68 for an example of flow re-routing after an injury).

In these studies, the model is defined on a network with conductances  $C_e$  on each link and where the total power

$$P = \frac{1}{2} \sum_k \sum_{j \in \Gamma(k)} C_{kj} (V_k - V_j)^2 \quad (217)$$

is minimized under the cost condition

$$\frac{1}{2} \sum_k \sum_{j \in \Gamma(k)} C_{jk}^\gamma = 1 \quad (218)$$

where in this equation it is assumed that the cost of a conductance  $C_{kj}$  is given by  $C_{kj}^\gamma$  where  $\gamma$  is a real number.

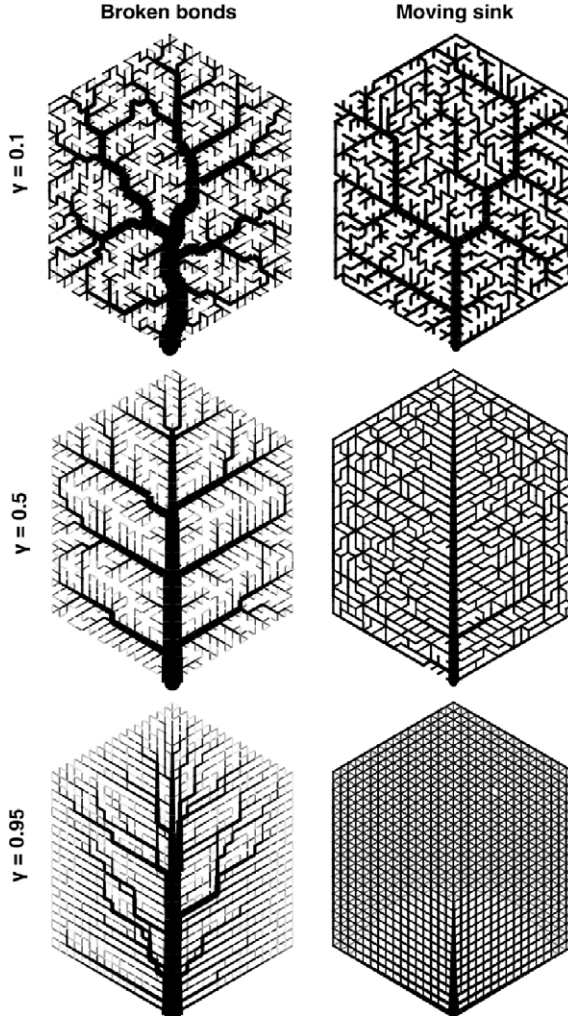


**Fig. 69.** Optimal networks for the resilience to damage (left) and to a fluctuating load (right panels).  
Source: From [282].

Following [282], we can introduce two variants of this model. The first one, which represents the resilience to damage is defined as follows. We cut a link  $e$  and compute for this system the total dissipated power denoted by  $P^e$ . The resilience to this damage can then be rephrased as the minimization of the functional

$$R = \sum_{e \in E} P^e. \quad (219)$$

Note that if breaking  $e$  disconnects the network, there is therefore one link with infinite resistance in the system and the dissipated power  $P^e$  is infinite. The finiteness of  $R$  implies the existence of loops in the optimal network. In another model, [282] Katifori et al. introduces time fluctuating load by introducing a system with one source at the stem of the leaf and one single moving sink at position  $a$ . For this system, one can compute the total dissipated power  $P^a$  and the resilience to fluctuations can be rephrased as the minimization of the functional

$$F = \sum_a P^a. \quad (220)$$

In these models, one observes the formation of loops (see Fig. 69), reminiscent of the ones seen in real leaves. These recent studies shed a new light in the formation and the evolution of real-world networks and open interesting directions of research. In particular, it would be very interesting to understand more quantitatively the condition of appearance of loops for example.

#### 4.6. Summary: effect of space on networks

We presented in this chapter the most important classes of models of spatial network formation. When spatial constraints are present, the network structure is affected and we summarize the main effects below.

- *Effect of space embedding on degree distribution, assortativity, clustering, and average shortest path.*

Spatial constraints imply that the tendency to connect to hubs is limited by the need to use small-range links. This explains why the degree distribution has a cut-off depending on the node density and the almost flat behavior observed for the assortativity. Connection costs also favor the formation of cliques between spatially close nodes and thus increase the clustering coefficient. The increasing tendency to establish connections in the geographical neighborhood leads to a large average shortest path. If the density of shortcuts is too low, the average shortest path can behave as  $N^{1/d}$  as in a  $d$ -dimensional lattice. In the opposite case, a large density of shortcuts leads to a logarithmic behavior typical of small-world networks.

- *Effect of space embedding on centrality.*

Spatial constraints also induce large betweenness centrality fluctuations. While hubs are usually very central, when space is important central nodes tend to get closer to the gravity center of all points. Correlations between spatial position and centrality compete with the usual correlations between degree and centrality, leading to the observed large fluctuations of centrality at fixed degree: many paths go through the neighborhood of the barycenter, reinforcing the centrality of less-connected nodes that happen to be in the right place; this yields larger fluctuations of the betweenness centrality and a larger number of ‘anomalies’.

- *Effect of spatial embedding on topology-traffic correlations.*

As we can see with growing network models where preferential attachment plays a role, spatial constraints induce strong nonlinear correlations between topology and traffic. The reason for this behavior is that spatial constraints favor the formation of regional hubs and reinforce locally the preferential attachment, leading for a given degree to a larger strength than the one observed without spatial constraints. Moreover, long-distance links can connect only to hubs, which yields a non-linear behavior of the distance-strength with values  $\beta_d > 1$ : the existence of constraints such as spatial distance selection induces some strong correlations between topology (degree) and non-topological quantities such as weights or distances.

- *Space and optimal networks.*

Spatial constraints combined with efficiency lead to a large variety of networks, with the existence of hub-and-spoke organization. Also, the emergence of complex structure in traffic organization could be explained by an optimization principle. In particular, strong correlations between distance and traffic arise naturally as a consequence of optimizing the average weighted shortest path. In the optimal network, long-range links carry large traffic and connect regional hubs dispatching traffic on a smaller scale ensuring an efficient global distribution. These results suggest that the organization of the traffic on complex networks and more generally the architecture of weighted networks could in part result from an evolutionary process. In the case of optimal networks, fluctuations and resilience to attack lead naturally to the formation of loops which shed some light on the evolution of various systems.

### 5. Processes on spatial networks

We will focus in this chapter on various processes which take place on spatial networks, and the guiding idea is to focus on the effects of space. In this respect, we will not address the general results concerning complex scale-free networks as there are already many reviews and books on these (see for example [7,9,10]), but we will try to address specifically effects which can be related to the spatial aspects of networks. In particular, we will essentially focus on studies using the small-world model with shortcuts located at random on a  $d$ -dimensional underlying lattice. This model which interpolates nicely between a ‘pure’ spatial lattice and a ‘pure’ random graph with one parameter only, represents an interesting playground to test theoretical ideas and models.

We will discuss six different processes. We will begin with the study of an Ising model on spatial networks, as it represents the archetype of phase transition and could be used in the modeling of very different systems. We will then discuss random walks and synchronization on spatial networks, followed by the important problem of navigating and searching in a spatial network. We will then discuss the robustness and resilience of spatial networks, having in mind more practical examples such as the robustness of power grids for example. Finally, we will discuss the effect of space on the spread of disease.

#### 5.1. Ising model

It is well known in statistical physics that long-range interactions affect the behavior of most systems (see for example [283]) and we expect that long shortcuts in the small-world lattice will indeed change the thermodynamics of the usual Ising model on a regular lattice. In this section, we start by recalling the main results on the Ising model on lattices and we will then review the results on spatial networks such as the Watts–Strogatz small-world and Apollonian networks. We will end this section with a general discussion on the effect of a spatial embedding on the critical behavior of phase transitions.

### 5.1.1. Generalities on the Ising model on lattices

The Ising model is a pillar of statistical physics and numerous books and reviews can be found on this subject. It was developed and studied in the framework of phase transitions, but the simplicity of the Ising model is the main reason for its ubiquity and for its various applications to many fields, even far from traditional physics. Indeed, in a first approach it is tempting for example to describe the behavior of an agent by a binary variable. It could be the answer ‘yes’ or ‘no’ to a certain question or the choice between ‘A’ or ‘B’ for example. The Ising model then appears as a very useful model for describing collective phenomena in social systems, such as opinion formation and dynamics for example (for applications of statistical physics to social systems, we refer the interested reader to the review [284] and references therein).

The Ising model is usually defined on a lattice and on each node, there is an Ising spin which is an object which can take two values only:  $\sigma_i = \pm 1$ . The interaction between spins is described by the Hamiltonian

$$H = - \sum_{i \neq j} J_{ij} \sigma_i \sigma_j \quad (221)$$

where  $J_{ij}$  represents the energy gain if two spins are aligned. The usual ferromagnetic Ising model on a lattice is obtained for  $J_{ij} = J > 0$  for neighbors on a lattice. At zero temperature  $T = 0$ , the ground state of the Hamiltonian equation (221) with ferromagnetic couplings is obtained for all spins aligned, and the magnetization is then  $M = \sum_i \sigma_i / N = \pm 1$ . Depending on the dimension of the lattice, we obtain different collective behaviors that we recall here briefly (for the ferromagnetic case).

- For one-dimensional systems, the ordered ferromagnetic configuration is obtained only for  $T = 0$  and there is no phase transition at finite temperature.
- For  $d \geq 2$ , the situation is different: at temperatures low enough, an ordered state is possible (with  $M = \pm 1$ ) while at high temperature this order is destroyed and  $M = 0$  (for large  $N$ ). The competition between the thermal agitation and the interaction leads in fact to a non-zero temperature transition  $T_c > 0$  (for  $N \rightarrow \infty$ ).
- The upper critical dimension of the Ising model is  $d_c = 4$  which means that above 4, the critical exponents are those of the mean-field obtained in the infinite dimensional case.
- In the infinite dimensional case, or equivalently in the case of a fully connected graph, the behavior of the Ising model is completely understood with the so-called mean-field theory. This approach is appropriate when the number of neighbors is very large, in which case fluctuations are negligible and only the average number of spins up and down is important.

### 5.1.2. Ising model on small-world networks

The first studies on the Ising model were done on lattices and later on planar networks. In particular, the critical behavior on a random planar lattice has been elucidated by Boulatov and Kazakov in an important paper [24]. More recently, Ising models were also studied on complex networks (see for example [7]) and we will focus here on the Watts–Strogatz network, where we will discuss the effect of long-range links on the nature and existence of a transition in the model.

In the complex network field, very quickly after Watts and Strogatz published their paper, Barrat and Weigt [215] studied the one-dimensional WS model, where at  $p = 0$  the network is a one-dimensional ring where each node is connected to its  $2m$  nearest neighbors by ferromagnetic bonds. In this situation the transition temperature is  $T_c = 0$  and the question is how the long-range links will modify this one-dimensional result. In [215], the authors use the replica approach to study this problem. They found that at high temperature, the paramagnetic phase is stable for any value of  $p$ . For small values of  $p$ , an expansion in terms of  $p\xi_0$  can be performed, where  $\xi_0 \sim \exp(Jm(m+1)/T)$  is the correlation length of the  $1d$  system, and implies that the first order approximation breaks down for  $p\xi_0 \sim 1$ . This result means that for finite  $p$ , there is a transition temperature given by [215]

$$T_c \sim \frac{1}{\log p}. \quad (222)$$

We can understand this result using the following argument. In the one-dimensional Ising model, the correlation length is  $\xi_0$ , which is the typical size of domains of correlated spins (i.e. having the same value). The average number of long-range links connected to a domain is then of order  $p\xi_0$  and it is thus clear that when  $p\xi_0 \gg 1$  the numerous shortcuts will lead to a mean-field behavior.

In [285], Herrero studied numerically the Ising model on WS networks constructed with lattices of larger dimensions ( $d = 2, 3$ ). In these networks, the presence of disorder, even small, leads to a change of universality class going from Ising-like at  $p = 0$  to mean-field type for  $p > 0$  (as signalled by mean-field values of the critical exponents). The  $1d$  argument for the transition temperature is also still correct and  $T_c$  is such that the spin correlation length  $\xi_0$  is of order the typical size of small-world clusters  $N^* \sim 1/p$  (see Section 4.3.1) leading to the behavior

$$T_c(p) \sim -1/\log p \quad (223)$$

for  $d = 1$ , and for  $d > 1$ :

$$T_c(p) - T_c(0) \sim p^{1/vd}. \quad (224)$$

Chatterjee and Sen [286] and Chang et al. [287] studied the Ising model on a one-dimensional WS network with shortcuts whose length is distributed according to  $P(\ell) \sim \ell^{-\alpha}$  (see [135] and Section 4.3.2). According to [286], there is a finite transition temperature for  $0 < \alpha < 2$ . Their results seem to indicate that for  $\alpha < 1$  the behavior is mean-field and that for  $1 < \alpha < 2$ , the system has a finite-dimensional behavior. This last result is however still under debate, as in [287] the numerical results seem to indicate that for the whole range  $0 < \alpha < 2$ , the behavior is mean-field like.

The Ising model was also studied on Apollonian networks in [199], where it is shown that for a model with decaying interaction constants of the form  $J_n \propto n^{-\alpha}$  (where  $n$  denotes the generation number), the critical temperature depends on the number of generations  $n$  as  $T_c(n) \sim n^{\tau(\alpha)}$ , where  $\tau$  varies continuously from  $\tau(0) = 1$  to  $\tau(\infty) = 1/2$ , indicating a new kind of critical behavior.

### 5.1.3. Critical fluctuations

In [288], Bradde et al. investigate from a general point of view the role of the spatial embedding on the critical behavior of phase transitions. They considered the Ising model as a prototype for studying the complex behavior induced by space. The Ising spins are located on the nodes of a  $d$ -dimensional Euclidean space and two nodes  $i$  and  $j$  are connected with a probability  $p_{ij}$ , which reads

$$p_{ij} \simeq \theta_i \theta_j J(|r_i - r_j|) \quad (225)$$

where  $r_{i(j)}$  denotes the position of node  $i(j)$ . The hidden variables  $\theta_i$  are found by fixing some conditions, such as the average degree for example.

The important quantity here appears to be the spectrum  $\rho(\lambda)$  associated to the matrix  $p_{ij}$  (which is similar to the adjacency matrix). We denote by  $\Lambda$  its largest eigenvalue, and by  $\lambda_c$  the spectral edge equal to the average value of the second largest eigenvalue  $\lambda_c = \langle \lambda_2 \rangle$  and such that for  $\lambda < \lambda_c$  the spectrum is self-averaging. The spectral gap is defined as  $\Delta_N \equiv \Lambda - \lambda_c$ . Under the assumption that the gap is self-averaging in the thermodynamic limit and  $\Delta_N \rightarrow \Delta$ , Bradde et al. distinguish two possible behaviors according to the value  $\Delta$ . If  $\Delta > 0$  when  $T \rightarrow T_c$ , the fluctuations are mean-field. If  $\Delta = 0$  then the fluctuations are mean-field or not depending on whether  $\rho(\lambda)$  is vanishing faster or slower than  $\lambda_c - \lambda$  close to the edge.

For homogeneous networks (obtained with  $\theta_i = \theta$ ), Bradde et al. recovered in the exponential case for  $J(r)$  the classical Ginsburg result stating that for  $d < 4$  critical fluctuations are relevant. For a power law behavior  $J(r) \sim r^{-\alpha}$  [289], the mean-field approximation is exact for  $d < \alpha < 3d/2$ , and for  $\alpha > 3d/2$ , non-trivial exponents are expected. For  $\alpha < d$ , a non-zero gap appears in the spectrum, suggesting a mean-field behavior. In addition, Bradde et al. studied the case of complex networks embedded in a  $d = 2$  space with a power-law degree distribution with exponent  $\gamma$  and with an exponential function for  $J(r) = \exp(-r/d_0)$ . For small  $d_0$ , the effect of space is important and we expect non-trivial effects of space with a spectrum close to  $\lambda_c$  behaving as  $\rho(\lambda) \sim (\lambda_c - \lambda)^\delta$ . For instance, they showed that for  $\gamma = 4$ , the mean-field behavior holds, while for a larger value  $\gamma = 6$ , the critical fluctuations are not captured by the mean-field. From a more general perspective, these first results seem to indicate that this approach opens interesting perspectives in the understanding of phase transitions in spatial complex networks.

## 5.2. Random walks in spatial networks

Random walks on graphs is an important and old subject in both statistical physics and in mathematics. Many books can be found on this subject (see for example [290]) and in this chapter we will focus on how shortcuts in a Watts–Strogatz network will affect the usual lattice behavior. For more results and details on random walks on general complex networks, we refer the interested reader to the review [14] or to the book [7]. We also note that random walks are also studied in connection with spectral graph theory, and we refer the interested reader to the book [40].

### 5.2.1. Quantifying the effect of shortcuts

The random walk can easily be defined on a  $d$ -dimensional lattice, for example in  $\mathbb{Z}^d$  where the walker jumps at every time step to one of its  $2d$  neighbors with equal probability. We just recall here the most important results.

If we denote by  $p_{ij}$  the probability that a walker at node  $i$  will jump to node  $j$ , the master equation for the probability  $P(i, t|i_0, 0)$  that a walker starting at node  $i_0$  at time  $t = 0$  is visiting the node  $i$  at time  $t$  is

$$\partial_t P(i, t|i_0, 0) = \sum_j A_{ji} p_{ji} P(j, t|i_0, 0) - A_{ij} p_{ij} P(i, t|i_0, 0) \quad (226)$$

where  $A_{ij}$  is the adjacency matrix. A usual choice for the transition rate is given by

$$p_{ij} = \frac{r}{k_i} \quad (227)$$

where  $k_i$  is the degree of node  $i$ . This choice corresponds to the case of uniform jumping probabilities to the neighbors of  $i$  and where  $r = \sum_j p_{ij}$  is the total escape rate. With this simple choice, the stationary solution of Eq. (226) is

$$P(i, \infty|i_0, 0) = \frac{k_i}{N\langle k \rangle} \quad (228)$$

**5.2.1.1. Return probability.** Many important quantities can be calculated with the use of the (modified) Laplacian operator on the network, which can be defined as

$$L_{ij} = k_i \delta_{ij} - A_{ij} \quad (229)$$

where  $k_i$  is the degree of node  $i$ . The link between random walks on a graph and spectral graph theory has been known for a long time (see for example [40]). In particular, the eigenvalue density  $\rho(\lambda)$  of this operator gives the return probability  $P_0(t)$  (which is the probability that starting from the origin the walker returns to it at time  $t$ )

$$P_0(t) = \int_0^\infty e^{-\lambda t} \rho(\lambda) d\lambda. \quad (230)$$

This relation implies, in particular, that the long time limit of  $P_0(t)$  is controlled by the behavior of  $\rho(\lambda)$  for  $\lambda \rightarrow 0$ .

For example, for a  $d$ -dimensional lattice, the spectral density behaves as [291]

$$\rho_L(\lambda) \sim \lambda^{d/2-1} \quad (231)$$

which gives the classical result

$$P_0^L(t) \sim \frac{1}{t^{d/2}}. \quad (232)$$

This quantity allows us to construct a typology of walks for an infinite lattice. For finite lattices, the walk is always recurrent and for an infinite lattice, the nature of the walk can be characterized by the behavior of the quantity

$$I = \int_0^T P_0(t) dt \quad (233)$$

for  $T \rightarrow \infty$ . We thus find the usual results, namely that for  $d \leq 2$ , the walk is recurrent and for  $d \geq 3$  it is transient.

In the case of an ER graph, Rodgers and Bray [292] showed that the density of states behaves as

$$\rho_{ER}(\lambda) \sim e^{-c/\sqrt{\lambda}} \quad (234)$$

leading to the following long time limit

$$P_0^{ER}(t) \sim e^{-at^{1/3}} \quad (235)$$

where  $a$  and  $c$  are non-universal parameters. In the case of the ER random graph the return probability thus decreases faster than the lattice: the random links allow the walker to explore other regions of the network and make its return more difficult.

If we now think of a  $d$ -dimensional variant of the Watts–Strogatz (see Section 4.3.1), we add a fraction  $p$  of shortcuts to a  $d$ -dimensional lattice and the natural question is how these shortcuts will affect the diffusion process. This problem was studied numerically in [293] and an analytical answer was given by Monasson in [294], who showed that the eigenvalue density for the WS model can be approximately written as

$$\rho_{WS}(\lambda) \sim \rho_L(\lambda) \times \rho_{ER}(\lambda) \sim \lambda^{d/2-1} e^{-p/\sqrt{\lambda}} \quad (236)$$

leading to the following behavior for the return probability

$$P_0(t) - P_0(\infty) \sim \begin{cases} t^{-d/2} & t \ll t_1 \\ e^{-(p^2 t)^{1/3}} & t \gg t_1 \end{cases} \quad (237)$$

where  $P_0(\infty) = 1/N$ , and where  $t_1$  is the crossover time. In the first regime, at short times, the walker does not encounter shortcuts and we recover the  $d$ -dimensional behavior. After a time  $t$ , the volume explored is of order  $V \sim t^{d/2}$  and the number of shortcuts in this volume is given by  $pV$ . The crossover time is thus such that  $pV \sim 1$ , leading to

$$t_1 \sim 1/p^{2/d}. \quad (238)$$

After this time, the walkers ‘feel’ the small-world nature of the network and we recover the ER behavior given by a stretched exponential.

**5.2.1.2. Number of distinct nodes, mean-square displacement and first-time return probability.** In [295], the authors study the effect of shortcuts on different quantities, such as the number  $N_{cov}$  of distinct sites visited at time  $t$  (which was also studied in [296]), the mean-square displacement  $\langle r^2(t) \rangle$  and the first-return time distribution.

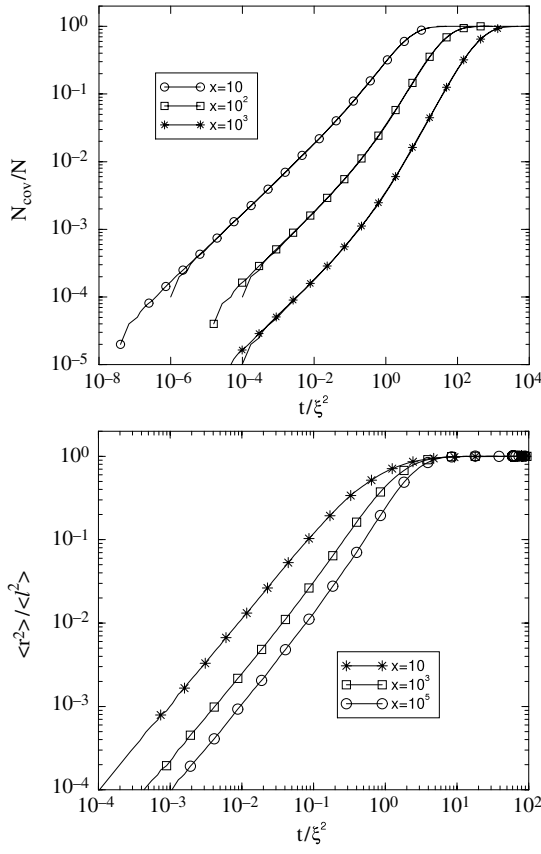


**Fig. 70.** (a) Rescaled number of distinct sites visited at time  $t$  versus the rescaled time. The symbols correspond to different values of  $x$  (circles:  $x = 10$ , squares:  $x = 10^2$ , stars:  $x = 10^3$ ) and for each value of  $x$  two values of  $p$  are used (0.0002 and 0.01). The collapse is very good, making it difficult to identify the two curves for each  $x$ . (b) Rescaled mean-square displacement versus rescaled time, showing a perfect collapse (for each  $x$  there are two curves for two different values of  $p$ ).  
Source: From [295].

In the case of  $d$ -dimensional lattices and with a transition probability  $p_{ij} = 1/k_i$ , Dvoretzky and Erdos [297] studied the average number of distinct sites and found the following behavior

$$N_{cov}(t) \sim \begin{cases} \sqrt{t} & d = 1 \\ t/\ln t & d = 2 \\ t & d \geq 3. \end{cases} \quad (239)$$

In the case of a one-dimensional WS network with a probability  $p$  to have a shortcut and an average number of shortcuts given by  $x = pN$ , these behaviors will be modified and simple scaling arguments can help us to understand the effect of the shortcuts [295]. In the WS network, the typical size of a cluster is  $\xi \sim 1/p$  (see Section 4.3.1) and for a time  $t \ll \xi^2$ , the random walker does not encounter any shortcuts and we expect a lattice-like behavior with  $N_{cov} \sim \sqrt{t}$ . For very large times  $t \gg N\xi$ , the walker has visited the whole network and we have  $N_{cov} \sim N$ . For intermediate times  $\xi^2 \ll t \ll N\xi$ , the walker spends on average a time  $t_1 \sim \xi^2$  before encountering a shortcut. At time  $t$  the number of shortcuts and thus of different segments visited is  $t/t_1 \sim t/\xi^2$  and the total number of distinct visited sites is then  $N_{cov} \sim (t/\xi^2) \times \xi^2 \sim t$  [295, 296]. We can summarize these behaviors in the following scaling form

$$N_{cov} = NS \left( \frac{t}{\xi^2}, x \right) \quad (240)$$

with

$$S(y, x) \sim \begin{cases} \sqrt{y}/x, & y \ll 1 \\ y/x, & 1 \ll y \ll x \\ 1, & y \gg x. \end{cases} \quad (241)$$

This scaling is confirmed by the excellent collapse observed numerically (see Fig. 70).

A similar line of reasoning can be applied to the mean-square displacement  $\langle r^2(t) \rangle$ , where the distance is here computed in terms of hops from the origin (i.e. the length of the shortest path from the origin to the node where the walker is located). On a  $d$ -dimensional lattice the mean-square displacement behaves as  $\langle r^2(t) \rangle \sim t$ , a behavior that we expect on the WS networks for times such that  $t \ll \xi^2$ . For large times, the mean-squared displacement saturates to a value equal to the diameter squared (we recall here that the diameter is defined as the maximum of all distances between pairs and is well approximated by the average shortest path  $\langle \ell \rangle$ ) and the saturation thus reads  $\langle r^2(t) \rangle \rightarrow \langle \ell \rangle^2$ . These behaviors can be encoded in the following scaling form [295]

$$\langle r^2(t) \rangle = \langle \ell \rangle^2 R\left(\frac{t}{\xi^2}, x\right) \quad (242)$$

with

$$R(y, x) \sim \begin{cases} y/\langle \ell \rangle^2 & t \ll \xi^2 \\ 1 & t \gg \xi^2 \end{cases} \quad (243)$$

which is confirmed numerically (see Fig. 70).

### 5.2.2. Diffusion on power law Watts–Strogatz networks

In [298], Kozma et al. study diffusion in a  $d$ -dimensional Watts–Strogatz networks of linear size  $L$ , where the shortcuts are connecting two nodes  $i$  and  $j$  (located at  $r$  and  $r'$ , respectively) with a probability decaying as  $p|r - r'|^{-\alpha}$ . The exponent  $\alpha$  thus characterizes the length of shortcuts and  $p$  is essentially the probability of a site to have a shortcut. Analytical calculations are simpler in the case (which is believed not to modify the universality) where multiple links are allowed with a Poisson distribution of links with average  $p/\mathcal{N}|r - r'|^\alpha$ , where  $\mathcal{N}$  is a normalization constant.

The equation studied in [298] and which describes the random walk process is

$$\partial_t P(r, t) = - \sum_{r'} (\Delta_{rr'} + q \Delta_{rr'}^{rand}) P(r', t) \quad (244)$$

where  $P(r, t)$  is the probability to find the walker at site  $r$  at time  $t$ ,  $-\Delta_{rr'}$  is the discretized Laplace (diffusion) operator. For example for  $d = 1$ , one has  $-\Delta_{ij} M_j = M_{i+1} - M_i - (M_i - M_{i-1})$  giving

$$\Delta_{ij} = 2\delta_{i,j} - \delta_{j,i-1} - \delta_{j,i+1}. \quad (245)$$

The quantity  $-\Delta_{rr'}^{rand}$  is the diffusion operator for the random links with diffusion coefficient  $q$ . On the  $d = 1$  lattice, one has  $\Delta_{ij}^{rand} = \delta_{ij} \sum_{l \neq i} J_{il} - J_{ij}$ , where  $J_{ij}$  is the number of links connecting the nodes  $i$  and  $j$ .

The Green's function  $G(r, r', t)$  for this model is the solution of Eq. (244) with the initial condition  $G(r, r', t = 0) = \delta(r - r')$ . The Fourier transformed Green's function in the limit  $\omega \rightarrow 0$

$$G(r, r') = \lim_{\omega \rightarrow 0} (i\omega + \Delta + q \Delta^{rand})^{-1}(r, r') \quad (246)$$

averaged over disorder gives a translation invariant quantity depending on  $|r - r'|$  only. For  $r = r'$ , we obtain  $\langle G(0) \rangle$ , which is related to the return probability (and is in fact the quantity  $I$  defined in Eq. (233)) and its scaling with the size  $L \rightarrow \infty$  determines if the random walk is transient or recurrent.

The authors of [298] used a self-consistent perturbation theory and obtained the phase diagram for all dimensions and values of  $\alpha$  (a detailed version of this work can be found in [299]). The results in the one-dimensional case can be summarized in Fig. 71, where a comparison is made with an annealed approximation where  $\Delta^{rand}$  is replaced by its average. In particular, for  $d = 1$ , these results are in agreement with the analysis presented in [217], which predicted  $\alpha = 2$  as a crossover between a recurrent and transient regime. In other words, for  $\alpha \geq 2$  the shortcuts do not affect the lattice behavior, while when  $\alpha < 2$  there are long shortcuts leading to entirely different regions of the networks. They modify qualitatively the lattice behavior and make it look like a large  $d$ -dimensional lattice, in agreement with other processes such as spin models where the mean-field behavior is recovered for  $p \neq 0$  (in the case  $\alpha = 0$ ).

### 5.3. Synchronization

Many natural phenomena can be described as a set of coupled oscillators. This is the case for cardiac cells, fireflies, etc. The synchronization properties depend on the coupling pattern, and many studies were devoted to the effect of the coupling network structure (see the review [277]).

Each oscillator  $i$  can be described by a scalar degree of freedom  $\phi_i$ , and each unit evolves according to an internal dynamics governed by  $\dot{\phi}_i = f(\phi_i)$ . If these oscillators are linearly coupled by a network, the output is a linear superposition of the outputs of the neighboring units and the evolution equations take the form of

$$\frac{d\phi_i}{dt} = f(\phi_i) + \sigma \sum_j C_{ij} h(\phi_j) \quad (247)$$

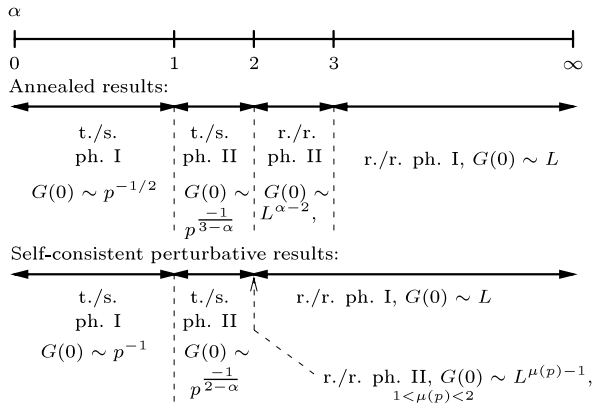


**Fig. 71.** Phase diagram for  $d = 1$ . The annealed approximation shows some differences with the self-consistent approximation for the quenched case. In the quenched case, the walk is transient for  $\alpha < 2$  and recurrent for  $\alpha \geq 2$ .

Source: From [298].

where  $C_{ij}$  is the coupling matrix,  $\sigma$  is the interaction strength and  $h$  a fixed output function. An important case corresponds to  $C_{ij} = L_{ij}$ , where  $L$  is the graph Laplacian. In an important paper, Pecora and Carroll [43] showed that the stability of synchronized solutions is related to the ratio

$$e = \frac{\lambda_N}{\lambda_1} \quad (248)$$

and that the smaller  $e$ , the more stable the synchronized solutions.

After Watts and Strogatz published their paper [3], synchronization properties were studied on SW networks, which showed that these networks were both able to sustain fast response, due to the long-range links, and coherent oscillations, thanks to the large clustering [173]. In particular, the ratio  $e$  was determined for SW networks [44], where additional edges are randomly wired on a one-dimensional ring. They obtained the general result that the small-world topology exhibits better synchronizability properties than ordered rings (but with less stability [300]) and that it can be achieved with a small density of shortcuts [301].

Finally, let us mention [302], which presents a study of coherence in various networks, including Apollonian networks (see [199] and Section 4.1.4). The main result is that for the Apollonian network, the coupling threshold beyond which coherence disappears decreases when the heterogeneity is increased. Also, the transition to coherence in this case is shown to be of the first order [302].

## 5.4. Navigating and searching

### 5.4.1. Searchable networks

The original 1967 experiment of Milgram [303], showing that the average shortest path in North-America is around 6, raises a number of questions. The first one is about the structure of the social network, and it is now relatively clear that enough shortcuts will modify the scaling of  $\langle \ell \rangle$  and induce a logarithmic behavior. Another question raised by Kleinberg [135] is actually how a node can find a target efficiently with only a local knowledge of the network (the answer being trivial if you know the whole network). It thus seems that in some way the social network is search-efficient, or is a *searchable* or *navigable* network, meaning that the shortcuts are easy to find, even by having access to local information only. In these cases, one speaks of navigability or searchability when the greedy search is efficient.

This problem goes beyond social networks, as decentralized searches, where nodes only possess local information (such as the degree or the location of their neighbors for example), in complex networks have many applications, ranging from sensor data in wireless sensor networks, and locating data files in peer-to-peer networks, to finding information in distributed databases (see for examples [304] and references therein). It is thus important to understand the efficiency of local search routines and the effect of the network structure on such decentralized algorithms.

In the case of social networks, it seems that they are composed by a spatial part constituted of the neighbors of a node belonging to its spatial neighborhood (such as in a regular lattice) and a purely social component, not correlated to space and which can connect regions which are geographically very far apart. In a search process, it is thus natural to try those links which open the way to very different parts of the world (in Milgram's experiment it is indeed interesting to note that individuals were passing the message only according to geography or proximity in the space of professional activities [305], as it was known to them that the target individual was a lawyer). In order to quantify this, Kleinberg [135] constructed a  $d$ -dimensional Watts–Strogatz model where each node  $i$  of the lattice

- (i) is connected to all neighbors such that their lattice distance is less than  $p$  (with  $p \geq 1$ ).

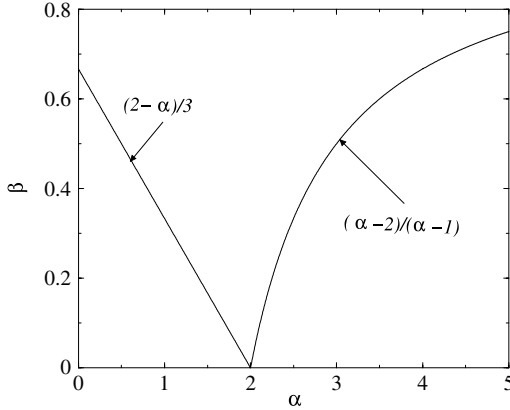


**Fig. 72.** Lower bounds for the two-dimensional case of the exponent governing the behavior of the average delivery time  $\bar{T}$  as a function of the exponent  $\alpha$  controlling the distribution of shortcuts. After [135].

- (ii) has  $q$  shortcuts to node  $j$  with a probability decreasing with the distance

$$p(i \rightarrow j) \sim d_E(i, j)^{-\alpha} \quad (249)$$

where  $\alpha$  is a tunable parameter.

The search process is the following one: a message needs to be sent to a target node  $t$  whose geographical position is known, and a node  $i$  which receives the message forwards it to one of its neighbor  $j$  that is the closest (geographically) to  $t$ . This is the simplest decentralized algorithm that we can construct (and which requires only geographical information). The most important figure of merit for this type of algorithm is the delivery time  $T$  (or its average  $\bar{T}$ , which is easier to estimate analytically) and its scaling with the number of nodes  $N$ . Kleinberg found bounds on the exponent of  $\bar{T}$  (see Fig. 72) and the important result is that the delivery time is optimal for  $\alpha = d$ , for which it scales as  $\log^2 N$ , while for  $\alpha \neq d$ , it scales faster (as a power of  $N$ ). This behavior can be intuitively understood: for  $\alpha > d$ , long links are rare and the network looks essentially like a lattice (with renormalized spacing). In the opposite case  $\alpha < d$ , shortcuts are all long and not necessarily useful. The best case is obtained when the shortcuts explore all spatial scales, which is obtained for  $\alpha = d$  (This result was extended in [306] to the case of small-world network constructed by adding shortcuts to a fractal set of dimension  $d_f$ ).

#### 5.4.2. Sketch of Kleinberg's proof

Inspired from Kleinberg's original rigorous derivation [307] of the bounds shown in Fig. 72, we can give the following hand-waving arguments in order to grasp some intuition on the effects of the link distribution on the average number of steps to reach a target in a decentralized algorithm (we will discuss in detail here for the case for  $d = 2$  but the extension to a generic  $d$  is trivial). For the interested reader, we also note that a detailed study of the  $d = 1$  case is done in [308], that exact asymptotic results were obtained in [309], and that the 'greedy' paths connecting a source to the target were studied in [310] by defining a greedy connectivity.

For  $\alpha = 2$  (and we assume here that  $p = q = 1$ ), the probability to jump from node  $u$  to node  $v$  is given by

$$P(u \rightarrow v) = \frac{1}{Z} \frac{1}{d_E(u, v)^2} \quad (250)$$

where  $Z$  is the normalization constant given by

$$Z = \sum_{v \neq u} \frac{1}{d_E(u, v)^2} \simeq 2\pi \int_1^{N/2} \frac{r dr}{r^2} \simeq 2\pi \ln N \quad (251)$$

implying that  $P(u \rightarrow v) \sim 1/\ln N d_E(u, v)^2$  (here and in the following we will use continuous approximation and neglect irrelevant prefactors, for rigorous bounds we refer to [307]). Following Kleinberg [307], we say that the execution of the algorithm is in phase  $j$  when the lattice distance  $d$  from the current node (which is holding the message) is such that  $2^j \leq d < 2^{j+1}$ . The largest phase is then  $\ln N$  and the smallest 0 when the message reaches the target node. The goal at this point is to compute the average number of steps  $\bar{T}$  to reach the target. For this we decompose the problem into computing the average time duration  $\bar{T}_j$  that the message stays in phase  $j$ . For this we have to compute the probability that the message leaves the phase  $j$  and jumps in the domain  $B_j$ , defined as the set of nodes within a distance  $2^j$  to the target node  $t$  (see Fig. 73). The size of this set  $B_j$  is  $|B_j| \sim 2^{2j}$  and the distance between  $u$  and any node of  $B_j$  is  $d(u, v \in B_j) \leq 2^{j+2}$ . The

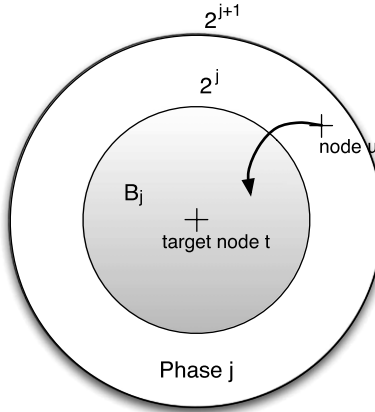


**Fig. 73.** Line: jump out of the phase  $j$  into the domain  $B_j$ .

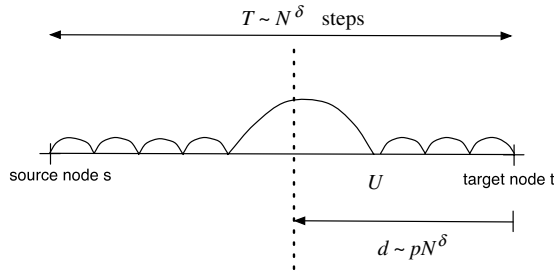


**Fig. 74.** One dimensional representation of Kleinberg's theorem in the case  $\alpha < 2$ .

probability to get out of phase  $j$  by using a long-range link is thus

$$P_{out} \sim \frac{|B_j|}{(2^{j+2})^2 \ln N} \sim \frac{1}{\ln N} \quad (252)$$

(the actual exact bound found by Kleinberg is  $P_{out} \geq 1/(136 \ln N)$ ). We then have  $P(T_j = i) = [1 - P_{out}]^i P_{out}$ , from which we obtain  $\bar{T}_j \sim \ln N$ . The average time to reach the target is then

$$\bar{T} = \sum_{j=0}^{\ln N} \bar{T}_j \sim \ln^2 N \quad (253)$$

which is the minimum time obtained for a decentralized algorithm for  $\alpha = 2$  (and  $\alpha = d$  for the general  $d$ -dimensional case).

We now consider the minimum scaling of  $\bar{T}$  in the case  $\alpha < 2$  (and general  $p$  and  $q$ ). The normalization constant behaves then as

$$\begin{aligned} Z &= \sum_{v \neq u} d_E(u, v)^{-\alpha} \simeq 2\pi \int_1^{N/2} r^{-\alpha} r dr \\ &\sim \left(\frac{N}{2}\right)^{2-\alpha}. \end{aligned} \quad (254)$$

We assume now that the minimum number of steps to reach the target scales as  $N^\delta$ . In this case, there is necessarily a last step along a long-range link leading to a node which is different from the target node and which is in the region  $U$  centered at  $t$  and of size  $\sim pN^\delta$  (Fig. 74). The probability  $P_i$  that this long-range link leading to  $U$  at step  $i$  is given by

$$P_i \leq \frac{q|U|}{Z} \sim N^{2\delta-2+\alpha} \quad (255)$$

and the probability that it happens at any step less than  $N^\delta$  is

$$P = \sum_{i \leq N^\delta} P_i \leq N^{3\delta-2+\alpha}. \quad (256)$$

This probability is non-zero only if  $3\delta - 2 + \alpha \geq 0$ , leading to the minimum possible value for  $\delta$  such that  $\bar{T} \sim N^\delta$

$$\delta_{min} = \frac{2 - \alpha}{3} \quad (257)$$

(the  $d$ -dimensional generalization would give  $\delta_{min} = (d - \alpha)/(d + 1)$ ).

In the last case,  $\alpha > 2$ , we will have mostly short links and the probability to have a link larger than  $m$  is given by

$$\begin{aligned} P(d_E(u, v) > m) &\sim \int_m^N \frac{r dr}{r^\alpha} \\ &\sim m^{2-\alpha}. \end{aligned} \quad (258)$$

In the following we will use the notation  $\epsilon = \alpha - 2$ . The probability to have a jump larger than  $N^\gamma$  for  $T < N^\beta$  is then given by

$$\begin{aligned} P(N^\gamma, T < N^\beta) &\sim qN^\beta(N^\gamma)^{-\epsilon} \\ &\sim qN^{\beta-\gamma\epsilon}. \end{aligned} \quad (259)$$

This probability will be non-zero for

$$\beta - \gamma\epsilon \geq 0. \quad (260)$$

Also, if at every step during a time  $T \sim N^\beta$ , we perform a jump of size  $N^\gamma$ , the traveled distance must be of order  $N$ , which implies that  $N^\beta N^\gamma \sim N$ , leading to the condition  $\beta + \gamma = 1$ . This last condition together with Eq. (260) leads to the minimum value of  $\beta$

$$\beta_{min} = \frac{\alpha - 2}{\alpha - 1} \quad (261)$$

which can be easily generalized to  $(\alpha - d)/(\alpha - d + 1)$  in  $d$ -dimensions. We thus recover the bounds  $\delta_{min}$  and  $\beta_{min}$  shown in Fig. 72.

#### 5.4.3. Searching in spatial scale-free networks

Kleinberg thus showed that a simple greedy search passing the message to the neighbor which is the nearest to the target is then able to find its target in a logarithmic time for a lattice with  $\alpha = d$ . The lattice considered in Kleinberg's paper is a variant of the WS model and has a low degree heterogeneity. When a large degree heterogeneity is present it is not clear that the greedy search used in [135] will work well, as it might be best to jump to a hub even if there is neighbor closer to the target node. In order to understand the effect of heterogeneity in spatial networks, Thadakamalla et al. [304] studied decentralized searches in a family of spatial scale-free networks where the nodes are located in a  $d$ -dimensional space:

- With probability  $1 - p$  a new node  $n$  is added and is connected to an existing node  $i$  with a preferential attachment probability weighted by the distance (see Section 4.4)

$$\Pi_{n \rightarrow i} \propto k_i F(d_E(i, j)) \quad (262)$$

where  $F(d)$  is a decreasing function of distance (and can be chosen as a power law  $d^{-\sigma}$ ) or as an exponential  $\exp(-d/d_0)$ .

- With probability  $p$ , a new edge connects existing nodes with probability

$$\Pi_{i \leftrightarrow j} \propto k_i k_j F(d_E(i, j)) \quad (263)$$

The authors of [304] investigated the following search algorithms, which cover a broad spectrum of possibilities:

- Random walk*: The message goes from a node to one of its randomly chosen neighbors.
- High-degree search*: The node passes the message to the neighbor which has the largest degree. This algorithm is already very efficient for a non-spatial network [311].
- Greedy search*: This is the algorithm used in Kleinberg's study [135] and where the node  $i$  passes the message to the neighbor which is the closest to the target (i.e. with the smallest  $d_E(i, t)$ ).
- Algorithms 4–8*: The node passes the message to the neighbor which minimizes a function  $F[k_i, d_E(i, t)]$  which depends both on the degree of the node and its distance to the target. The functions  $F$  considered here are: (i)  $F_1[k, d] = d - f(k)$  where  $f(k)$  is the expected maximum length of an edge from a node with degree  $k$ ; (ii)  $F_2[k, d] \propto d^k$ ; (iii)  $F_3[k, d] = d/k$ ; (iv)  $F_4[k, d] \propto d^{\ln k + 1}$ ; (v)  $F_5[k, d] = d/(\ln k + 1)$ .

The main result obtained in [304] is that algorithms (4–8) perform very well and are able to find a path between the source and the target whose length is at most one hop more than the average shortest path. This result is surprising: the calculation of the shortest average path requires the knowledge of the whole network, while the algorithms used here have only local information. This success can be attributed to the fact that the scale-free networks considered in this study have hubs which allow one efficiently to find the target. It should also be noted that the greedy search performance is not too bad,

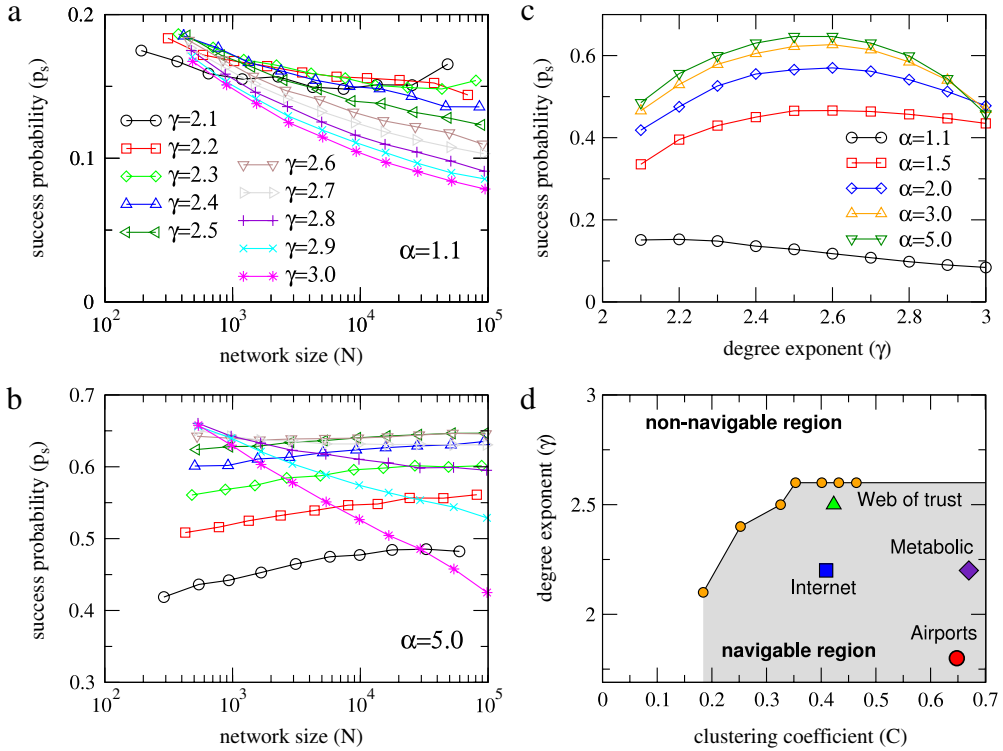


**Fig. 75.** (a), (b) Success probability  $p_s$  versus  $N$  for various values of  $\gamma$  and for (a) weak clustering and (b) strong clustering. (c) Success probability  $p_s$  versus  $\gamma$  for various values of  $\alpha$  and for fixed system size  $N \approx 10^5$ . (d) The solid line separates the navigable from the non-navigable region.  
Source: From [313].

but has the severe drawback that in some cases it does not find the target and stays stuck in a loop, which never happens with algorithms (4–8). Similar results were obtained for different values of  $p$  and  $\sigma$ . These results allow the authors to claim that the class of spatial networks considered here belong to the class of searchable networks. The authors checked with these different algorithms that it is also the case for the US airline network.

Finally, we mention Hajra and Sen [312] who studied the effect of the transition scale-free/homogeneous network ([226] and Section 4.4.2.2) on the navigability for three different search algorithms. In particular, they showed that the effect of the transition on navigability is marginal and is the most pronounced on the highest degree-based search strategy, which is less efficient in the power-law regime.

#### 5.4.4. Navigability and metric space

In [313], Boguñá et al. studied the navigability on a network constructed on a hidden metric space (see Section 4.2.3) where the probability to connect two nodes (with degree  $k$  and  $k'$  drawn from  $P(k) \sim k^{-\gamma}$ ) lying for example on a one-dimensional space is given by

$$r(d; k, k') = \left(1 + \frac{d}{d_c(k, k')} \right)^{-\alpha} \quad (264)$$

where  $\alpha > 1$  controls the clustering (the larger the  $\alpha$ , the larger the clustering coefficient) and where  $d_c(k, k') \sim kk'$  (other forms are possible). Boguñá, Krioukov and Claffy analyzed the result of a greedy algorithm on these networks with different values of  $\alpha$  and  $\gamma$  and found that the average shortest path decreases with smaller  $\gamma$  and larger  $\alpha$ . A large clustering and degree homogeneity thus favors the greedy algorithm, a somewhat expected result, since hubs allow a fast routing and large clustering an efficient local search. Strong clustering also favors the fraction of successful paths (i.e. finding the target). If  $\gamma$  is too large (larger than 2.6), the percentage of successful paths becomes too small, which is related to the small number of hubs. These results can be summarized in Fig. 75d, where real-world networks are shown in the clustering-degree distribution exponent plane ( $C, \gamma$ ). The solid lines indicate the separation between a navigable region and a non-navigable one where the efficiency of the greedy algorithm decreases with the system size. Interestingly enough, we see that all the real-world examples of communication and transportation, social and biological networks considered here are in the navigable region.

These various results (summarized in [196]) show that many real-world networks are navigable, which means that they support efficient communication without a global knowledge of the network. From a more theoretical perspective, the

authors of [196] suggest the interesting idea that real-world networks have an underlying hidden metric space which could be the source of their navigability.

However, in the case of the Internet it is important to note that the navigability is not due to the knowledge of geography alone. Indeed, the Internet can be mapped to a hyperbolic space [314], but the distance in this hyperbolic space encodes multiple factors (such as geography and also political, economical, communities, etc.), so that navigability results from a combination of all these factors.

#### 5.4.5. Effect of cost

In [315], Li et al. study navigability on a Watts–Strogatz network constructed on a two-dimensional square lattice where the pairs of nodes are connected with a probability  $p \sim 1/d^\alpha$ . The important difference from the case considered by Kleinberg [135] is that there is cost associated to the long-range shortcuts and that their number is limited by a total value  $\sum_{ij} d_E(i, j) < \Lambda$ , where  $\Lambda$  represents the amount of resources available for the shortcuts. Li et al. study, in particular, the average delivery time and found numerically that it has a minimum value for  $\alpha \approx 3$  (and  $\alpha = 2$  for  $d = 1$ ), suggesting that the optimal value might be  $\alpha = d + 1$ , in contrast with Kleinberg's result  $\alpha = d$ . In addition, the optimal delivery time seems to behave as  $N^{1/d}$ , in sharp contrast with the behavior  $(\log N)^2$  obtained by Kleinberg. These results suggest that cost constraints are relevant for the navigability condition, and it would be interesting to extend Kleinberg's result in this case and to understand the main mechanisms and how Kleinberg's derivation is affected by the cost constraint.

#### 5.4.6. Routing in social networks

In [136], the authors tested navigability on a social network of bloggers and showed that geographic information is sufficient to perform global routing (as in Kleinberg's case on a small-world network [135]) in a non-negligible fraction of cases: for 13% of the source-target pairs, the message reaches the target based on geographic information only. On the other hand, these authors also showed that the probability for two nodes separated by a distance  $d$  decays as  $P(d) \sim 1/d^\alpha$  with  $\alpha \approx 1$  (see Section 3.2.4). We are thus facing an apparent contradiction here: for a two-dimensional space (which is a good approximation of the US), the navigability is obtained for  $\alpha = 2$  according to Kleinberg's result and not for  $\alpha = 1$  (see previous section). The authors of [136] suggest in fact that the Kleinberg navigability condition can be generalized for different networks and is obtained when the probability  $P(u, v)$  that two nodes are connected scales as

$$P(u, v) \sim \frac{1}{R(u, v)} \quad (265)$$

where  $R(u, v)$  is the ‘rank’ of  $v$  with respect to  $u$ , and counts the number of individuals living between  $u$  and  $v$ . This results from the argument that distance alone has no meaning and that one should include the density. Indeed, two individuals separated by a distance of 500 m in rural areas probably know each other, which is certainly not the case in a dense urban area. If the two-dimensional density  $\rho$  is uniform, the rank then scales with distance  $d$  as

$$R \sim d^2 \quad (266)$$

which leads to  $P(d) \sim 1/d^2$  and the navigability condition  $\alpha = d$  is recovered. The navigability condition of Kleinberg thus implicitly assumes a uniform density and could be modified for other distributions. Indeed, the authors of [136] showed that networks based on the friendship condition of Eq. (265) are indeed navigable and contain discoverable shortcuts. The apparent paradox is thus solved: for the social network studied in [136], we observe  $R \sim d$ , which explains  $P(d) \sim 1/d$  and the network still being navigable.

#### 5.5. Effect of space on robustness and resilience

Many important infrastructures in modern society are structured in the form of networks, and it is natural to question their robustness. Large-scale collapses, such as blackouts or Internet outages, are spectacular illustrations of this problem. Indeed, very quickly after the first publications on small-worlds and scale-free networks, the first studies on robustness appeared [316]. In particular, an important distinction appeared between robustness in the case of random failures and in the case of targeted attacks. In particular, one of the most important results [316] states that scale-free networks are very resilient to random failures but very sensitive to targeted attacks, on hubs for example.

We will review in this chapter, essentially two types of study which considered the effect of space on the resilience of networks. The first type concerns percolation studies which analyze the effect of the underlying lattice on the breaking process. Other studies considered the effects of additional shortcuts on a lattice with the study of Watts–Strogatz networks. Another set of studies focused on the vulnerability of power grids and on the failure cascade process.

##### 5.5.1. Percolation and small-worlds

The topological effect of the removal of bonds or nodes can be understood in the framework of percolation (see for example the books [129,317]). In the case of regular lattices and bond percolation with a probability  $p$  that a bond is present,

we observe a percolation transition at a finite, non-universal value  $p_c$  which depends on the lattice. Below the threshold, we observe finite clusters whose size diverges at  $p_c$  (which is  $p_c = 1/2$  for a 2d square lattice and behaves as  $p_c \sim 1/2d$  for large dimensions  $d$ ). At the threshold there is a giant component, or infinite percolating cluster, which has a universal fractal dimension  $d_f$  independent of the lattice. In addition, in the vicinity of  $p_c$ , the correlation length  $\xi$ , which measures the linear size of finite clusters, and the probability  $P_\infty$  for a node to belong to the infinite percolating cluster scale as

$$\xi \sim |p_c - p|^{-\nu} \quad (267)$$

$$P_\infty \sim (p - p_c)\beta \quad (268)$$

where the exponents in the two dimensional case are  $\beta_2 = 5/36$ , and  $\nu_2 = 4/3$  and in the mean-field case (i.e. for  $d \geq 6$ ) are  $\beta_{MF} = 1$  and  $\nu_{MF} = 1/2$ .

The natural question to ask at this point concerns the effect of shortcuts on this standard percolation behavior. In [318, 319], the authors use a generating function formalism in order to compute various quantities, and we briefly recall this derivation for the one-dimensional WS network where each site is connected to its  $k$ th nearest neighbors and where additional shortcuts are added between randomly chosen pairs of sites with probability  $\phi$ , giving an average of  $\phi kN$  shortcuts in total. The first quantity which is needed is the generating function

$$H(z) = \sum_{n=0}^{\infty} P(n)z^n \quad (269)$$

where  $P(n)$  denotes the probability that a randomly chosen node belongs to a cluster of  $n$  sites other than the giant percolating cluster. In other words, below the transition  $H(1) = 1$  and above the percolation threshold, we have  $H(1) = 1 - P_\infty$ . The quantity  $P_0(n)$ , which is the probability that a randomly chosen node belongs to a cluster of  $n$  sites on the underlying lattice, is given by (for the one-dimensional case and for  $n > 0$ )

$$P_0(n) = npq^{n-1}(1-q)^2 \quad (270)$$

where  $q = 1 - (1-p)^k$ . We now define the probability  $P(m|n)$  that there are exactly  $m$  shortcuts emerging from a cluster of size  $n$ , which is given by

$$P(m|n) = \binom{2\phi kN}{m} \left[ \frac{n}{N} \right]^m \left[ 1 - \frac{n}{N} \right]^{2\phi kN - m} \quad (271)$$

which indeed represents the number of possible ways to choose  $m$  end shortcuts with uniform probability  $n/N$  within a total of  $2\phi kN$ .

If we assume that there are no loops involving shortcuts, we can now write a recursive equation on  $H(z)$  by noticing that a finite cluster consists of a local cluster of  $n$  sites and with  $m$  shortcuts leading to other clusters

$$H(z) = \sum_{n=0}^{\infty} P_0(n)z^n \sum_{m=0}^{\infty} P(m|n)[H(z)]^m \quad (272)$$

(this equation can be understood if we note that the prefactor of  $z^l$  is the probability to belong to a finite cluster of size  $l$ ). For large  $N$ , we then obtain

$$H(z) = H_0(z e^{2\phi k(H(z)-1)}) \quad (273)$$

where

$$H_0(z) = 1 - p + pz \frac{(1-q)^2}{(1-qz)^2}. \quad (274)$$

From this Eq. (273), we can then estimate various quantities such as the average cluster size

$$\langle s \rangle = H'(1) = \frac{p(1+q)}{1-q-2k\phi p(1+q)}. \quad (275)$$

At the percolation threshold  $p = p_c$ , this size diverges and we thus obtain an implicit equation for the threshold

$$\phi = \frac{(1-p_c)^k}{2kp_c(2-(1-p_c)^k)}. \quad (276)$$

The numerical solution for the percolation threshold versus the density of shortcuts  $\phi$  is shown in Fig. 76. Close to  $p_c$  we also obtain  $\langle s \rangle \sim (p_c - p)^{1/\sigma}$  with  $\sigma = 1$ ,  $P(n) \sim n^{-\tau} e^{-n/n^*}$  with  $\tau = 3/2$ .

These values  $\tau = 3/2$  and  $\sigma = 1$  correspond actually to the mean-field values of percolation. This result means that the shortcuts not only modify the percolation threshold (which is expected since  $p_c$  is not universal) but also the universality class: the WS model resembles more a random graph in infinite dimension. This result is actually consistent

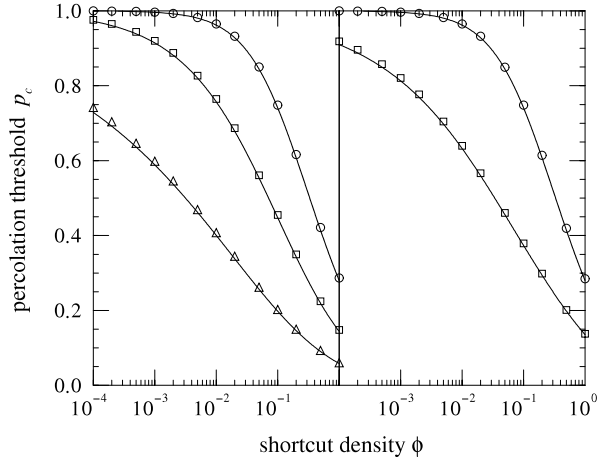


**Fig. 76.** Numerical solution for the percolation threshold for  $N = 10^6$  for site and bond percolation (shown left and right, respectively). Circles represent the case  $k = 1$ , squares  $k = 2$ , and triangles  $k = 5$ .

Source: From [319].

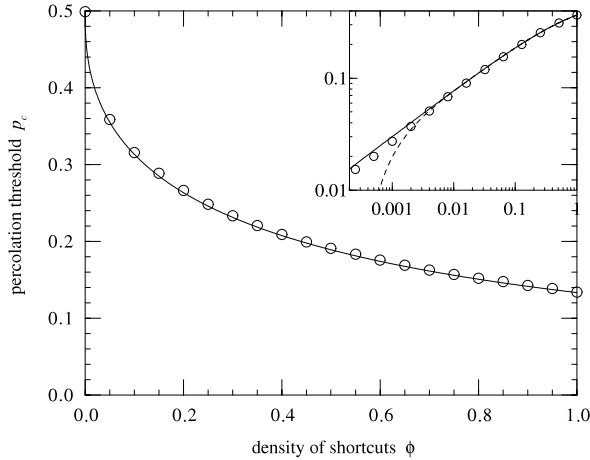


**Fig. 77.** Percolation threshold for a two-dimensional Watts–Strogatz network with a fraction  $\phi$  of shortcuts (the lines are the analytical calculations and the circles represent the numerical simulation). The inset is the zoom in loglog on the small  $\phi$  region (the numerical simulation is compared with the analytical calculation for the quantity  $1/2 - p_c$ ).

Source: From [320].

with what happens, for example for the Ising model, which is mean-field like as long as the shortcut density is non-zero (see Section 5.1).

This one-dimensional model was extended to the  $d = 2$  case with the help of high-order series expansion [320], and Ozana [321] discussed finite-size scaling for this problem by noting that we have two length scales in the problem: the length  $\xi_{SW} \sim 1/p^{1/d}$ , which gives the typical size of clusters connected by the shortcuts, and the length  $\xi$ , which is the usual cluster size for the percolation on the underlying lattice. The main result is that shortcuts indeed lead to a mean-field behavior and the larger their density, the smaller the percolation threshold (see Fig. 77).

In [198] the authors study the percolation on a model of lattice-based scale-free network where each node is connected to all the neighbors in a radius  $R$  distributed according to a law  $P(R) \sim R^{-\beta}$ , which implies that  $P(k) \sim k^{-\gamma}$  with  $\beta = d(\gamma - 1) + 1$ . The main result is that the percolation threshold is non-zero for  $\gamma > 2$ , in contrast with scale-free networks with  $\gamma < 3$ , which display the behavior (see for example [7])  $p_c(N) \rightarrow 0$ . In fact, for  $\gamma > 2$ , the radius distribution behaves with an exponent  $\beta > d+1$  and most of the links are short. In other words, the behavior should be that of an almost regular lattice (with a rescaled lattice spacing of order  $\langle R \rangle < \infty$ ) thus leading to a finite percolation threshold. We note here that it would be interesting to extend to the length, for example, the study made in [322], where the probability that an edge depends on the degree of its endpoints, allowing an interpolation between random failures and targeted attacks.

In [323], Auto et al. studied percolation on Apollonian networks (see [199] and Section 4.1.4) using real-space renormalization. For this two-dimensional spatial, scale-free, and planar network, the percolation threshold goes to zero in

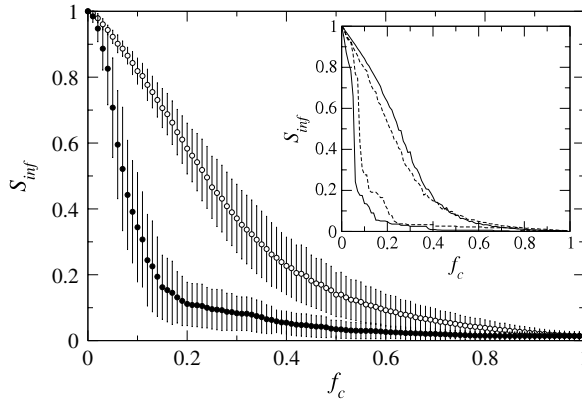


**Fig. 78.** Effect of random removal of nodes (white circles) and targeted attacks (black circles) on the relative size of the largest component of the EU power grid. In the inset, the effect of random removal and targeted attacks are shown for Italy (dashed lines) and France (continuous line).  
Source: From [123].

the thermodynamic limit, in agreement with general results for scale-free networks with  $\gamma < 3$ . The mass of the percolating cluster, however, behaves as  $M \sim e^{-\lambda/p}$  (where  $\lambda$  is a constant), a result reminiscent of the marginal case  $\gamma = 3$ .

### 5.5.2. Cascade of failures in infrastructures

A small local failure will lead to a major breakdown when it can propagate and reinforce itself. A simple illustration of this phenomenon is displayed in the example of the random fuse network introduced in 1985 by de Arcangelis, Redner and Herrmann [324]. The random fuse network is an electrical metaphor of material breakdown and consists of a lattice where the bonds are fuses with threshold  $i_c$  distributed according to a given law  $P(i_c)$ . If the current going through a fuse is larger than its threshold, the fuse breaks and its conductance goes to zero. The randomness of the thresholds models the heterogeneity of a material, and the main question here is what happens if a macroscopic current  $I$  is injected in this system. If we assume that a given bond fails, the current will be redistributed according to Kirchoff's laws on the neighbors of the failed fuse. For example, for an infinite two-dimensional square lattice, the current on the nearest neighbors of the failed bond is multiplied by  $\zeta = 4/\pi$  (see for example [325]). If the distribution  $P(i_c)$  has a finite support  $[i_m, i_M]$ , we can then produce the following argument. In the worst case, the failed bond had the smallest threshold possible  $i_m$ . The current on the neighbors is then  $\zeta i_m$  and the failure will certainly propagate if

$$\zeta i_m > i_M. \quad (277)$$

This result implies that if the disorder is weak (i.e. the difference  $\delta = i_M - i_m$  is small), the failure will very likely propagate across the system and create a macroscopic avalanche (which in material science is known as a 'brittle' behavior). In the opposite case of large  $\delta$ , we will observe the formation of microcracks which will grow and eventually coalesce when the applied current  $I$  is increased ('ductile' behavior). This simple example shows that the flow redistribution process after a failure is a crucial element, and combined with the heterogeneity of the system can lead to a wide variety of behavior. A general model of failure and current redistribution was for example discussed in [326], but we will focus in this chapter on cases where space plays a dominant role.

Various studies examined the vulnerability of infrastructures such as power grids [122,123,327], Internet, or transportation networks [178,328,329] and most of these studies are not concerned with spatial aspects but rather focused on how to measure the damage and the effect of various attack strategies. In particular, nodes with large betweenness centrality seem to be the weak points for all these networks, leading to the idea that global properties of the network are needed in order to understand the stability of these systems.

As with many spatial networks with strong physical constraints, power grids have an exponentially distributed degree (see Section 3.2.2), and in this case we can compute the effect of different removal strategies. In particular, if we remove nodes at random, the critical fraction  $f_c$  is given by [316]

$$f_c = 1 - \frac{1}{\kappa - 1} \quad (278)$$

where  $\kappa = \langle k^2 \rangle_0 / \langle k \rangle_0$  (where the subscript 0 indicates that we compute the corresponding quantities before any node removal). Another strategy consists in attacking the most connected nodes, in which case we can also compute a critical fraction using the argument developed in [316] (see Fig. 78 where the two strategies are illustrated in the case of the European power grid). One obtains for a network, with a degree distribution of the form  $P(k) \sim \exp(-k/\gamma)$ , the following condition for the critical fraction  $f_c$

$$1 + f_c(\ln f_c - 1) = \frac{1}{2\gamma - 1}. \quad (279)$$

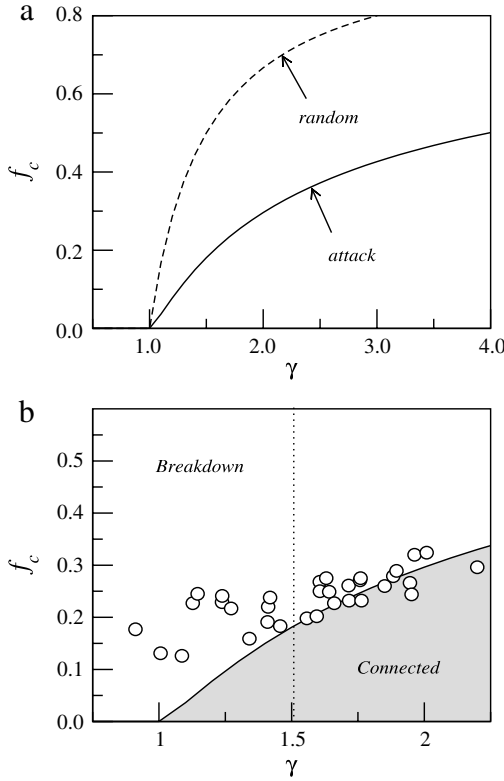


**Fig. 79.** (a) Comparison of the critical fraction needed to disrupt an exponential network with distribution  $P(k) \sim \exp(-k/\gamma)$ . (b) Estimated values for attacks on 33 different European power grids (circles) and the mean-field prediction of Eq. (279) (continuous line).  
Source: From [123].

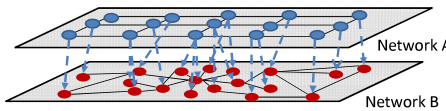


**Fig. 80.** Schematic representation of two interdependent networks. Nodes in network B (communications network) are dependent on nodes in network A (power grid) for power; nodes in network A are dependent on network B for control information.  
Source: From [330].

In the Fig. 79a, we see that the critical fraction of node removal is obviously smaller in the targeted attack strategy. In the Fig. 79b, the authors of [123] compare the theoretical mean-field value of  $f_c$  with actual simulation results. The agreement is relatively good, but there are some deviations for small values of  $\gamma$ : the simulated values of  $f_c$  seem to be relatively constant (of order  $0.2 \pm 0.1$ ), while the mean-field value goes to zero for  $\gamma \rightarrow 1$  (which corresponds roughly to the one-dimensional case).

### 5.5.3. Failure of interdependent networks

Space leads naturally to an increased level of interconnection between critical infrastructure networks. Recent events, such as the 2003 blackout, have reinforced the need for understanding the vulnerabilities of this spatially coupled network. In particular, in [330], the authors modeled the effect of the coupling between the electrical network and the Internet. They considered that the electrical blackout in Italy in September 2003 caused the shutdown of power stations which led to the failure of Internet nodes, and which in turn caused the breakdown of other power stations. The model proposed in [330] is made of two interconnected networks (see Fig. 80). The two interconnected networks have their own dynamics and can therefore not be considered as forming one single large network. The ability of a node in A to function will depend on its B-node (and vice-versa), which leads to the following process proposed in [330]: all B-nodes connected to A-nodes which do not belong the giant cluster in A have to be disrupted and vice-versa. This dynamics leads to surprising effects, such the lowering of critical thresholds and the appearance of an abrupt first-order transition with the size of the giant component going abruptly to zero at the transition point. In particular, for two connected scale-free networks, the interdependent dynamics leads to an additional fragility: while the degree heterogeneity is an asset against failure with many small degree nodes and a few hubs, when two networks are interdependent, hubs can be dependent on small degree nodes, which leads to

an increased vulnerability of the system. We note here that this problem is not equivalent to one dynamics on two connected networks, which obviously reduces to the usual case of one single network.

### 5.6. Space and the spread of disease

The importance of space and mobility networks appears very clearly in the study of epidemic spread. Infectious diseases indeed spread because people interact and travel, and the modeling of disease spread thus requires – ideally – the knowledge of the origin–destination matrix and of the social network.

We first recall here the main results for a prototype of disease spreading (the SIR model) on lattices and small-world networks. In particular, we discuss the effect of shortcuts on the spreading process. We then discuss the metapopulation model which enters the description of the disease spread among several subpopulations connected by a network. Finally, we end this chapter by describing recent studies of malware propagation among WiFi routers and virus spread using Bluetooth and MMS.

#### 5.6.1. SIR on lattices and small-world networks

In theoretical epidemiology, it is customary to divide the population into compartments, such as infectious ( $I$ ), susceptible ( $S$ ), or removed individuals ( $R$ ), and where the number of compartments depends on the specific nature of the disease [331]. This description assumes that we neglect fluctuations among individuals in the same state. The two main models which have been studied in the literature are:

- The SIS model. In this case, a susceptible individual in contact with infected individuals can himself become infected and will heal after a certain time and come back to a susceptible state, meaning that he can again catch the disease. This could for example describe the common cold, which does not confer long lasting immunity and for which individuals become susceptible again after infection.
- The SIR model. The difference here is that an infected individual becomes immunized (or has recovered) after a certain time immunized and cannot catch the disease again. This is for example the case for infantile diseases that we cannot catch a second time (in the vast majority of cases).

In the homogeneous mixing approximation, the equations governing the evolution of the number of susceptibles, infected, and recovered are in the SIR case

$$\begin{cases} \partial_t S = -\lambda S \frac{I}{N} \\ \partial_t I = +\lambda S \frac{I}{N} - \mu I \\ \partial_t R = +\mu I \end{cases} \quad (280)$$

along with the condition  $S + I + R = N$ , where  $\lambda$  is the probability per unit time to catch the disease and  $\mu$  is the recovery rate (i.e.  $1/\mu$  is the typical recovery time). The basic reproductive rate [331] is here given by  $R_0 = \lambda/\mu$  and represents the average number of secondary infections when one infected individual is introduced into a susceptible population. We thus have an epidemic threshold  $\lambda_c = \mu$  below which the disease is not contagious enough to spread in the population and above which an extensive fraction of the population gets infected.

In the homogeneous approximation, any pair of individuals can interact, which is not realistic in many cases (but which usually allows for an analytical approach). We have then to introduce the contact network, for which the nodes are the individuals and the presence of a link between  $i$  and  $j$  denotes the possibility that the virus can spread from  $i$  to  $j$  (or from  $j$  to  $i$ ). When we introduce a contact network, the important question which immediately arises is the one of the epidemic threshold and the effect of the network structure on its value. In this section, we will examine two cases. We will first examine the SIR model in the case of a lattice, and we then proceed to the Watts–Strogatz case where long-range links are added to a lattice.

**5.6.1.1. SIR model in space.** In pre-industrial times, disease spread was mainly a spatial diffusion phenomenon. For instance, during the spread of the so-called Black Death, which occurred in the 14th century (see for example [332]), only few means of travelling were available and typical trips were limited to relatively short distances on the time scale of one day. Historical studies confirm that the propagation (see Fig. 81) indeed followed a simple scheme, with a spatio-temporal spread mainly dominated by spatial diffusion.

The simplest way to describe the spatio-temporal evolution of a disease can be found for example in the book [334], which described a spatial SIR model where  $S(x, t)$  denotes the susceptible individuals and  $I(x, t)$  the infected and infectious individuals at time  $t$  and at location  $x$ . In the non-spatial version, the evolution of the densities  $s = S/N$ ,  $i = I/N$  and  $r = R/N$  is described by the set of equations (see for example [7,331])

$$\begin{cases} \frac{\partial s}{\partial t} = -\lambda s i \\ \frac{\partial i}{\partial t} = +\lambda s i - \mu i \end{cases} \quad (281)$$

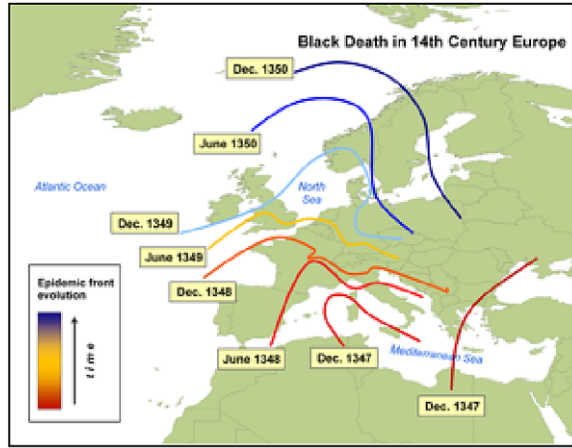


**Fig. 81.** Spread of the Black Death during the 14th century. The epidemic front spreads in Europe with a velocity of the order of 200–400 miles per year. Source: From [333].

along with the condition that the sum of the three densities is one  $s + i + r = 1$ . In these equations, the number of individuals is absorbed into the definition of the quantity  $\lambda$ . In the spatial version, the quantities  $s$  and  $i$  now depend on space, and in the simplest version it is assumed that simple diffusion is the cause of their dispersion and that they have the same diffusion constant. The equations governing their evolution then become

$$\begin{cases} \frac{\partial s}{\partial t} = -\lambda s i + D \nabla^2 s \\ \frac{\partial i}{\partial t} = +\lambda s i - \mu i + D \nabla^2 i. \end{cases} \quad (282)$$

When  $D \neq 0$  and  $\lambda = \mu = 0$ , the infection front grows as  $\sqrt{t}$  while the combination of  $D \neq 0$  and  $\lambda \neq 0$  leads in fact to a finite velocity. A simple way to see this is given by the following argument for the one-dimensional case [334]. Using dimensional arguments, we will use the following rescaling

$$i \rightarrow \frac{I}{S_0}, \quad s \rightarrow \frac{S}{S_0}, \quad x \rightarrow \sqrt{\frac{\lambda S_0}{D}} x, \quad t \rightarrow \lambda S_0 t \quad (283)$$

and where  $R_0 = \lambda S_0 / \mu$  is the basic reproductive rate and must be larger than one in order to observe an outbreak [331] (the quantity  $S_0$  is the initial number of susceptibles). We then obtain

$$\begin{cases} \frac{\partial s}{\partial t} = -s i + \frac{\partial^2 s}{\partial x^2} \\ \frac{\partial i}{\partial t} = +s i - \frac{1}{R_0} i + \frac{\partial^2 i}{\partial x^2}. \end{cases} \quad (284)$$

We look now for a traveling wave solution of Eq. (284) of the form

$$\begin{cases} i(x, t) = i(x - vt) \\ s(x, t) = s(x - vt) \end{cases} \quad (285)$$

where  $v$  is the wavespeed which needs to be determined. Inserting this form in the system Eq. (284) we obtain

$$\begin{cases} i'' + v i' + i \left( s - \frac{1}{R_0} \right) = 0 \\ s'' + v s' - i s = 0 \end{cases} \quad (286)$$

where the prime denotes differentiation with respect to the variable  $z = x - vt$ . We look for a solution such that  $i(-\infty) = i(\infty) = 0$  and  $0 \leq s(-\infty) < s(\infty) = 1$ . Near the wave front,  $s \approx 1$  and  $i \approx 0$  and we obtain

$$i'' + v i' + i \left( 1 - \frac{1}{R_0} \right) \approx 0 \quad (287)$$

which can be solved and leads to

$$i(z) \propto \exp \left[ \left( -v \pm \sqrt{v^2 - 4 \left( 1 - \frac{1}{R_0} \right)} \right) z / 2 \right]. \quad (288)$$

This solution cannot oscillate around  $i = 0$ , which implies that the wavespeed  $v$  and  $R_0$  must satisfy the conditions  $R_0 > 1$  and

$$v \geq 2 \left( 1 - \frac{1}{R_0} \right)^{1/2}. \quad (289)$$

For most initial conditions, the travelling wave computed in the full non-linear system will evolve at the minimal velocity and we eventually obtain the epidemic wave velocity

$$V = 2(\lambda S_0 D)^{1/2} \sqrt{1 - \frac{1}{R_0}}. \quad (290)$$

We can apply this simple model to the historical case of the Black Death. Following [334], the number of individuals in Europe at that time was  $\approx 85$  million, which gives a density  $S_0 \approx 20/\text{km}^2$ . The quantities  $\lambda$  and  $\mu$  are more difficult to determine as the plague is transmitted by fleas jumping from rats to humans. In [332] these parameters are estimated to be  $\mu \approx 15/\text{year}$  and  $\lambda \approx 1.0 \text{ km}^2/\text{year}$ . The basic reproductive rate is then  $R_0 \approx 1.33$ , which is not very large. The main difficulty here is the estimate of the diffusion coefficient, and if we assume that news spreads at a velocity of around 160 km/year, we obtain  $D \approx 10^4 \text{ km}^2/\text{year}$ . Putting all the numbers together we then find a velocity of the order  $v \approx 700 \text{ km/year}$ , which is larger than historical estimates, put in the range [300, 600] km/year. However, given the uncertainties on the parameter (especially for  $D$ ), the spatial diffusion approximation is not unreasonable.

**5.6.1.2. SIR model in small-worlds.** An important observation which was made by Grassberger [335] is that the SIR model on a graph can be mapped to the corresponding bond percolation problem. This mapping is, however, valid only for at least a very peaked distribution of infection time [336] (the main reason for the failure of the mapping in the case of random infection times is the existence of correlations introduced between neighbors of the same site). As in [335], the authors of [337,338] consider a SIR model where nodes stay infectious during a time  $\tau$  and where the transmission rate between two connected nodes is a random variable distributed according to the distribution  $P(\lambda)$ . For a given value of  $\lambda$ , the probability  $1 - p$  not to transmit the disease is given by

$$1 - p = (1 - \lambda \delta t)^{\tau/\delta t} \quad (291)$$

which in the continuous time limit and averaged over all values of  $\lambda$  gives

$$p(\tau) = 1 - \int d\lambda P(\lambda) e^{-\lambda \tau}. \quad (292)$$

This quantity  $p$  gives the fraction of bonds completed in a given epidemic, and we thus obtain a mapping between the SIR model and a bond percolation problem. If  $p$  is larger than the percolation threshold on the underlying lattice, there is a giant cluster, which means that an extensive number of nodes were infected. For a peaked distribution of  $\lambda$ , the epidemic threshold is given by

$$\lambda_c = -\tau \ln(1 - p_c) \quad (293)$$

and indicates the general trend that if  $p_c$  is smaller then  $\lambda_c$  is smaller too. On a square lattice, for  $p > p_c = 1/2$ , we obtain results such as the one shown in Fig. 82a, where we see some large regions unaffected by the disease. The authors of [337,338] studied the SIR model on a two-dimensional Watts–Strogatz model with a fraction  $\phi$  of shortcuts connecting randomly chosen nodes. The result is shown in the Fig. 82b and displays evidence that even a small fraction of long-range links is enough to ‘homogenize’ the system and to break down the large unaffected regions. In addition, as shown in [320], the percolation threshold decreases with  $\phi$  (see Fig. 77), which implies that the epidemic threshold is also smaller due to the shortcuts which facilitate the spread of the disease.

The same mapping between the SIR model and bond percolation implies that for the scale-free network with exponent  $\gamma$  and constructed on a lattice (such as in [198]) the epidemic threshold is non-zero for  $\gamma > 2$ , while for a non-spatial scale-free network, we expect  $p_c = 0$  (in the limit of infinite networks, see for example the book [5]). In this spatial lattice, it thus seems that the addition of shortcuts and the existence of hubs is not enough to counterbalance the effect of the short links and the underlying spatial structure.

### 5.6.2. From Euclidean space to networks

However, in modern times, the simple picture of pure spatial diffusion, with the possible addition of few shortcuts, no longer holds. A striking example can be seen in the SARS outbreak in 2003. In Fig. 83 we show the spatio-temporal evolution of this disease, which started in China. We can see on this figure that there is a clear spatial component with the disease spreading in south-west Asia but also with long-range jumps to Europe and the US. This clearly shows that pure spatial diffusion is no longer a good model and that the global aspect of transportation networks needs to be included in the modeling. At a smaller scale, it has also been observed that epizootics, such as the foot-and-mouth disease outbreak in 2001

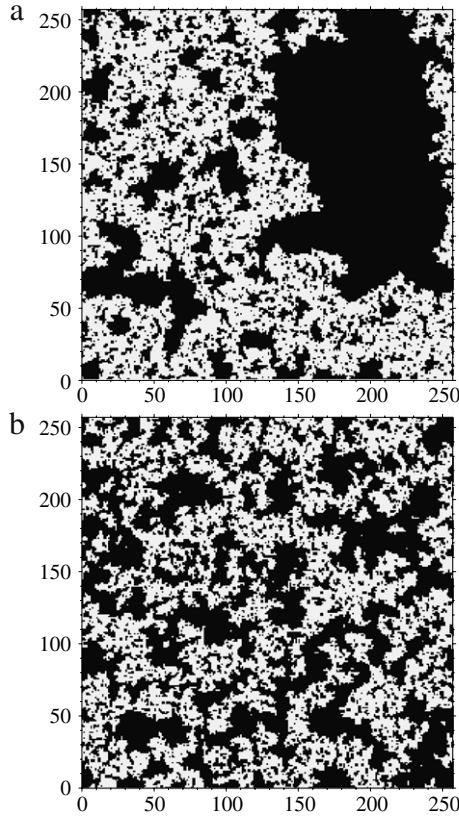


**Fig. 82.** Snapshot of the final cluster of recovered nodes (gray nodes) after the epidemics has died out on (a) a lattice with periodic boundary conditions, and (b) on a two-dimensional Watts–Strogatz network with a fraction of shortcuts  $\phi = 0.01$ .  
Source: From [337].

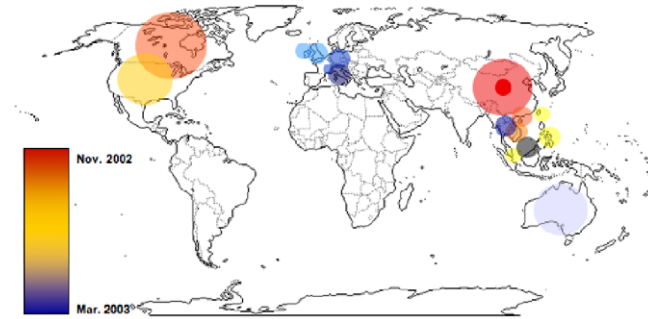


**Fig. 83.** Global evolution of the SARS disease which started in China in 2002. The color code corresponds to time and goes from the Hong Kong outbreak in November 2002 to the end of the disease spread in March 2003. Courtesy V. Colizza.

in Great Britain's livestock did not follow a purely spatial pattern [339], but instead, the epidemic showed local stochastic spread and rare long-distance jumps.

An approach to the problem is provided by metapopulation models that describe the spread of an infectious disease at a scale where a transportation network dominates. These models describe spatially structured populations such as cities or urban areas which interact through a given transportation network and have been the subject of many studies (we refer the interested reader to [7] and references therein). In the simplest version of the metapopulation model, the nodes of the network are the cities (or urban areas) and these cities are connected through a network defined by a weighted adjacency matrix  $p_{ij}$ . The element  $p_{ij}$  represents the probability per unit time that an individual chosen at random in city  $i$  will travel to city  $j$ . In the case where we assume that any individual of a city has the same probability to travel (in other words if we neglect any social structure), the  $p_{ij}$  can then be estimated as  $w_{ij}/N_i$ , where  $w_{ij}$  is the flow of travelers between  $i$  and  $j$ , and  $N_i$  is the population of city  $i$ . The evolution of the number  $I_i(t)$  of infected individuals in the city  $i$  at time  $t$  is then given by

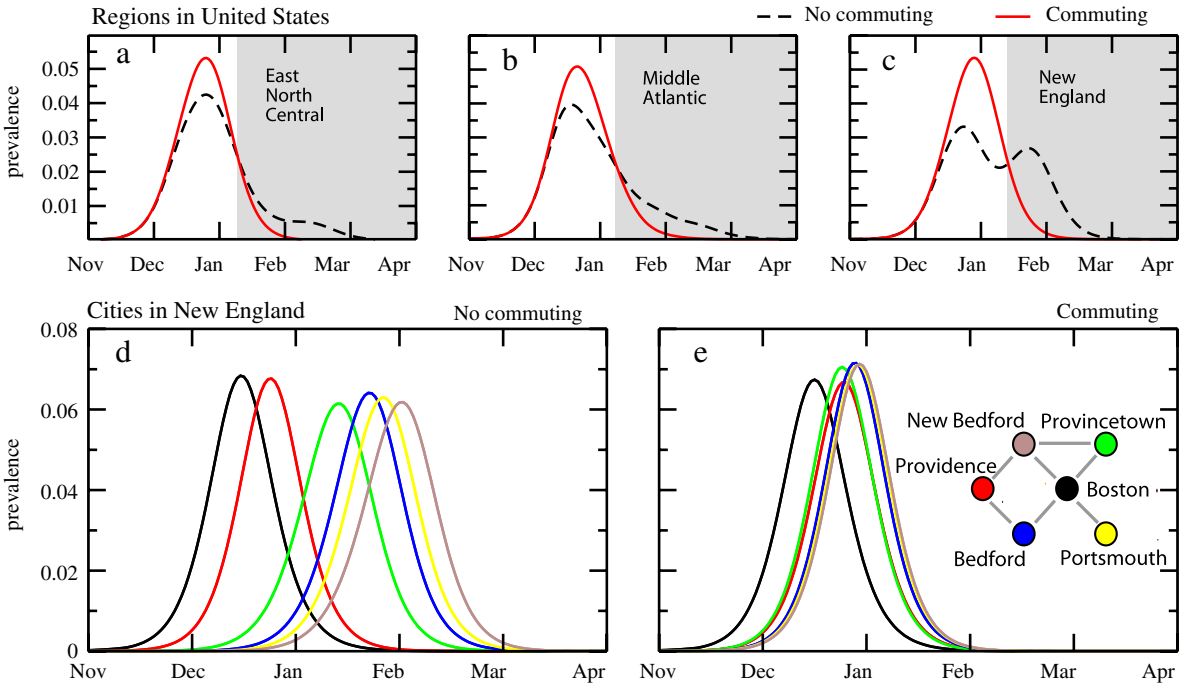


**Fig. 84.** Comparison of prevalence profiles without and with commuting flows. (a)–(c) Prevalence profiles for three continental US regions. (d)–(e) Prevalence profiles for cities in New England.  
Source: From [162].

an equation of the form

$$\partial_t I_i(t) = K(S_i, I_i, R_i, \dots) + \Omega_i(\{I\}) \quad (294)$$

where  $K$  represents the local term and corresponds to the spread of the disease due to intra-city contamination. The travel term  $\Omega$  depends on the mobility network and, in the simple case of uniform travel probability, can be written as (in the limit of large  $I_l$ )

$$\Omega_i = \sum_j p_{ji} I_j - p_{ij} I_i. \quad (295)$$

If the probability is constant,  $\Omega$  is essentially the Laplacian on the underlying network and if the mobility graph is a lattice, we recover the usual Laplacian diffusion term. From a theoretical perspective it would be interesting to understand precisely the crossovers when we have different scales and networks interacting with each other.

Theoretical studies on the metapopulation model, such as the existence of a pandemic threshold, were done in [143,340–342]. In particular, if we assume that the travel probability is constant  $p_{ij} = p$ , the pandemic threshold has an expression of the form

$$R_* \propto (R_0 - 1)p \frac{\langle k^2 \rangle}{\langle k \rangle}. \quad (296)$$

The disease will then spread all over the world if  $R_* > 1$ , which implies that  $R_0 > 1$  (i.e. the disease spreads in each subpopulation) and that the product  $p\langle k^2 \rangle$  is large enough. For scale-free networks (such as for the worldwide airline network), the quantity  $\langle k^2 \rangle$  is large, which suggests that reducing travel (i.e. decreasing  $p$ ) is not efficient. The fact that reducing travel is not an efficient strategy was also confirmed in theoretical and numerical studies [340–343]. Other studies on applications of metapopulation models to the SARS or influenza can be found in [162,343,344].

More recently, in [162], small-scale commuting flows were added to the large-scale airline network. This is an interesting problem, since we have now the superimposition of networks at different scales. In Fig. 84, we show the different prevalence (defined as the fraction of infected individuals in the population) profiles obtained with and without commuting flows. At a regional level, the prevalence is increased when commuting flows are added in the model, but the more spectacular effect is at a local level: the inclusion of short-range mobility does not change the magnitude of prevalences but largely increases the synchrony between outbreaks in neighboring cities [162].

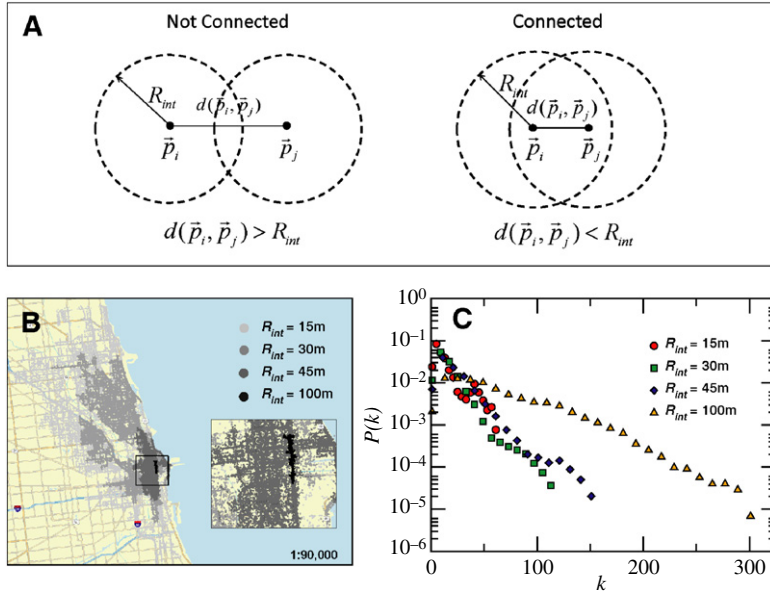


**Fig. 85.** (a) Construction of the WiFi network as a random geometric graph (see Section 4.1.1). (b) Giant component of the WiFi network in Chicago for different values  $R_{int}$ . (c) Degree distribution for different values of  $R_{int}$ .

Source: From [345].

### 5.6.3. WiFi and Bluetooth epidemiology

**5.6.3.1. WiFi epidemiology.** In densely populated areas, the range of the WiFi routers is such that the corresponding geometric graph can percolate through the whole urban area (see Fig. 85). This fact could be used to spread a computer virus or malware that could have large-scale consequences. An epidemiological model was developed in [345] in order to study various scenarios and to assess the vulnerability of these networks. Using a database containing the geographic location of the wireless routers, Hu et al. [345] focused on seven urban areas in the US. From the set of vertices (which are here the routers), the geometric network can be constructed for a given value of the router's range  $R_{int}$ . In practice, the value of  $R_{int}$  fluctuates from 10 to 100 m depending on the environment and the specific router type. In this study, this value  $R_{int}$  is assumed to be the same for all routers (but actually the study of geometric random graphs with random  $R_{int}$  could be of interest). An example of such a geometric network is shown in Fig. 85 for the Chicago area, with  $R_{int} = 45$  m.

Hu et al. then use the compartmental approach of standard epidemiology in order to describe the spread of a computer virus. The usual scheme must, however, be enlarged in order to take into account the heterogeneity observed in the security levels of WiFi routers. For details of the epidemiological model, we refer the interested reader to the paper [345]. Once this epidemiological description is set up, the authors studied the spread of the virus in various settings and on the giant component. An example of the spread of the virus is shown for the Chicago area in Fig. 86. This figure displays a clear spatial diffusion of the disease which takes place on the giant component of the WiFi network. The time scales are actually very important in this case, and Hu et al. estimated that in the Chicago case, the malware rapidly propagates in a few hours and infects about 40% two weeks after the beginning of the infection (and about 10% to 55% for most areas considered in this study).

The fraction of encrypted routers and geometrical constraints of the urban area may have large consequences on the spread of the malware. In particular, areas with small bottlenecks may be very sensitive to the local density of encrypted routers. This study allows the future possibility to have an estimate of the immunization threshold in order to stop the spread of malware.

**5.6.3.2. Mobile phone disease.** In [346], Wang et al. study the spreading patterns of a mobile phone virus. A mobile phone virus can spread through two very different mechanisms. The first mechanism is through Bluetooth connections, provided that the infected phone and the susceptible one are separated by a short distance (typically from 10 to 30 m). In the second mechanism, a MMS virus can send a copy of itself to all the numbers found in the infected phone's contact book. We thus have a short range, spatial infection pattern superimposed with long-range infections. However, a cell phone virus can infect only phones with the right operating system. The market share  $m$  of an OS is then an important parameter in the study of the spread of mobile phone viruses. The authors of [346] used the database of a mobile phone provider and simulated the spread of disease using a SI type compartment model and studied the effect of various values of  $m$ . They found the existence of a threshold value (of order  $m_c \approx 10\%$ ) above which there is a giant component of phones using the same OS, allows a MMS virus to spread (added to the fact that even for  $m > m_c$ , the dynamics still depends on  $m$ , and the larger this parameter,



**Fig. 86.** Spatial spread of a SIR type disease in the Chicago area (results obtained for  $R_{int} = 45m$ ).  
Source: From [345].

the faster the dynamics). At the time of this study, the share of the largest OS was about 3% and could explain why we had not yet seen a major mobile virus outbreak.

## 6. Summary and outlook

In this article we review the most important effects of space on the structure of networks. In particular, the existence of a cost associated to the length of edges leads to many important consequences, such as a large clustering and a flat assortativity. The degree distribution is usually peaked due to the existence of strong physical constraints, although broad degree distributions can be observed for spatial, non-planar networks. The betweenness centrality displays strong fluctuations which can be related to the interplay of space and degree. These different effects are by now relatively well understood and, as shown in Section 4, there is now a wealth of various models which incorporate space at different levels. Finally, in Section 5 we discussed various processes, such as the random walk, diseases spread etc., on spatial networks.

Despite these various advances, there are still many open problems which could represent interesting research directions both at the theoretical and the applied levels. We give here a non-exhaustive, subjective list of such open problems that seem particularly interesting.

- *Scale and description.* In problems such as disease spread, the description depends strongly on the scale of interest. At a small spatial scale (but large enough in order to allow for the use of continuous limits), we can use partial differential equations. In contrast, at a larger scale, of the order given by a typical link of the relevant transportation network, the system is better described by metapopulation models. Given the interest of interdependent scales and networks, an interesting question is how we could integrate a ‘mixed’ description able to interpolate between a continuous partial differential equation to a discrete network, metapopulation-like description. Another way to look at this question is to look for a continuous, pde-like, description of the spread over a network at a large scale.
- *Interdependent networks.* Recent studies showed the importance of connected networks and, in particular, that coupled dynamics could lead to new and surprising results. In particular, we saw that networks are coupled via space, and this can lead to a cascade of failures more critical than what could be expected. However, a number of questions remain unsolved at this point. For example, what are the conditions for a coupling to be relevant and to affect the single-network behavior? In particular, in the development of failures, it would be interesting to understand the space-time properties of blackouts.
- *Optimal spatial networks.* Optimal networks are very important, as we saw in this review (see Section 4.5). In particular, there are many different directions, such as understanding the hub location problem in presence of congestion, and more generally we believe that statistical physics could bring interesting insights on these problems usually tackled by mathematicians and engineers expert in optimization. Also, as recent studies suggested, evolution through resilience and noise shaped loopy networks. It would be interesting to understand quantitatively the formation and the statistics of these loops.

- **Connection with socio-economical indicators.** Data on spatial networks and in particular, road and other infrastructure networks are now available, and these networks have been the subject of many studies. Also, with the emergence of geosocial applications, for example on mobile phones, we can expect interesting studies connecting spatial distributions and social behavior. This line of research has already appeared in recent studies which tried to relate topological structures of networks to socio-economical indicators. In these studies, an important question concerns the correlations between topological quantities and social factors. For example, it would be interesting to know if we can understand some aspects of the spatial distribution of crime rates in terms of topological indicators of the road network (such as the betweenness centrality for example).
- **Evolution of transportation (and spatial) networks.** How transportation networks evolve is an old problem and was already the subject of many studies in the 1970s (see for example [16]). However, apart from some exceptions (see for example [106] and references therein) this problem is still not very well understood. We are now in a position where data and tools are available and we can expect some interesting developments in this area. In parallel to empirical studies, we also need to develop theoretical ideas and models in order to describe the evolution of spatial networks.
- **Urban studies.** More generally, infrastructure and transportation networks are part of urban systems and we believe that the current understanding of spatial networks could help in understanding the structure and evolution of these systems. In particular, our knowledge of spatial networks could help in the understanding of important phenomenon such as urban sprawl and in the design of sustainable cities.

## Acknowledgements

I am indebted to A. Banos, A. Barrat, M. Batty, H. Berestycki, G. Bianconi, M. Boguna, S. Boettcher, P. Bonnin, P. Bordin, J. Bouttier, V. Blondel, M. Brede, A. Chessa, V. Colizza, T. Courtat, L. Dall'Asta, C.-N. Douady, S. Douady, Y. Duan, J.-P. Frey, S. Fortunato, A. Flammini, M. Gastner, C. Godrèche, E. Guittet, D. Helbing, H.J. Herrmann, S. Havlin, B. Jiang, S.M. Kang, D. Krioukov, R. Lambiotte, M. Latapy, V. Latora, D. Levinson, J.-M. Luck, J.-P. Nadal, S. Porta, C. Roth, G. Santoboni, A. Scala, P. Sen, E. Strano, F. Tarissan, P. Thiran, C. Uzan, A. Vespignani, Z. Zhang, and R.M. Ziff, for giving useful suggestions and advice to improve this manuscript at various stages.

## References

- [1] P. Erdős, A. Rényi, On random graphs, *Publ. Math.* 6 (1959) 290–297.
- [2] P. Erdős, P. Rényi, On the evolution of random graphs, *Publ. Math. Inst. Hung. Acad. Sci.* 5 (1960) 17–60.
- [3] D.J. Watts, D.H. Strogatz, Collective dynamics of small-world networks, *Nature* 393 (1998) 440.
- [4] A.-L. Barabási, R. Albert, Emergence of scaling in random networks, *Science* 286 (1999) 509–511.
- [5] R. Pastor-Satorras, A. Vespignani, *Evolution and Structure of the Internet: A Statistical Physics Approach*, Cambridge University Press, Cambridge, 2003.
- [6] S.N. Dorogovtsev, J.F.F. Mendes, *Evolution of Networks: From Biological Nets to the Internet and WWW*, Oxford University Press, Oxford, 2003.
- [7] A. Barrat, M. Barthélémy, A. Vespignani, *Dynamical Processes in Complex Networks*, Cambridge University Press, Cambridge, UK, 2008.
- [8] G. Caldarelli, *Scale-free Networks*, Oxford University Press, Oxford, 2007.
- [9] M.E.J. Newman, *Networks: An Introduction*, Oxford University Press, Oxford, UK, 2010.
- [10] R. Cohen, S. Havlin, *Complex Networks: Structure, Robustness and Function*, Cambridge University Press, Cambridge, 2010.
- [11] R. Albert, A.-L. Barabási, Statistical mechanics of complex networks, *Rev. Modern Phys.* 74 (2002) 47–97.
- [12] S.N. Dorogovtsev, J.F.F. Mendes, Evolution of networks, *Adv. Phys.* 51 (2002) 1079–1187.
- [13] M.E.J. Newman, The structure and function of complex networks, *SIAM Rev.* 45 (2003) 167–256.
- [14] S. Boccaletti, V. Latora, Y. Moreno, M. Chavez, D.-Ung. Hwa, Complex networks: structure and dynamics, *Phys. Rep.* 424 (2006) 175–308.
- [15] E. Bullmore, O. Sporns, Complex brain networks: graph theoretical analysis of structural and functional systems, *Nature Rev. Neurosci.* 10 (2009) 186–198.
- [16] P. Haggett, R.J. Chorley, *Network Analysis in Geography*, Edward Arnold, London, 1969.
- [17] R.J. Chorley, P. Haggett (Eds.), *Models in Geography*, Methuen and Co., London, 1967.
- [18] F. Bavaud, C. Mager (Eds.), *Handbook of Theoretical and Quantitative Geography*, FGSE, University of Lausanne, Lausanne, Switzerland, 2009.
- [19] I. Rodriguez-Iturbe, A. Rinaldo, *Fractal River Basins: Chance and Self-organization*, Cambridge University Press, Cambridge, 1997.
- [20] I.F. Akyildiz, S. Weilian, Y. Sankarasubramaniam, E. Cayirci, A survey on sensor networks, *Comm. Mag. IEEE* 40 (2002) 102–114.
- [21] M.A. Nowak, S. Bonhoeffer, R.M. May, Spatial games and the maintenance of cooperation, *Proc. Natl. Acad. Sci. (USA)* 91 (1994) 4877–4881.
- [22] C. Hauert, G. Szabo, Game theory and physics, *Amer. J. Phys.* 73 (2005) 405–414.
- [23] W. Tutte, A census of planar maps, *Canad. J. Math.* 15 (1963) 249–271.
- [24] D. Boulatov, V. Kazakov, The Ising model on a random planar lattice: the structure of the phase transition and the exact critical exponents, *Phys. Lett. B* 187 (1987) 379–384.
- [25] J. Ambjorn, B. Durhuss, T. Jonsson, *Quantum Geometry. A Statistical Field Theory Approach*, Cambridge University Press, Cambridge, UK, 1997.
- [26] J. Clark, D.A. Holton, *A First Look at Graph Theory*, World Scientific, 1991.
- [27] D. Jungnickel, *Graphs, networks and algorithms*, in: *Algorithm and Computation in Mathematics*, vol. 5, Springer Verlag, Heidelberg, 1999.
- [28] S. Lammer, B. Gehlsen, D. Helbing, Scaling laws in the spatial structure of urban road networks, *Physica A* 363 (2006) 89.
- [29] H.J. Hilhorst, Statistical properties of planar Voronoi tessellations, *Eur. Phys. J. B* 64 (2008) 437–441.
- [30] H.J. Hilhorst, The perimeter of large planar Voronoi cells: a double-stranded random walk, *J. Stat. Mech.* 2005 (2005) L02003.
- [31] H.J. Hilhorst, Asymptotic statistics of the  $n$ -sided planar Poisson–Voronoi cell: I. exact results, *J. Stat. Mech.* 2005 (2005) P09005.
- [32] L.A.N. Amaral, A. Scala, M. Barthélémy, H.E. Stanley, Classes of small-world networks, *Proc. Natl. Acad. Sci. (USA)* 97 (2000) 11149–11152.
- [33] S. Porta, P. Crucitti, V. Latora, The network analysis of urban streets: a dual approach, *Physica A* 369 (2006) 853–866.
- [34] V. Kalapala, V. Sanwalani, A. Clauset, C. Moore, Scale invariance in road networks, *Phys. Rev. E* 73 (2006) 026130.
- [35] G. Bianconi, M. Marsili, Loops of any size and Hamilton cycles in random scale-free networks, *J. Stat. Mech.* 2005 (2005) P06005.
- [36] H.D. Rozenfeld, J.E. Kirk, E.M. Boltt, D. ben Avraham, Statistics of cycles: how loopy is your network, *J. Phys. A* 38 (2005) 4589–4595.
- [37] R. Pastor-Satorras, A. Vázquez, A. Vespignani, Dynamical and correlation properties of the Internet, *Phys. Rev. Lett.* 87 (2001) 258701.
- [38] A. Vázquez, R. Pastor-Satorras, A. Vespignani, Large-scale topological and dynamical properties of the Internet, *Phys. Rev. E* 65 (2002) 066130.
- [39] M. Barthélémy, L.A.N. Amaral, Small-world networks: evidence for a crossover, *Phys. Rev. Lett.* 82 (1999) 3180.

- [40] F.R.K. Chung, Spectral Graph Theory, AMS Press, Providence, RI, 1997.
- [41] M. Fiedler, Algebraic connectivity of graphs, *Czechoslovak Math. J.* 23 (1973) 298–305.
- [42] B. Luo, R.C. Wilson, E.R. Hancock, Spectral embedding of graphs, *Pattern Recog.* 36 (2003) 2213–2230.
- [43] L.M. Pecora, T.L. Carroll, Master stability functions for synchronized coupled systems, *Phys. Rev. Lett.* 80 (1998) 2109.
- [44] M. Barahona, L.M. Pecora, Synchronization in small-world systems, *Phys. Rev. Lett.* 89 (2002) 054101.
- [45] L.C. Freeman, A set of measures of centrality based on betweenness, *Sociometry* 40 (1977) 35–41.
- [46] M.E.J. Newman, Scientific collaboration networks: shortest paths, weighted networks, and centrality, *Phys. Rev. E* 64 (2001) 016132.
- [47] K.-I. Goh, B. Kahng, D. Kim, Universal behavior of load distribution in scale-free networks, *Phys. Rev. Lett.* 87 (2001) 278701.
- [48] M. Barthélémy, Comment on: ‘universal behavior of load distribution in scale-free networks’, *Phys. Rev. Lett.* 91 (2003) 189803.
- [49] M. Barthélémy, Betweenness centrality in large complex networks, *Eur. Phys. J. B* 38 (2004) 163.
- [50] A. Barrat, M. Barthélémy, A. Vespignani, The effects of spatial constraints on the evolution of weighted complex networks, *J. Stat. Mech.* (2005) P05003.
- [51] M. Molloy, B. Reed, A critical point for random graphs with a given degree sequence, *Random Struct. Algorithms* 6 (1995) 161.
- [52] A. Barrat, M. Barthélémy, R. Pastor-Satorras, A. Vespignani, The architecture of complex weighted networks, *Proc. Natl. Acad. Sci.* 101 (2004) 3747–3752.
- [53] S.-H. Yook, H. Jeong, A.-L. Barabasi, Y. Tu, Weighted evolving networks, *Phys. Rev. Lett.* 86 (2001) 5835–5838.
- [54] E.J. Taffee, H.L. Gauthier Jr., Geography of Transportation, Prentice Hall, Englewood Cliffs, New Jersey, 1973.
- [55] J.-P. Rodrigue, C. Comtois, B. Slack, The Geography of Transport Systems, Routledge, New York, NY, 2006.
- [56] F. Xie, D. Levinson, Measuring the structure of road networks, *Geograph. Anal.* 39 (2007) 336–356.
- [57] W.L. Garrison, Connectivity of the interstate highway system, *Region. Sci. 6* (1960) 121–137.
- [58] K. Kansky, Structure of Transportation Networks: Relationships Between Network Geometry and Regional Characteristics, University of Chicago Press, Chicago, 1969.
- [59] J. Buhl, J. Gautrais, N. Reeves, R.V. Solé, S. Valverde, P. Kuntz, G. Theraulaz, Topological patterns in street networks of self-organized urban settlements, *Eur. Phys. J. B* 49 (2006) 513–522.
- [60] T. Courtaud, C. Glaouen, S. Douady, Mathematics and morphogenesis of the city: a geometrical approach, *Phys. Rev. E* (2010).
- [61] D. Levinson, A. El-Geneidy, The minimum circuitry frontier and the journey to work, *Region. Sci. Urban Econom.* 39 (2007) 732–738.
- [62] M. Batty, Accessibility: in search of a unified theory, *Environ. Plan. B: Plan. Design* 36 (2009) 191–194.
- [63] S. Handy, D.A. Niemeier, Measuring accessibility: an exploration of issues and alternatives, *Environ. Plan. A* 29 (1997) 1175–1194.
- [64] D. Levinson, K.J. Krizek (Eds.), Planning for Place and Plexus: Metropolitan Land Use and Transport, Routledge, New York, NY, 2008.
- [65] A. El-Geneidy, D. Levinson, Place rank: valuing spatial interactions, *Netw. Spatial Econom.* (2010).
- [66] P. Crucitti, V. Latora, S. Porta, Centrality in networks of urban streets, *Chaos* 16 (2006) 015113.
- [67] I. Vragovic, E. Louis, A. Diaz-Guilera, Efficiency of informational transfer in regular and complex networks, *Phys. Rev. E* 71 (2005) 036122.
- [68] D.J. Aldous, J. Shunn, Connected spatial networks over random points and a route-length statistic, *arXiv:1003.3700*, 2010.
- [69] V. Latora, M. Marchiori, Efficient behavior of small-world networks, *Phys. Rev. Lett.* 87 (2001) 198701.
- [70] V. Latora, M. Marchiori, Economic small-world behavior in weighted networks, *Eur. Phys. J. B* 32 (2003) 249.
- [71] A. Tero, S. Takagi, T. Saigusa, K. Ito, D.P. Bebbert, M.D. Fricker, K. Yumiki, R. Kobayashi, T. Nakagaki, Rules for biologically inspired adaptive network design, *Science* 327 (2010) 439–442.
- [72] S. Fortunato, Community detection in graphs, *Phys. Rep.* 486 (2010) 75–174.
- [73] M.E.J. Newman, M. Girvan, Finding and evaluating community structure in networks, *Phys. Rev. E* 69 (2004) 026113.
- [74] S. Fortunato, M. Barthélémy, Resolution limit in community detection, *Proc. Natl. Acad. Sci. (USA)* 104 (2007) 36–41.
- [75] R. Guimerà, L.A.N. Amaral, Cartography of complex networks: modules and universal roles, *J. Stat. Mech.* 2005 (2005) P02001.
- [76] R. Milo, S. Shen-Orr, S. Itzkovitz, N. Kashtan, D. Chklovskii, U. Alon, Network motifs: simple building blocks of complex networks, *Science* 298 (2002) 824.
- [77] A. Cardillo, S. Scellato, V. Latora, S. Porta, Structural properties of planar graphs of urban street patterns, *Phys. Rev. E* 73 (2006) 066107.
- [78] A. Runions, A.M. Fuhrer, P.B. Federl lane, A.-G. Rolland-Lagan, P. Prusinkiewicz, Modeling and visualization of leaf venation patterns, *ACM Trans. Graphics* 24 (2005) 702–711.
- [79] G.B. West, J.H. Brown, The origin of allometric scaling laws in biology from genomes to ecosystems: towards a quantitative unifying theory of biological structure and organization, *J. Exp. Biol.* 208 (2003) 1575–1592.
- [80] M.T. Gastner, M.E.J. Newman, Optimal design of spatial distribution networks, *Phys. Rev. E* 74 (2006) 016117.
- [81] M. Schwartz, Telecommunication Networks: Protocols, Modelling and Analysis, Addison-Wesley Longman Publishing, Boston, 1986.
- [82] D.M. Levinson, K.J. Krizek, Planning for Place and Plexus, Routledge, New York (NY), 2008.
- [83] M. Kurant, P. Thiran, Extraction and analysis of traffic and topologies of transportation networks, *Phys. Rev. E* 74 (2006) 036114.
- [84] P. Sen, S. Dasgupta, A. Chatterjee, P.A. Seeram, G. Mukherjee, S.S. Manna, Small-world properties of the Indian railway network, *Phys. Rev. E* 67 (2003) 036106.
- [85] V. Latora, M. Marchiori, Is the Boston subway a small-world network, *Physica A* 314 (2001) 109–113.
- [86] J. Sienkiewicz, J.A. Holyst, Statistical analysis of 22 public transport networks in Poland, *Phys. Rev. E* 72 (2005) 046127.
- [87] Y. Hu, D. Zhu, Empirical analysis of the worldwide maritime transportation network, *Physica A* 388 (2009) 2061–2071.
- [88] W. Li, X. Cai, Statistical analysis of airport network of China, *Phys. Rev. E* 69 (2004) 046106.
- [89] R. Guimerà, L.A.N. Amaral, Modeling the world-wide airport network, *Eur. Phys. J. B* 38 (2004) 381–385.
- [90] R. Guimerà, S. Mossa, A. Turtschi, L.A.N. Amaral, The worldwide air transportation network: anomalous centrality, community structure, and cities’ global roles, *Proc. Natl. Acad. Sci. (USA)* 102 (2005) 7794–7799.
- [91] G. Bianconi, P. Pin, M. Marsili, Assessing the relevance of node features for network structure, *Proc. Natl. Acad. Sci. (USA)* 106 (2009) 11433.
- [92] C. von Ferber, T. Holovatch, Y. Holovach, V. Palchykov, Public transport networks: empirical analysis and modeling, *Eur. Phys. J. B* 68 (2009) 261–275.
- [93] K.A. Seaton, L.M. Hackett, Stations, trains and small-world networks, *Physica A* 339 (2004) 635–644.
- [94] K. Lee, W.-S. Jung, J.S. Park, M.Y. Choi, Statistical analysis of the metropolitan Seoul subway system: network structure and passenger flows, *Physica A* 387 (2008) 6231–6234.
- [95] C. Roth, S. Kang, M. Batty, M. Barthélémy, Commuting in polycentric cities, *PLoS One* (in press).
- [96] M. Kurant, P. Thiran, Layered complex networks, *Phys. Rev. Lett.* 96 (2006) 138701.
- [97] G. Chowell, J.M. Hyman, S. Eubank, C. Castillo-Chavez, Scaling laws for the movement of people between locations in a large city, *Phys. Rev. E* 68 (2003) 066102.
- [98] A.de Montis, M. Barthélémy, A. Chessa, A. Vespignani, Structure of inter-cities traffic: a weighted network analysis, *Environ. Plan. A* 39 (2007) 905–924.
- [99] S. Caschili, A.De Montis, A. Chessa, G. Deplano, Weighted networks and community detection: planning productive districts in Sardinia, in: G. Rabino and M. Caglioli (Eds.) Planning, Complexity and New ICT Alinea Editrice s.r.l., 2009, pp. 27–36.
- [100] C. Thiemann, F. Theis, D. Grady, R. Brune, D. Brockmann, The structure of borders in a small world, *arXiv:1001.0943*, 2010.
- [101] V.D. Blondel, J.-L. Guillaume, R. Lambiotte, E. Lefebvre, Fast unfolding of communities in large networks, *J. Stat. Mech.* 2008 (2008) P10008.
- [102] V.D. Blondel, G.M. Krings, I. Thomas, Regions and borders of mobile telephony in Belgium and around Brussels, *Brussels Stud.* 42 (2010) 1–13.
- [103] X. Xu, J. Hu, P. Liu, Empirical analysis of the ship-transport network of China, *Chaos* 17 (2007) 023129.
- [104] P. Kaluza, A. Koelsch, M.T. Gastner, B. Blasius, The complex network of global cargo ship movements, *J. R. Soc. Interface* 7 (2010) 1093–1103.
- [105] V. Colizza, M. Barthélémy, A. Vespignani, Typology of nodes in weighted directed networks, 2008 (unpublished).
- [106] D. Levinson, B. Yerra, Self-organization of surface transportation networks, *Transport. Sci.* 40 (2006) 179–188.
- [107] M. Batty, Cities and Complexity, MIT Press, Cambridge, 2005.

- [108] H. Makse, J.S. Andrade, M. Batty, S. Havlin, Modeling urban growth patterns with correlated percolation, *Phys. Rev. E* 58 (1998) 7054.
- [109] C. Clark, Urban population densities, *J. R. Stat. Soc. Ser. A* 114 (1951) 490–496.
- [110] P. Crucitti, V. Latora, S. Porta, Centrality measures in spatial networks of urban streets, *Phys. Rev. E* 73 (2006) 036125.
- [111] B. Jiang, C. Claramunt, Topological analysis of urban street networks, *Environ. Plan. B* 31 (2004) 151–162.
- [112] B. Jiang, A topological pattern of urban street networks: universality and peculiarity, *Physica A* 384 (2007) 647–655.
- [113] B. Hillier, J. Hanson, *The Social Logic of Space*, Cambridge University Press, Cambridge, 1984.
- [114] M. Barthélémy, A. Flammini, Modeling urban street patterns, *Phys. Rev. Lett.* 100 (2008) 138702.
- [115] S. Gerke, C. Mcdiarmid, On the number of edges in random planar graphs, *Combin. Probab. Comput.* 13 (2004) 165.
- [116] A.P. Masucci, D. Smith, A. Crooks, M. Batty, Random planar graphs and the London street network, *Eur. Phys. J. B* 71 (2009) 259–271.
- [117] M. Schreckenberg, R. Selten, *Human Behaviour and Traffic Networks*, Springer Verlag, Berlin, 2004.
- [118] B.M. Yerra, D.M. Levinson, The emergence of hierarchy in transportation networks, *Ann. Reg. Sci.* 39 (2005) 541–553.
- [119] S. Scellato, A. Cardillo, V. Latora, S. Porta, The backbone of a city, *Eur. Phys. J. B* 50 (2006) 221–225.
- [120] E. Strano, A. Cardillo, V. Iacoviello, V. Latora, R. Messora, S. Porta, S. Scellato, Street centrality vs. commerce and service locations in cities: a kernel density correlation case study in Bologna, Italy, *Environ. Plan. B: Plan. Design* 36 (2009) 450–465.
- [121] L.Da.F. Costa, B.A.N. Travencolo, M.P. Viana, E. Strano, On the efficiency of transportation systems in large cities, *Europhys. Lett.* 91 (2010) 18003.
- [122] R. Albert, I. Albert, G.L. Nakarado, Structural vulnerability of the North American power grid, *Phys. Rev. E* 69 (2004) 025103.
- [123] R.V. Solé, M. Rosas-Casals, B. Corominas-Murtra, S. Valverde, Robustness of the European power grids under intentional attack, *Phys. Rev. E* 77 (2008) 026102.
- [124] E. Ravasz, A.-L. Barabási, Hierarchical organization in complex networks, *Phys. Rev. E* 67 (2003) 026112.
- [125] A. Yazdani, P. Jeffrey, A complex network approach to robustness and vulnerability of spatially organized water distribution networks, *arXiv: 1008.1770*, 2010.
- [126] T.M. Walski, E.D. Brill, J. Gessler, I.C. Goulter, R.M. Jeppson, K. Lansey, L. Han-Lin, J.C. Liebman, L. Mays, D.R. Morgan, L. Ormsbee, Battle of the network models: epilogue, *J. Water Resour. Plan. Manage.* 113 (1987) 191–203.
- [127] R. Farmani, D.A. Savic, G.A. Walters, Exnet benchmark problem for multi-objective optimization of large water systems, in: *Modelling and Control for Participatory Planning and Managing Water Systems*, IFAC Workshop, Venice, Italy, 2004.
- [128] S.-H. Yook, H. Jeong, A.-L. Barabasi, Modeling the Internet's large-scale topology, *Proc. Natl. Acad. Sci. (USA)* 99 (2002) 13382.
- [129] A. Bunde, S. Havlin, Percolation, in: A. Bunde, S. Havlin (Eds.), *Fractals and Disordered Systems*, Springer Verlag, Heidelberg, 1991, pp. 51–95.
- [130] C. Song, S. Havlin, H. Makse, Self-similarity in complex networks, *Nature* 433 (2005) 392–395.
- [131] B.M. Waxman, Routing of multipoint connections, *IEEE J. Select. Areas Commun.* 6 (1988) 1617.
- [132] G.K. Zipf, *Human Behaviour and the Principle of Least Effort*, Addison-Wesley, Cambridge, MA, 1949.
- [133] R. Lambiotte, V.D. Blondel, C. de Kerchove, E. Huens, C. Prieur, Z. Smoreda, P. Van dooren, Geographical dispersal of mobile communication networks, *Physica A* 387 (2008) 5317–5325.
- [134] G. Krings, F. Calabrese, C. Ratti, V.D. Blondel, A gravity model for inter-city telephone communication networks, *J. Stat. Mech* 2009 (2009) L07003.
- [135] J.M. Kleinberg, Navigation in a small world, *Nature* 406 (2000) 845.
- [136] D. Liben-Nowell, J. Nowak, R. Kumar, P. Raghavan, A. Tomkins, Geographic routing in social networks, *Proc. Natl. Acad. Sci. (USA)* 102 (2005) 11623–11628.
- [137] J. Goldenberg, M. Levy, Distance is not dead: social interaction and geographical distance in the Internet era, *arXiv:0906.3202*, 2009.
- [138] L. Backstrom, E. Sun, C. Marlow, Find me if you can: improving geographical prediction with social and spatial proximity, in: *Proceedings of the 19th international conference on World Wide Web*, Raleigh, North Carolina, USA, ACM, New York, NY, USA, 2010, pp. 61–70.
- [139] L. Adamic, E. Adar, How to search a social network, *Soc. Netw.* 27 (2005) 187–203.
- [140] Y. Hu, Y. Wang, D. Li, S. Havlin, Z. Di, Maximizing entropy yields spatial scaling in social networks, *arXiv:1002.1802*, 2010.
- [141] S. Scellato, C. Mascolo, M. Musolesi, V. Latora, Distance matters: geo-social metrics for online social networks, in: *Proceedings of the 3rd Workshop on Online Social Networks*, WOSN 2010, Boston, USA, 2010.
- [142] A.K. Chandra, K.B. Hajra, P.K. Das, P. Sen, Modeling temporal and spatial features of collaboration networks, *Int. J. Modern Phys. C* 18 (2007) 1157–1172.
- [143] V. Colizza, A. Barrat, M. Barthélémy, A. Vespignani, Prediction and predictability of global epidemics: the role of the airline transportation network, *Proc. Natl. Acad. Sci. (USA)* 103 (2006) 2015.
- [144] P.L. Mokhtarian, C. Chen, Ttb or not ttb, that is the question: a review and analysis of the empirical literature on travel time (and money) budgets, *Transport. Res. Part A: Policy Practice* 38 (2004) 643–675.
- [145] Y. Zahavi, *The UMOT Model*, The World Bank, Washington, DC, 1977.
- [146] D. Levinson, Y. Wu, The rational locator reexamined: are travel times still stable, *Transportation* 32 (2005) 187–202.
- [147] R. Koelbl, D. Helbing, Energy and scaling laws in human travel behaviour, *New J. Phys.* 5 (2003) 48.
- [148] J.-P. Hubert, P.L. Toint, From average travel time budgets to daily travel time distributions: appraisal of two conjectures by Koelbl and Helbing and some consequences, *J. Transport. Rese. Board* 1985 (2007) 135–143.
- [149] R. Ahas, U. Mark, A. Aasa, H. Kalle, Mapping human behavior in Tallinn, in: *Tallinn, Delft: TU Delft*, 2001.
- [150] A. Aasa, O. Järv, E. Saluveer, S. Slim, R. Ahas, Methodology of determination of the anchor points based on passive mobile positioning database, *Social Positioning Method*, 2008.
- [151] N. Eagle, S. Pentland, Eigenbehaviors: identifying structure in routine, *Behav. Ecol. Sociobiol.* 63 (2009) 1057–1066.
- [152] M.C. Gonzalez, C.A. Hidalgo, A.-L. Barabasi, Understanding individual human mobility patterns, *Nature* 453 (2008) 779–782.
- [153] A. Sevtsuk, C. Ratti, Does urban mobility have a daily routine? learning from the aggregate data of mobile networks, *J. Urban Technol.* 17 (2010) 41–60.
- [154] D. Brockmann, L. Hufnagel, T. Geisel, The scaling laws of human travel, *Nature* 439 (2006) 462–465.
- [155] C. Song, T. Koren, P. Wang, A.-L. Barabasi, Modelling the scaling properties of human mobility, *Nature Phys.* (2010).
- [156] S. Rambaldi, A. Bazzani, B. Giorgini, L. Giovannini, Mobility in modern cities: looking for physical laws, in: *Proceedings of the ECCS'07*, 2007, p. 132.
- [157] A. Bazzani, B. Giorgini, S. Rambaldi, R. Gallotti, L. Giovannini, Statistical laws in urban mobility from microscopic gps data in area of florence, *J. Stat. Mech.* 2010 (2010) P05001.
- [158] S. Erlander, N.F. Stewart, *The Gravity Model in Transportation Analysis*, VSP, Utrecht, The Netherlands, 1990.
- [159] J.E. Anderson, Theoretical foundation for the gravity equation, *Amer. Econom. Rev.* 69 (1979) 106–116.
- [160] J.H. Bergstrand, The gravity equation in international trade: some microeconomic foundations and empirical evidence, *Rev. Econ. Statist.* 67 (1985) 474–481.
- [161] W.-S. Jung, F. Wang, H.E. Stanley, Gravity model in the Korean highway, *Europhys. Lett.* 81 (2008) 48005.
- [162] D. Balcan, V. Colizza, B. Goncalves, H. Hu, J.R. Ramasco, A. Vespignani, Multiscale mobility networks and the large spreading of infectious diseases, *Proc. Natl. Acad. Sci. (USA)* 106 (2009) 21484.
- [163] C. Viboud, O.N. Bjornstad, D.L. Smith, L. Simonsen, M.A. Miller, B.T. Grenfell, Synchrony, waves, and spatial hierarchies in the spread of influenza, *Science* 312 (2006) 447–451.
- [164] G.K. Zipf, The  $p_1 p_2/d$  hypothesis: on the intercity movement of persons, *Amer. Sociol. Rev.* 11 (1946) 677–686.
- [165] A.G. Wilson, A statistical theory of spatial distribution models, *Transport. Res.* 1 (1967) 253–269.
- [166] H. Samaniego, M.E. Moses, Cities as organisms: allometric scaling of urban road networks, *J. Transport Land Use* 1 (2008) 21–39.
- [167] G.B. West, J.H. Brown, B.J. Enquist, General model for the origin of allometric scaling laws in biology, *Science* 276 (1997) 122.
- [168] J.R. Banavar, A. Maritan, A. Rinaldo, Size and form in efficient transportation networks, *Nature* 399 (1999) 130.

- [169] M. Chavez, M. Valencia, V. Latora, J. Martinic, Complex networks: new trends for the analysis of brain connectivity, *Int. J. Bif. Chaos* 20 (2010) 1677–1686.
- [170] V.M. Eguiluz, D.R. Chialvo, G.A. Cecchi, M. Baliki, A.V. Apkarian, Scale-free brain functional networks, *Phys. Rev. Lett.* 94 (2005) 018102.
- [171] M. Kaiser, C.C. Hilgetag, Modelling the development of cortical systems networks, *Neurocomputing* 58–60 (2004) 297–302.
- [172] M. Kaiser, C.C. Hilgetag, Nonoptimal component placement, but short processing paths, due to long-distance projections in neural systems, *PLoS Comp. Biol.* 2 (2005) 0805–0815.
- [173] L.F. Lago-Fernandez, R. Huerta, F. Corbacho, J.A. Siguenza, Fast response and temporal coding on coherent oscillations in small-world networks, *Phys. Rev. Lett.* 84 (2000) 2758.
- [174] D.S. Modha, R. Singh, Network architecture of the long-distance pathways in the macaque brain, *Proc. Natl. Acad. Sci. (USA)* 107 (2009) 13485–13490.
- [175] A. Zalesky, A. Fornito, I.H. Harding, L. Cocchi, M. Yucel, C. Pantelis, E.T. Bullmore, Whole-brain anatomical networks: does the choice of node matters, *NeuroImage* 50 (2010) 970–983.
- [176] C.J. Honey, O. Sporns, L. Cammoun, X. Gigandet, J.-P. Thiran, R. Meuli, P. Hagmann, Predicting human resting-state functional connectivity from structural connectivity, *Proc. Natl. Acad. Sci. (USA)* 106 (2010) 2035–2040.
- [177] G. Bagler, Analysis of the airport network of India as a complex weighted network, *Physica A* 387 (2008) 2972–2980.
- [178] L. Dall'asta, A. Barrat, M. Barthélémy, A. Vespignani, Vulnerability of weighted networks, *J. Stat. Mech.* (2006) P04006.
- [179] X. Xu, J. Hu, F. Liu, L. Liu, Scaling and correlations in 3 bus-transport networks of China, *Physica A* 374 (2007) 441.
- [180] P. Crucitti, V. Latora, M. Marchiori, A topological analysis of the Italian electric power grid, *Physica A* 338 (2004) 92–97.
- [181] C.C. Hilgetag, G.A.P.C. Burns, M.A. O'Neill, J.W. Scannell, M.P. Young, Theoretical neuroanatomy: relating anatomical and functional connectivity in graphs and cortical connection matrices, *Phil. Trans. R. Soc. Lond. B* 355 (2000) 91.
- [182] R. Albert, H. Jeong, A.-L. Barabasi, Diameter of the World Wide Web, *Nature* 401 (1999) 130–131.
- [183] E.N. Gilbert, Random plane networks, *J. Soc. Ind. Appl. Math.* 9 (1961) 533–543.
- [184] I. Balberg, Universal percolation-threshold limits in the continuum, *Phys. Rev. B* 31 (1985) 4053.
- [185] J. Quantanilla, S. Torquato, R.M. Ziff, Efficient measurement of the percolation threshold for fully penetrable discs, *Physica A* 33 (2000) L399.
- [186] J. Dall, M. Christensen, Random geometric graphs, *Phys. Rev. E* 66 (2002) 016121.
- [187] J.B. Gouéré, Subcritical regimes in the Poisson Boolean model of continuum percolation, *Ann. Probab.* 36 (2008) 1209–1220.
- [188] M.L. Huson, A. Sen, Broadcast scheduling algorithms for radio networks, in: *Militart Communications Conference, IEEE MILCOM'95* vol. 2, 1995 647–651.
- [189] C. Herrmann, M. Barthélémy, P. Provero, Connectivity distribution of spatial networks, *Phys. Rev. E* 68 (2003) 026128.
- [190] G. Nemeth, G. Vattay, Giant clusters in random ad hoc networks, *Phys. Rev. E* 67 (2003) 036110.
- [191] M.E.J. Newman, S.H. Strogatz, D.J. Watts, Random graphs with arbitrary degree distributions and their applications, *Phys. Rev. E* 64 (2001) 026118.
- [192] M.C. Gonzalez, H.J. Herrmann, Scaling of the propagation of epidemics in a system of mobile agents, *Physica A* 340 (2004) 741–748.
- [193] M.C. Gonzalez, P.G. Lind, H.J. Herrmann, System of mobile agents to model social networks, *Phys. Rev. Lett.* 96 (2006) 088702.
- [194] M.C. Gonzalez, P.G. Lind, H.J. Herrmann, Model of mobile agents for sexual interaction networks, *Eur. Phys. J. B* 49 (2006) 371–376.
- [195] M. Angeles serrano, D. Krioukov, M. Boguñá, Self-similarity of complex networks and hidden metric spaces, *Phys. Rev. Lett.* 100 (2008) 078701.
- [196] D. Krioukov, F. Papadopoulos, M. Kitsak, A. Vahdat, M. Boguñá, Hyperbolic geometry of complex networks, *Phys. Rev. E* 82 (2010) 036106.
- [197] A.F. Rozenfeld, R. Cohen, D. ben Avraham, S. Havlin, Scale-free networks on lattices, *Phys. Rev. Lett.* 89 (2002) 218701.
- [198] C.P. Warren, L.M. Sander, I.M. Sokolov, Geography in a scale-free network model, *Phys. Rev. E* 66 (2002) 056105.
- [199] J.S. Andrade Jr., H.J. Herrmann, R.F.S. Andrade, L.R. da Silva, Apollonian networks, *Phys. Rev. Lett.* 94 (2005) 018702.
- [200] Z. Zhang, L. Chen, S. Zhou, L. Fang, J. Guan, T. Zou, Analytical solution of average path length for Apollonian networks, *Phys. Rev. E* 77 (2008) 017102.
- [201] Z. Zhang, J. Guang, B. Ding, L. Chen, S. Zhou, Contact graphs of disk packings as a model of spatial planar networks, *New J. Phys.* 11 (2009) 083007.
- [202] P. Erdős, P. Rényi, On the strength of connectedness of random graphs, *Acta. Math. Sci. Hung.* 12 (1961) 261–267.
- [203] R.M. Ziff, R.D. Vigil, Kinetics and fractal properties of the random sequential adsorption of line segments, *J. Phys. A: Math. Gen.* 23 (1990) 5103–5108.
- [204] A. Denise, M. Vasconcellos, D. Welsh, The random planar graph, *Congr. Numer.* 113 (1996) 61–79.
- [205] C. Mcdiarmid, A. Steger, D.J.A. Welsh, Random planar graphs, *J Combin. Theory* 93 (2005) 187–205.
- [206] G. Caldarelli, A. Capocci, P. De Los Rios, M.A. Munoz, Scale-free networks from varying vertex intrinsic fitness, *Phys. Rev. Lett.* 89 (2002) 258702.
- [207] M. Boguñá, R. Pastor-Satorras, Class of correlated random networks with hidden variables, *Phys. Rev. E* 68 (2003) 036112.
- [208] N. Masuda, H. Miwa, N. Konno, Geographical threshold graphs with small-world and scale-free properties, *Phys. Rev. E* 71 (2005) 036108.
- [209] Y. Hayashi, A review of recent studies of geographical scale-free networks, *IPSJ Trans. Netw. Ecol.* 47 (2006) 776–785 (special issue).
- [210] M. Boguñá, R. Pastor-Satorras, A. Diaz-Guilera, A. Arenas, Model of social networks based on social distance attachment, *Phys. Rev. E* 70 (2004) 056122.
- [211] L.H. Wong, P. Pattison, G. Robins, A spatial model for social networks, *Physica A* 360 (2006) 99–120.
- [212] E.W. Zegura, K.L. Calvert, S. Bhattacharjee, How to model an internetwork, *Proc. IEEE Infocom.* (1996) 594–602.
- [213] M. Kaiser, C.C. Hilgetag, Spatial growth of real-world networks, *Phys. Rev. E* 69 (2004) 036103.
- [214] A.K.M. Stoneham, The small-world problem in a spatial context, *Environ. Plan. A* 9 (1977) 185–195.
- [215] A. Barrat, M. Weigt, On the properties of small-world network models, *Eur. Phys. J. B* 13 (2000) 547.
- [216] M. Barthélémy, L.A.N. Amaral, Erratum: small-world networks: evidence for a crossover, *Phys. Rev. Lett.* 82 (1999) 5180.
- [217] S. Jespersen, A. Blumen, Small-world networks with long-tailed distributions, *Phys. Rev. E* 62 (2000) 6270–6274.
- [218] P. Sen, B.K. Chakrabarti, Small-world phenomena and the statistics of linear polymer, *J. Phys. A* 34 (2001) 7749.
- [219] P. Sen, K. Banerjee, T. Biswas, Phase transitions in a network with a range-dependent connection probability, *Phys. Rev. E* 66 (2002) 037102.
- [220] C.F. Moukarzel, M. Argollo de Menezes, Shortest paths on systems with power-law distributed long-range connections, *Phys. Rev. E* 65 (2002) 056709.
- [221] T. Petermann, P. De Los Rios, Spatial small-worlds networks: a wiring-cost perspective, *arXiv:cond-mat/0501420*, 2005.
- [222] M.E.J. Newman, D.J. Watts, Scaling and percolation in the small-world network model, *Phys. Rev. E* 60 (1999) 7332–7342.
- [223] K. Kosmidis, S. Havlin, A. Bunde, Structural properties of spatially embedded networks, *Europhys. Lett.* 82 (2008) 48005.
- [224] H.A. Simon, On a class of skew distribution functions, *Biometrika* 42 (1955) 425.
- [225] J. Jost, M.P. Joy, Evolving networks with distance preferences, *Phys. Rev. E* 66 (2002) 036126.
- [226] S.S. Manna, P. Sen, Modulated scale-free network in Euclidean space, *Phys. Rev. E* 66 (2002) 066114.
- [227] R. Xulvi-Brunet, I.M. Sokolov, Evolving networks with disadvantaged long-range connections, *Phys. Rev. E* 66 (2002) 026118.
- [228] M. Barthélémy, Crossover from spatial to scale-free networks, *Europhys. Lett.* 63 (2003) 915–921.
- [229] A. Barrat, M. Barthélémy, A. Vespignani, Weighted evolving networks: coupling topology and weights dynamics, *Phys. Rev. Lett.* 92 (2004) 228701.
- [230] P. Sen, S.S. Manna, Clustering properties of a generalized critical Euclidean network, *Phys. Rev. E* 68 (2003) 026104.
- [231] A. Fabrikant, E. Koutsoupias, C.H. Papadimitriou, Heuristically optimized trade-offs: a new paradigm for power laws in the Internet, in: *Proceeding of the 29th International Colloquium on Automata, Languages, and Programming, ICALP*, in: *Lecture Notes in Computer Science*, vol. 2380, Springer, 2002, pp. 110–122.
- [232] M.T. Gastner, M.E.J. Newman, Shape and efficiency in spatial distribution networks, *J. Stat. Mech.* (2006) P01015.
- [233] A. Bejan, G.A. Ledeza, Streets tree networks and urban growth: optimal geometry for quickest access between a finite-size volume and one point, *Physica A* 255 (1998) 211–217.
- [234] B. Duplantier, Statistical mechanics of polymer networks of any topology, *J. Stat. Phys.* 54 (1989) 581–680.
- [235] A. Coniglio, Fractal structure of Ising and Potts clusters: exact results, *Phys. Rev. Lett.* 62 (1989) 3054.
- [236] M. Barthélémy, A. Flammini, Co-evolution of density and topology in a simple model of city formation, *Netw. Spatial Econom.* 9 (2009) 401–425.
- [237] J.G. Wardrop, *Proc. Institut. Civil Eng.* 1 (1952) 325–378.
- [238] R.K. Ahuja, T.L. Magnanti, J.B. Orlin, *Network Flows*, Prentice Hall, New Jersey, 1993.

- [239] G. Kirchoff, Über die auslosung der gleichungen, auf welche man bei der untersuchung der linearen verteilung galvanischer strome gefurhrt wird, Ann. Phys. und Chemie 72 (1847) 497–508.
- [240] P.G. Doyle, J.L. Snell, Random walks and electric networks, The Mathematical Association of America, USA, 1984, pp. 83–149.
- [241] T.A. McMahon, J.T. Bonner, On Size and Life, Scientific American Library, New York, 1983.
- [242] D. Garlaschelli, G. Caldarelli, L. Pietronero, Universal scaling relations in food webs, Nature 423 (2003) 165.
- [243] A. Maritan, F. Colaiori, A. Flammini, M. Cieplak, J.R. Banavar, Universality classes of optimal networks, Science 272 (1996) 984–986.
- [244] N. Mathias, V. Gopal, Small-worlds: how and why, Phys. Rev. E 63 (2001) 021117.
- [245] J. Berg, M. Lassig, Correlated random networks, Phys. Rev. Lett. 89 (2002) 228701.
- [246] S. Valverde, R. Ferrer Cancho, R.V. Solé, Scale-free networks from optimal design, Europhys. Lett. 60 (2002) 512–517.
- [247] R. Ferrer i Cancho, R.V. Solé, Optimization in complex networks, in: Statistical Mechanics of Complex Networks, in: Lecture Notes in Physics, vol. 625, Springer, 2003, pp. 114–125.
- [248] R. Guimerà, A. Diaz-Guilera, F. Vega-Redondo, A. Cabrales, A. Arenas, Optimal network topologies for local search with congestion, Phys. Rev. Lett. 89 (2002) 248701.
- [249] V. Colizza, J.R. Banavar, A. Maritan, A. Rinaldo, Network structures from selection principles, Phys. Rev. Lett. 92 (2004) 198701.
- [250] M.E. O'Kelly, A quadratic integer program for the location of interaction hub facilities, J. Oper. Res. 32 (1987) 393–404.
- [251] D.L. Bryan, M.E. O'Kelly, Hub-and-spoke networks in air transportation: an analytical review, J. Reg. Sci. 39 (1999) 275–295.
- [252] M.E. O'Kelly, Routing traffic at hub facilities, Netw. Spat. Econ. 10 (2010) 173–191.
- [253] D.J. Aldous, Spatial transportation networks with transfer costs: asymptotic optimality of hub and spoke models, in: Mathematical Proceedings of the Cambridge Philosophical Society, Cambridge University Press, 2008, pp. 471–487.
- [254] D.J. Ashton, T.C. Jarrett, N.F. Johnson, Effect of congestion costs on shortest paths through complex networks, Phys. Rev. Lett. 94 (2005) 058701.
- [255] T.C. Jarrett, D.J. Ashton, M. Fricker, N.F. Johnson, Interplay between function and structure in complex networks, Phys. Rev. E 74 (2006) 026116.
- [256] S.N. Dorogovtsev, J.F.F. Mendes, Exactly solvable small-world network, Europhys. Lett. 50 (2000) 1.
- [257] D.J. Aldous, Optimal spatial transportation networks where link-costs are sublinear in link-capacity, J. Stat. Mech. 2008 (2008) P03006.
- [258] M. Barthélémy, A. Flammini, Optimal traffic networks, J. Stat. Mech. (2006) L07002.
- [259] M.D. Penrose, The longest edge of the random minimal spanning tree, Ann. Appl. Probab. 7 (1997) 340–361.
- [260] J. Beardwood, J.H. Halton, J.M. Hammersley, The shortest path through many points, Proc. Cambridge Philos. Soc. 55 (1959) 299–327.
- [261] J.M. Steele, Growth rates of Euclidean minimal spanning trees with power weighted edges, Ann. Probab. 16 (1988) 1767–1787.
- [262] Z. Wu, L.A. Braunstein, S. Havlin, H.E. Stanley, Transport in weighted networks: partition into superhighways and roads, Phys. Rev. Lett. 96 (2006) 148702.
- [263] R. Dobrin, P.M. Duxbury, Minimum spanning trees on random networks, Phys. Rev. Lett. 86 (2001) 5076–5079.
- [264] N. Read, Minimum spanning trees and random resistor networks in  $d$  dimensions, Phys. Rev. E 72 (2005) 036114.
- [265] T.S. Jackson, N. Read, Theory of minimum spanning trees. i. mean-field theory and strongly disordered spin-glass model, Phys. Rev. E 81 (2010) 021130.
- [266] H. Takayasu, M. Takayasu, A. Provata, G. Huber, Statistical properties of aggregation with injection, J. Stat. Phys. 65 (1991) 725.
- [267] S.S. Manna, D. Dhar, S.N. Majumdar, Spanning trees in two dimensions, Phys. Rev. A 46 (1992) R4471.
- [268] P. De Los Rios, Power law size distribution of supercritical random trees, Europhys. Lett. 56 (2001) 898–903.
- [269] K.I. Goh, E. Oh, H. Jeong, B. Kahng, D. Kim, Classification of scale-free networks, Proc. Natl. Acad. Sci. (USA) 99 (2002) 12583.
- [270] S. Khuller, B. Raghavachari, N. Young, Balancing minimum spanning trees and shortest-path trees, Algorithmica 14 (1995) 305–321.
- [271] M. Bayati, C. Borgs, A. Braunstein, J. Chayes, A. Ramezanpour, R. Zecchin, Statistical mechanics of Steiner trees, Phys. Rev. Lett. 101 (2010) 037208.
- [272] M. Mézard, G. Parisi, M.-A. Virasoro, Spin Glass and Beyond, World Scientific, 1987.
- [273] J.W. Billheimer, P. Gray, Network design with fixed and variable cost elements, Transport. Sci. 7 (1973) 49–74.
- [274] K.A.K. Bhattacharyya, S.S. Manna, Optimal network for passenger traffic, Physica A 388 (2009) 3651–3656.
- [275] M.T. Gastner, M.E.J. Newman, The spatial structure of networks, Eur. Phys. J. B 49 (2006) 247–252.
- [276] M. Brede, Coordinated and uncoordinated optimization of networks, Phys. Rev. E 81 (2010) 066104.
- [277] A. Arenas, A. Diaz-Guilera, J. Kurths, Y. Moreno, C. Zhou, Synchronization in complex networks, Phys. Rep. 469 (2008) 93–153.
- [278] L. Donetti, P.I. Hurtado, M.A. Munoz, Entangled networks, synchronization and optimal network topology, Phys. Rev. Lett. 95 (2005) 188701.
- [279] M. Brede, Optimal synchronization in space, Phys. Rev. E (2010) 025202(R).
- [280] M. Brede, Small worlds in space: synchronization, spatial and relational modularity, Europhys. Lett. 90 (2010) 60005.
- [281] F. Corson, Fluctuations and redundancy in optimal transport networks, Phys. Rev. Lett. 104 (2010) 048703.
- [282] E. Katifori, Damage and fluctuations induce loops in optimal transport networks, Phys. Rev. Lett. 104 (2010) 048704.
- [283] D. Mukamel, Statistical mechanics of systems with long range interactions, in: A. Campa, A. Giansanti, G. Morigi, F. Sylos Labini, (Eds.), AIP Conference Proceedings: Dynamics and Thermodynamics of Systems with Long-Range Interactions: Theory and Experiments, vol. 22, 2008, p. 970.
- [284] C. Castellano, S. Fortunato, V. Loreto, Statistical physics of social dynamics, Rev. Modern Phys. 81 (2009) 591–646.
- [285] C. Herrero, Ising model in small-world networks, Phys. Rev. E 65 (2002) 066110.
- [286] A. Chatterjee, P. Sen, Phase transition on Ising model on a Euclidean network, Phys. Rev. E 74 (2006) 036117.
- [287] Y.F. Chang, L. Sun, X. Cai, Phase transition of a one-dimensional Ising model with distance dependent connections, Phys. Rev. E 76 (2007) 021101.
- [288] S. Bradde, F. Caccioli, L. Dall'asta, G. Bianconi, Critical fluctuations in spatial complex networks, Phys. Rev. Lett. 104 (2010) 218701.
- [289] M. Fisher, S.-K. Ma, B.G. Nickel, Critical exponents for long-range interactions, Phys. Rev. Lett. 29 (1972) 917–920.
- [290] G.H. Weiss, Aspects and Applications of Random Walk, North-Holland, Amsterdam, 1994.
- [291] E.N. Economou, Green's Functions in Quantum Physics, Springer, 2006.
- [292] G.J. Rodgers, A.J. Bray, Density of states of a sparse random matrix, Phys. Rev. B 37 (1988) 3557–3562.
- [293] S. Jespersen, I.M. Sokolov, A. Blumen, Relaxation properties of small-world networks, Phys. Rev. E 62 (2000) 4405–4408.
- [294] R. Monasson, Diffusion, localization and dispersion relations on small-world lattices, Eur. Phys. B 12 (1999) 555–567.
- [295] E. Almasi, R.V. Kulkarni, D. Stroud, Scaling properties of random walks on small-world networks, Phys. Rev. E 68 (2003) 056105.
- [296] F. Jasch, A. Blumen, Target problem on small-world networks, Phys. Rev. E 63 (2001) 041108.
- [297] A. Dvoretzky, P. Erdos, Some problems on random walks in space, in: Proceedings of the 2nd Berkeley Symposium on Mathematical Statistics and Probability, University of California Press, Berkeley, California, 1950, pp. 353–367.
- [298] B. Kozma, M.B. Hastings, G. Korniss, Diffusion process on power-law small-world networks, Phys. Rev. Lett. 95 (2005) 018701.
- [299] B. Kozma, M.B. Hastings, G. Korniss, Processes on small-world networks with distance-dependent random links, J. Stat. Mech. (2007) P08014.
- [300] A. Diaz-Guilera, J. Gomez-Gardenes, Y. Moreno, M. Nekovee, Synchronization in random geometric graphs, Internat. J. Bifur. Chaos 19 (2009) 687–693.
- [301] H. Hong, M.Y. Choi, B.J. Kim, Synchronization on small-world networks, Phys. Rev. E 65 (2002) 026139.
- [302] P.G. Lind, J.A.C. Gallas, H.J. Herrmann, Coherence in scale-free networks of chaotic maps, Phys. Rev. E 70 (2004) 056207.
- [303] S. Milgram, The small world problem, Psychol. Today 2 (1967) 60–67.
- [304] H.P. Thadakamalia, R. Albert, S.R.T. Kumara, Search in spatial scale-free networks, New J. Phys. 9 (2007) 190.
- [305] P.D. Killworth, H.R. Bernard, The reversal small-world experiment, Soc. Networks 1 (1978) 159–192.
- [306] M.R. Roberson, D. ben Avraham, Kleinberg navigation in fractal small world networks, Phys. Rev. E 74 (2006) 017101.
- [307] J. Kleinberg, The small-world phenomenon: an algorithmic perspective, Technical Report 99–1776, Cornell Computer Science, 1999.
- [308] H. Zhu, Z.-X. Huang, Navigation in a small world with local information, Phys. Rev. E 70 (2004) 021101.
- [309] C.C. Cartozo, P. De Los Rios, Extended navigability of small world networks: exact results and new insights, arXiv:0901.4710 2009.
- [310] J. Sun, D. ben Avraham, Greedy connectivity of geographically embedded graphs, Phys. Rev. E 82 (2010) 016109.
- [311] L.A. Adamic, R.M. Lukose, A.R. Puniyani, B.A. Huberman, Search in power-law networks, Phys. Rev. E 64 (2001) 046135.

- [312] K.B. Hajra, P. Sen, Effect of a static phase transition on searching dynamics, *J. Stat. Mech.* 2007 (2007) P06015.
- [313] M. Boguñá, D. Krioukov, kc. Claffy, Navigability of complex networks, *Nature Phys.* 5 (2009) 74–80.
- [314] M. Boguñá, F. Papadopoulos, D. Krioukov, Sustaining the Internet with hyperbolic mapping, *Nature Commun.* (2010) 1.
- [315] C. Li, S.D.S. Reis, A.A. Moreira, S. Havlin, H.E. Stanley, J.S. Andrade Jr., Towards design principles for optimal transport networks, *Phys. Rev. Lett.* 104 (2010) 018701.
- [316] R. Cohen, K. Erez, D. ben Avraham, S. Havlin, Resilience of the Internet to random breakdowns, *Phys. Rev. Lett.* 85 (2000) 4626.
- [317] D. Stauffer, A. Aharony, *Introduction to Percolation Theory*, Taylor & Francis, London, 1992.
- [318] D.S. Callaway, M.E.J. Newman, S.H. Strogatz, D.J. Watts, Network robustness and fragility: percolation on random graphs, *Phys. Rev. Lett.* 85 (2000) 5468–5471.
- [319] C. Moore, M.E.J. Newman, Exact solution of site and bond percolation on small-world networks, *Phys. Rev. E* 62 (2000) 7059–7064.
- [320] M.E.J. Newman, I. Jensen, R.M. Ziff, Percolation and epidemics in a two-dimensional small world, *Phys. Rev. E* 65 (2002) 021904.
- [321] M. Ozana, Incipient spanning cluster on small-world networks, *Europhys. Lett.* 55 (2001) 762.
- [322] A.A. Moreira, J.S. Andrade Jr., H.J. Herrmann, J.O. Indekeu, How to make a fragile network robust and vice-versa, *Phys. Rev. Lett.* 102 (2009) 018701.
- [323] D.M. Auto, A.A. Moreira, H.J. Herrmann, J.S. Andrade Jr., Finite-size effects for percolation on Apollonian networks, *Phys. Rev. E* 78 (2008) 066112.
- [324] L.de Arcangelis, S. Redner, H.J. Herrmann, A random fuse model for breaking processes, *J. Phys. Lett.* 46 (1985) L585.
- [325] J.-P. Clerc, G. Giraud, J.-M. Laugier, J.-M. Luck, The electrical conductivity of binary disordered systems, percolation clusters, fractals and related models, *Adv. Phys.* 39 (1990) 191–309.
- [326] Y. Moreno, M. Nekovee, A. Vespignani, Efficiency and reliability of epidemic data dissemination in complex networks, *Phys. Rev. E* 69 (2004) 055101.
- [327] R. Kinney, P. Crucitti, R. Albert, V. Latora, Modeling cascading failures in the North American power grid, *Eur. Phys. J. B* 46 (2005) 101.
- [328] V. Latora, M. Marchiori, Vulnerability and protection of infrastructure networks, *Phys. Rev. E* 71 (2005) 015103(R).
- [329] D.R. Wuellner, S. Roy, R.M. D’souza, Structure and resilience of networks: airlines in USA, [arXiv:0901.0774](https://arxiv.org/abs/0901.0774), 2009.
- [330] S.V. Buldyrev, R. Parshani, G. Paul, H.E. Stanley, S. Havlin, Catastrophic cascade of failures in interdependent networks, *Nature* 464 (2010) 1025–1028.
- [331] R.M. Anderson, R.M. May, *Infectious Diseases of Humans: Dynamics and Control*, Oxford University Press, Oxford, 1992.
- [332] J.V. Noble, Geographic and temporal development of plagues, *Nature* 250 (1974) 726–728.
- [333] V. Colizza, M. Barthélémy, A. Barrat, A. Vespignani, Epidemic modeling in complex realities, *C.R. Biologies* 330 (2007) 364–374.
- [334] J.D. Murray, *Mathematical Biology*, 2nd ed., Springer, New-York, 1993.
- [335] P. Grassberger, On the critical behavior of the general epidemic process and dynamical percolation, *Math. Biosci.* 63 (1983) 157–172.
- [336] E. Kenah, J.M. Robins, Second look at the spread of epidemics on networks, *Phys. Rev. E* 76 (2007) 036113.
- [337] C.P. Warren, L.M. Sander, I.M. Sokolov, Firewalls, disorder and percolation in epidemics, [arXiv:cond-mat/0106450v1](https://arxiv.org/abs/cond-mat/0106450v1), 2001.
- [338] C.P. Warren, L.M. Sander, I.M. Sokolov, Epidemics, disorder, and percolation, *Physica A* (2003) 1–8.
- [339] M.J. Keeling, M.E.J. Woolhouse, R.M. May, G. Davies, B.T. Grenfell, Modelling vaccination strategies against foot-and-mouth disease, *Nature* 421 (2003) 136–142.
- [340] V. Colizza, R. Pastor-Satorras, A. Vespignani, Reaction–diffusion processes and metapopulation models in heterogeneous networks, *Nature Phys.* 3 (2007) 276–282.
- [341] V. Colizza, A. Vespignani, Invasion threshold in heterogeneous metapopulation networks, *Phys. Rev. Lett.* 99 (2007) 148701.
- [342] M. Barthélémy, C. Godrèche, J.-M. Luck, Fluctuation effects in metapopulation models: percolation and pandemic threshold, *J. Theoret. Biol.* (2010).
- [343] V. Colizza, A. Barrat, M. Barthélémy, A.-J. Valleron, A. Vespignani, Modeling the worldwide spread of pandemic influenza: baseline case and containment interventions, *PLoS Medicine* 4 (2007) e13.
- [344] V. Colizza, A. Barrat, M. Barthélémy, A. Vespignani, Predictability and epidemic pathways in global outbreaks of infectious diseases: the SARS case study, *BMC Medicine* 5 (2007) 34.
- [345] H. Hu, S. Myers, V. Colizza, A. Vespignani, WiFi epidemiology: can your neighbors’ router make you sick, *Proc. Natl. Acad. Sci. (USA)* 106 (2009) 1318–1323.
- [346] P. Wang, M. Gonzalez, C.A. Hidalgo, A.-L. Barabasi, Understanding the spreading patterns of mobile phone viruses, *Science* 324 (2009) 1071–1076.